Constructing Responsive Self-Assemblies Through Dynamic Disulphide Linkages

Submitted By

Sumit Chowdhuri

Registration No.: 176122040

Supervisor

Prof. Debapratim Das

Department of Chemistry
Indian Institute Technology Guwahati
Guwahati, Assam-781039 (India)

A thesis submitted for the partial fulfilment

of the requirements of the degree of

Doctor of Philosophy
in
Chemistry
IIT Guwahati, July 2022

Indian Institute of Technology Guwahati

This thesis is dedicated to my Lord, Parampremamoy Sree Sree Thakur Anukulchandra,

&

His living embodiment, Parampujyapada Sree Sree Acharyadev

Indian Institute of Technology Guwahati

Declaration

I hereby declare that all the matters embodied in the thesis result from the experiments and investigations performed by me in the Department of Chemistry, Indian Institute of Technology, Guwahati, India, under the supervision of Prof. Debapratim Das. In keeping with the general practice of reporting scientific observations, due acknowledgements have been made wherever the work described is based on the findings of the other investigators.

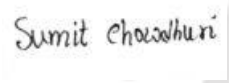

(Sumit Chowdhuri)

Indian Institute of Technology Guwahati

भारतीय प्रौद्योगिकी संस्थान गुवाहाटी
INDIAN INSTITUTE OF TECHNOLOGY GUWAHATI

Dr. Debapratim Das
Professor
Department of Chemistry
Ph: + 91 361 258 3301
Fax: + 91 361 258 2349
E-mail: ddas@iitg.ac.in

July 12th 2022

To whom it may concern.

This is to certify that the thesis entitled "Constructing Responsive Self-Assemblies Through Dynamic Disulphide Linkages" submitted by Sumit Chowdhuri (Roll No. 176122040) for the award of PhD degree to IIT Guwahati, is absolutely based on his own research work and that neither this thesis nor any part of it has been submitted for any degree/diploma or any academic award anywhere before.

(Prof. Debapratim Das)

भारतीय प्रौद्योगिकी संस्थान गुवाहाटी
Indian Institute of Technology Guwahati

Acknowledgement

This thesis represents the final stage on my path to completing my PhD It has been maintained on track with help from many people, including my family, lab mates, well-wishers, and friends. I want to express my gratitude to everyone who helped make this thesis a success and a memorable experience for me. Additionally, it's a great opportunity for me to thank everyone who helped this journey to be a successful one in countless ways.

In the first place, I want to thank my supervisor, Professor Debapratim Das for giving me the opportunity to work in his lab. I've been able to expand my scientific abilities and thoughts because of his consistent motivation, support, and encouragement. In addition to treating me as a student, he also treated me as a part of the family, which gave me the support I needed to overcome whatever difficulties and challenges I could have had with my work. I feel incredibly fortunate to have had a supervisor who genuinely cares for me and who promptly addresses my questions and concerns.

Additionally, I would like to express my sincere gratitude to the members of my doctoral committee, Prof. Chandan Mukherjee, Dr. Kalyan Raidongia, and Dr. Dipankar Srimani, for their advice and critical assessment of my research, which undoubtedly contributed to the development and enhancement of the research work.

I also want to sincerely thank to my seniors, Dr. Nilotpal Singha, Dr. Bapan Pramanik, Dr. Basab Kanti Das, and Dr. Payel Dowari, for their initial direction, encouragement, and assistance in the lab. Additionally, I am also thankful to Dr. Subhajit Ghosh and Dr. Tanur Sinha. My labmate Saurav Das deserves a big thank you for his tremendous support in a number of areas. I sincerely appreciate Priyam, Tanushree, Malay, and Ritvika's cooperation during the course of my work.

I appreciate the assistance in numerous experiments provided by Professor Lihi Abramovich (Tel Aviv University, Israel) and Dr. Anindita Ukil (University of Calcutta, India).

I want to extend my sincere acknowledgement to the Department of Chemistry, IIT Guwahati and the Central Instrument Facility (CIF) for providing me with high-end instrumental facilities. I am also grateful to IIT Guwahati for providing the financial assistance.

My family has given me plenty of encouragement and support to put in all my efforts and attention towards my research career. They constantly encouraged me to achieve all my goals in life and helped me through all ups and downs in life.

My profound acknowledgement also extends to my close friends for their unending support, especially Srijeeb, Pulak da, Bhargabi, Mahesh, Pranjal and Subhasish.

My everlasting gratitude is devoted toward my beloved God, my Lord, Sree Sree Thakur Anukulchandra, who has given me the strength to confront all of my life's challenges. I am fortunate to have experienced the presence of my lord through, Sree Sree Dada (Rev. Ashok Chakravarty) and my Acharyadev (Rev. Arkadyuti Chakravarty) who had constantly elevated me with their celestial guidance.

Indian Institute of Technology Guwahati

Abstract

The thesis, "Constructing Responsive Self-Assemblies Through Dynamic Disulphide Linkages" discusses how dynamic covalent chemistry can be used to create various self-assemblies. These self-assemblies have been created using biopolymers, peptides containing cysteine, and synthetic polymers and they have been applied in a variety of biological systems.

Chapter 1 is about the understanding of several self-assembly processes and their applications along with a review of the literature.

In Chapter 2, a detailed and systematic investigation of the creation of smart thixotropic hydrogels utilizing cysteine-containing peptides and their uses in 3D cell proliferation is provided.

Chapter 3 is about peptides and biopolymer based composite hydrogels and their application in bone cell regeneration.

Chapter 4, is a thorough investigation of the design and construction of coacervate using various peptides and polymers, as well as the compartmentalization of various proteins and dyes inside the coacervate,

Chapter 5 demonstrated the responsiveness of the coacervates by using a wide range of stimuli and by utilizing the dual dynamic nature of coacervate we have created transience of coacervates in a multimodal manner.

List of Abbreviations

1	Py	Pyrene butyric acid
2	Lys (K)	Lysine
3	Cys (C)	Cysteine
4	Phe (F)	Phenylalanine
5	Val (V)	Valine
6	Ala (A)	Alanine
7	Leu (L)	Leucine
8	Ill (I)	Isoleucine
9	Gly (G)	Glycine
10	ECM	Extracellular matrix
11	DIPEA	N, N-Diisopropylethylamine
12	HBTU	N, N, N′, N′-Tetramethyl-O-(1H-benzotriazol-1-yl) uronium hexafluorophosphate
13	HOBT	Hydroxybenzotriazole hydrate
14	TFA	Trifluoroacetic acid
15	TES	Triethylsilane
16	DMF	Dimethyl formamide
17	GSH	Glutathione
18	TCEP	Tris(2-carboxyethyl) phosphine hydrochloride
19	DTT	1,4-Dithiothreitol
20	RT	Room Temperature
21	T_g	Gel Melting Temperature
22	HI	Hydropathy index
23	H_2O_2	Hydrogen Peroxide
24	HPLC	High Performance Liquid Chromatography
25	CD	Circular Dichroism
26	NMR	Nuclear Magnetic Resonance
27	FESEM	Field Emission Scanning Electron Microscopy
28	FETEM	Field Emission Transmission Electron Microscopy
29	AFM	Atomic Force Microscopy
30	MALDI-TOF	Matrix-assisted laser desorption/ionization-Time Of Flight
31	G′	Storage Modulus
32	G″	Lost Modulus
33	MGC	Minimum Gelation Concentration
34	HA	Hyaluronic Acid
35	Alg	Sodium Alginate
36	Gel	Gelation
37	Cht	Chitosan
38	RhB	Rhodamine B
39	MTT	3-(4,5-Dimethylthiazol-2-yl)-2,5-Diphenyltetrazolium Bromide
40	Wt. %	Weight percentage
41	ESI-MS	Electrospray Ionization-Mass Spectrometry
42	SPPS	Solid Phase Peptide Synthesis
43	HOBT	Hydroxy benzotriazole
44	Fmoc	Fluorenylmethyloxycarbonyl
45	Boc	tert-Butyloxycarbonyl
46	Trt	Triphenylmethyl
47	DCM	Dichloromethane

48	ACN	Acetonitrile
49	DFT	Density Functional Theory
50	DMEM	Dulbecco's Modified Eagle Medium
51	PBS	Phosphate Buffer Saline
52	PI	Propidium iodide
53	HLB	Hydrophilic/Lipophilic Balance
54	ALP	Alkaline phosphatase
55	4-MUP	4-Methylumbelliferyl Phosphate
55	αMEM	Minimum Essential Medium Eagle
56	THF	Tetrahydrofuran
57	CDI	Carbonyl diimidazole
60	NaOD	Sodium deuteroxide
61	DCl	Deuterium Chloride
62	Na_2SO_4	Sodium Sulphate
63	HEPES	4-(2-hydroxyethyl)-1-piperazineethanesulfonic acid
64	LVE	Linear Viscoelastic Range
65	LLPS	Liquid Liquid Phase Separation
66	Py1	Pyrene Carboxylic Acid
67	FITC	Fluorescein isothiocyanate
68	BSA	Bovine Serum Albumin
69	HRP	Peroxidase from Horseradish
70	$(Boc)_2O$	Di-tert-butyl dicarbonate
71	HCl	Hydrochloric acid
72	NaOH	Sodium Hydroxide
73	(AIBN)	2,2'-azobis(2-methylpropionitrile)
74	GPC	Gel Permeation Chromatography
75	UV-Vis	Ultraviolet-visible spectrophotometry

CONTENTS

1. Chapter 1: Introduction

1.1 Prelude 21
1.2 Self-assemblies of peptide amphiphiles 20-24
1.2.1 Hierarchical self-assembly process of peptide 22-23
1.2.2 Non-Covalent interactions involved in peptide self-assembly 23
1.2.2.1 Hydrogen bonding interaction 23
1.2.2.2 π–π stacking interaction 23-24
1.2.2.3 Hydrophobic interaction 24
1.3 Different types of self-assemblies 24-34
1.3.1 Hydrogel 25-30

1.3.1.1 Supramolecular hydrogelator 25-27
1.3.1.2 Peptide-based gelators 26-27
1.3.1.3 Stimuli-responsive peptide hydrogel 27
1.3.1.4 pH-responsive peptide hydrogel 27
1.3.1.5 Redox-responsive peptide hydrogel 28-20
1.3.2 Polymeric hydrogel 20-30
1.3.3 Polymer–Peptide based composite Hydrogels 30-31
1.4 Gelation driven by Cysteine: 32-32
1.5 Transient self-assembly 32-32
1.6 Coacervates 33-37
1.6.1 Simple coacervation 35
1.6.2 Complex Coacervation 35-36
1.6.3 Covalently crosslinked coacervate 36
1.6.4 Transient coacervation 36-37
1.7 Applications of Self-assembly 37-40
1.7.1 Hydrogels as an extracellular matrix for tissue engineering 38-39
1.7.2 Osteogenesis 40
1.7.3 Drug delivery vehicle 40-41
1.8 The present thesis 41-43

2. Chapter 2: Effective Three-Dimensional Cell Proliferation Using a Smart Thixotropic Hydrogel Made of Disulphide Linked Short Peptides.

2.1 Introduction 47-48
2.2 Results and discussion 48-64
2.3 Conclusion 64
2.4 Experimental section 64-71
2.4.1 General information and materials 64
2.4.2 Syntheses of peptides (1-12) 64-67
2.4.3 Determination of solubility of the peptides 67
2.4.4 Preparation of hydrogel 67-68
2.4.5 Determination of sol–gel transition temperature (T_g) 68
2.4.6 Electron microscopy 68
2.4.7 Rheology 68-69
2.4.8 HPLC 69
2.4.9 Circular dichroism (CD) 69
2.4.10 Dye release study 69-70
2.4.11 NMR studies 70

2.4.12 Density Functional Theory (DFT) 70
2.4.13 Cell culture 70
2.4.14 Cytotoxicity assay 70-71
2.4.15 Confocal microscopy 71
2.4.16 Cell proliferation assay 71
2.4.17 Statistical analysis 71

3. Chapter 3: Modulation of Physical and Biological Properties of Biopolymer Hydrogels in The Presence of Short Self-Assembling Peptide
3.1 Introduction 75-76
3.2 Results and discussion 76-88
3.3 Conclusion 89-89
3.4 Experimental section 89-96
3.4.1 General information and materials 89
3.4.2 Synthesis 90-92
3.4.3 Preparation of the hydrogel 92-93
3.4.4 Field emission scanning electron microscopy (FESEM) 93
3.4.5 Swelling property 93
3.4.6 Stability of Hydrogels toward proteolytic digestion 93-94
3.4.7 Stability of hydrogel in cell culture medium 94
3.4.8 Rheology 94
3.4.9 Cell Viability on the composite hydrogel 94-95
3.4.10 Alkaline phosphatase (ALP) activity 95
3.4.11 Mineralization assay 95-96

4. Chapter 4:Dual Dynamic Covalent Bond Mediated Polymer-Peptide Coacervation
4.1 Introduction 99-100
4.2 Results and discussion 100-106
4.3 Conclusion 107
4.4 Experimental section 107
4.4.1 General information and materials 107
4.4.2 Synthesis of polymers 108
4.4.2.1 Synthesis of Boc-EDA (18) 108
4.4.2.2 Synthesis of methacryloyl chloride 108
4.4.2.3 Synthesis of MA-EDA-Boc (19) 109
4.4.2.4 Synthesis of MA-EDA.HCl (20) 109
4.4.2.5 Synthesis of MA-CHO (21) 109
4.4.2.6 Synthesis of MA-Benz (22) 109-110
4.4.2.7 Syntheses of Poly-CHO (23) and Poly-Benz (24) 110-111
4.4.4 Syntheses of Peptides 111-113
4.4.5 Optical microscopy 113
4.4.6 Field Emission Scanning Electron Microscopy (FESEM) 113
4.4.7 Transmission Electron Microscopy (TEM) 113
4.4.8 Turbidity measurement 113
4.4.9 ^{1}H-NMR analysis showing the reversible formation of imine linkage 113-114
4.4.10 Preparation of coacervates using PolyCHO and PyKC 114
4.4.11 Estimation of water content 114
4.4.12 Fluorophore labelling of proteins 114-115
4.4.13 Preparation of protein and dye entrapped coacervates 115
4.4.14 Enzyme activity measurements 115
4.4.15 Phase diagram 116

4.4.16 Effect of H_2O_2 on the aldehyde groups of the polymer. 116

5. Chapter 5: Creating Multimodal Transience in a Polymer–Peptide Composite Coacervate
5.1 Introduction 119
5.2 Results and discussion 120-126
5.3 Conclusion 126-127
5.4 Experimental section 127
5.4.1 Optical microscopy 127
5.4.2 Turbidity measurement 127
5.4.3 Stock Solutions for Different Experiments 127
5.4.4 Preparation of Coacervates using PolyCHO and PyKC 128
5.4.5 Transient pH Cycle 128
5.4.6 Transient Redox Cycle 128
5.4.7 Response of the Coacervates Toward Different Stimuli 129
5.4.8 Transient Formation of the Coacervates Under the Influence of Two Different Triggers 129
5.4.9 Estimation of PyKC and $(PyKC)_2$ during Transient Redox Cycle 129

6. References 131
7. Characterisation Data 147

Chapter 1: Introduction

1.1 Prelude

"Supramolecular chemistry, the designed chemistry of the intermolecular bond, is rapidly expanding at the frontiers of molecular science with physical and biological phenomena."-Jean-Marie Lehn.[1]Self-assembly is ubiquitous in nature, and it is thought to play a key role in the emergence, maintenance, and progression of life.[2, 3]Unlike traditional chemistry which deals with the strong irreversible covalent bonds, Supramolecular chemistry is associated with the self-assembly of molecules, which occurs when molecules in equilibrium are connected by weak reversible noncovalent interactions to form stable, structurally well-defined aggregates.[4]Supramolecular chemistry began in 1894 when Emil Fischer proposed the famous 'Lock and Key' model to explain the enzyme-substrate mechanism. Since then, two tenets have emerged:'molecular recognition' and 'supramolecular function,' which have since been incorporated as a topic of a new subject known as supramolecular chemistry.[5]Supramolecular chemistry comprises molecular self-assembly, folding, host-guest chemistry, mechanically interlocked molecular structures, and, more recently, dynamic covalent chemistry, as well as transient assembly.

Scientists have used molecular self-assembly, a powerful natural phenomenon, to develop smart supramolecular architectures.[6] This is mainly governed by weak non-covalent interactions like electrostatic interactions (ionic bonds), hydrogen bonding, metal coordination, hydrophobic forces, van der Waals forces, π–π stacking interactions, etc.[7]Even though these forces are weak, their combined effects can generate structurally and chemically stable frameworks.Condensates, micelles, vesicles, gels, and other similar structures are common examples of self-assembly. Natural amino acids are a great candidate for self-assembly due to the presence of various functional units. Peptides self-assemble hierarchically, and produce a variety of primary, secondary, and tertiary structures, resulting in a wide range of structural soft materials with applications in drug delivery, tissue engineering, scaffolds for cell proliferation, wound healing, nano fabrication, and other fields.[8]

The current thesis is concerned with various types of self-assemblies, specifically hydrogels, coacervates, and transient assemblies, as well as their responsiveness to environmental cues and applications in diverse biological fields. The following is a summary of the current state of different assemblies with respect to their preparation, physical significance, mechanistic aspects, and numerus applications.

1.2 Self-assemblies of peptide amphiphiles

Amphiphiles are molecules that have a hydrophilic "head" group and a hydrophobic "tail". Polar, Ionic, or hydrogen-bond-forming groups may be present in the head groups, making them water-soluble. Saturated or unsaturated hydrocarbon chains or aromatic groups make up the tail regions.[9]Amphiphiles can achieve an optimal hydrophilic-lipophilic balance (HLB) with the appropriate use of functional groups, allowing them to further self-organize. Tuning the aggregation of these amphiphilic molecules

is thus possible by altering their architectures. One important class of amphiphilic molecules is the peptide amphiphiles (PA)[10]. Amphiphilic peptides made entirely of amino acids are structured in so-called amphipathic sequences, which means they have both hydrophobic and hydrophilic domains when folded properly. To improve their interaction with the environment, the peptides fold into helices and sheets and self-assemble in a lipid bilayer. Furthermore, the natural amino acids' vast spectrum of functional groups allows PAs to be designed with the appropriate functionality. By combining peptide sequences with other functional groups to create novel PAs, new soft materials with hitherto unseen characteristics and uses can be created.

1.2.1 Hierarchical self-assemblyprocess of peptide

All of the key properties that aid in the self-assembly process may be found in natural amino acids. A peptide molecule with the appropriate amino acid sequence could easily self-assemble.

The hierarchical process of peptide self-assembly that results in hydrogelation can be simplified as shown in Fig. 1.1 In solution, peptide molecules adopt a specific secondary conformation, whichself-assembles into nanofibers in the presence of appropriatestimuli or favourable physical conditions. Elongation of these fibres in three-dimensional space results in thicker and longer fibres, which then join together to form a fibrillar network. This self-supporting hydrogel is made up of three-dimensional peptide networks that can trap water molecules. The physical properties of these hydrogels can be fine-tuned and various functional materials can be generated by tweaking the amino acid sequences. Several attempts to make and comprehend peptide-based hydrogels with diverse secondary structural motifs such as α-helix, β-sheet, β-hairpin, and coiled-coil have been performed in the previous two decades.[7]

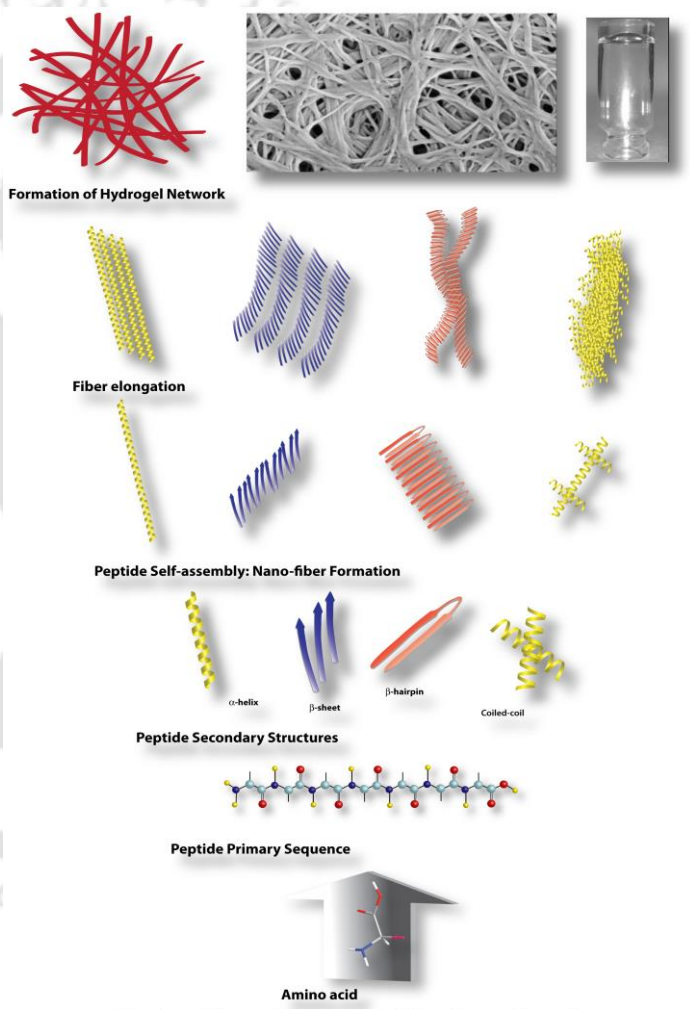

Fig. 1.1 Hierarchical assembly of peptides.[7]

1.2.2 Non-Covalent interactions involved in peptide self-assembly

As a result of the cooperative effects of several relatively weak intermolecular interactions, stable and orderly self-assembled peptide nanostructures are created. I'll go over a few distinct sorts of non-covalent interactions in the next few paragraphs.

1.2.2.1 Hydrogen bonding interaction

The longitudinal packing of peptide monomers is driven by hydrogen bonding between the backbone amine group and the carbonyl group of peptide chains, which is a key feature in peptide self-assembly[11]. The peptide backbone comprises hydrogen bond donor (amide-NH) and acceptor (amide carbonyl) groups, which enable the peptide molecule to generate intermolecular hydrogen bonds and assemble easily via various secondary structures.

In peptides and proteins, the β -sheet is a common secondary structure that consists of two or three backbone hydrogen bonds joining strands laterally, resulting in antiparallel and parallel structures in this pleated sheet.[11] By inserting a β -turn stabilizing DPro-LPro unit in between two β -strands, a β -hairpin can be created in a similar method.[12, 13] Furthermore, hydrogen-bonding interactions between peptide side chains (between residues at positions i, i+3 and i, i+4), electrostatic interactions between charged polar residues, and capping interactions between residues adjacent between strands all affect the stability of α-helical protein conformations formed by winding the polypeptide backbone.[14, 15] Moreover, Hydrophobic interactions govern the connections between the helices when favourable interactions at the α-helix surfaces pull α-helices together to create a coiled-coil shape, which is stabilized by hydrogen bonding iinteractions.[16]

1.2.2.2π–π stacking interaction

Aromatic interactions are the most important non-covalent interactions since they not only aid in the self-assembly and gelation of peptides, but they can also help to balance the hydrophobicity of peptides.[17, 18] Another strategy is to use aromatic functionalities to impart the amphiphilicity needed to drive self-assembly, in which case self-assembly will be controlled by the directionality of the resulting aromatic stacking interactions or π– π staking interaction. Appropriate alignments of the aromatic rings in the peptide sequences of naturally occurring aromatic amino acids, Phenylalanine (Phe), Tyrosine (Tyr), and Tryptophan (W) lead to peptide self-assembly. Additionally, aromatic moieties, such as Fmoc, naphthalene, pyrene, anthracene, naphthalene diimide (NDI), and perylene diimide (PDI), are commonly attached to synthetic peptides to produce self-assembling sequences.[19-21]Figure 1.2 shows different types of π– π staking between two aromatic rings.

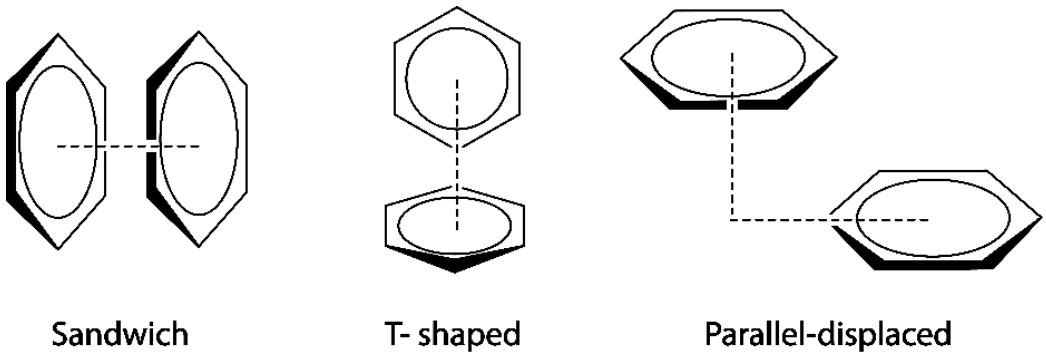

Figure 1.2 Different types of π–π staking of benzene dimer.

1.2.2.3 Hydrophobic interaction

Hydrophobic interactions are one of the most common noncovalent interactions in biological systems, and they occur when water molecules rearrange as two hydrophobic species approach each other.[22]To induce hydrophobicity into the peptide self-assembly process, we can introduce hydrophobic side chains (Alanine, Leucine, Isoleucine, aromatic amino acids) to the backbone of the peptide.

1.3 Different types of self-assemblies

Over the last decade, Scientists have developed an elegant and simple library of functional amphiphilic small moleculeswith remarkable abilities to form supramolecular self-assemblies such as micelles,[23, 24] reverse micelles,[25, 26] vesicles,[27] fibres,[28] supramolecular gels,[29] coacervates[30] and so on. Each of the forms of the self-aggregated structure has its own prominence and has important applications in chemistry, physics, biology, and other fields. Precise control over the formation of different well-defined supramolecular self-assemblies can be achieved through the careful design of low-molecular-weight amphiphiles. Only the functional moieties of the amphiphilic structure can be tuned to produce a wide range of supramolecular structures with task-specific applications.[31]

1.3.1 Hydrogel

Hydrogel is a semisolid material more specifically a cross-linked three-dimensional network structure that can entrap a considerable amount of water molecule inside its network. Hydrogels are a class of materials that have already gained significant interest in different biomedical applications over the last 60 years due to their high-water content, which mimics hydrated tissues.The first molecular gelator, reported by Hoffman in 1921, was dibenzoyl-L-cystine (Figure 1.3A) which was able to form a self-supportinghydrogel.[32]The hydrogel was rigid enough to hold its shape, as evidenced by the vial inversion test.Aromatic moieties are highly effective at enhancing intermolecular interactions in water, which is one of the most revealing design principles revealed in the study of dibenzoyl-L-cystine.This principle is largely responsible for the successful use of aromatic–aromatic interactions to design

hydrogelators of small peptides.[13, 15]Various classes of hydrogels have been developed in this regard to make this class of biomaterial applicable in various spheres of human life.

Types of hydrogels

Hydrogels are classified as either physically (supramolecular) or chemically cross-linked (Polymeric) based on the nature of the crosslinks in their three-dimensional networks. Cross linking in polymeric hydrogels is accomplished through the formation of irreversible covalent bonds between monomer units via an appropriate synthetic route.[33, 34]In many ways, supramolecular hydrogels differ from polymeric hydrogels. One significant difference is that, unlike polymeric hydrogels, which form from a randomly cross-linked network of permanent covalent bonds, supramolecular hydrogels form as a result of molecular self-assembly driven by weak, reversible non-covalent interactions among hydrogelators in water.This specific but fundamental difference not only results in more organised molecular arrangements in supramolecular hydrogels, but it also manifests itself during the hydrogelation process.While simple swelling typically results in a polymeric hydrogel, a stimulus or triggering force is required to shift thermodynamic equilibrium and initiate the self-assembly process in order to achieve a supramolecular hydrogel.As a result, there are several stimuli or triggers (for example, pH change, chemical or photochemical reactions, redox, and catalysis) that can be used to modify the weak interactions.

1.3.1.1 Supramolecular hydrogelator

Non-covalent interactions such as hydrogen bonding, electrostatics, hydrophobic forces, metal-ligand coordination, and host-guest recognition hold supramolecular hydrogels together, making them one of the most promising soft material platforms that significantly reduce structural flexibility and change macroscopic performance, resulting in the formation of 3D cross-linked networks in modern biomedical applications[35]. Because of the presence of non-covalent interactions, supramolecular hydrogels exhibit moderate mechanical properties as well as reversible sol-gel transition behaviour in response to a wide range of biological stimuli (e.g., pH, redox agents, enzymes, bioactive molecules) and processability intrinsic to supramolecular cross-linking units, which can serve as a smart carrier for delivering various therapeutic agents.[36]Anumerus number of host macrocyclic molecules, including cyclodextrin (CD) and cucurbituril (CB[n]), have already been reported to form supramolecular hydrogels by host guest interactions, and the hydrogels are also applicable in many biochemical applications due to their nontoxic nature.[37, 38] Furthermore, the development of highly strong, opaque materials is frequently the result of strong, multivalent electrostatic interaction between two oppositely charged polyelectrolytes.[39] Shinkai and colleagues have described a variety of stimuli-responsive supramolecular gels. The majority of these gelators are made from cholesterol found in nature. An n-butanol gel of cholesterol derivatized with an azobenzyl group (Figure 1.3B) was demonstrated to be photo responsive in one of the earliest

examples.[40] A gel of decyl ammonium salt of anthracene-9-carboxylate (S3, Figure 1.3B), on the other hand, was demonstrated to be photochemically and thermally responsive in another case.[41]

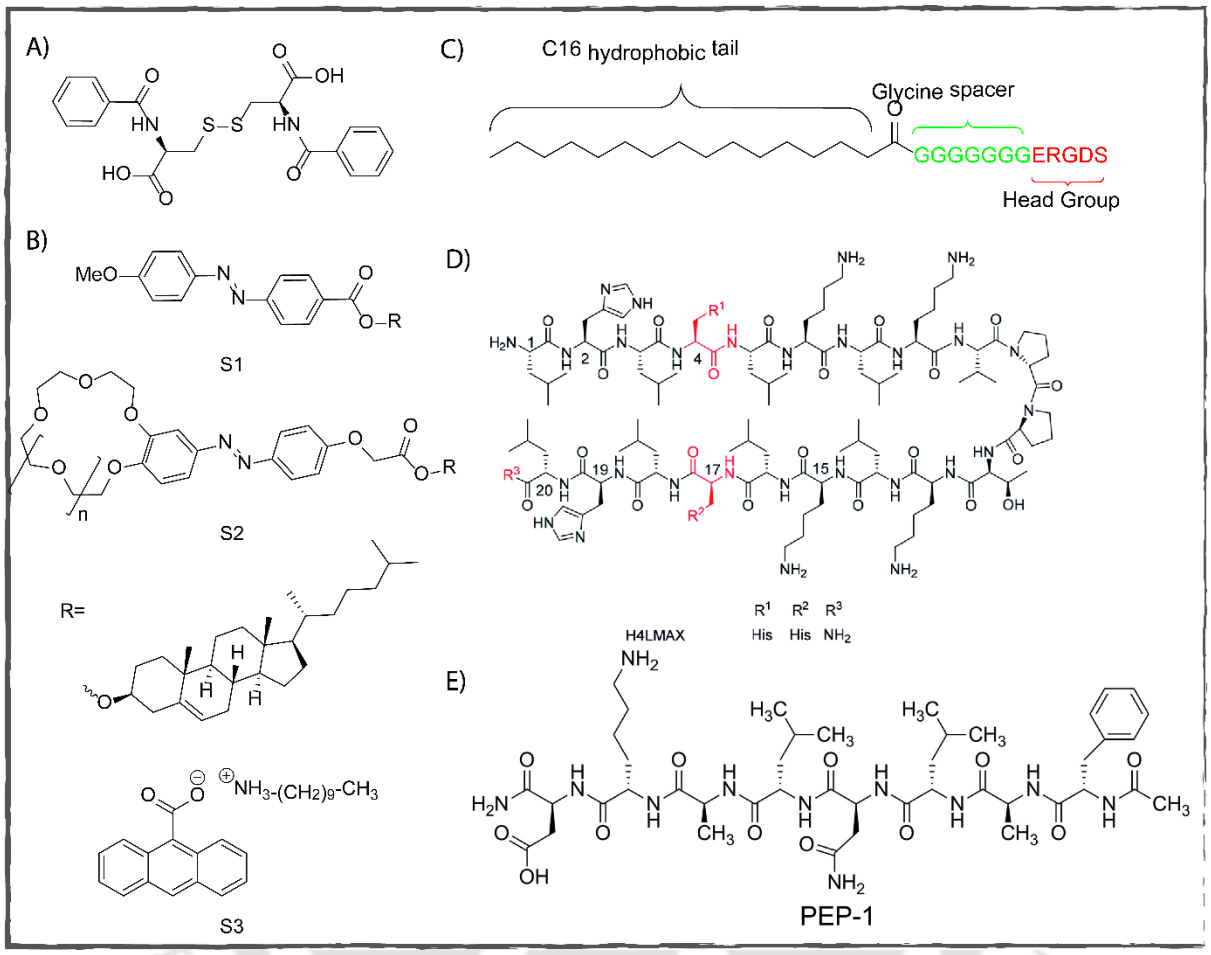

Fig. 1.3 Chemical structures of different peptide hydrogelators. Figure adapted with permission.[40, 44, 47, 50]

1.3.1.2 Peptide-based gelator:

Because of their inherent biocompatibility, amino acid or peptide hydrogelators are extremely important in addition to small organic and inorganic hydrogelators. Peptide hydrogels are composed by using amino acids with some driving forces known as non-covalent or supramolecular interaction such as hydrogen bonding, hydrophobic interaction, π–π staking to give a very stable structure.[42] For each non-covalent interaction there required some specific interactions. For hydrogel bonding, the donor and acceptor should be properly positioned. Efficient π–π interaction requires proper superimposition of aromatic rings and being in the order of 3.4 Å. For hydrophobic interaction and ionic interactions, the force is not directional and so specific. These intermolecular interactions result in the formation of organised supramolecular structures that entrap water when stimulated.Overall, there should be a proper balance of hydrophobicity and hydrophilicity in the peptide structure.[43] Paramonov et al.

reported a peptide amphiphile (Figure 1.3 C) which was an oligo-peptide. These peptides are self-assembled by forming a hydrophobic core, followed by β-sheets in the region closest to the core.[44]

1.3.1.3 Stimuli-responsive peptide hydrogel

The nature and amount of non-covalent interactions, as well as the mechanical strength and robustness of the hydrogels, are determined by factors such as gelation medium temperature, pH, and ionic strength.The most common method for creating stimuli-responsive hydrogels is to strategically incorporate destabilizing functionalities in the hydrogel framework that may disrupt the hydrogel's structural integrity in response to a specific environmental situation such as light, temperature, electric or magnetic field, pH, chemicals, shear stress, and redox reagents. Stimuli-responsive hydrogels have recently sparked a lot of interest in the chemistry and material fields.[45]

1.3.1.4 pH-responsive peptide hydrogel

One of the most prevalent approaches to modulate the gelation propensity of peptide hydrogels has been pH-driven regulation of charged interactions between pH-sensitive amino acids such as lysine, arginine, histidine, aspartic acid, and glutamic acid in the peptide gelator backbone.[46]Schneider et al. demonstrated the importance of pH in achieving secondary structural conformations that are required for hydrogelation utilizing their -hairpin peptides. MAX1 (Figure 1.3 D) showed that changes in sol-gel characteristics are influenced by pH.[13, 47]Changes in pH influence the gelation of the 21-residue peptide AFD19, according to Dexter and co-workers, with highly charged peptide states creating low-viscosity solutions and thermostable gels at pH 6. Although at high pH, the peptide generates insoluble fibrils. Switching between the peptide's liquid, gel, and insoluble phases is possible by adding acid or base.[48]Peptide RATEA16 can form stable at neutral pH. However, the hydrogels dissolved at acidic pH[49] Another finding revealed that PEP-1 (Figure 1.3 E, a naturally occurring β-strand peptide fragment of Galectin-1), a highly biocompatible amphiphilic peptide identified in bovine spleen gels spontaneously at pH 7.4 .with a high yield stress of 88.0 Pa and a gel-to-sol temperature of 84 °C. The gel network could entrap water-soluble guest molecules like Calcein, which could be selectively released at acidic pH.[50]

1.3.1.5 Redox-responsive peptide hydrogel

The reducing agent can cleave disulphide bonds in a reversible manner. This characteristic can be used to create redox-responsive hydrogels. Makhlynets and co-workers reported an unnatural nine-residue peptide F9 3'PyA (Figure 1.4 A) may produce a hydrogel in the presence of Ag (I), but not in the presence of Cu(II), whereas the same peptide, but with the nitrogen in a different place in the pyridyl ring (F9 4'PyA, Figure 1.4 B), can form a hydrogel in the presence of Cu(II), but not in the presence of Ag (I). When ascorbic acid is introduced as a reducing agent, the Cu (II) ion is converted to Cu (I) ion, and the hydrogel dissolves.[51]

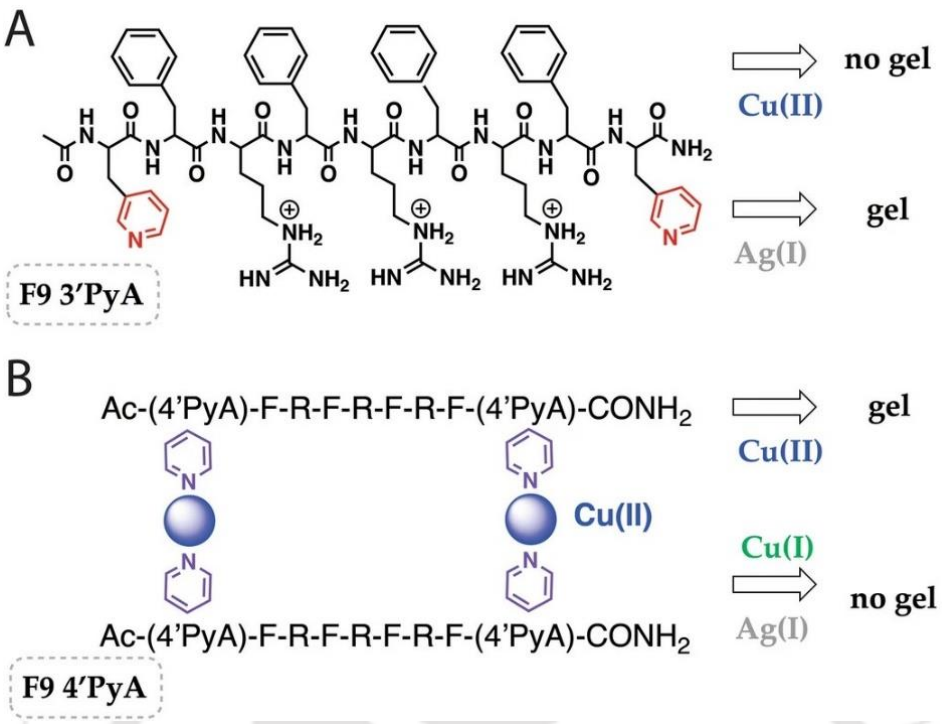

Fig. 1.4 This study outlines nine-residue peptides containing non-natural amino acids. A) F9 3PyA gels with Ag(I) but not with Cu (II). B) In the presence of Cu (II), F9 4PyA forms a gel but not in the presence of Cu(I) or Ag (I). Figure reproduced with permission.[51]

Ferrocene phenylalanine (Figure 1.5 A-B) conjugate is another example, which can form a hydrogel at physiological pH and disintegrate at higher pH. Due to the presence of the Ferrocene unit, hydrogel breaks and reforms in the presence of H_2O_2 and ascorbic acid respectively.[52]Incorporating Cys residue into the hydrogel is another strategy to provide it a redox responsive feature. The peptide Ac-C$(FKFE)_2$CG-NH_2 (Figure 1.5C) is an example of a redox driven gelation. Two Cys residues in this peptide can undergo intramolecular cyclization via disulphide bond formation. The cyclopeptide that results do not self-assemble, and the solutions remain stable for months with no discernible alterations. However, when the disulphide is reduced with tris(2-carboxyethyl) phosphine (TCEP), the resultant linearized peptide quickly assembles into a fibrous network hydrogel[53].

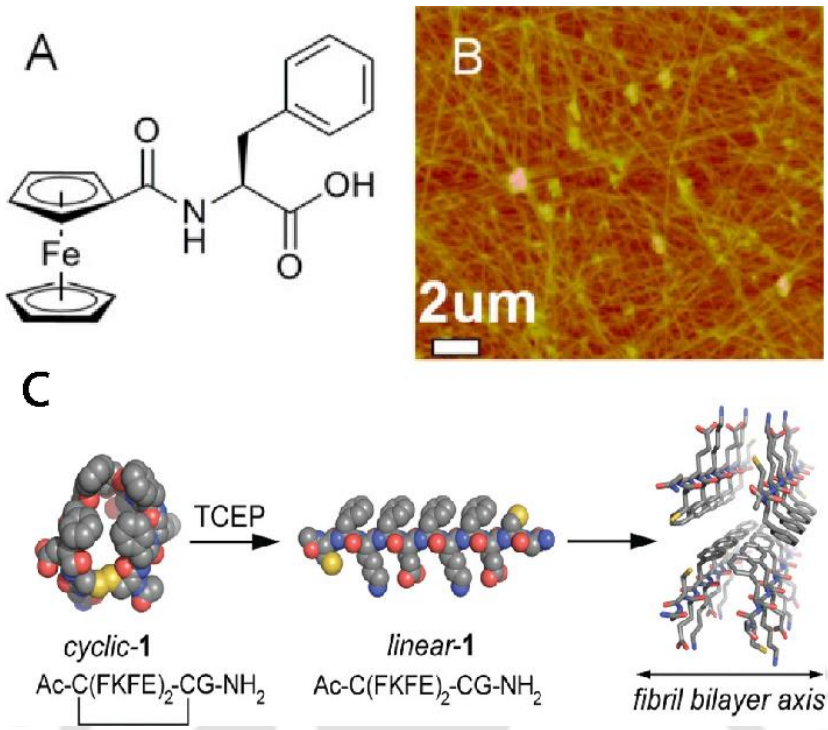

Figure 1.5 A) Chemical structure of the gelator Fc-F. B) image of the cryo-dried hydrogel. C) Cyclic to Linear Peptide Conformational Switch Using a Reductive Trigger. Figure reproduced with permissions. [52,53]

1.3.2 Polymeric hydrogel

Polymeric hydrogels are formed by crossing the polymeric chains to create a stable polymeric network that can entrap water molecules within the spaces between the polymeric chains. Polymeric hydrogels (PHG) are viscoelastic materials with a network structure due to the cross-linker and the solvent, respectively.[54] They are mainly composed of simple biopolymers or by using synthesised polymers. PHG materials, such as soap, shampoo, toothpaste, hair gel, and contact lenses, have recently become commonplace in everyday life in a variety of forms, depending on their intended use. Oil recovery, medicines, agriculture, textiles, and water treatment are just a few of the advanced industrial applications for PHGs. As a result, gel materials are now among the most common in our daily lives.[55] Researchers have been able to develop and tune hydrogel materials employing a wide range of polymers (both natural and synthetic) and varied crosslinking between the polymer chains via irreversible covalent bonds such as Schiff base formation,[56] click reaction,[57]disulphide linking,[58]photopolymerization of thiol and terminal alkenes[59] etc.Furthermore, the mechanical strength of these chemical crosslinks can be fine-tuned to create robust and stable hydrogels. The inclusion of hydrophilic groups in the polymer chains, such as amino, carboxyl, and hydroxyl groups, contributes to the hydrogels' water holding ability. The amount of water in a hydrogel, according to Hoffmann, can range from 10% to thousands of times the weight of the xerogel.[60] The greater the number of hydrophilic groups, the greater the water retaining capacity; however, as the cross-linking density

increases, the equilibrium swelling decreases due to the reduction in hydrophilic groups. Naturally available biopolymers like silk, natural rubber, The most common materials utilised in the production and manufacture of PHG include synthesized monomers or polymers, as well as natural polymers are Methacrylic acid (MA), Acrylic acis (AA), Acrylamide (AM), Hydroxyethyl methacrylate (HEMA), Hydroxyethoxyethyl methacrylate (HEEMA), Hydroxydiethoxy- ethylmethacrylate (HDEEMA), Methoxyethyl methacrylate (MEMA),Gelatin methacrylate (GelMA) etc.[61]

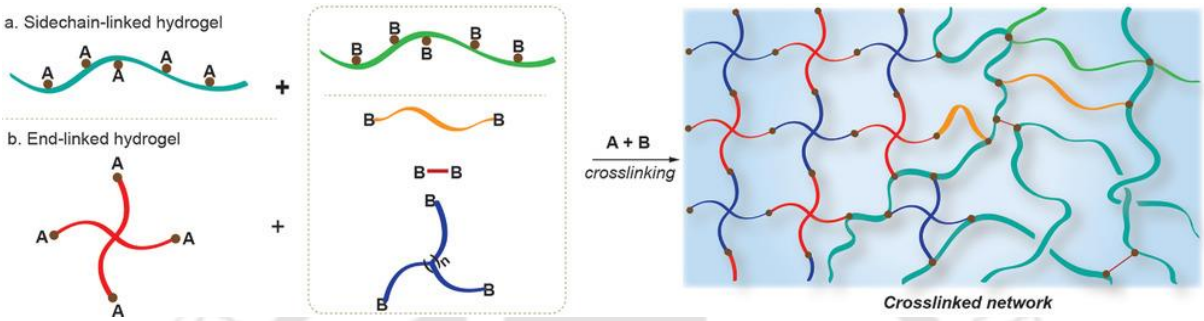

Figure 1.6 Different crosslinking technique in polymeric hydrogelation.Figure reproduced with permission.[301]

1.3.3 Polymer–Peptide based composite Hydrogels

The lack of mechanical strength and toughness in hydrogels limits their use in several applications. Despite having high swelling ratios (10-100), conventionally manufactured peptide hydrogels have low Young's modulus (1–100 kPa), storage modulus (1–100 kPa), and fracture energy, making them weak in nature.[62] There are numerous literature reports that show how hydrogels can be toughened using various methods, allowing them to be used in load-bearing applications.

Among the methods available for producing tough hydrogels are slip-link networks, nanocomposite hydrogels, double network hydrogels, multi-functional crosslinked hydrogels, homogeneous hydrogels, and hybrid ionic–covalent IPN hydrogels. All of the methods mentioned above have been shown to improve hydrogel strength as well as hydrogel toughness.[63]A recent report demonstrated that Fmoc-RGD peptide can form hydrogels via slow gelation kinetics, but in the presence of Chitosan, the strength and rate of hydrogelation increase significantly, and the composite hydrogels (Figure 1.1) were used in both 2D and 3D cell culture. Chitosan's inherent antibacterial properties make the composite hydrogel an ideal candidate for antibacterial activity.[64]

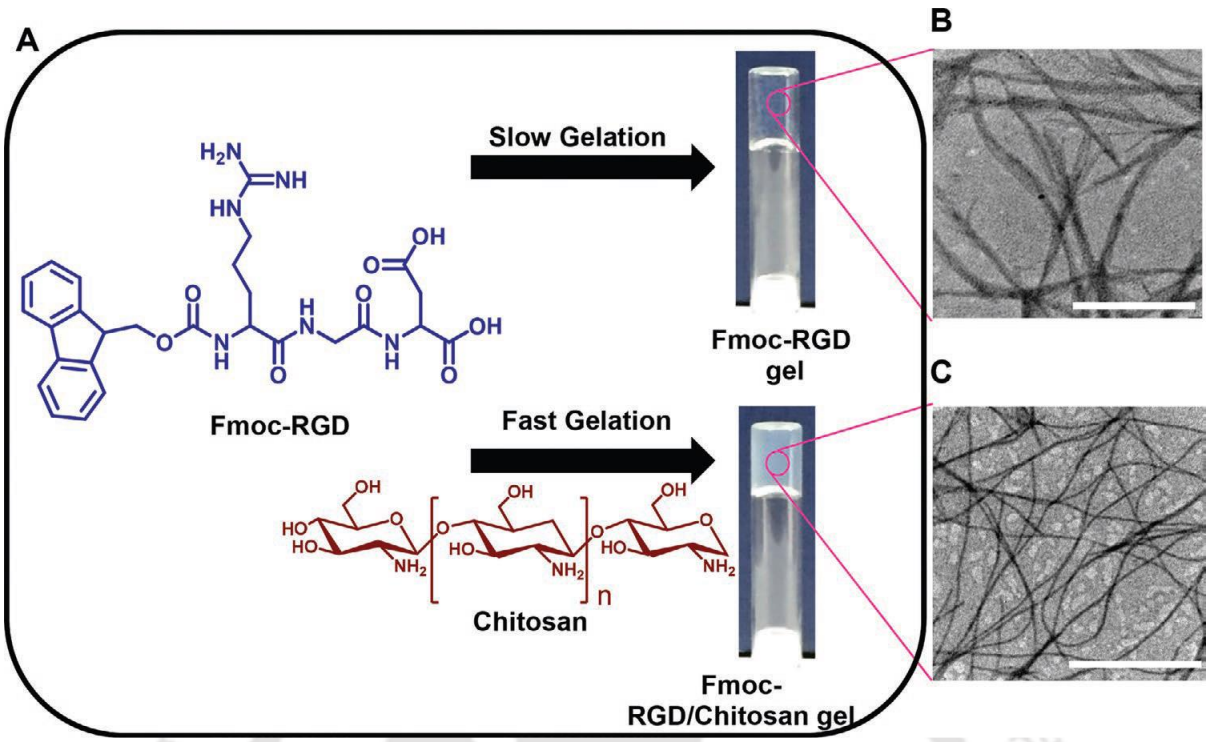

Figure 1.7 Preparation and morphology of the Fmoc-RGD and Fmoc-RGD/chitosan composite hydrogels. A) Chemical structures of Fmoc-RGD and chitosan, and digital images of the hydrogels. TEM images of B) Fmoc-RGD and C) Fmoc-RGD/chitosan composite hydrogels (Scale bars are 1 μm). Figure reproduced with permission.[64]

1.4 Gelation driven by Cysteine

Because of their degradability in response to redox stimuli, disulphide-cross-linked hydrogels have been widely used in biological applications.[65] Incorporating L-lysine, which is easily converted into an amphiphile, not only acts as a hydrogelator, but has also inspired the development of new L-lysine-based hydrogelators.Cysteine with a free sulfhydryl group, when incorporated into the peptide backbone, is capable of forming disulphide linkages in the presence of an oxidising agent (H_2O_2, $[Fe(CN)_6]^{4-}$), and generating the free sulfhydryl group in the presence of a reducing agent (TCEP, DTT, GSH) to produce redox responsive hydrogel.Peptide-based hydrogels are normally weak as noncovalent force is the only driving force for hydrogelation. However, by introducing cysteine, we can improve the mechanical properties of the hydrogel through chemical ligation via the formation of redox responsive disulphide groups.

Yang et. Al.[66] reported a tuneable simple disulphide shuffling technique to generate keratin hydrogels (Figure 1.8) through the shuffling between intramolecular disulphide bonds to intermolecular disulphide bonds. To begin, intramolecular disulphide bonds were cleaved by using Cysteine as a reducing agent to liberate the thiol group, and the free thiol groups can form intermolecular disulphide linkages via thiol oxidation. Controlling the cysteine level results in tuneable disulphide crosslinking density, altering network structure, gel degradation, and drug release rate.

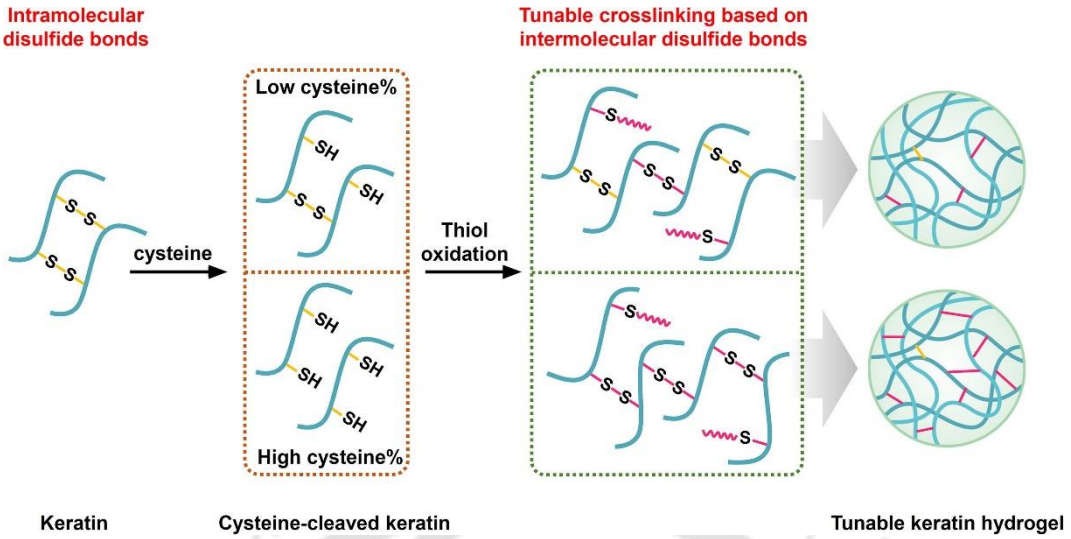

Figure 1.8 Gelation mechanism illustrated schematically using the disulphide shuffling strategy. The density of intermolecular disulphide crosslinking can be tuned by changing the cysteine levels, resulting in a different microstructure and properties such as mechanical strength, gel degradation, and drug release. Figure reproduced with permission.[66]

In order to create smart responsive materials, our team used a simple design philosophy to create Azo-KC (Azo-Lys-Cys-$CONH_2$), a tripeptide gelator that generated a robust and water insoluble hydrogel. AzoKC molecules form dimers in aqueous media through in situ disulphide production, which then self-assemble in a stepwise manner to create tightly packed fibrillar networks of the hydrogel having light responsive as well as syneresis property.[67]

1.5 Transient self-assembly

Recently, in an attempt to develop biomimetic cycles, there has been an increasing interest to achieve synthetic chemical systems out of equilibrium.[68, 69] To achieve such interactive, life-like materials, a fuel source and feedback control are important. The continuous energy supply in the form of chemical fuel helps to maintain the transient self-assembly[70] far from thermodynamic equilibrium, to which the typical synthetic systems spontaneously assemble. The behaviour of such transient systems is driven by the kinetics of fuel consumption, rather than thermodynamic stability, and so the self-assembly process and its kinetics[71, 72] need to be acutely understood. So far, mostly biological components like enzymes, DNA, or proteins have shown such artificial, chemically fuelled, active self-assembling behaviour.

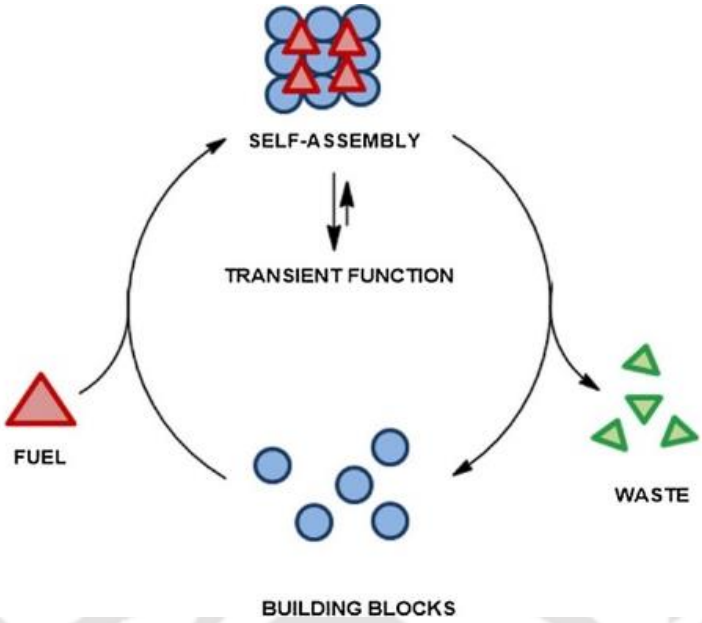

Figure 1.9 Schematic presentation of transient self-assembly driven by fuel. Figure reproduced with permission.[301]

In this regard, of late short peptide gelators have emerged which in addition to exhibiting exceptional stimuli responsiveness, lack the complexity of that of natural system. Such hydrogel networks, on account of their exceptional spatial control have successfully been able to be selectively assembled or removed.[73]

However, the temporal control of these materials is yet to be tuned by delicately balancing theactivation and deactivation kinetics of gelation (Figure 1.9).[69, 70] Once optimised, such artificial active materials achieved via a fuel-driven self-assembly process can successfully be used for drug delivery, active separation, self-healing, and autonomous control of chemical processes.[74]

1.6 Coacervates

In the 1930s, Oparin suggested the concept of coacervates in his work on the origins of life, which was followed by Bungenberg-de Jong's introduction of coacervates in 1929. Coacervate dropletsform spontaneously as a result of liquid-liquid phase separation, which occurs when a liquid condensed phase rich in macromolecules separates from an aqueous solution.Due to the differing affinity of molecules for the coexisting phases, coacervates can easily absorb and concentrate solutes from the environment because they lack a membrane.Coacervations happens through multiple weak non-covalent interactions (electrostatic interactions, hydrogen bonding, hydrophobic forces, van der Waals forces, Cation-π interaction, π–π stacking interaction (Figure 1.10).

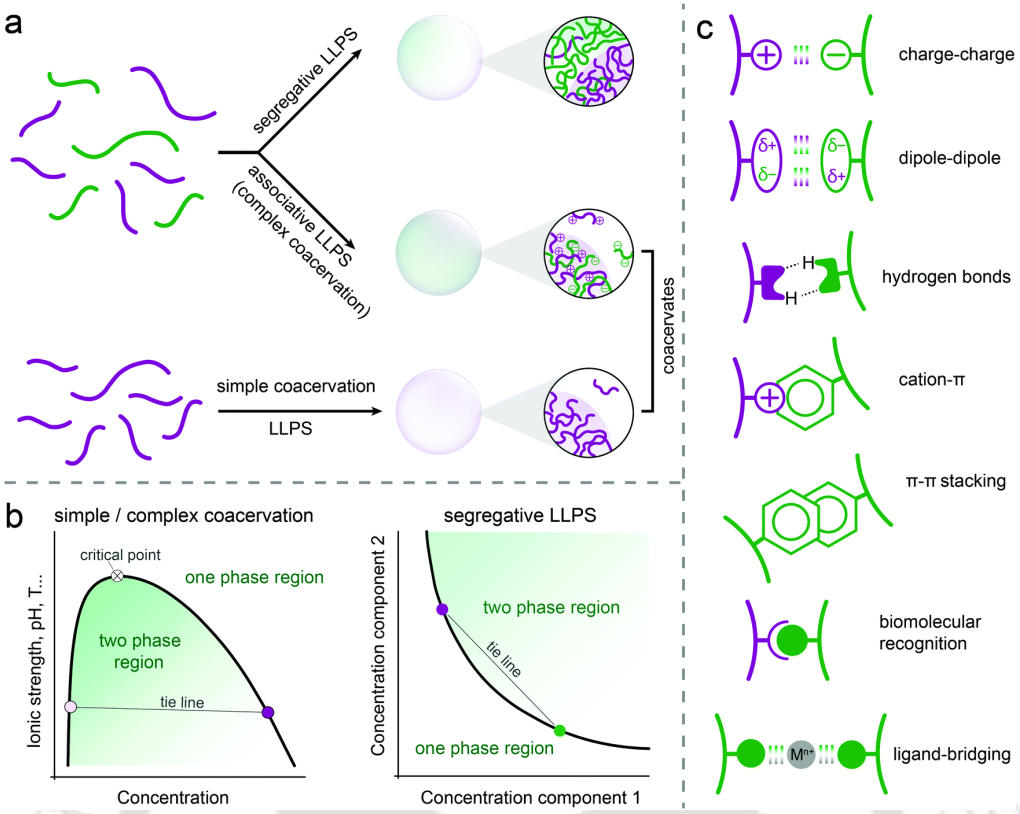

Figure 1.10 (a) Different types of liquid–liquid phase separation and coacervate formation, (b) schematic phase diagrams of simple or complex coacervation and segregative phase separation, (c) potential interactions involved in the formation of peptide-based coacervates. Figure reproduced with permission.[76]

Changes in solution temperature, pH, ionic strength, or composition can induce phase separation, which can occur via nucleation and growth of coacervate droplets when an energy barrier must be overcome to nucleate the coacervate phase. However, these types of equilibrium characterizations do not provide sufficientinsight into the dynamic behaviour of coacervates. Typical approaches for determining coacervate phase behaviour include turbidity and light scattering, which take use of the light dispersed by these small droplets in solution. While an increase in viscosity can be utilised to detect the onset of complex formation.[75] Based on the driving factor for the LLPS, Coacervates[76] can be categorized as complex or simple. Complex coacervate[77, 78] is of two types, associative and segregative. Associative LLPs are formed by attractive electrostatic interactions between oppositely charged macromolecules, whereas segregative LLPs are formed by minimising repulsive interactions such as hydrophobic effects and contain a single component that is responsible for phase separation.[79-81]

1.6.1 Simple coacervation

Simple coacervation[82] is a liquid-liquid phase separation that results in a condensed droplet of a single macromolecule.

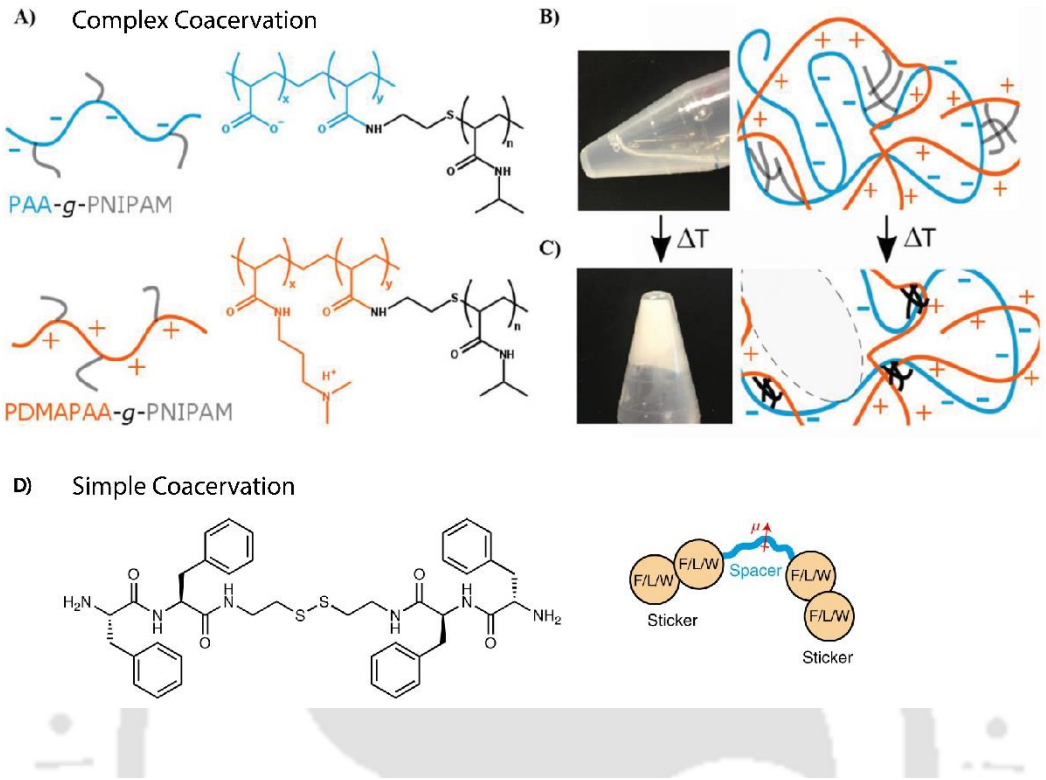

Figure 1.11 A) The complex coacervate phase's composition and temperature responsiveness. Molecular structures of PAA-g-PNIPAM and PDMAPAA-g-PNIPAM. B) Illustration and schematic of the complex coacervate structure below the LCST. C) Illustration and schematic representation of the solidification caused by increasing the temperature above the PNIPAM LCST, D) Structure of FFssFF and schematic illustration of a synthon motif consisting of two dipeptide stickers and a polar spacer. Figure reproduced with permission. [79, 93]

This is induced by changes in the polymer-solvent interactions as a result of factors including temperature, pH of the medium and solvent composition.[83] In simple coacervation process of gelatin, the liquid liquid phase separation happens through the intermolecular self charge neutralisation of the side chain amino acids of gelatin.[84]

Although coacervates derived from polyelectrolytes with the same charge should technically be categorised as 'simple' coacervates[85].Kitamoto et al. reported first time facile coacervate production from a single "natural" glycolipid biosurfactant.[86] Coacervation is difficult to achieve with a single peptide molecule and there are very few reports. Most recently, self-coacervation has been achieved using a short peptide synthon made up of only two dipeptide stickers joined by a disulphide linked hydrophilic spacer (Figure 1.11 D).[79]

1.6.2 Complex Coacervation

Complex coacervates are water-dispersed condensed droplets formed by the spontaneous liquid–liquid phase separation of two oppositely charged polyelectrolytes in aqueous solution.[87] Tiebackx initially

noticed the phenomena when he was studying the mixture of gum arabic (or acacia gum) with gelatin and discovered insoluble gelatin–gum arabic complexes.[88]The electrostatic interactions of oppositely charged macro-ions result in the release of tiny, bound counter-ions and the restructuring of water molecules, which drives the self-assembly of these materials.[75] Many studies have shown that oppositely charged polypeptides,[30, 89, 90]Peptide–Nucleotide,[91] protein-anionic polysacaride[92] can form complex coacervate through electrostatic attraction. A recent study found that electrostatic interaction between two oppositely charged polyelcectrolites can generate complex coacervate that is also thermoresponsive (Figure 1.11a-c).[93]

1.5.3 Covalently crosslinked coacervate

There are very few reports where along with noncovalent interaction covalent bond formation through imine bond formation or disulphide linkages also plays a vital role in the coacervate formation. Alsberg et al. discovered that complex coacervate microdroplets can form as a result of a Schiff base reaction between the aldehyde groups of oxidised sodium alginate and the amine groups of Gelatin-Methacrylate (GelMA)[94]. Miserez and co-workers reported a histidine-responsive beak peptide coupled with a disulphide link containing self-immolative moieties can generate a coacervate, which is self-destructive[95].

1.6.3 Transient coacervation

The ability of self-assembled structures in biological systems to adapt to changes in external conditions is one of the most interesting features of these structures. Incorporating similar capabilities into synthetic self-assembly holds a lot of promise for developing smart systems[96]. Membrane less organelles like coacervates are involved in many intracellular processes. However, the exact process of controlling the dynamic nature of the coacervates remains poorly understood. Boekhoven and co-workers reported transient coacervation based on complexation of RNA and apeptide molecule (Figure 1.12) where the activation step, EDC molecule converts the negatively charged aspartate to the corresponding anhydride and the deactivation step driven by spontaneous hydrolysis of the anhydride molecule[97]. Mixtures of Polylysine (PLL), ATP, and polysaccharide have been used to generate transient multiphase droplet organization.The lifetime of these multiphase coacervate droplets can be altered in response to GOx's catalytic activity in the presence of various amounts of glucose.[98] Chemical reaction network for reversible polyamine ionisation leading to transient coacervate micelle when polyamine mixed with polyanion where allyl acetate act as a activator and thiol or amine-functionalized small molecules act as a deactivator.[99]

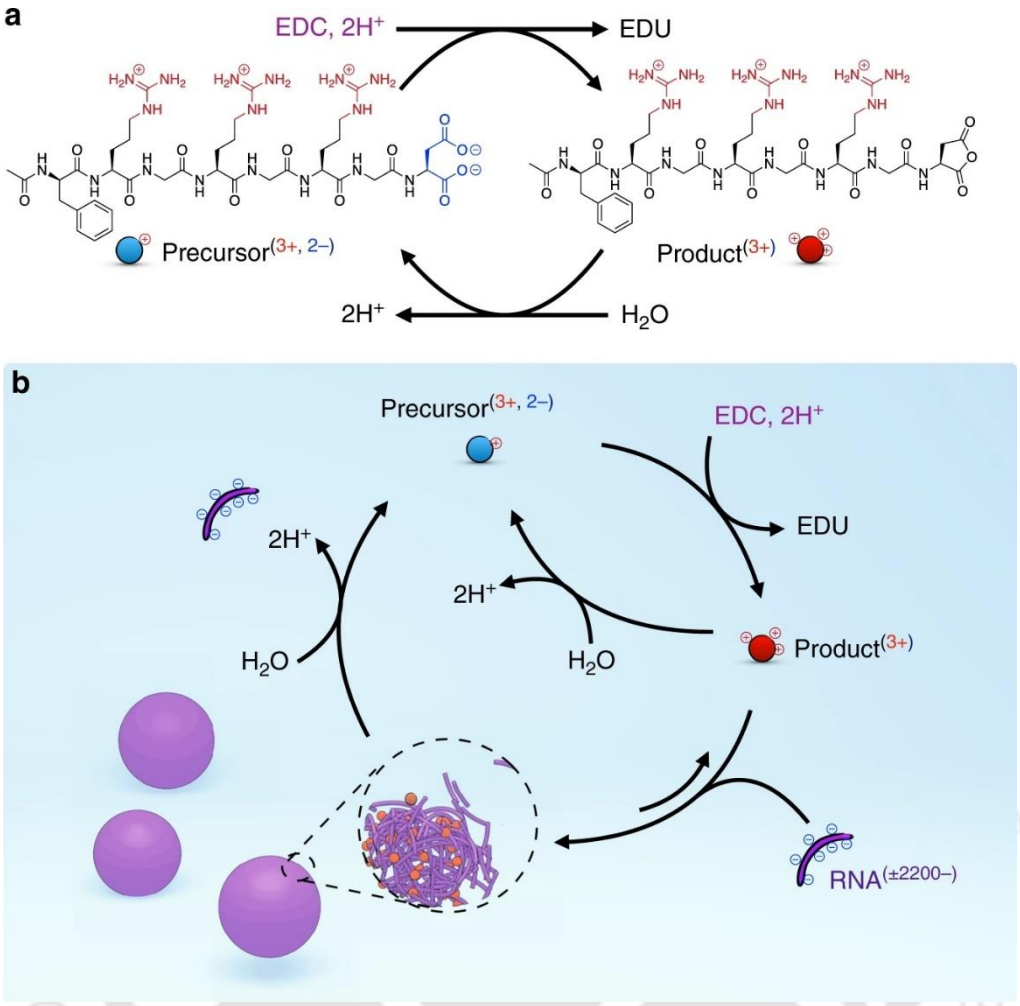

Figure 1.12 a) The chemical reaction cycle that converts a chemical fuel (EDC) into waste (EDU) while removing two negative charges on a peptide (precursor) resulting in a cationic transient anhydride (product). b) A schematic representation of the chemical reaction cycle combined with complex coacervation with RNA (poly-U). The influx and efflux of droplet materials are regulated by the chemical reaction cycle. Figure recreated with permission.[97]

1.7 Applications of Self-assembly

Peptides, which are found all over nature, are made up of a short chain of amino acids and have the ability to perform specific biological functions due to their highly ordered assembly structures[100]. Due to their tuneable mechanical stability, high biocompatibility, and excellent injectability, peptide-based hydrogels with a high amount of water inside their three-dimensional network have been used in a variety of prominent biomedical fields.All of the above characteristics provide extracellular matrix-mimicking environments for peptide-based hydrogels, opening up opportunities for biomedical applications in drug delivery[101], tissue engineering,[102, 103] wound healing[104, 105] and antitumor therapy.[106-108]

1.7.1 Hydrogels as an extracellular matrix for tissue engineering

As short peptide hydrogelators are soft in nature and contain a high amount of water, they can mimic the extracellular matrix in cell culture applications.Cell culture is a commonly employed in vitro approach for improving our understanding of cell biology, tissue architecture, and disease causes, as well as medication action, protein production, and tissue engineering application.

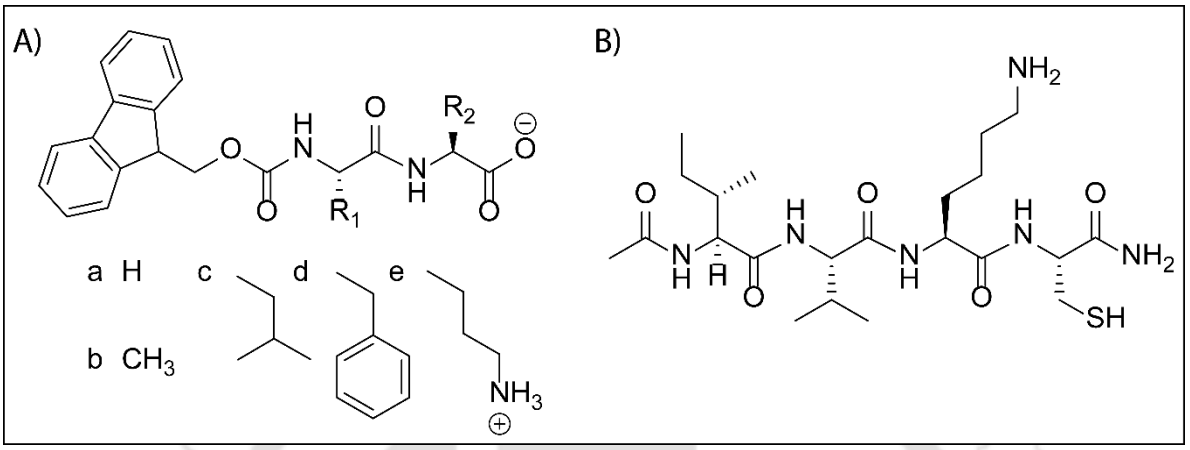

Figure 1.13 A) Molecular structure of Fmoc–dipeptides. The R groups are the amino acids Gly (a), Ala (b), Leu (c), Phe (d), and Lys (e). B) Chemical Structure of AcIVKC. Figure adapted with permission.[110]

The majority of cancer biology research is conducted in vitro utilizing two-dimensional (2-D) cell cultures which have been used since the early 1900s. 2-D cell culture, primarily involves cultures of cells on flat plastic dishes. 2D cultures, on the other hand, have several drawbacks, including disruption of interactions between the cellular and extracellular environments, changes in cell shape, polarity, and division mechanism. These drawbacks prompted the development of models that are better suited to simulate in vivo situations. Three-dimensional (3-d) culture is one such way where the cells are mixed with the hydrogel in particular proportion and the cell can proliferate inside the 3-d network of the hydrogel.[109] Ulijin et. Al. first report Fmoc protected dipeptide hydro-gelator used as a matrix for 3-D cell culture.[110]Under physiological conditions, peptides (Figure 1.13A) spontaneously assemble into fibrous hydrogels. The structural and physical properties of these gels were discovered to be determined by the sequence of the amino acid present in peptide building blocks. Whereas, Fmoc–dipeptide combinations were found to produce fibrous hydrogels capable of supporting chondrocyte cell culture in two and three dimensions.

The RADA16 peptide family is one of the most explored peptide hydrogels for 3-D nanofibrous scaffolds promoting cell differentiation. These ionic peptides can self-assemble into cross-linked network structures and create stable β-sheets, which could imitate the ECM of tissue cells.Through C-terminal functionalization of the RADA16 peptide (Figure 1.13A) with physiologically active peptide sequences,

three distinct peptide hydrogels were employed to produce a 3D cell environment for human adipose stem cells.[111]

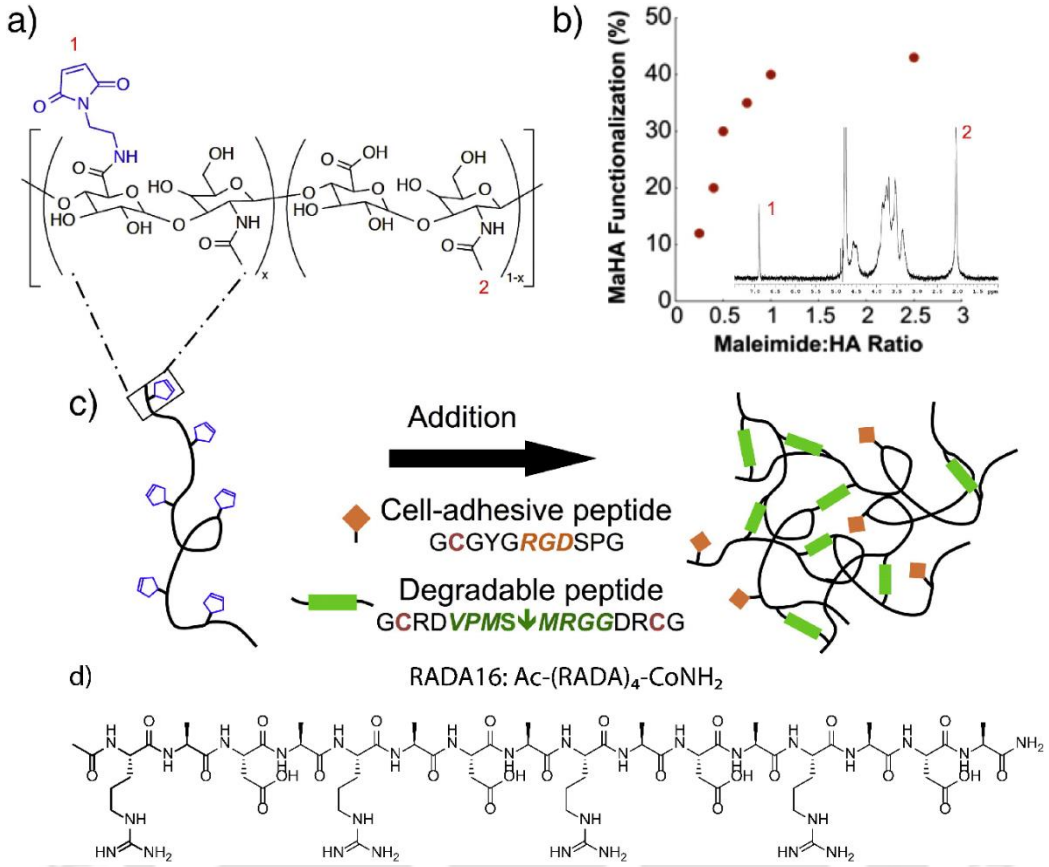

Figure 1.14 (a) Maleimide-functionalized hyaluronic acid (MaHA) and (b) MaHA functionalization with respect to maleimide to HA ratio during synthesis determined using 1H NMR (inset; numbered peaks are for 1: pendent acetyl protons on the HA backbone or 2: maleimide protons). (c) Cell-adhesive MaHA hydrogels were formed through an addition reaction between maleimides on MaHA and thiols on cysteine groups within cell-adhesive peptides (RGD, pendant) or MMP-sensitive peptides (VPMS↓MRGG, crosslinker). (d) Chemical structure of RADA16 peptide. Figure adapted with permission.[127]

Another study found that in the presence of H_2O_2, Ac-IVKC (Figure 1.13B), a short tetramer peptide, converted to (Ac-IVKC)2 dimers via disulphide bond formation, resulting in the spontaneous formation of a hydrogel with ahigh elastic modulus, which has never been seen in peptide-based hydrogels before. Various cells were seeded onto the hydrogel membrane, including primary human corneal stromal and epithelial cells, and the viability of the cells was demonstrated.[112]

1.7.2 Osteogenesis

Bone-engineered tissues have been developed as an alternative to autografts and allografts for the repair and reconstruction of bone defects throughout the last decade.Hydrogels offer great application possibilities as an articular cartilage repair material due to their similarities to the extracellular matrix, large adjustable range of water content, and good lubricity[113]. Conventional hydrogels are unsuitable for

use as biostructural materials due to their poor mechanical properties compared to biological soft tissues. Polymeric tough and robust hydrogels, on the other hand, appeal as next-generation structural biomaterials, particularly for the replacement of soft connective tissues like cartilage, tendons, and ligaments, due to their soft and wet nature and high mechanical strength achieved through toughening techniques.[114] The former technique has been used to create exceedingly homogeneous polymer networks (e.g., a tetra-PEG gel)[115] and a structure that averages the force by using slide-ring crosslinkers like a pulley.[116]The sacrificial bond principle, which is used in the latter technique, is characterized as "a weak and brittle structure introduced to a soft and flexible structure is preferentially fractured in a wide area and releases huge amounts of energy when deformed, resulting in toughening material." Hydrogels containing two interpenetrating polymer networks with differing physical properties, known as double network (DN) hydrogels, are a good example.[117] Numerous studies have shown that naturally occurring biomaterials such as gelatin,[118, 119] alginate[120], hyaluronic acid[29, 121, 122], chitosan[123], silk fibroin[124, 125] and combinations[126] of these biomaterials are highly helpful in bone cell regeneration. Holloway et al. developed a cell-interactive BMP-2 delivery device (Figure 1.14 a-c) with tunable degradation using a maleimide-hyaluronic acid hydrogel functionalized with both RGD and MMP-cleavable domains[127].It's attractive to drive osteogenic differentiation only through the scaffold, without the use of exogenous substances. In another report mineralization and osteogenic differentiation have been demonstrated to be aided by the inclusion of calcium phosphate or hydroxyapatite particles, or the production of a composite with these particles.[128]

1.7.3 Drug delivery vehicle

Because of the increased need for targeted controlled drug delivery (TCDD), amazing biomaterials with higher biocompatibility and biodegradability have been developed. Many drug delivery vehicles have been developed over the last few decades using a variety of materials, including synthetic polymers,[129] natural polymers,[130]and liposomes.[131] peptides,[132] metalloid nanotubes[133] and metal nanorods.[134] Small molecule drugs, proteins, and nucleic acids have all been successfully delivered using these drug carriers.[135, 136] Peptides are becoming increasingly significant in the field of drug administration because of their intrinsic biodegradability, biocompatibility, and ability to self-assemble into nanostructures.[137] In recent years, "Smart Polymers" have emerged as a possible candidate for controlled drug delivery, competing with established hydrogel systems.[138]Hydrogels have been widely investigated for the encapsulation and regulated release of medicinal drugs and proteins due to their highly hydrated and porous design. Small molecules and macromolecules can be modified with a variety of techniques that allow them to interact with pharmaceuticals via covalent or non-covalent connections. Using a low molecular weight gelator, there are three basic drug delivery techniques. The compound can be physically captured inside an inert gelator and then released from the gel via diffusion or gel

disintegration. 2) The drug can be covalently attached to a functional group, resulting in a prodrug that self-assembles and degrades slowly when exposed to enzymes. 3) A functionalized linker can be covalently attached to a therapeutic, and the amphiphilic prodrug can self-assemble after enzymatic cleavage of part of the linker.

Vegners[139] reported the first peptide-based drug delivery vehicle in 1995, where adamantanamine derivatives were encapsulated in Fmoc-Leu-Asp hydrogels and administered to rabbits; they were discovered to impact the rabbit's immune system. In another report Zhang and his colleagues utilized a long peptide (Acetyl-(Arg-Ala-Asp-Ala)$_4$–CONH$_2$) and conducted a dye release investigation.[140] Yang et al. discovered that glutathione promoted gelation of conjugated Folic acid-Taxol complexes (Figure 1.15) and sustained Taxol release via ester hydrolysis in another study.[141]

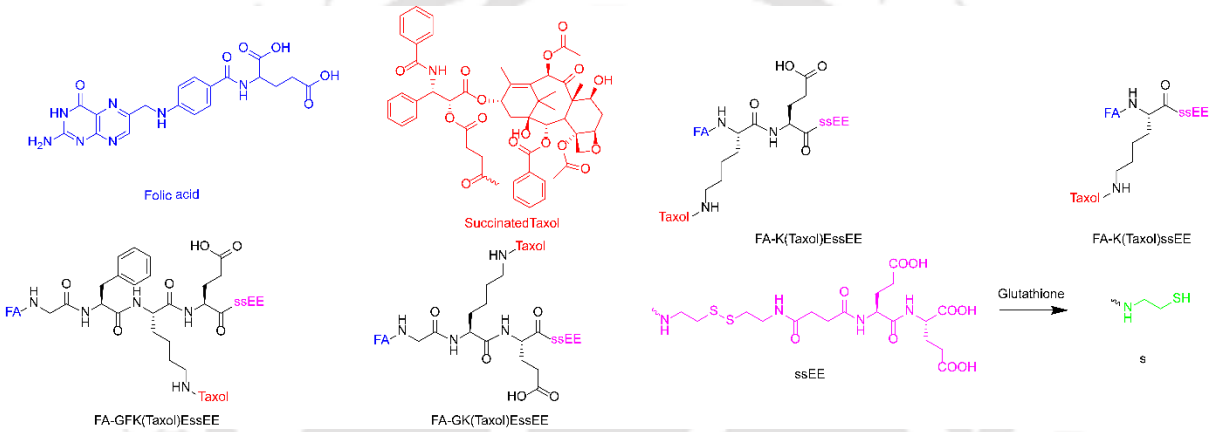

Figure 1.15 Chemical structures of all folic acid (FA)–Taxol conjugates used for GSH-triggered hydrogelations. Figure adapted with permission.[141]

1.8 The present thesis

In this thesis, we used short peptide amphiphiles, natural biopolymers, and synthetic polymers containing aldehyde to create several smart self-assembling systems. cysteine has been purposefully included in the peptide backbone to provide redox responsiveness to the self-assembled systems. Pyrene moiety was employed in two examples to add π–π staking and hydrophobicity into the self-assembly process. We have demonstrated different tissue engineering applications employing peptide and peptide-biopolymer based composite hydrogels. In the last two chapters, we used a cysteine-containing peptide and an aldehyde-functional polymer to make coacervates with multi-responsive characteristics. Finally, the dual responsive property of the coacervates was utilized to establish dual transience in the coacervate system.

Chapter 2

The hydrogelation of short peptides containing "Lys–Cys" (KC) residues at the C-terminus was investigated in the thisstudy. Two of the 12 peptides we investigatedwere capable of producing hydrogels, with the Cys residue dimerization controlling the aggregation process. NMR, CD, and rheological studies were used to investigate peptide aggregation, although the Ac-FFKC-NH_2 hydrogel was found to be stronger and more effective. Within the 3D matrix of the noncytotoxic Ac-FFKC-NH_2 hydrogel, both differentiated RAW macrophages and undifferentiated THP-1 monocytes were found to grow significantly.

Chapter 3

In this chapter, Pyrene-Lys-Cys (PyKC), a Pyrene-capped dipeptide, was employed as a doping agent with different biopolymers to generate four composite hydrogels. The addition of a very little amount of PyKC enhances the hydrogel's strength and provides thixotropic behaviour, according to the mechanical investigations. The Hyaluronic acid-PyKC composite hydrogels were discovered to be biocompatible and capable of supporting osteogenesis after MC_3 T_3-E1 osteoblast progenitor cells cultured on the materials demonstrated matrix calcification and osteogenic differentiation.

Chapter 4

Utilizing dynamic covalent chemistry, we generated coacervates using an aldehyde-containing polymer (Poly-CHO) and the PyKC dimer. The formation of imine and disulphide bonds promotes coacervation to happen. A detailed investigation was carried out to validate the coacervation. The coacervates can effectively entrap a variety of proteins and enzymes. The coacervates can also entrap the Peroxidase from horseradish (HRP) enzyme, protecting it from the H_2O_2 present in bulk solution.

Chapter 5

We demonstrated the coacervate's multiresponsive characteristic due to the presence of a dual dynamic bond. We used transient coacervation in a pH-dependent and redox-dependent way because of the dual responsiveness of the Coacervates. We used urea and urease as activators and Glucono delta-lactone (GdL) as deactivators for pH-dependent transient coacervation. The combination of H_2O_2 and TCEP was applied in the redox-responsivesive transient coacervation. The lifetime of the coacervates can be controlled by altering the activator-to-deactivator ratio.

Indian Institute of Technology Guwahati

Chapter 2: Effective Three-Dimensional Cell Proliferation Using a Smart Thixotropic Hydrogel Made of Disulphide Linked Short Peptides

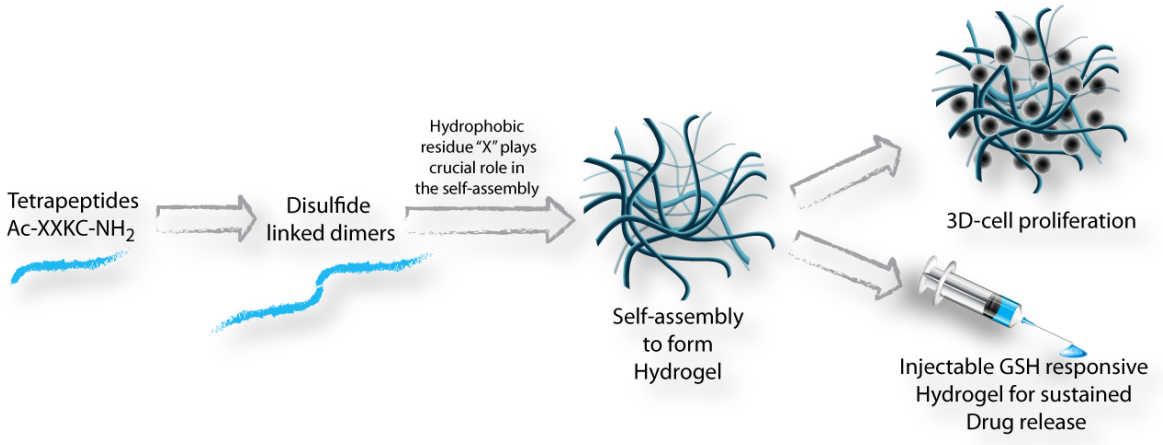

Indian Institute of Technology Guwahati

2.1 Introduction

Short peptide based self-assembled systems are receiving significant interest as biomaterials mainly because of their biocompatibility, stimuli responsiveness and bio-degradability.[142-145] These smart soft-materials have found applications in various fields including, drug delivery,[146, 147] matrix for cell-proliferation,[148, 149] protective storage of proteins,[150] sensor,[151, 152] nano-fabrication,[153-155] organic methodology[156, 157] organic electronics[158] to name a few. One of the most common outcome of the self-assembly of these short peptides is the formation of hydrogels.[159, 160] According to the need, with proper permutation and combination of the constituent amino acids, properties of these hydrogels can be altered. Moreover, introduction of stimuli-responsiveness can also be achieved easily through attachment of appropriate functional groups.[161-163]Disulphide linkage through Cysteine (Cys) residues of the sequence is one of the effective ways to incorporate stimuli responsiveness. Reducing agents like, glutathione (GSH), Tris(2-carboxyethyl) phosphine hydrochloride (TCEP) or Dithiothreitol (DTT) act as stimuli as they are capable of breaking the disulphide linkages and thereby disrupt the self-assemblies. Several disulphide-linked peptide hydrogels have been reported in the literature.[164-166] For example, Nilsson and group reported an11 amino acid peptide consisting of two Cys residues that cyclizes thorough intramolecular disulphide linkage and the cyclic form is unable to aggregate.[165] The aggregation and hence the hydrogelation is achieved through a reductive trigger that breaks the disulphide linkage to create the linear β-sheet forming peptide. Hauser et al. reported several such disulphide linked peptide hydrogels for various applications like, cell proliferation, tissue engineering, wound healing etc.[112, 167, 168] Recently, our group reported a tripeptide (Pyrene butyric acid functionalized Lys-Cys, PyKC), which forms disulphide linkage in neutral condition and self-assemble to form a hydrogel.[150] The hydrogel showed some unique properties like, insolubility in water. Additionally, it did not allow any exchange of solute and solvent to and from the hydrogel. This unique insolubility property was exploited to entrap and protect protein molecules from extreme conditions. In continuation with this work, we reported another peptide with the C-terminal "KC" sequence that forms a light sensitive hydrogel with water insoluble property like PyKC.[169] The hydrogel showed light triggered syneresis and used for efficient removal of organic contaminants from water. Interestingly, Hauser et al. on several occasions reported peptide hydrogels containing the C-terminal "KC" unit. One such peptide is Ac-IVKC-NH_2, which forms one of the strongest peptide based hydrogel (elastic modulus of ~0.9 MPa) reported so far.[112]

All these reports prompted us to explore the possibility of creating new smart soft-materials from short peptides containing "KC" sequence at the N-terminal. It is important to note that all these reported "KC" peptides bear a short hydrophobic sequence/group at the N-terminal. The "KC" unit is hydrophilic in nature and a hydrophobic group is needed to gain the appropriate hydrophobic-lipophilic balance

(HLB)[170] which allows the self-aggregation. We envisioned that a thorough screening of the N-terminal sequence with hydrophobic residues could be beneficial to understand the self-assembly behavior of the "KC" sequences. We have prepared two series of peptides with the general formulas, Ac-XXKC-NH_2 and H-XXKC-NH_2 (Scheme 2.1) where X stands for the hydrophobic amino acid residue (Gly, Ala, Val, Ile, Leu, Phe). The self-aggregation of these peptides in aqueous medium are thoroughly analyzed to find the effect of the N-terminal hydrophobic character on the self-assembly process. Among all these peptides, 11 and 12 could form stable hydrogels.

To this end, cell-based assays have become an essential requirement for drug discovery process providing simple, fast, and economic alternative to animal testing. The majority of cell-based assays traditionally use two-dimensional (2D) monolayer cells that are cultured on flat and rigid substrates.[171] However, 2D cell culture cannot effectively take into account the natural 3D environment of cells since all cells in the in vivo environment are embedded in the extracellular matrix (ECM) in a three-dimensional (3D) fashion and are surrounded by other cells. Thus, 3D cell culture systems is much preferred over the 2D culture systems.[172] In this context, development of artificial ECM emerged as an important field of research in recent years.[173, 174] Various approaches involving synthetic polymers and peptides have been examined for this purpose.[174-177] The three dimensional network created through self-assembly of peptide based soft-materials offers excellent support for cell proliferation and tissue growth.[177] In recent years, many such peptide-based soft-materials have been successfully utilized as a cell-proliferation platform.[178-182] However, in order to use these hydrogels as effective surface for cell-proliferation, the hydrogel needs to provide a network structure, should be non-toxic, and have an optimum rheological property.[172] In the present case, the hydrogel obtained from **12**proved to be an excellent platform for 3D cell-proliferation for RAW macrophages and THP-1 monocytes.

2.2 Results and discussion

As discussed in the introduction, our previous experiences with short peptides having C-terminal "KC" unit revealed that the presence of hydrophobic residues are essential for these peptides to self-assemble.[150, 169] In this work, first, we wanted to assess the role of different hydrophobic amino acids toward the self-assembly of these peptides. Two series of peptides (NH_2-XXKC-NH_2 and Ac-XXKC-NH_2, Scheme 2) are synthesized where X stands for natural hydrophobic amino acids. Both free (**1**-**6**) and N-acylated (**7**-**12**) sequences are prepared to compare the role of the N-terminal capping.

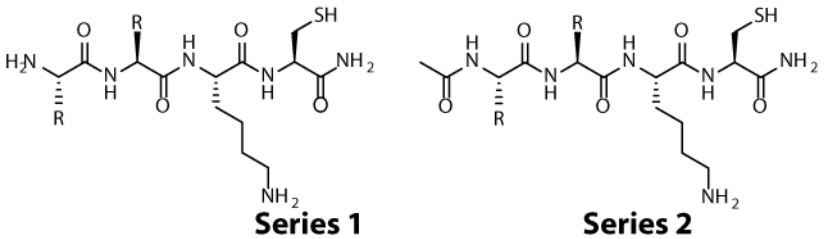

		Series 1	Series 2
		NH_2-XXKC-NH_2	Ac-XXKC-NH_2
R = H	X = G	**1**	**7**
CH_3	A	**2**	**8**
$CH(CH_3)CH_2CH_3$	I	**3**	**9**
$CH_2CH(CH_3)_2$	L	**4**	**10**
$CH(CH_3)_2$	V	**5**	**11**
CH_2Ph	F	**6**	**12**

Scheme 2.1 Chemical structures of the "KC" peptides used in this study.

Once the peptides are ready, their solubility in aqueous medium are tested. Except Ac-IIKC-NH_2 (**9**), all the other peptides are found to be soluble in water (solubility range: 15 mg/mL to hygroscopic, Table 2.1). However, none of them could form hydrogel in plain water even at a very high concentration. To test the hydrogel formation, all the soluble peptides are dissolved in different buffers (pH 1-11) at various concentrations. Various techniques like, incubation at room temperature (RT) for 24 h, sonication followed by incubation at RT or heating to 60 °C followed by incubation at RT are applied to form the hydrogels. However, only Ac-VVKC-NH_2 (11) and Ac-FFKC-NH_2 (12) could form self-supporting hydrogels when dissolved in buffers at and above pH 8 (Tris, Phosphate, carbonate/bicarbonate) and incubated at room temperature for several hours. For the present study, we have chosen 20 mM Tris buffer (pH 8) as the gelation medium. The time required to form hydrogel were 12 h and 2 h respectively for 11 and 12. Techniques like sonication and heating/cooling resulted in hydrogelation for these peptides. However, for all further studies we used the RT incubation method to prepare the hydrogels in Tris buffer (pH 8).

Though the acetylated peptides, 11 and 12 could form hydrogels, their non-acylated counterparts (5 and 6) failed to do so. This clearly shows that capping at the N-terminus of these peptides is necessary toward formation of the hydrogel. It is well-known that capping the peptide termini has a trivial impact on the overall charge distribution on the peptides that in turn significantly alter the aggregation pathway. [183, 184] It has been shown previously that neutralization of charged terminals of N- and C-termini capped peptides enhances the aggregation tendency and alter the morphoplogy.[185, 186] Notably, not all the acetylated peptides (7-12) are capable of hydrogelation. As mentioned earlier, in addition to other factors, peptides forming hydrogels need to have an optimum HLB.[187] Reports have shown the importance of the presence of hydrophobic amino acids in order to self-assemble to hydrogels and

influence of increasing hydrophobicity on the gelation kinetics and rheology.[188, 189] The hydrophobicity of an amino acid can be described through their hydropathy index (HI) values. The HI of the amino acids (X in the sequences) are shown in Table 2.1. It is understandable that the HI of Gly and Ala are too low to provide sufficient hydrophobic character to the sequences for self-aggregation. On the other extreme, the HI of Ile is too high and makes the sequence extremely hydrophobic and insoluble in water. The cases of Leu, Val and Phe do not really fall in line with hydrophobic character alone. The HI of Val is highest among these three and can be considered as the optimum hydrophobicity required for gelation. However, Leu has a much higher HI than Phe but peptide **10** failed to form hydrogel. This certainly indicates that though the hydrophobic side chains are important, some other parameters definitely playing the determining role.

Table 2.1 Various physicochemical parameters of **1-12** and the hydrogels of **11-12**

eptide Sequence (Number)	HI of X[190]	Solubility in water (mg/mL)	Solubilityin buffer[a] (mg/mL)	Sol/Gel[a]	MGC[a] (wt%)	Gelation Time (h)	T_g (°C)
NH_2-GGKC-$CONH_2$ (**1**)	-0.4	Hygroscopic	-	Sol	-	-	-
NH_2-AAKC-$CONH_2$(**2**)	1.8	Hygroscopic	-	Sol	-	-	-
NH_2-IIKC-$CONH_2$ (**3**)	4.5	15	0.5	Sol	-	-	-
NH_2-LLKC-$CONH_2$ (**4**)	3.8	150	10	Sol	-	-	-
NH_2-VVKC-$CONH_2$ (**5**)	4.2	300	18	Sol	-	-	-
NH_2-FFKC-$CONH_2$ (**6**)	2.8	200	14	Sol	-	-	-
Ac-GGKC-$CONH_2$ (**7**)	-0.4	Hygroscopic	-	Sol	-	-	-
Ac-AAKC-$CONH_2$ (**8**)	1.8	100	5	Sol	-	-	-
Ac-IIKC-$CONH_2$ (**9**)	4.5	Insoluble	Insoluble	Insoluble	-	-	-
Ac-LLKC-$CONH_2$ (**10**)	3.8	25	1.5	Sol	-	-	-
Ac-VVKC-$CONH_2$ (**11**)	4.2	100	9	Gel	0.5	12	61
Ac-FFKC-$CONH_2$ (**12**)	2.8	125	15	Gel	0.5	2	69

[a]In 20 mM Tris buffer at pH 8. [b] Minimum gelation concentration in 20 mM Tris buffer at pH **8.**

As mentioned in the introduction, we wanted to explore the possibility to utilize the hydrogels as an effective medium for 3D cell proliferation. For any application, it is extremely important to analyze the properties of the hydrogel as well as find the mechanistic detail behind the aggregation process. The hydrogels formed by 11 and 12 are thus investigated in detail. Since these gelators contain free thiol groups, in line with previous experiences,[112, 150, 169] it is expected that the gelator molecules form disulphide linked dimers during the gelation process and these dimers play crucial role in the aggregation. Hydrogels formed by 11 and 12 are analyzed by analytical HPLC, and only the peak corresponding to the disulphide-linked dimers are obtained (Figure 2.1). Moreover, when the gelation is tested for these two peptides in presence of GSH (glutathione, a well-known disulphide bond breaker), even at high concentrations of the gelators, no gelation is observed. A time dependent analyses of the gelation process shows that the dimerization completes within 12 h for 11 and 2 h for 12 which are

similar to the gelation time (Figure 2.1). These confirm the critical role of the dimers behind the aggregation process. Hydrogelation is also tested in presence of hydrogen peroxide (H_2O_2) to facilitate the dimerization process and indeed the time required to form the hydrogels are much lesser in presence of H_2O_2 (7 and 1 h for **11** and **12** respectively).

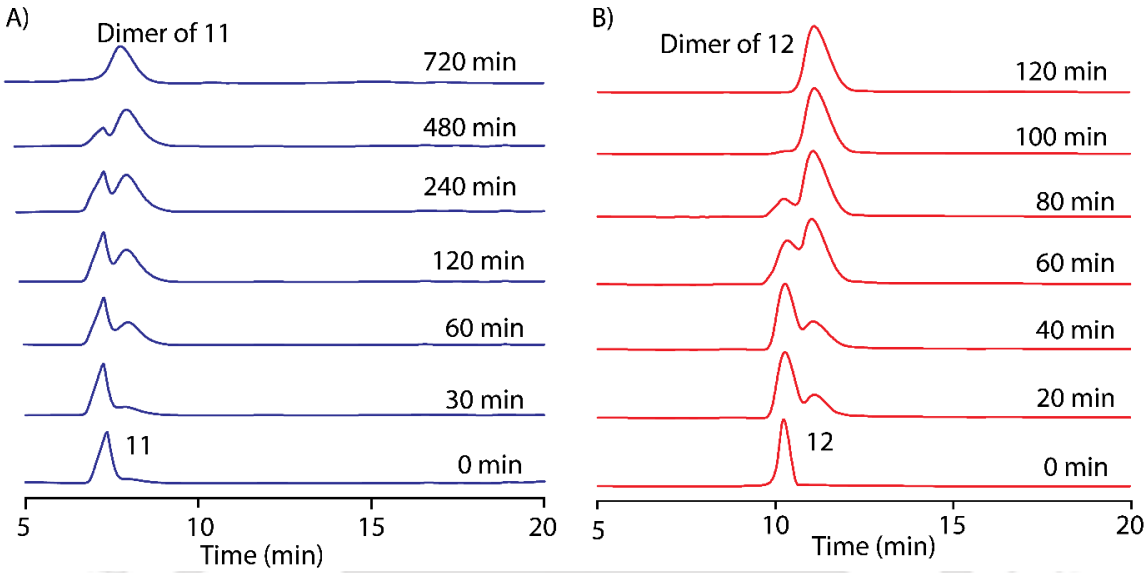

Figure 2.1. Time dependent dimerization profile of A)**11**and B)**12** obtained by analytical HPLC at room temperature in 20 mM Tris buffer.

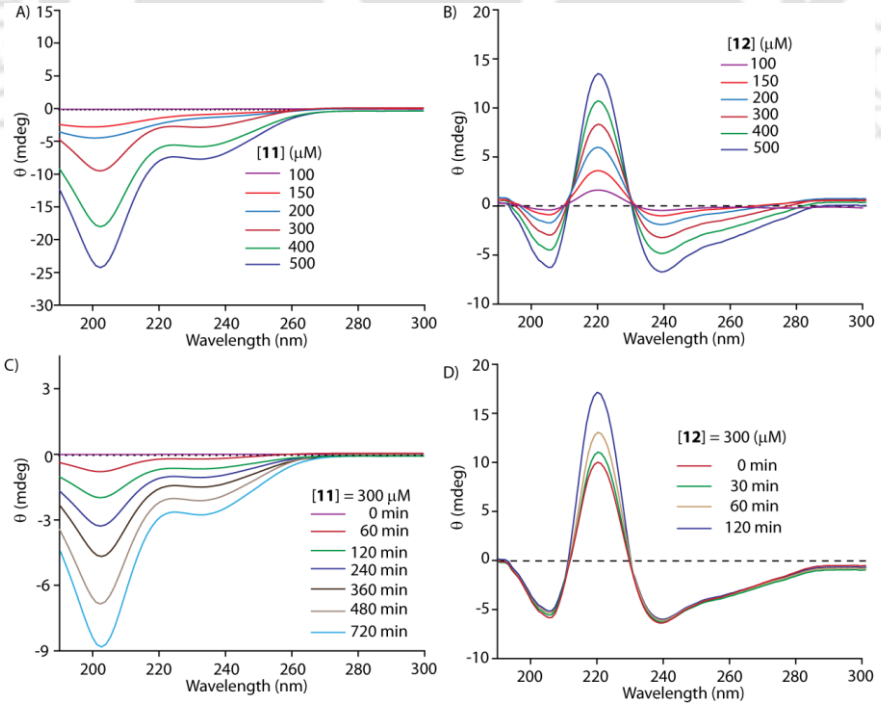

Figure 2.2A-B) Concentration dependent CD spectra of A) **11** and B) **12**. C-D) Time dependent changes in the CD spectra of C) **11** and D) **12** in Tris buffer. All the measurements are performed at room temperature.

In order to understand the situation, circular dichroism (CD) spectra of 11 and 12 are recorded with increasing concentrations of the gelators (Figure 2.2 and 2.3). To ensure complete dimerization, the stock solution is incubated at room temperature for 24 h prior to the experiments.

For 11, the system shows a negative peak at 205 nm suggesting random coil conformation at concentration below 300 μM. With further increase in concentration, above 300 μM, another negative peak appears at 235 nm. The CD pattern in this case is unusual as the peaks do not match with any typical secondary structures. One possibility is a helical structure consisting of turns through the disulphide linkages. However, detailed investigation is required to identify the exact situation which is beyond the scope of the present manuscript. On the other hand, peptide 12 shows two negative peaks at 205 nm and 240-270 nm (broad) along with a prominent positive cotton effect at 220 nm. The intensity of all these peaks increased with increase in concentration. In case of 12, a β-sheet arrangement peptide can be concluded from the CD spectra which matches with the previously reported examples containing FF residue and especially for FF nanotubes.[191-196] The broad peak in the aromatic region is due to the π–π* transitions of the phenyl groups. This near-UV CD signal is suggestive of a tertiary/higher-order structure around the aromatic groups.

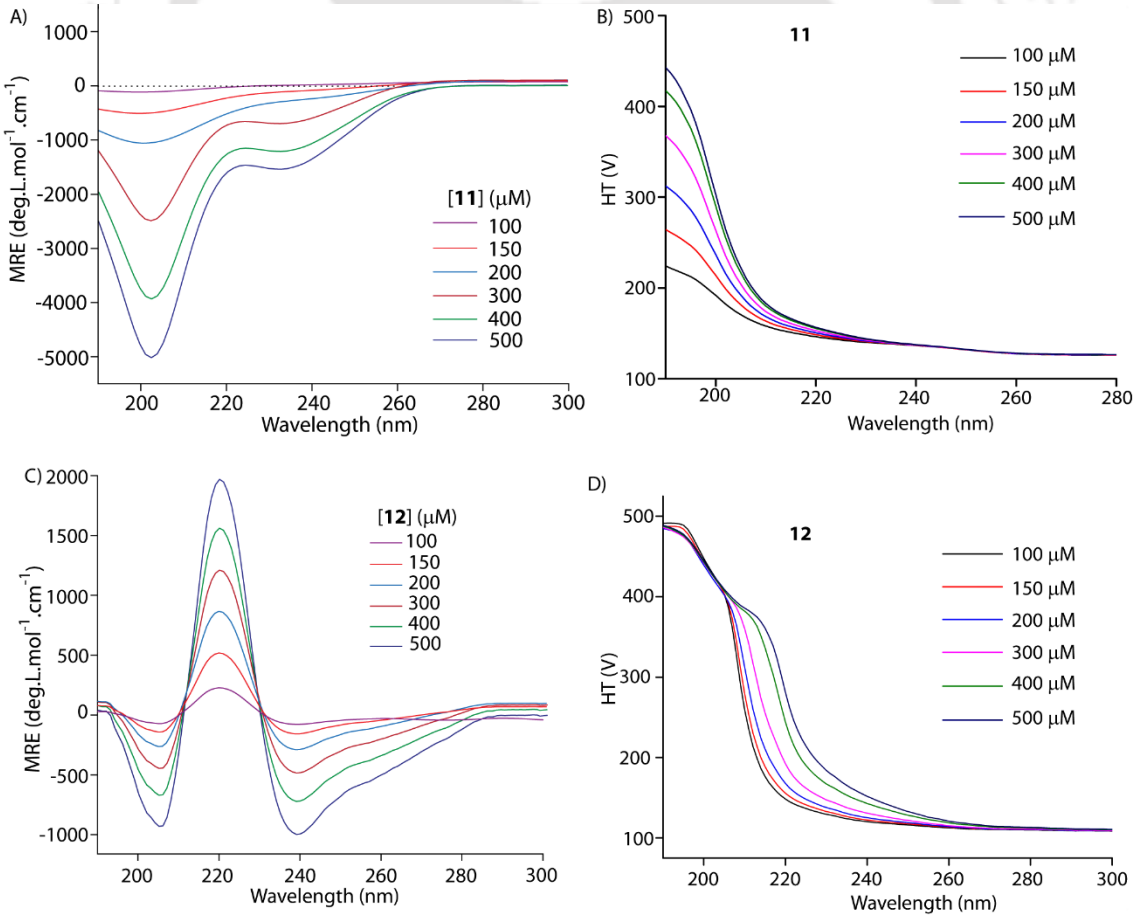

Figure 2.3 Mean Residual Ellipticity (MRE) plots andHT profiles of the CD spectra presented in Fig. 2.2A and B.

One interesting observation is the significant difference in the time required for completion of the dimerization processes in these two systems. Recently, we have shown the effect of molecular arrangement of two thiol molecules (in the aggregated state) on the disulphide formation possibility.[156] It was found that the thiols groups need to be in a very close proximity (~4 Å) in order to form the disulphide bonds. Following our previous report, energy minimized structures for two molecules of the same peptides are obtained using DFT calculation. It is observed that the distance between the thiol groups for two 12 molecules is 3.99 Å while the same for 11is 7.34 Å (Figure 2.4).

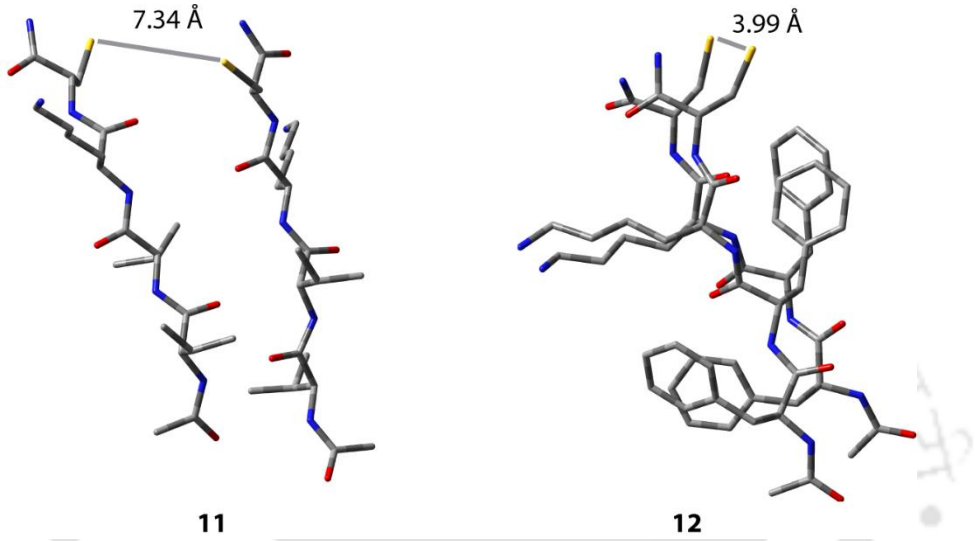

Figure 2.4 DFT calculations of compound **11** and **12**.

The closer proximity of the thiols in case of 12 explains the faster rate of dimerization. In order to examine further, a time dependent CD analyses is performed for both gelators. As can be seen from Figure 2.2 C, for 11, initially, the system remains CD inactive and measurable CD signals appear only after some time. With increase in time, the peak intensities enhanced and after 12 h no further change is observed. On the other hand, in case of 12 (Figure 2.2D) prominent CD signals are observed even at 0th minute. However, with further incubation, only the intensity corresponding to 220 nm peak enhanced while the other peaks remain unchanged. It is obvious from these observations that even in the monomeric state, at this concentration, 12 remain in lower order self-assembled state. However, as the molecules dimerize, higher order aggregates are formed leading to more intense peak.

Along with the hydrophobic interaction, hydrogen bonding also plays a crucial role in the self-aggregation processes. In the present cases, both the systems possess four amide N*H*s as well as two NH_2 groups, which can serve as hydrogen donors. On the other hand, there are four possible hydrogen bond acceptors (carbonyl oxygens) present in these peptides. To assess the role of hydrogen bonding in the self-assemblies, ^{1}H NMR studies are performed for these two gelators at MGC. The ^{1}H NMR spectra are recorded in DMSO-d_6 (the peptides do not aggregate in DMSO, see Figure 2.6 and the explanation

therein) with varying amounts of H_2O (Tris buffer (pH 8)). All the samples are incubated at room temperature for 24 h to ensure complete dimerization. In DMSO, both 11 and 12 failed to form any gel and thus it is assumed that the molecules are not in aggregated state in this solvent. As can be seen from Figure 2.5, in both cases, all the N*H*s and NH_2s show significant downfield shifts with increase in water content, which signifies the involvement of hydrogen bonding in the aggregation process.[197] Additionally, the aromatic protons from Phe residues of 12 showed moderate up-field shifts (~0.15 ppm) as the water content reaches 40%.[198] The shift of the aromatic

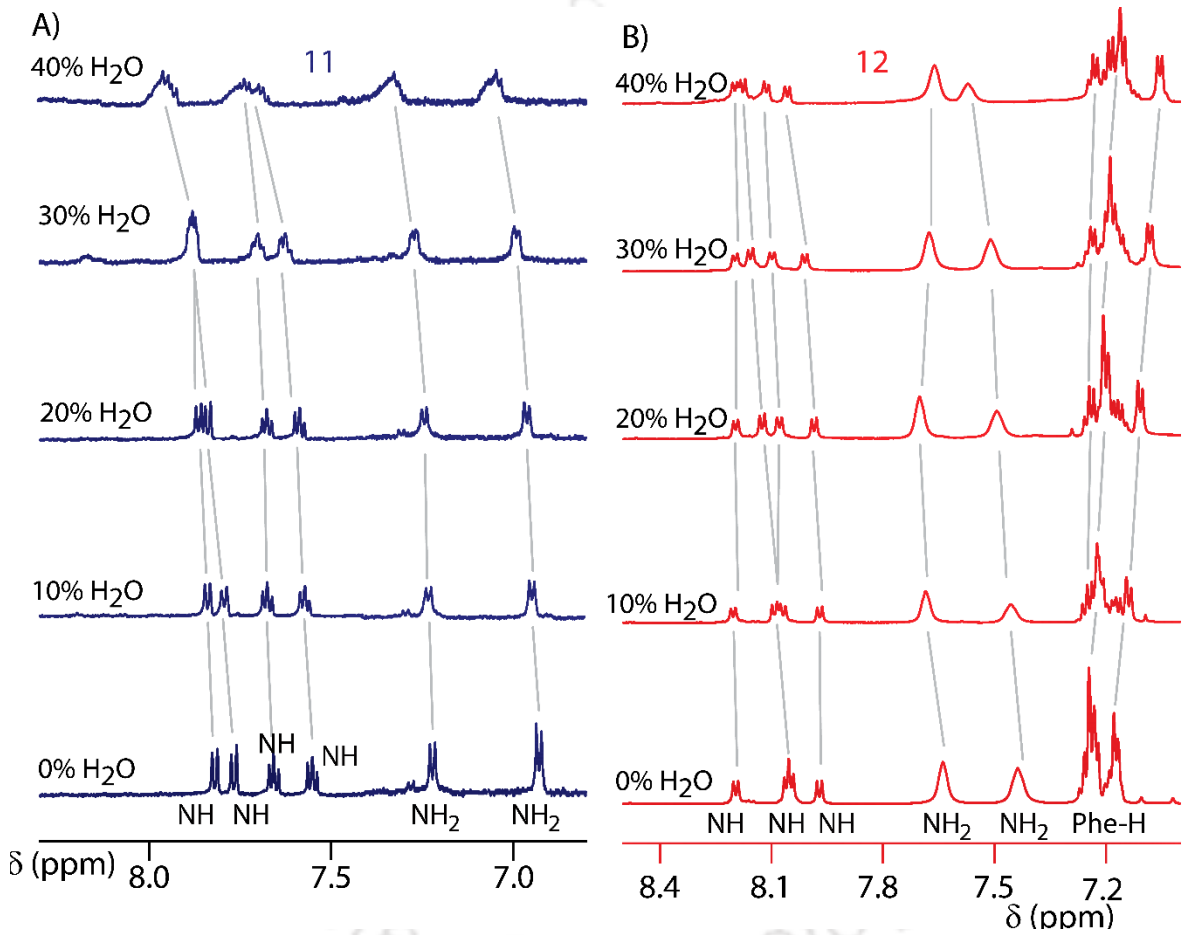

Figure 2.5 ^{1}H NMR spectra (aromatic region) of A) **11** and B) **12** in DMSO-d_6 with varying amount of H_2O showing the involvement of hydrogen bonding (**11** and **12**) and π–π stacking (**12**) in the aggregated state.

protons indicate possible π–π interactions between phenyl rings which is also observed from the CD spectra as discussed earlier. Moreover, a similar experiment monitored by the emission of the phenyl rings of 12 show a decrease in the emission intensity with increase in water content. This result additionally supports the involvement of the π–π interaction (Figure 2.7).

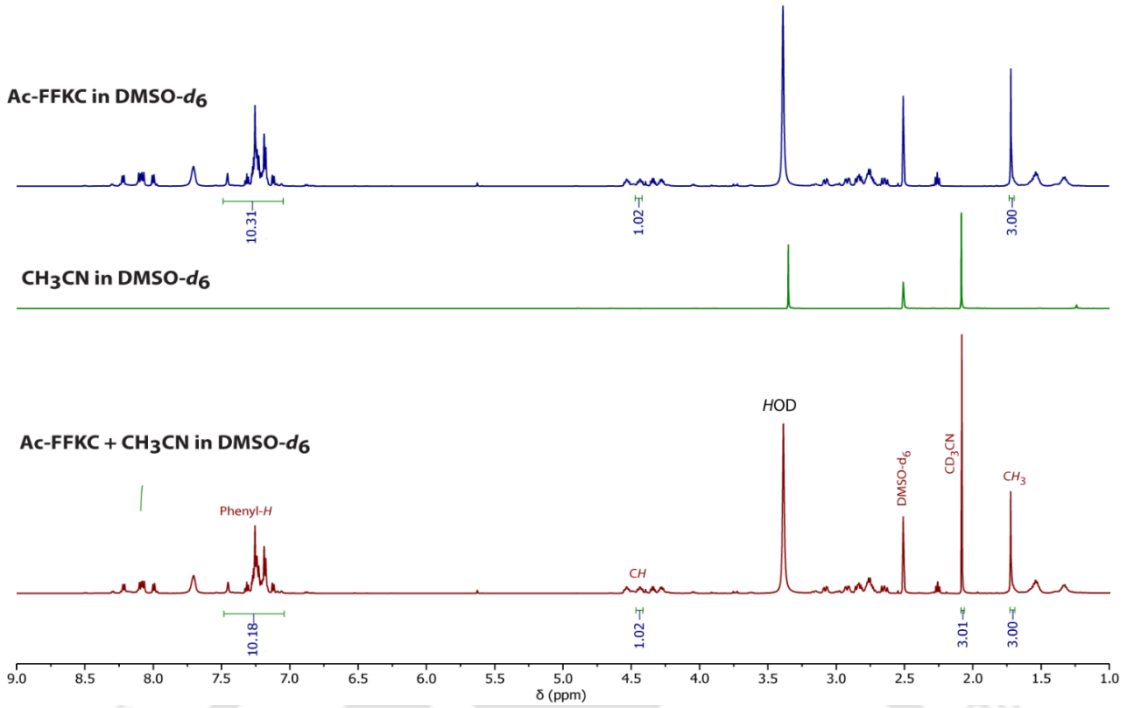

Figure 2.6 ^{1}H NMR spectra of **12**,acetonitrile and a 1:1 acetonitrile-**12** mixture in DMSO-d_6. As the integration for both acetonitrile protons and protons of **12** maintain the 1:1 ratio, it is concluded that the compound does not form aggregate in DMSO.

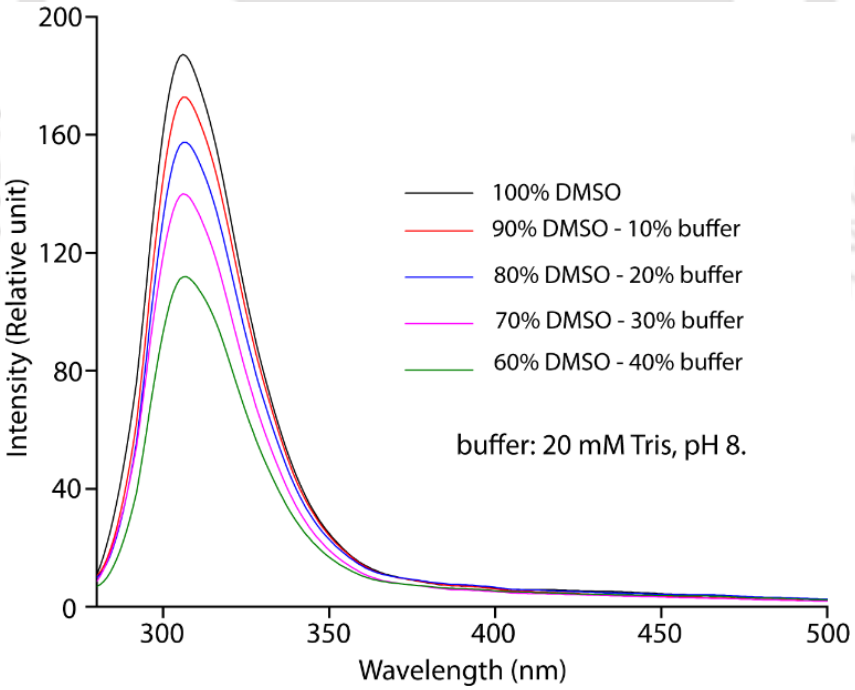

Figure 2.7Emission spectra of **12** in different compositions of DMSO and 20 mM Tris buffer pH8. All samples are 24 h matured and the experiments are carried out at RT (λ_{ex} = 265 nm).

The morphologies of the hydrogels formed by 11 and 12 are checked by FETEM and field emission scanning electron microscope FESEM. Both the hydrogels show network like structures. However, the

fibers are of different dimensions. Peptide 11 forms fibers of ~20 nm diameters and ~200 nm in length (Figure 4A, C). On the other hand, hydrogel of 12 consists of network of very long fibers (few μm) with ~ 50 nm diameter (Figure 4B, D). The hierarchical aggregation of the dimers of 11 and 12 lead to the formation of the fibers, which get cross-linked through supramolecular interactions forming the network structures. The water molecules are entrapped in these networks through cohesive forces. However, the presence of very long fibers suggests that the aggregation in case of 12 is much stronger than that in case of 11. It is important to note that the drying of hydrogels during sample preparation does affect the morphology as demonstrated by Adams et al.[199, 200] However, in the present case, additionally we checked the morphology of freeze-dried xerogels. Irrespective of the sample preparation method used, similar morphologies are obtained for both hydrogels.

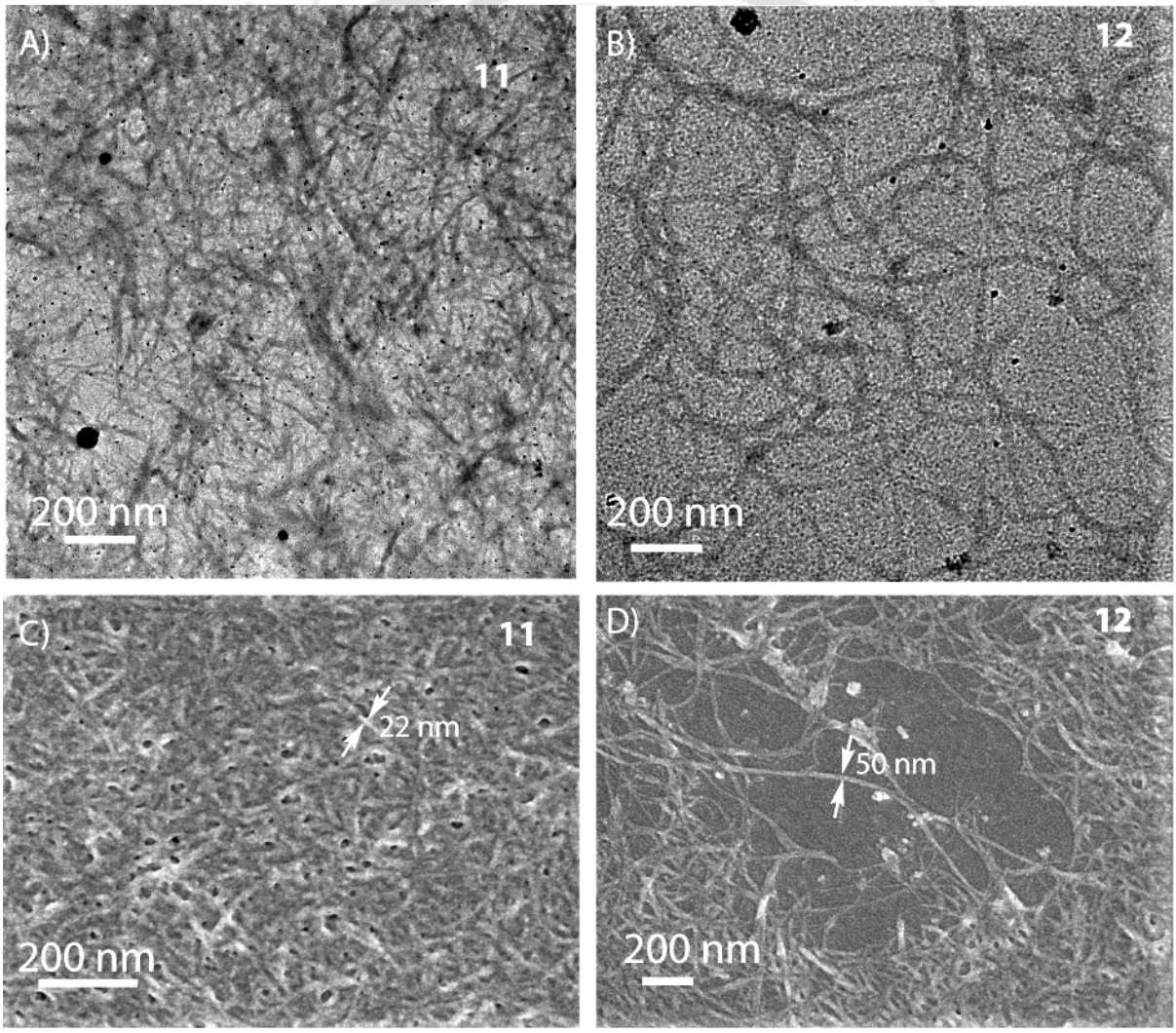

Figure 2.8 A-B) FETEM and C-D) FESEM images of hydrogels formed by **11** (A, C) and **12** (B, D) at MGC.

As mentioned in the introduction, the aim of this work is to explore the possibility of utilizing these hydrogels for 3D cell proliferation. In order to use a hydrogel for effective cell proliferation, it is

important to study its rheological behavior. A detailed study on the rheological properties of these hydrogels is carried out. Frequency and amplitude sweeps of the hydrogels prepared from 11 and 12 (2 wt%) are shown in Figure 2.8 A and B. In both cases, the storage modulus (G′) are found to be higher than that of the loss modulus (G″) which confirms the gel state of these two materials. However, the hydrogel from 12 is found to be much stronger in nature than 11 since both G′ and G″ values for 12 are higher than that of 11.[201] The amplitude sweep experiments also show that much higher strain is required for the hydrogel of 12 for gel-sol transition.

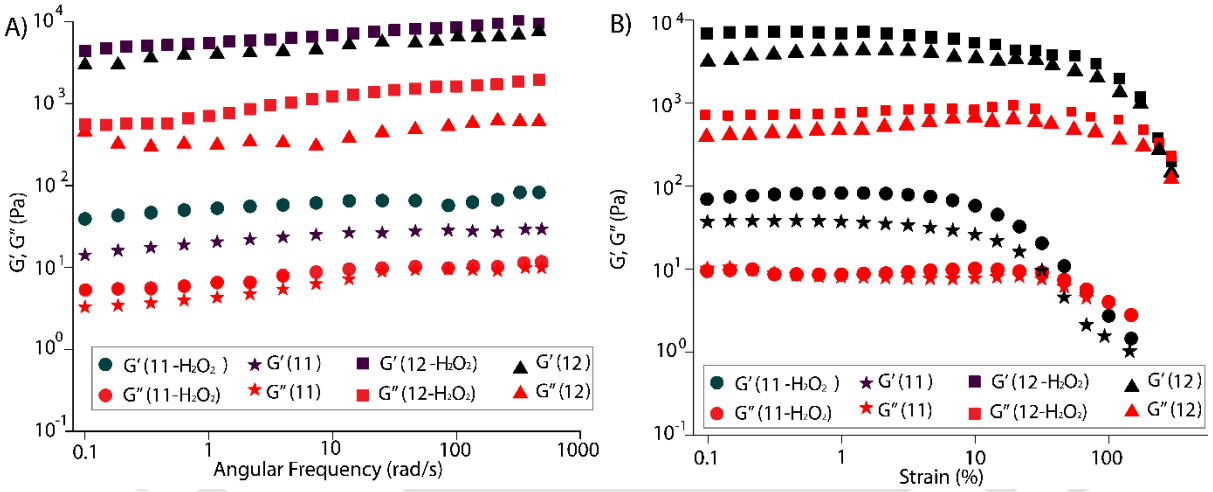

Figure 2.9 A) Frequency sweep and B) amplitude sweep profiles of hydrogels prepared by **11** and **12** at MGC in presence and absence of H_2O_2.

For disulphide linked gelation process, the presence of H_2O_2 not only facilitates the dimerization process but also produce stronger hydrogels.[112] In the present case, presence of H_2O_2 certainly expedites the dimerization of 11 and 12 as found from the HPLC analyses (Figure 2.1). To verify any effect on the gel-strength due to the presence of H_2O_2, rheological behavior of the hydrogels (24 h matured samples) prepared using H_2O_2 are determined. As can be seen from Figure 2.8 A and B, in both cases, no significant enhancement in the gel-strengths noticed. Please note that the hydrogels are made of disulphide-linked dimers of the gelators (11 and 12) and no cross-linking is possible. The presence of H_2O_2 could only make the oxidation process faster but the aggregation processes remain unchanged leading to similar gel-strength. However, it is also important to note that even though the gel strength does not change when the gels are prepared in presence of H_2O_2, the underlying structure could be different. To ensure that is not the case here, CD spectra are recorded in presence of H_2O_2 and compared to that obtained for samples without H_2O_2 (Figure 2.10). Interestingly, no reportable difference is observed clarifying that the presence of H_2O_2 only enhanced the disulphide bond formation rate without affecting the aggregation process.

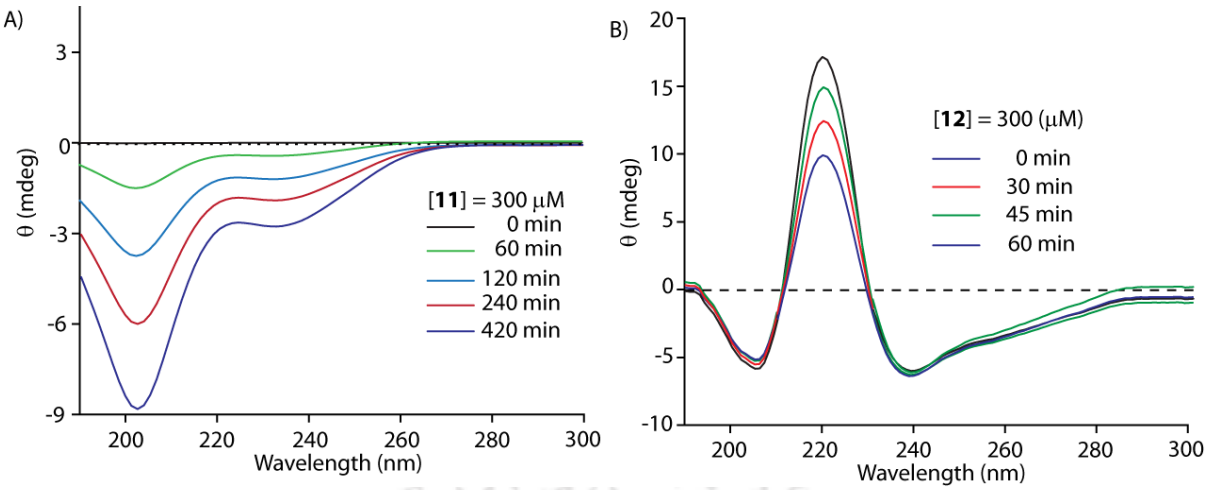

Figure 2.10Time dependent changes in the CD spectra of A) **11** and B) **12** in Tris buffer. All measurements are performed at room temperature.

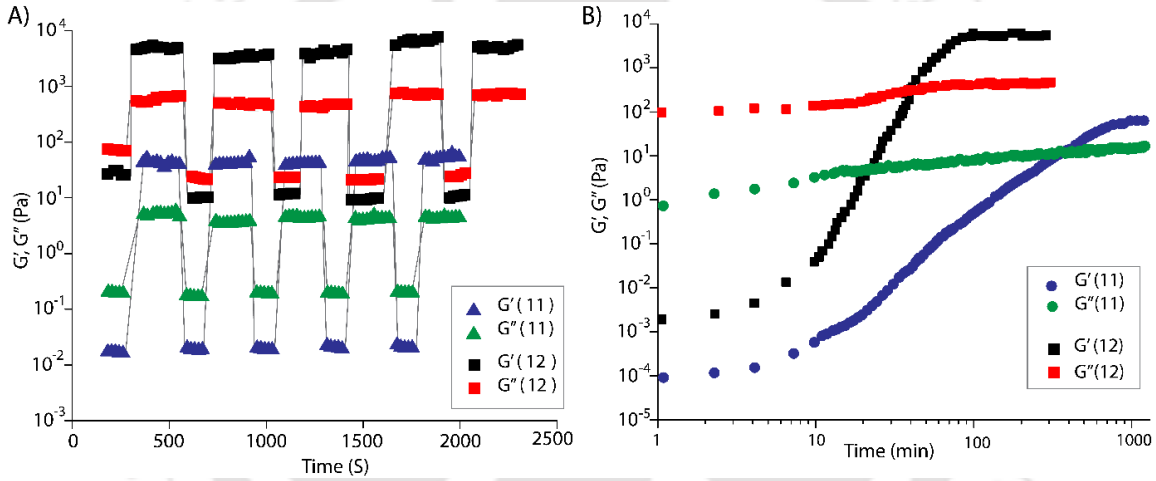

Figure 2.11 A) Time-dependent step-strain rheological data showing the thixotropic nature of hydrogels prepared by **11** and **12** (γ = 500 %). B) The gelation kinetics of hydrogels prepared by **11** and **12** as a function of time.

Thixotropy of hydrogels is an important property, which opens up the possibility to use these hydrogels for various applications including localized drug delivery and cell proliferation. For a regular gel, when a shear strain is applied, the G′ decreases and crosses the G″ and the gel turns into a sol but the G′ does not come back to its original value upon removal of the strain and the system remain as sol. However, in case of a thixotropic gel, as soon as the strain is removed, the system reverts to its initial rheological characteristics representing the gel state. In the present cases, both the hydrogels showed thixotropic nature.[202, 203]Figure 2.8 B shows that both hydrogels display a yield strain and transform to a quasi-liquid. These are the beginning of deformation of the gels, an essential character for thixotropic/injectable gels. Time dependent strain sweeps are performed at a fixed angular frequency of 1 rad s^{-1} and alternating the applied strains (Figure 2.12 A).

At a higher strain (γ = 500 % for Figure 2.10A), the gels lose their viscoelastic nature and regain it in every successive step while coming back to a lower strain. These experiments confirm that both the hydrogels are thixotropic in nature and can be used as injectable gels. Additionally, a set of experiments are performed where the hydrogels are prepared in syringes (in presence of RhB to make a colored gel) and then the pistons are pressed to liquefy the hydrogels. The liquids come out of the needle and immediately return back to their gel state (Figure 2.12 A-B). These simple experiments confirm the injectability of the hydrogels.

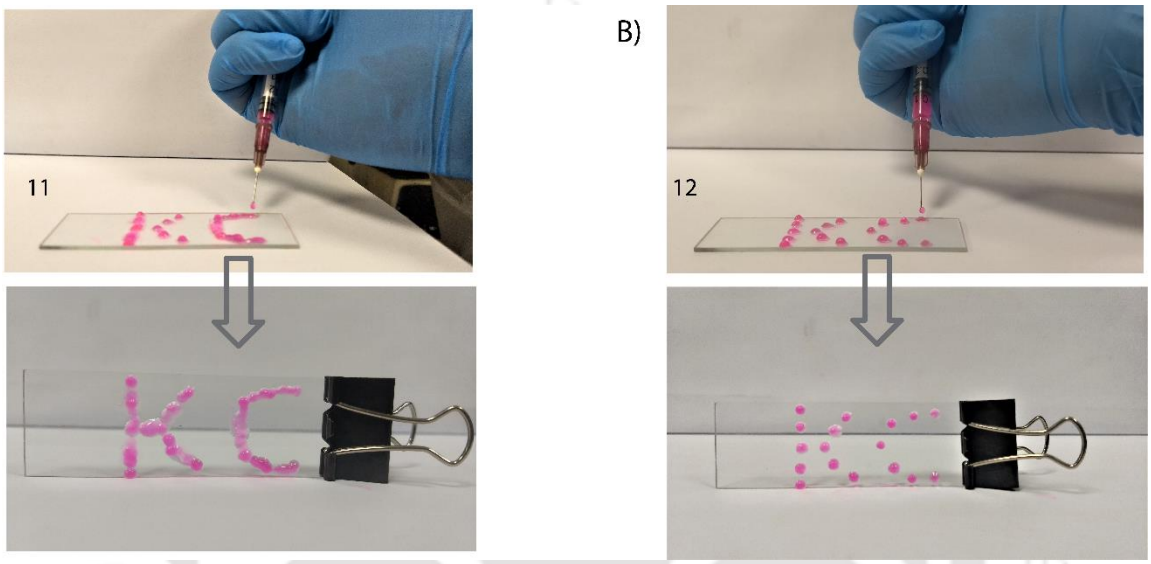

Figure 2.12A-B) Photographs showing the injectable property of the hydrogels formed by **11** (A) and **12** (B) at MGC. The hydrogels are prepared in presence of RhB in syringes and then drops of the hydrogel are injected on a glass slide to show that upon coming out of the needle, the solutions immediately return back to gel states.

Finally, time dependent rheology of the gels are recorded (Figure 2.10B). Initially, the G" values are found to be much higher indicating the sol state. However, the G' values continue to increase with time and at a certain point crosses the corresponding G" values. The crossover points are 422 and 42 minutes respectively for 11 and 12. The crossover points represent the sol to gel transitions. However, the equilibrium in the G' values are reached after 700 and 100 mins respectively. After that, no further change is observed. It is to be noted that the vial inversion tests to determine the gel formation as well as the time dependent dimerization studies also resulted similar time frame for self-sustained gel formation and complete dimerization respectively. These results indicate that the dimerization and the gel formation are complementary processes here. As the monomers get dimerized, the dimers start aggregating and after a particular time, the aggregation lead to a higher G' value than the G" indicating that the systems are no longer in sol state. However, after this crossover points, the dimerization

processes continue and so do the aggregation. Once all the monomers are converted to the dimers, the systems achieve their final self-sustaining gel state.

From the aforementioned studies, it is very clear that both the peptides (**11** and **12**) are efficient hydrogelators and in the gel state, they form nano-fribrous networks. Toward using any hydrogel for biological experiments, especially for cell-proliferation studies, the network structure is an essential criterion which allows the cells to adhere on the surface of the hydrogel and provide a template like extracellular matrix. However, the appropriate strength and elastic properties of the hydrogels are also crucial for this kind of application. An optimum strength of the hydrogel is required for the proper proliferation of the cells. In the present study, the hydrogel prepared from **12** showed much better properties than that of the hydrogel of **11** and thus we have chosen the hydrogel of **12** for all further experiments.

The gel to sol transition in response to a stimulus is an important parameter for any soft-material in order to find a suitable application. Since the hydrogels formed by these two short peptides are governed by disulphide-linked dimerization of the peptides, it is likely that these hydrogels can also be responsive toward disulphide bond breaking agents like GSH, DTT or TCEP. When a small portion of aqueous solutions of these reagents placed on top of the hydrogel, it transformed into sol. Though the experiment performed are qualitative in nature, it is very clear that the hydrogels responds strongly to these disulphide bond breaking agents. Among all these agents, GSH is abundant in biological systems and thus, we performed a quantitative analysis with GSH. Typically, 200 μL hydrogel of **12** at MGC is prepared in several glass vials. On top of them, 100 μL of 5 mM GSH solutions are placed. At different time intervals, one sample from each of the hydrogels are taken out and the hydrogels were dissolved in water. These aqueous solutions are then analyzed using analytical HPLC to find out the extent of dimer to monomer conversion. The % monomer are plotted against time and are shown in Figure 2.12 A. Full conversion takes place in ~ 21 h.

Since the hydrogels are thixotropic and responsive to GSH, we envisioned that the hydrogel of 12 could be a very good candidate for localized drug delivery vehicle. To verify the possibility, a model dye, RhB, is entrapped in the hydrogel and the gel is dipped into water and aqueous soultions of GSH (0.1-1 mM). The release profiles of RhB is shown in Figure 2.13 B. In water, the dye release is observed to be extremely slow as only 6 % of the dye is released from the hydrogel in 7 days. On the other hand, the rate of release increases with increase in the GSH concentration. The % release did not improve much when 0.01 mM GSH is applied (~11%). However, with increase in concentration of GSH, the release enhanced significantly. For 0.1 and 1 mM GSH, the overall release after 7 days are observed to be 23 and 57% respectively. As GSH breaks the disulphide bond of the gelator dimers, the self-assembly get disturbed and the entrapped dye gets released. With increase in concentration of the GSH in the

surrounding enhances the rate of the disulphide bond breaking and thus higher release rate is observed with higher GSH concentration. Though very preliminary, these results suggest that the hydrogel holds promise as localized delivery system where the cargo can be unloaded in response to the local GSH around the site of injection.

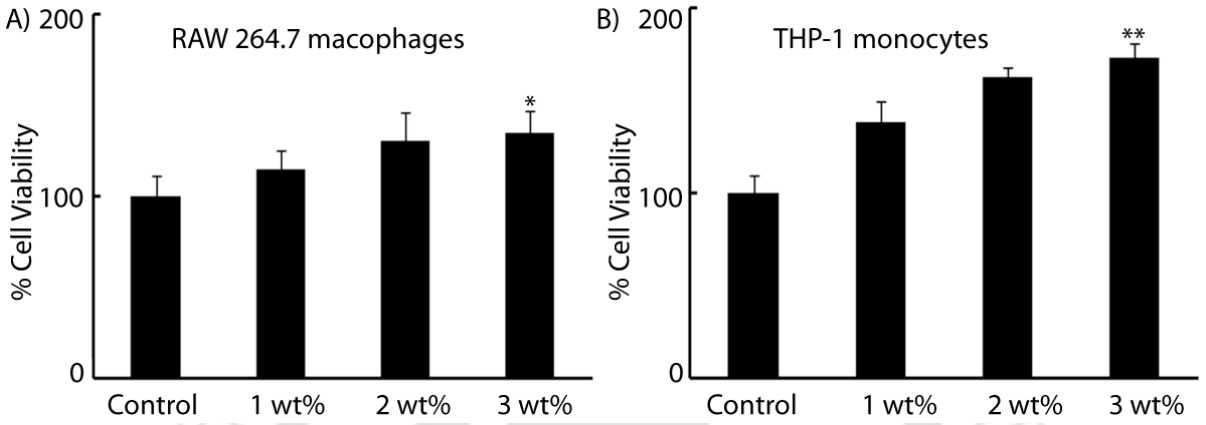

Figure 2.13A) GSH induced dimer to monomer formation in the hydrogel formed by **12**. B) Release profile of RhB from 1wt% hydrogel of **12** in response to different concentration of GSH. All experiments are performed in triplicate and at RT.

We wanted to investigate the biocompatible nature of the hydrogel by encapsulating the immune cells within the 3D environment of the peptide hydrogels. We chose two cell types: undifferentiated human THP-1 monocytes and relatively more differentiated RAW 264.7 mousemacrophages. Different concentrations of the peptide 12 (1, 2 and 3 wt%) are analyzed for cell cytotoxicity against both RAW macrophages (A) and THP-1 monocytes (B) after 24 h using MTT reagent. There has been a significant increase in cell viability when cells are incubated with 3 wt% concentrations of 12 ($p < 0.05$ and $p < 0.01$ for RAW and THP-1 cells respectively), within 3-D peptide hydrogels compared to 2-D cultured cells (Figure 2.14).

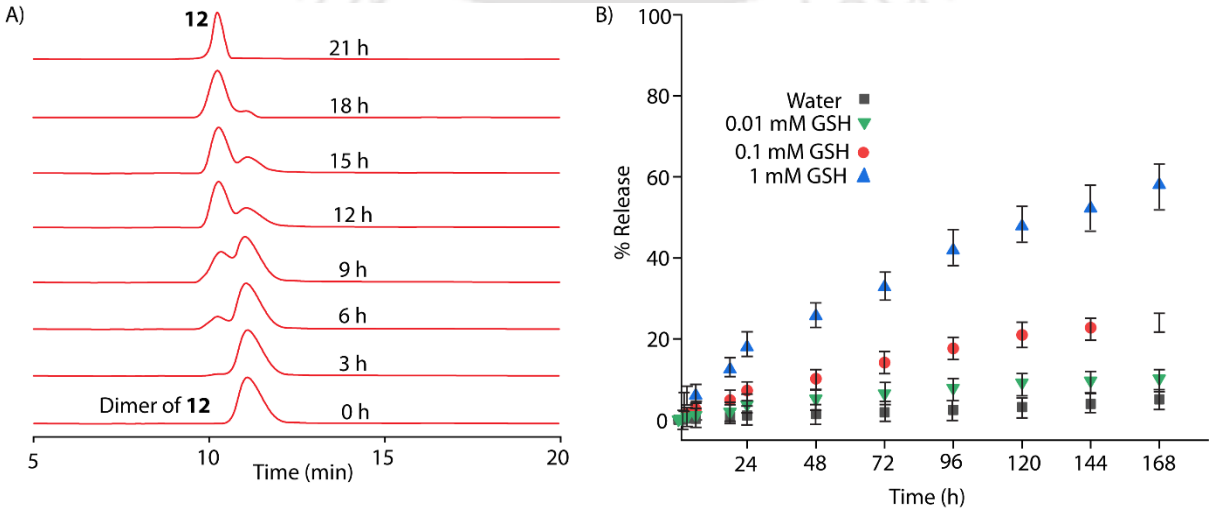

Figure 2.14Cytotoxic activity of different concentration of **12** against (A) RAW 264.7 macrophage (B) THP-1 monocytic cells. Cells are incubated within different concentration of **12** for 24 hrs. The cytotoxic effects are measured by MTT cell viability assay. 2-D cultured cells without peptide encapsulation served as control. The results are representative of means ± SD of three independent experiments. *$p < 0.05$, **$p < 0.01$ versus control, Student t test.

The cytotoxicity of peptide 12 is further assessed by confocal microscopy using Calcein AM and Propidium iodide (PI) for imaging of live and dead cells respectively in 3D cell-gel constructs. Microscopic images corroborated with cell viability results showing similar observations with no detrimental effect of 12 on overall cell survival rates (Figure 2.15). Taken together, these results suggest the biocompatible and non-toxic nature of the peptide, as both macrophages and monocytes survived within the encapsulation of hydrogel matrix.

The peptide hydrogel mimics the structure of ECM and macrophages actively associate with the ECM facilitating their integration in engineered tissues. The 3-Dimensional cell culture scaffolds play an important role in affecting cell behavior and proliferation. Therefore, we sought to find out whether the hydrogel of 12 support proliferation of macrophages and monocytes within the embedded structure. Cells are incubated with different concentrations of peptide (1, 2 and 3wt%) and cell proliferation was measured after 24, 48 and 72 hours using CyQUANT cell proliferation assay kit. As observed up to 72 hours, these hydrogels are stable and did not d egrade in cell culture media. After 24 hours of incubation, significant change in cell proliferation is observed in the hydrogel-encapsulated cells as compared to 2-D cultured cells ($p < 0.05$). After 48 hours, cellular proliferation of RAW macrophages and THP-1 monocytic cells present within encapsulation increased by 27.5 ± 4.1% (for 3 wt%) and 40.6 ± 6.1% (for 3 wt%) respectively, compared to 2-D cultured cells at 48 hour of incubation ($p < 0.01$).

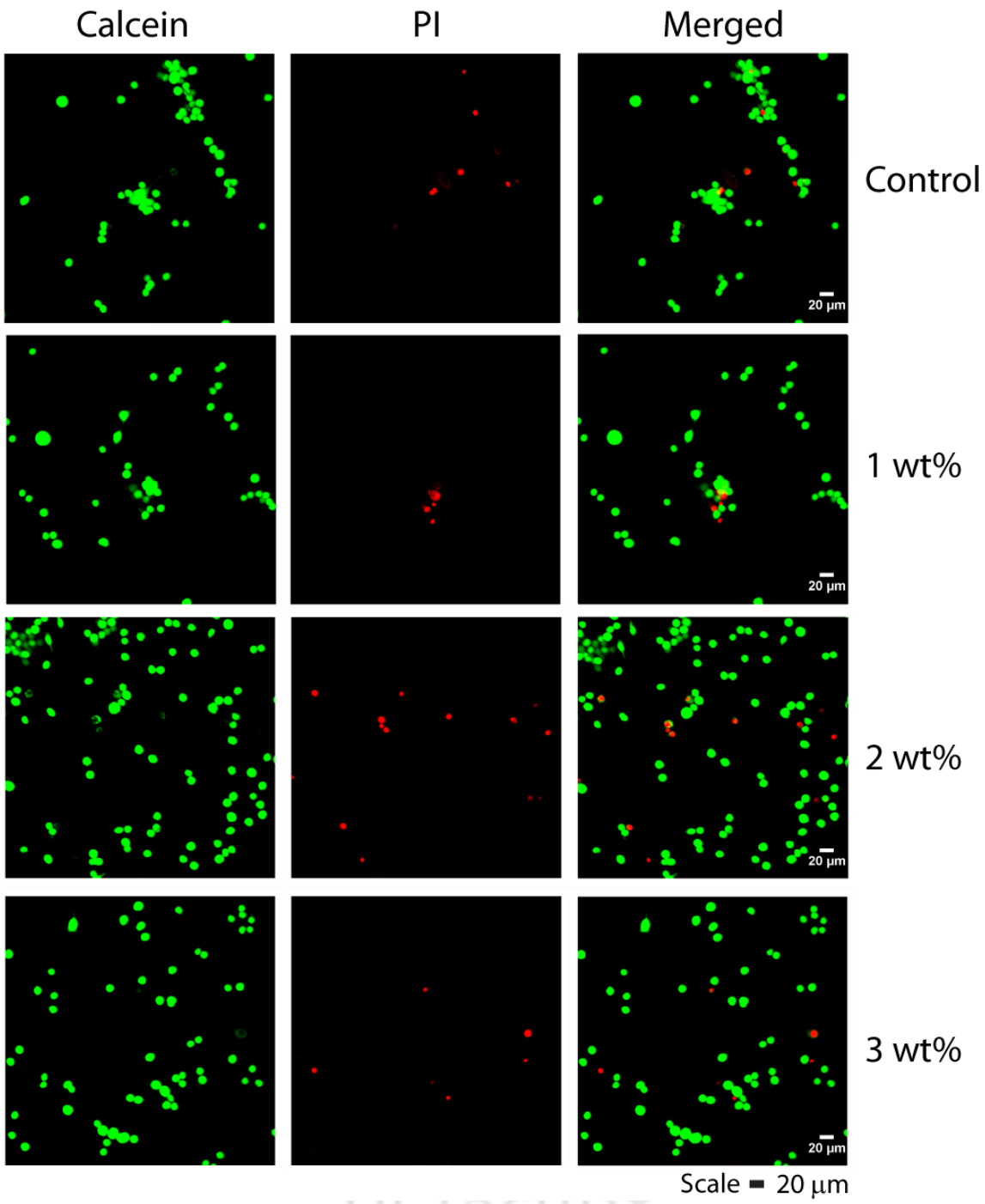

Figure 2.15 Microscopic analysis of viability of RAW 264.7 macrophages within different concentration of hydrogel of **12** by Live and Dead cell staining. Cells are incubated within different concentration of the peptide for 24 hrs. 2-D cultured cells without peptide encapsulation served as control. Green fluoroscence indicates live cells and red fluoroscence indicates dead cells. Scale bar: 20µm.

After 72 hours of incubation cellular proliferation increased by 47.1 ± 6.9% (for 3 wt%) and 43.9 ± 6.4% (for 3 wt%) respectively for RAW macrophages and THP-1 monocytes within peptide hydrogels compared to 2-D cultured cells after 72 hours ($p < 0.001$). Different concentrations of peptide did not hamper cell proliferation but aided the proliferation rates of both macrophages and monocytes (Figure

2.16 and Table 2.2). This result suggests that cells can proliferate more rapidly within these peptide matrices as a mode of 3-D cell multiplication compared to 2-D mode of cell proliferation.

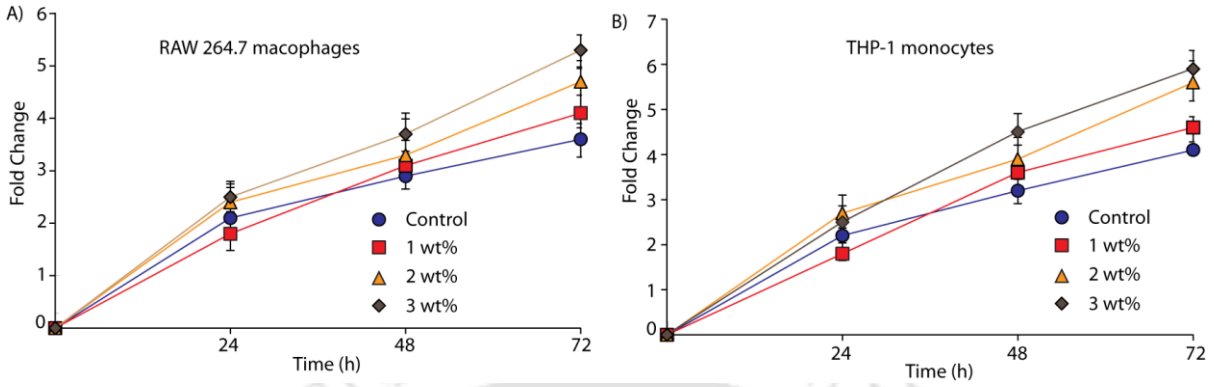

Figure 2.16 Cell Proliferation of macrophages without or within peptide encapsulation. Raw 264.7 macrophage (A) and THP-1 monocytic cells (B) are incubated within different concentration of **12** and proliferation is evaluated after 24, 48 and 72 h of incubation. 2-D cultured cells without peptide encapsulation served as control. The proliferation is evaluated using CyQUANT reagent and fluorescence intensity is measured on a microplate reader. Values are calculated as the fold change of proliferating cells. Mean values ± S.D.

Table 2.2 Fluorescence measurements to evaluate cell proliferation without or within hydrogel encapsulation after 24, 48 and 72h of incubation.

Treatments	Incubation Period											
	0 h			24 h			48 h			72 h		
Control (RAW cells)	30	32.3	31.6	62	66	73.3	100.6	91.6	81	125.3	112	103.6
Control (THP1 cells)	31.6	33.6	35.3	65.3	74.6	81.6	119.3	108.3	94.6	151	135.6	129
1 wt% (RAW cells)	28	34.3	32.6	63	55.6	53.3	97.6	107.3	89	143.3	129	120.3
1 wt% (THP1 cells)	31.3	34	27.6	61.6	58.3	51	118	112	101.3	149	143	132.6
2 wt% (RAW cells)	33.3	36.6	39	97.6	86	83.6	131.6	119.3	112	162	170.3	186
2 wt% (THP1 cells)	39	38.6	35	112.6	100.3	94.6	161	146.6	135	192	212	226.3
3 wt% (RAW cells)	32.6	37	33.3	75	85.6	93.3	117	125.3	140.6	169	180.6	195.3
3 wt% (THP1 cells)	35.6	37.3	32.6	96.6	87	80.6	140.3	159.6	164.6	223.3	207	194.3

2.3 Conclusion

In summary, a detailed and systematic analyses is reported to identify the role of N-terminal capping and hydrophobic residues of tetrapeptides containing C-terminal "KC" unit. Both Ac-VVKC-NH_2 and Ac-FFKC-NH_2could form self-supporting hydrogels and the dimerization of the peptides plays controlling role toward the hydrogelation. Both the hydrogels are found to be thixotropic and responsive toward GSH. A GSH mediated model-drug release study show that the hydrogel of Ac-FFKC-NH_2 have potential to be used as injectable localized drug delivery vehicle. The 3-dimensional matrix is found to

be non-toxic and effective for 3D cell proliferation for RAW macrophages and THP-1 monocytes. Overall, the hydrogel of Ac-FFKC-NH_2 shows high potential as an effective biomaterial for further use.

2.4 Experimental section

2.4.1 General information and materials

All the Fmoc-protected amino acids, HBTU, HOBT are acquired from from GL Biochem, China. Triethylsilane (TES), Trifluoroacetic acid (TFA), N,N-Diisopropylethylamine (DIPEA), Rhodamine B (RhB) and all solvents are purchased from Spectrochem (India). Milli-Q water with a conductivity of less than 2$\mu Scm^{-1}$is used for all sample preparations. Electrospray ionization mass spectrometry (ESI-MS) are performed with a Q-Tof-Micro Quadrupole mass spectrometer (Micromass) and data are analyzed using the built-in software).

2.4.2 Syntheses of peptides (1-12)

The peptides are synthesized using solid phase peptide synthesis (SPPS) technique. Standard Fmoc-protected amino acids and Rink-amide MBHA (4-(2′,4′-Dimethoxyphenyl-Fmoc-aminmethyl)-phenoxyacetamido-methylbenzhydryl amine) resin are used for the syntheses. Typically, 4 equiv. (with respect to the resin loading capacity) of the protected amino acid, 4 equiv. of HBTU, 4 equiv. of HOBT and 8 equiv. of DIPEA are pre-mixed in dimethyl formamide (DMF) and added to the resin. The coupling is continued for 1 h and the resins are thoroughly washed. The Fmoc-deprotection is achieved using 20% piperidine-DMF mixture and after washing the resin, the next amino acid is coupled following the above protocol. Once the sequences are complete, the resins are washed thoroughly and dried under reduced pressure. The cleavage of the peptides are done by shaking the resin with 95% TFA in dichloromethane (DCM) containing 1% TES for 1 h. The resins are then filtered and washed with DCM and the filtrates are reduced in volume under reduced pressure. The crude peptides are precipitated from dry cold ether, filtered and lyophilized. The pure peptides are then obtained by semi-preparative HPLC purification.

Characterisation of the peptides

Peptide 1

^{1}H NMR (600 MHz, Deuterium Oxide) δ (ppm) = 4.42 (dd, J = 7.7, 5.3 Hz, 1H), 4.29 (dd, J = 8.4, 5.9 Hz, 1H), 3.97 (d, J = 4.5 Hz, 2H), 3.82 (s, 2H), 2.92 (t, J = 7.5 Hz, 3H), 2.83 (dd, J = 14.2, 7.7 Hz, 1H), 1.79 (tt, J = 6.5, 2.7 Hz, 1H), 1.72 (dd, J = 9.4, 4.9 Hz, 1H), 1.67 – 1.58 (m, 2H), 1.39 (dddt, J = 16.3, 8.3, 6.3, 2.6 Hz, 2H). ^{13}C NMR (151 MHz, Deuterium Oxide) δ(ppm) = 174.09, 173.96, 171.16, 167.67, 163.16, 162.92, 65.97, 55.35, 53.68, 42.04, 40.28, 39.09, 30.25, 26.19, 25.10, 21.95, 21.93. ESI-MS (m/z):calculated 361.181for $C_{13}H_{27}N_6O_4S^+$ $[M+H]^+$found, 363.182. **HPLC:R_T = 3.59 min.**

Peptide 2

^{1}H NMR (600 MHz, Deuterium Oxide) δ(ppm) = 4.47 – 4.41 (m, 1H), 4.32 – 4.23 (m, 2H), 4.03 (q, J = 7.1 Hz, 1H), 2.94 (t, J = 7.5 Hz, 2H), 2.86 (qd, J = 14.2, 6.3 Hz, 2H), 1.84 – 1.70 (m, 2H), 1.64 (p, J = 7.7 Hz, 2H), 1.48 (d, J = 7.1 Hz, 3H), 1.41 (dt, J = 16.1, 8.3 Hz, 2H), 1.34 (d, J = 7.2 Hz, 3H). ^{13}C NMR (151 MHz, Deuterium Oxide) δ(ppm) = 174.77, 173.98, 173.68, 170.51, 55.18, 53.61, 49.47, 48.73, 39.10, 30.19, 26.21, 25.22, 21.95, 16.45. ESI-MS (m/z): calculated, 391.212for $C_{15}H_{31}N_6O_4S^+$ [M+H]$^+$; found, 391.211.**HPLC:R_T = 4.14 min.**

Peptide 3

^{1}H NMR (600 MHz, Deuterium Oxide) δ(ppm) = 4.45 (dd, J = 7.2, 5.5 Hz, 1H), 4.32 (dd, J = 8.1, 6.4 Hz, 1H), 4.18 (d, J = 8.7 Hz, 1H), 3.86 (d, J = 6.0 Hz, 1H), 2.94 (t, J = 7.7 Hz, 2H), 2.87 (qd, J = 14.2, 6.4 Hz, 2H), 1.92 (dd, J = 6.6, 3.3 Hz, 1H), 1.84 – 1.76 (m, 2H), 1.76 – 1.69 (m, 1H), 1.65 (p, J = 7.6 Hz, 2H), 1.51 – 1.32 (m, 5H), 1.20 – 1.12 (m, 2H), 0.94 (d, J = 6.9 Hz, 3H), 0.91 – 0.85 (m, 6H), 0.83 (t, J = 7.4 Hz, 3H). ^{13}C NMR (151 MHz, Deuterium Oxide) δ(ppm) = 173.93, 173.23, 172.80, 169.17, 58.16, 57.34, 55.27, 53.37, 39.03, 36.39, 35.86, 30.32, 30.16, 26.24, 25.19, 24.53, 23.95, 21.96, 14.51, 13.99, 10.38, 9.84. ESI-MS (m/z):calculated, 475.306 for $C_{21}H_{43}N_6O_4S^+$ [M+H]$^+$; found, 475.301.**HPLC:R_T = 8.15 min.**

Peptide 4

^{1}H NMR (400 MHz, Deuterium Oxide) δ(ppm) = 4.48 (dd, J = 7.1, 5.5 Hz, 1H), 4.42 (t, J = 7.3 Hz, 1H), 4.33 (dd, J = 8.1, 6.4 Hz, 1H), 3.98 (t, J = 7.2 Hz, 1H), 3.02 – 2.86 (m, 4H), 1.89 – 1.54 (m, 11H), 1.49 – 1.35 (m, 2H), 0.98 – 0.86 (m, 12H). **^{13}C NMR** (151 MHz, Deuterium Oxide) δ(ppm) = 173.96, 173.86, 173.36, 170.18, 55.17, 53.49, 52.31, 51.57, 39.83, 39.72, 39.07, 30.17, 26.24, 25.25, 24.21, 23.73, 21.94, 21.78, 21.60, 21.12, 21.06. **ESI-MS (m/z):** calculated, 475.306 for $C_{21}H_{43}N_6O_4S^+$ [M+H]$^+$; found, 475.300. **HPLC:R_T = 5.64 min.**

Peptide 5

^{1}H NMR (400 MHz, Deuterium Oxide) δ(ppm) = 4.48 (dd, J = 7.1, 5.5 Hz, 1H), 4.36 (t, J = 2.1 Hz, 1H), 4.21 – 4.10 (m, 1H), 3.86 (d, J = 6.1 Hz, 1H), 3.06 – 2.79 (m, 4H), 2.20 (d, J = 6.7 Hz, 1H), 2.04 (d, J = 6.7 Hz, 1H), 1.92 – 1.61 (m, 4H), 1.55 – 1.33 (m, 2H), 1.06 – 0.87 (m, 12H). **^{13}C NMR** (151 MHz, Deuterium Oxide) δ(ppm) = 172.84, 169.24, 162.86, 59.54, 58.16, 55.28, 53.41, 39.07, 30.33, 30.05, 26.23, 25.19, 21.97, 18.35, 18.27, 17.88, 17.56, 16.87, 16.84. **ESI-MS (m/z):** calculated, 447.275for $C_{19}H_{38}N_6O_4S$; found, 447.276 for [M+H]$^+$, 893.544.**HPLC:R_T = 6.82 min.**

Peptide 6

^{1}H NMR (600 MHz, D_2O) δ(ppm) = 7.37 – 7.23 (m, 6H), 7.23 – 7.11 (m, 4H), 4.57 (dt, J = 14.4, 7.2 Hz, 1H), 4.35 (dd, J = 7.0, 5.5 Hz, 1H), 4.20 (t, J = 7.4 Hz, 2H), 3.21 – 3.10 (m, 2H), 2.98 (d, J = 7.9 Hz, 1H), 2.91 (s, 2H), 2.90 – 2.81 (m, 2H), 1.77 – 1.57 (m, 4H), 1.33 (td, J = 17.0, 8.8 Hz, 2H). **^{13}C NMR** (151 MHz, D_2O) δ(ppm) = 173.94, 135.74, 133.46, 129.31, 129.10, 129.05, 128.72, 127.92, 127.18, 55.28, 54.75, 53.98, 53.25, 39.05, 37.21, 36.72, 30.56, 26.32, 25.11, 21.86. **ESI-MS (m/z):** calculated, 543.275for $C_{27}H_{38}N_6O_4S$; found, 543.270.**HPLC:R_T = 7.34 min.**

Peptide 7

^{1}H NMR (600 MHz, D_2O) δ(ppm) = 4.42 (dd, J = 7.8, 5.1 Hz, 1H), 4.30 (dd, J = 9.0, 5.5 Hz, 1H), 3.89 (d, J = 11.1 Hz, 4H), 2.92 (dt, J = 15.9, 6.4 Hz, 4H), 2.84 (dd, J = 14.2, 7.8 Hz, 1H), 2.01 (s, 3H), 1.86 – 1.78 (m, 1H), 1.73 (dq, J = 9.6, 4.6 Hz, 1H), 1.66 – 1.59 (m, 2H), 1.45 – 1.32 (m, 3H). **^{13}C NMR** (151 MHz, D_2O) δ(ppm) = 175.04, 174.16, 173.97, 172.44, 171.65, 65.99, 55.42, 53.58, 42.55, 42.35, 39.11, 30.12, 26.13, 25.08, 21.93, 21.68, 14.03. **ESI-MS (m/z):** calculated, 405.191 for $C_{15}H_{29}N_6O_5S^+$ [M+H]$^+$; found, 405.192. **HPLC:R_T = 3.52 min.**

Peptide 8

^{1}H NMR (600 MHz, D_2O) δ(ppm) = 4.43 (dd, J = 7.3, 5.4 Hz, 1H), 4.27 – 4.21 (m, 2H), 4.19 (q, J = 7.3 Hz, 1H), 2.94 (t, J = 7.5 Hz, 2H), 2.87 (qd, J = 14.2, 6.4 Hz, 2H), 1.95 (s, 3H), 1.80 (dd, J = 15.9, 6.2 Hz, 1H), 1.76 – 1.69 (m, 1H), 1.63 (p, J = 7.8 Hz, 2H), 1.46 – 1.36 (m, 2H), 1.32 (dd, J = 15.1, 7.2 Hz, 7H). **^{13}C NMR** (151 MHz, D_2O) δ(ppm) = 175.25, 175.14, 174.14, 174.06, 173.78, 55.26, 53.51, 49.63, 49.54, 39.11, 30.09, 26.14, 25.17, 21.95, 21.51, 16.41, 16.24. **ESI-MS (m/z):** calculated, 433.223 for $C_{17}H_{33}N_6O_5S^+$ $[M+H]^+$; found, 433.224. **HPLC:R_T = 5.36 min.**

Peptide 9

^{1}H NMR (600 MHz, DMSO-d_6) δ(ppm) = 7.76 (s, 3H), 7.45 – 7.42 (m, 1H), 7.22 (s, 1H), 4.33 – 4.27 (m, 1H), 4.27 – 4.22 (m, 1H), 4.14 (dt, J = 16.8, 8.1 Hz, 2H), 2.80 – 2.66 (m, 4H), 2.23 (t, J = 8.4 Hz, 1H), 2.08 (s, 5H), 1.85 (s, 3H), 1.68 (q, J = 10.5, 7.9 Hz, 3H), 1.41 (ddq, J = 9.7, 5.9, 3.3 Hz, 2H), 1.34 – 1.25 (m, 2H), 1.11 – 1.00 (m, 2H), 0.79 (t, J = 7.2 Hz, 14H). **^{13}C NMR** (151 MHz, DMSO-d_6) δ(ppm) = 171.45, 171.40, 171.16, 169.52, 57.12, 57.01, 54.74, 52.54, 38.77, 36.42, 36.39, 31.01, 30.80, 26.61, 26.20, 24.56, 24.47, 22.57, 22.18, 15.46, 15.41, 11.06, 11.02. **ESI-MS (m/z):** calculated, 517.317 for $C_{23}H_{45}N_6O_5S^+$ $[M+H]^+$; found, 517.322.**HPLC:R_T = 10.20 min.**

Peptide 10

^{1}H NMR (600 MHz, D_2O) δ(ppm) = 4.43 (dd, J = 7.2, 5.3 Hz, 1H), 4.32 (dd, J = 9.6, 5.2 Hz, 1H), 4.28 (dd, J = 8.7, 5.8 Hz, 1H), 4.21 (dd, J = 9.4, 5.6 Hz, 1H), 2.93 (t, J = 7.7 Hz, 2H), 2.91 – 2.81 (m, 2H), 1.95 (s, 3H), 1.83 – 1.68 (m, 2H), 1.63 – 1.45 (m, 8H), 1.42 – 1.32 (m, 2H), 0.87 (d, J = 6.2 Hz, 6H), 0.84 – 0.80 (m, 6H). **^{13}C NMR** (151 MHz, D_2O) δ(ppm) = 174.99, 174.47, 174.24, 174.03, 173.54, 55.20, 53.39, 52.59, 52.09, 39.64, 39.44, 39.07, 30.03, 26.13, 25.18, 24.21, 21.96, 21.90, 21.46, 20.74, 20.69. **ESI-MS (m/z):** calculated, 517.317 for $C_{23}H_{45}N_6O_5S^+$ $[M+H]^+$; found, 517.319. **HPLC:R_T = 7.29 min.**

Peptide 11

^{1}H NMR (600 MHz, D_2O) δ(ppm) = 4.44 (dd, J = 7.1, 5.5 Hz, 1H), 4.32 (dd, J = 8.6, 6.0 Hz, 1H), 4.07 (dd, J = 8.4, 5.8 Hz, 1H), 4.02 (dd, J = 7.8, 5.8 Hz, 1H), 2.95 (t, J = 7.9 Hz, 3H), 2.88 (dd, J = 10.6, 6.4 Hz, 2H), 1.99 (s, 6H), 1.80 (dd, J = 9.2, 4.6 Hz, 1H), 1.72 (dt, J = 10.1, 5.0 Hz, 1H), 1.67 – 1.61 (m, 2H), 1.47 – 1.34 (m, 3H), 0.92 – 0.90 (m, 7H), 0.88 (t, J = 6.2 Hz, 7H). **^{13}C NMR** (151 MHz, D_2O) δ(ppm) = 174.28, 173.97, 173.84, 173.42, 173.23, 59.77, 59.37, 55.27, 53.32, 39.06, 30.25, 29.99, 29.81, 26.17, 25.17, 21.95, 21.46, 18.43, 18.33, 18.27, 17.87, 17.78. **ESI-MS (m/z):** calculated, 489.278 for $C_{21}H_{41}N_6O_5S^+$ $[M+H]^+$; found, 489.285.**HPLC:R_T = 8.15 min.**

Peptide 12

^{1}H NMR (600 MHz, DMSO-d_6) δ (ppm) = 8.20 (d, J = 7.7 Hz, 1H), 8.06 (t, J = 7.4 Hz, 2H), 7.97 (d, J = 8.0 Hz, 1H), 7.64 (s, 2H), 7.44 (s, 1H), 7.26 – 7.23 (m, 4H), 7.21 – 7.15 (m, 3H), 4.53 (d, J = 4.6 Hz, 1H), 4.43 (d, J = 2.4 Hz, 1H), 4.34 (d, J = 5.2 Hz, 1H), 4.28 (d, J = 5.2 Hz, 1H), 3.06 (d, J = 4.3 Hz, 1H), 2.91 (dd, J = 14.1, 4.3 Hz, 1H), 2.88 – 2.79 (m, 2H), 2.80 – 2.71 (m, 3H), 2.69 – 2.61 (m, 1H), 2.24 (s, 1H), 1.72 (s, 3H), 1.58 – 1.49 (m, 2H), 1.32 (d, J = 8.7 Hz, 2H). **^{13}C NMR** (151 MHz, DMSO-d_6) δ (ppm) = 171.37, 171.31, 171.02, 169.31, 137.95, 137.59, 129.02, 128.01, 126.20, 54.59, 22.41, 22.11. **ESI-MS (m/z):** calculated, 585.285 for $C_{29}H_{41}N_6O_5S^+$ $[M+H]^+$; found, 585.295. **HPLC:R_T = 10.2 min.**

2.4.3 Determination of solubility of the peptides

To determine the solubility of the peptides, 1 mg of a peptide is taken in a glass vial containing a magnetic bar and inserted in a water bath maintaining the temperature at 25 °C and placed on a magnetic stirrer. To these vials, 25 μL water/buffer) is added at a time and stirred for 5 mins. The samples are checked visually to see any insoluble particle or haziness. If the solid does not get dissolved completely, more water/buffer (25 μL each time) are added and the process repeated till visually clear solutions are obtained. The clear solutions are then subjected to Tindal effect experiments by passing LASER light through them to confirm complete solubilization.

2.4.4 Preparation of hydrogel

To prepare the hydrogel, 2 mg of individual peptide was added in required volume of 100 μL of 20 mM Tris buffer at pH 8 and agitated by shaking the solution to completely dissolve the solid (2 mins). The solution was kept undisturbed at room temperature (12 h for **11** and 2 h for **12**) to get the self-supporting hydrogel.

2.4.5 Determination of sol–gel transition temperature (T_g)

Glass vials containing the gel samples are kept in a water bath and the temperature of the bath was raised at a rate of 0.5 °C per minute. On top of the gels small steel balls are placed. The temperature at which the steel ball fall down to the bottom is noted as T_g. The experiments are performed in triplicate.

2.4.6 Electron microscopy

Small portions (5 μL) of 48 h matured gels are casted either on carbon coated copper grids (Field emission transmission electron microscope, FETEM) or on silicon wafers (Field emission scanning electron microscope, FESEM) and dried under ambient condition for 24 hours. Images are taken on JEOL, 2100F (FETEM) or Gemini SEM 300, Sigma Zeiss (FESEM) instruments.

2.4.7 Rheology

The viscoelastic properties of the hydrogels are characterized using Anton Paar MCR 102 rheometer equipped with a 20 mm parallel plate (with 0.5 mm zero gap) measuring system at 25 °C. Appropriate amounts of Peptides **11** and **12** are dissolved in Tris buffer of pH 8 at the gelation concentration and kept at room temperature undisturbed for 2 h and 12 h respectively to get the hydrogels. Appropriate amounts of hydrogels are taken with the help of a spatula very carefully to avoid any damage to the hydrogel samples and placed on the lower plate of the rheometer. The measuring system are then lowered until it reached the position where the gap between the two plates was 0.3 mm. Then the respective rheological measurements are performed. All the experiments are performed in triplicate.

Strain sweep tests are performed to identify the linear viscoelastic region (LVR) over a range from 0.01 to 1000 % strain at a fixed oscillatory frequency of 1 rad/s. The LVR can be defined as, where strain has no impact upon G′ and G″. Frequency sweep tests are carried out under an appropriate strain (= 0.1 %) selected from the LVR with the frequency ranging from 0.1 to 1000 rad/s at 25 °C. For the time sweep experiment, pre-gel solutions of each peptide are prepared. Once the peptides get dissolved, the rheological experiments are started with appropriate aliquots considering it as time zero. As the rheological experiment cannot be continued for a longer time period with one sample, the G' and G" are measured at different time points with samples from the stocks and noted the exact time of measurements. The G' and G" values obtained from these experiments are plotted against time of measurements. The experiments are performed in triplicate. To investigate the thixotropic property of the gels (2 wt%), cyclic dynamic strain sweep experiment is performed at a constant angular frequency of 1 rad s^{-1} by altering the applied strain from 0.1 to 100%. In this experiment, a higher strain (γ = 50%) and a lower strain (γ = 0.1%) are applied on the gel alternatively over a period of 2300 s and 5 successive cycles.

2.4.8 HPLC

Chromatographic purifications are performed on a Luna 5 μm (C18) column (Phenomenex) using a Dionex Ultimate 3000 HPLC. Acetonitrile and water with 0.1% TFA used as the mobile phase. A program is created as, 5% ACN to 100% ACN within a time interval of 20 min and this program is used for all the analyses. For the dimerization experiment, solutions of the peptides are prepared in Tris buffer and incubated at RT. Equal volume of samples from these solutions are injected at different time intervals. For the GSH mediated dimer to monomer conversion study, several sets of 1 wt.% hydrogel (200 μL) of 12 is prepared and 100 μL of 5 mM GSH solution in water was added on top of these hydrogels. At different interval one such sample was diluted up to 2 mL by adding distilled water. These solutions are then analyzed on HPLC using the previously mentioned program.

2.4.9 Circular dichroism (CD)

Circular Dichroism (CD) experiments are performed by using Jasco J-1500 spectropolarimeter and all the samples are recorded at room temperature. All measurements are done in 0.2 cm path length cuvette with 800 μL sample volume. Each CD profile is an average of 3 scans of the same sample collected at a scan rate 100 nm min^{-1}, with a proper baseline correction from the water medium. For concentration dependent studies, stock of the peptides are prepared in Tris buffer and incubated at room temperature for 24 h. These stock solutions are then used to prepare solutions of different concentration. For time dependent study, freshly prepared 300 μM solutions of the peptides are used for the study and the CD spectra are recorded at different time interval.

2.4.10 Dye release study

For dye release experiment, Rhodamine B (RhB) is used as a model dye because it is an organic molecule with absorption maxima of ~ 550 nm and the absorption profile does not overlap with the absorption of the gelator molecule. 1 mg/mL RhB solution is prepared in distilled water. Appropriate amount of **12** (to maintain the MGC in the final sample) is dissolved in 190 μL of Tris buffer and 10 μL of the RhB solution is added and the solution is agitated to get a clear solution. The solution is kept at RT to get the dye encapsulated hydrogel. Four such sets of dye encapsulated hydrogels are prepared. These hydrogels are then suspended in 1.8 mL solutions of 3 different concentrations of GSH (0.01 mM, 0.1 mM, 1 mM) and water. 100 μL of the bulk solutions are taken time to time and replaced with the same amounts of fresh GSH solution to keep the overall volume intact. The absorbance of these aliquots are then measured to find the cumulative release of the dye. The experiments are performed in triplicate.

2.4.11 NMR studies

^{1}H NMR and ^{13}C NMR spectra are recorded using a Bruker Ascend 600 MHz (Bruker, Coventry, UK) spectrometer and referenced to deuterated solvents. To understand the role of hydrogen bonding and π–π stacking, solutions of **11** and **12** are prepared in DMSO-d_6 containing varying amount of 20 mM Tris buffer at pH 8. The solutions are incubated at room temperature for 24 h before recording the ^{1}H NMR. Amount of buffer could not be increased above 40% due to the appearance of large solvent peak.

2.4.12 Density Functional Theory (DFT)

The M06 family of functions was chosen over other conventional DFT functions as they are proven to be more accurate toward geometries and energy calculations for a variety of dispersion-dominated systems like DNA base-pair stacks and D-A CT complexes.[203] Energy minimized structures of the monomers and their corresponding supramolecular dimers were obtained using the density functional theory (DFT) at the B3LYP/6-31G (d,p) accuracy level using the Gaussian 09 package of programs.

2.4.13 Cell culture

RAW 264.7 macrophages are maintained in DMEM, supplemented with 10% fetal bovine serum, 100 U/mL penicillin, and 100 μg/mL streptomycin while the THP1 monocytes are maintained in RPMI, supplemented with 14% fetal bovine serum, 100 U/mL penicillin, and 100 μg/ml streptomycin. The peptide is dissolved in different concentrations in 100 μL of 20 mM Tris buffer (pH 8). The cells (murine macrophages and human monocytic cells) are washed twice in the medium, and seeded directly within the peptide scaffolds during the gelation stage. This infusion of the peptide hydrogel with the media helped to regulate the pH, thereby maintaining a constant pH between 7.45 and 7.55, which is suitable

for cell growth. The cultures are maintained in an incubator at 37 °C with a humidified atmosphere of 5% CO2.

2.4.14 Cytotoxicity assay

The cytotoxicity assay is performed by MTT. 10^4 cells are seeded onto the hydrogels of varying concentrations in a 96 well plate and incubated for 24 h. MTT (5 mg/mL) is then added onto the constructs and incubated at 37 °C for 4 h. After the period, formazan crystals were solubilized in DMSO and absorbance is measured at 570 nm. The extent of cell viability is measured as the percent viability within peptide hydrogels with respect to 2-D cultured cells.

2.4.15 Confocal microscopy

The viability of the cells is further assessed by fluorescent live-dead staining. 2-D cultured RAW macrophages without hydrogel encapsulation served as control. Macrophages are plated in glass-bottomed culture dishes, cultured in DMEM and 10% FCS and maintained at 37 °C and 5% CO_2 in a humidified incubator for 24 h. For microscopic analysis, the DMEM medium is removed and the cell-gel constructs are washed twice with PBS. Thereafter, 200µL of PBS solution containing 2 µM of calcein AM and 4 µM Propidium iodide (PI) are added onto the cell-gel constructs for analyzing viable and non-viable cells. After 15 min of incubation at 37 °C/5% CO_2, the labeled cells are viewed under Olympus IX81 microscope equipped with a FV1000 confocal system 10X objective and further 30X magnification. Images obtained are analyzed by Olympus Fluoview (version 3.1a; Tokyo, Japan) and analyzed using Image J software.

2.4.16 Cell proliferation assay

Cells are plated at a density of 10^4 cells/well withsolutions of **12** of varying concentrations in a 48 well plate and incubated for 2 h. The cells are then further incubated either for 24, 48, or 72 h. Cell proliferation is analyzed by using CyQUANT Direct Cell Proliferation Assay Kit. When the incubation period is over, the medium was removed and the constructs were incubated with CyQUANT reagent for 1 h at 37 °C according to manufacturer's instructions. Plates are analyzed by using a fluorometric plate reader with excitation at 508 nm and emission at 527 nm. 2-D cultured cells are termed as control.

2.4.17 Statistical analysis

All experiments are performed in triplicates. The results are expressed as the mean ± SD. Student t test was used to calculate the statistical significances of differences among paired data sets, and a p value < 0.05 was regarded to be significant.

Chapter 3: Modulation of Physical and Biological Properties of Biopolymer Hydrogels in the Presence of Short Self-Assembling Peptide

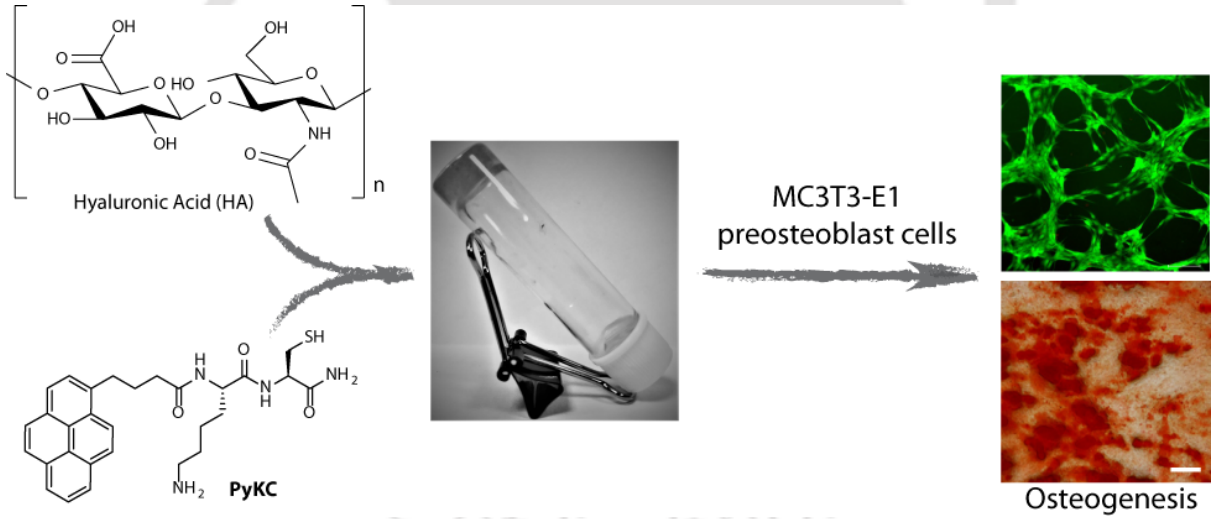

Indian Institute of Technology Guwahati

3.1 Introduction

Scaffold that mimics the natural state of the tissue by forming three-dimensional surroundings, which is biocompatible, non-immunogenic and act as an artificial extracellular matrix (ECM) is essential for tissue engineering applications. Several types of materials have been used as scaffolds for tissue engineering purpose till date. Currently, the well-known materials for tissue engineering scaffold are a combination of inorganic or organic materials and natural polymers.[204-209] These scaffolds provide mechanical and structural support for cell growth. Hydrogels of natural or synthetic molecules have emerged as one of the most promising candidates. In recent years, biodegradable and injectable hydrogels are getting significant attention as promising candidates for matrix and scaffolds for tissue engineering.[210-212] Natural polysaccharide based hydrogels like, chitosan, hyaluronic acid and alginate are commonly used as a scaffold for tissue engineering.[210, 211, 213-217] They fulfil the basic criteria of bio-compatibility, hydrophilic nature and huge water storage in their long entangled network, which mimics the natural extracellular matrix and allows the cells to adhere and differentiate. However, these biopolymer-based hydrogels suffer from mechanical properties which are weaker than the natural ECM and thus cannot be implanted.[209, 213, 218]

The mechanical properties of these biopolymers can be enhance by the synthesis of composite hydrogel to make it suitable for tissue engineering.[219] In this respect, an additive that does not compromise with the biocompatibility and biodegradability but enhance the usability of these bio-polymeric hydrogels for bone tissue engineering application is essential.[219, 220] Peptide hydrogelators appear to be a favourable choice as their material properties can be tuned by manipulating the assembly process, which in turn enables to modulate cellular functionality and tissue morphogenesis.[144, 160, 221-224] Peptides can self-assemble in aqueous medium to form fibrous network like structures that can immobilize water molecules through cohesive forces leading to self-supporting hydrogels. The advantage of these hydrogels are, a) they are made of natural amino acids, generally biocompatible and biodegradable in nature, b) by fine-tuning the extent and proportions of different noncovalent interactions, the properties including the mechanical ones can be tuned easily, c) easy incorporation of specific functional groups allows to create smart stimuli-responsive materials.[160] Control over the mechanical and functional properties can also be tailored by combining two or more gelator molecules to form composite hydrogels.[225-227] Co-assembly of two building blocks have been previously observed to have resulted in hybrid materials with superior physical properties and biocompatibility not shown by individual building blocks.[223, 226, 228-230]

To this end, recently we have demonstrated a tripeptide, PyKC (Scheme 1), that formed, in the hydrogel state, very tightly knitted network of thin fibers.[150, 156] The glutathione responsive supramolecular hydrogel of PyKC remained insoluble in water and other water miscible organic medium, buffers of different pH (3 – 11) as well as in human blood serum. Additionally, the formed hydrogel showed extreme confinement property as exchange of solvent or solute was highly restricted to and from the gel. In continuation to that work, we have recently reported another series of similar peptides with KC unit at the C-terminal and the hydrogels of those peptides showed excellent cell-proliferation in the hydrogel network.[231] Based on these successes, we envisioned that PyKC could be an excellent candidate to prepare two-component composite hydrogel with biopolymers. The tendency to form very tightly woven network may possibly enhance the mechanical properties, introduce thixotropic/injectable nature to the composite hydrogels and make them attractive plat-form for bone tissue engineering.

Herein, we report the effect of combining PyKC with four different biopolymers on their hydrogel properties and especially on the mechanical behaviour. We observed that only 10% doping of PyKC results in significant improvement of the composite hydrogels. Based on the overall properties of these materials, the composite hydrogel prepared in combination of HA and PyKC was further tested for bone cell proliferation and differentiation and found that the combination is an excellent platform for supporting osteogenic differentiation.

3.2 Results and Discussions

To prepare the composite hydrogels for an effective 3D artificial ECM for bone tissue engineering, we have combined PyKC with different biopolymers. Four different polymers were chosen for this purpose chitosan (Cht), sodium alginate (Alg), gelatin (Gel), and hyaluronic acid (HA) (Scheme 3.1). All these polymers are capable of forming hydrogels under different experimental conditions and are used as artificial ECM either in combination with other materials or as the sole component and showed promising results.[232] Our idea was to incorporate the PyKC molecules to these polymeric systems and create composite hydrogels that may possess superior properties compared to that of the pristine polymers. To form Polymer/PyKC composite hydrogels, initially, the two components were mixed in 1:1 ratio by volume to attain 1 wt% polymer and 1 wt% PyKC in the respective composite hydrogels. However, the hydrogels prepared using this ratio resulted into very weak hydrogels (data not shown) and therefore, polymer–PyKC ratio was changed to 10:1 (wt%). All the studies were per-formed with these gels. However, in the case of gelatin, it wasdifficult to construct such composite hydrogel and thus the 1 wt% gelatin and 1 wt% PyKC hydrogel was used for further

studies. Hereafter, the composites are denoted as, polymer short name (Cht, Alg, Gel, or HA)/ PyKC. Notably, for Alg and Gel, no hydrogel could be formed at 10 and 1 wt% concentrations respectively in absence of PyKC.

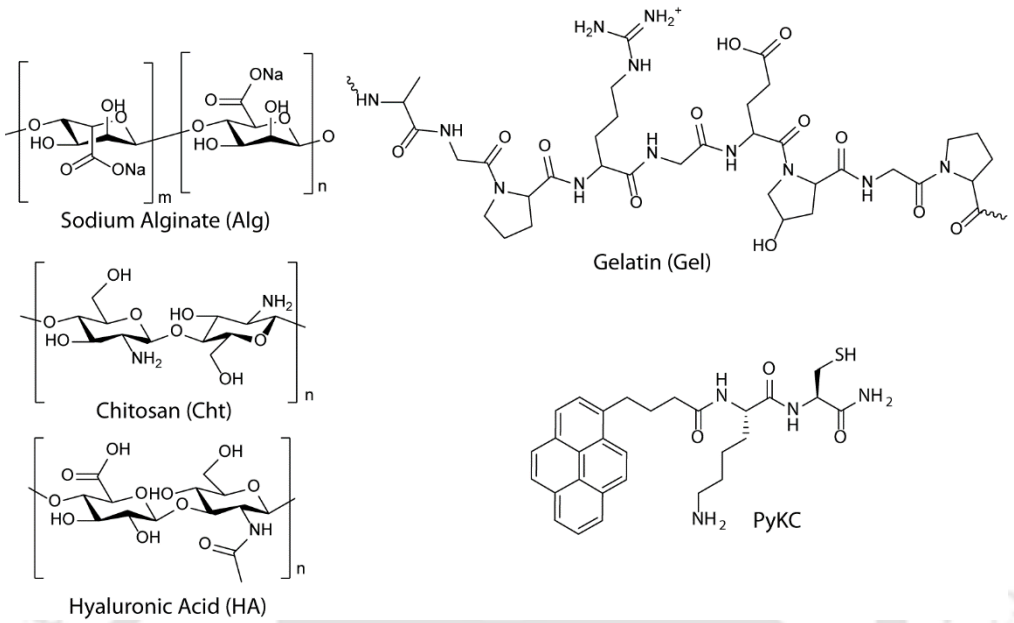

Scheme 3.1 Chemical structures of different biopolymers and PyKC used in this study to construct composite hydrogels.

Various characterization studies were performed to under-stand and compare the properties of the composite hydrogels with that of the hydrogels prepared by the polymers alone or by PyKC. Due to the presence of Cysteine residue in the sequence, PyKC forms disulphide linked dimer in neutral to basic condition.[150] Previously we observed that the formation of the dimers is crucial for the hydrogelation of PyKC.[150] Analytical HPLC analyses of these composites show that indeed, for the first two cases, no trace of the PyKC monomer could be seen whereas incomplete dimerization was observed for the other two (Figure 3.1). The extent of dimerization for Cht and Alg composites were found to be 65 and 70% respectively. The % conversion did not improve even after incubation for seven days. The gel melting temperatures (T_g) were then measured for all the composites by ball dropping method (Table 3.1). HA/PyKC and Gel/PyKC hydrogels were found to be stable up to 90 °C and no sign of melting were observed at this temperature. On the other hand, the Alg/PyKC and Cht/PyKC composites registered their melting temperatures at 80 and 72 °C respectively. Importantly, the T_g of PyKC was recorded as 75 °C.[150]

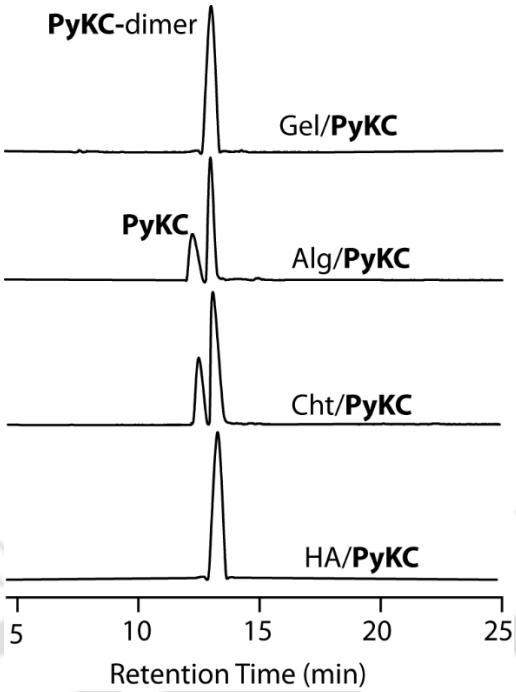

Figure 3.1 HPLC traces of 24 h samples of different composite hydrogels showing the extent of monomer to dimer conversion of PyKC.

Table 3.1. Compositions and different properties of the hydrogels studied.

Hydrogels	PyKC (wt%)	Biopolymer (wt%)	Sol/Gel	T_g (°C)	Swelling ratio	Average (Pa)	G'Average (Pa)	G"
Gel/PyKC	1	1	gel	80	32.50	2500	1020	
Alg/PyKC	1	10	gel	> 90	12.41	2400	920	
Cht/PyKC	1	10	gel	72	16.08	120	80	
HA/PyKC	1	10	gel	> 90	14.81	5000	1130	
Gel	-	1	sol	-	-	2.3	8.3	
Alg	-	10	viscous sol	-	-	4.5	9.5	
Cht	-	10	gel	73	12.24	140	90	
HA	-	10	gel	> 90	10.52	2050	580	

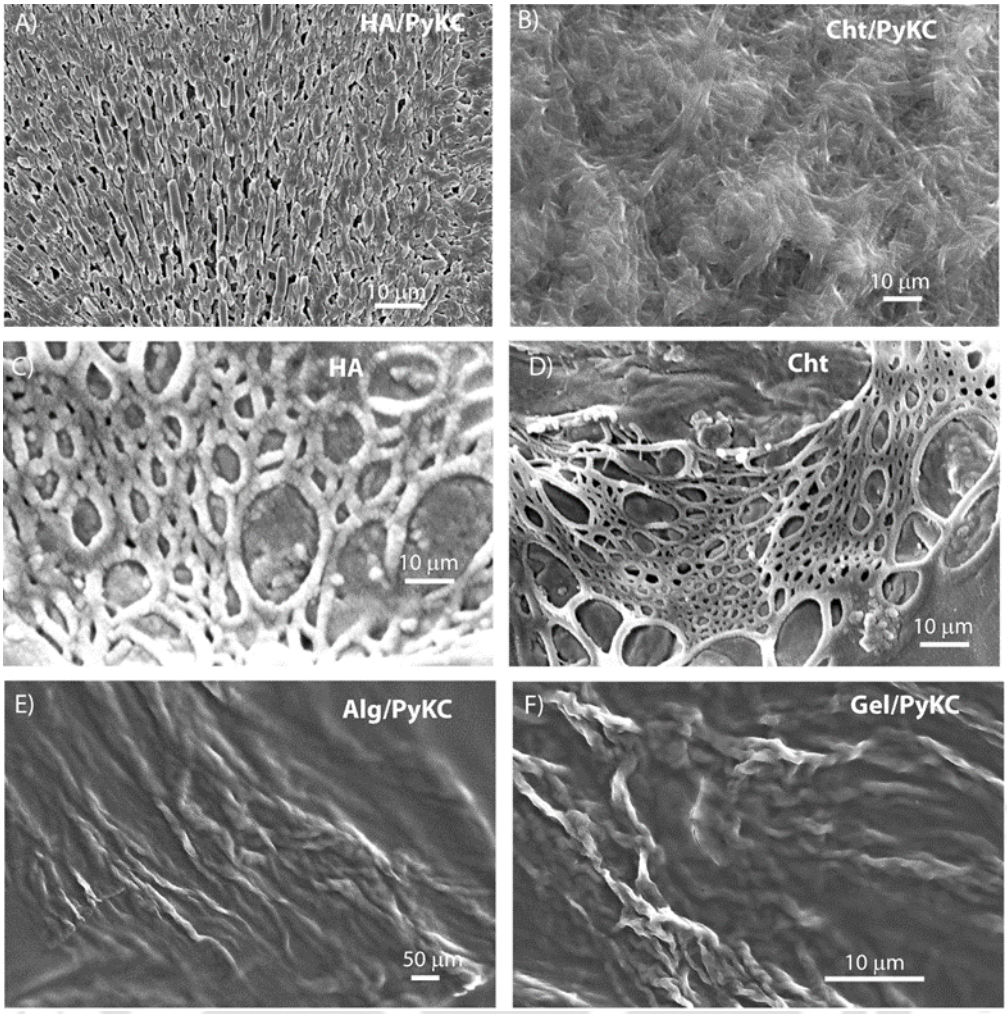

Figure 3.2 FESEM images of different hydrogels. A) HA/PyKC (10-1 wt%); B) Cht/PyKC (10-1 wt%); C) HA (10 wt%); D) Cht (10 wt%); E) Alg/PyKC (10-1 wt%); and F) Gel/PyKC (1-1 wt%).

The morphologies of the composite hydrogels were evaluated using Field Emission Scanning Electron Microscopic (FESEM) analyses. For HA/PyKC, well arranged brick like structures were observed (Figure 3.2 A). Whereas, for Cht/PyKC composite hydrogel, long entangled fibrillary network several micrometer long fibers could be seen under FESEM (Figure 3.2 B). These morphologies are significantly different than that of the hydrogels formed by the corresponding polymers alone at this concentration, as can be seen in Figure 3.2 C-D. Such fibrillar network was also not observed in Alg/PyKC and Gel/PyKC which displayed dense bundle like morphology.

Next, the swelling behavior of these composite hydrogels were studied.[233] As can be seen in Figure 3.3, the highest swelling ratio (Table 3.1) was noted for Gel/PyKC with a value of 3250% while the lowest was found for Alg/PyKC (1241%). For Cht and HA composites, the swelling obtained was 1608 and 1481%, respectively. Importantly, the presence of PyKC resulted in an enhancement in the swelling ratio when compared to the respective polymer hydrogels. The presence of PyKC in the composites certainly

allows enhanced water retention in the 3D hydrogel structure presumably by contributing the tightly knitted network as previously seen for PyKC hydrogel.

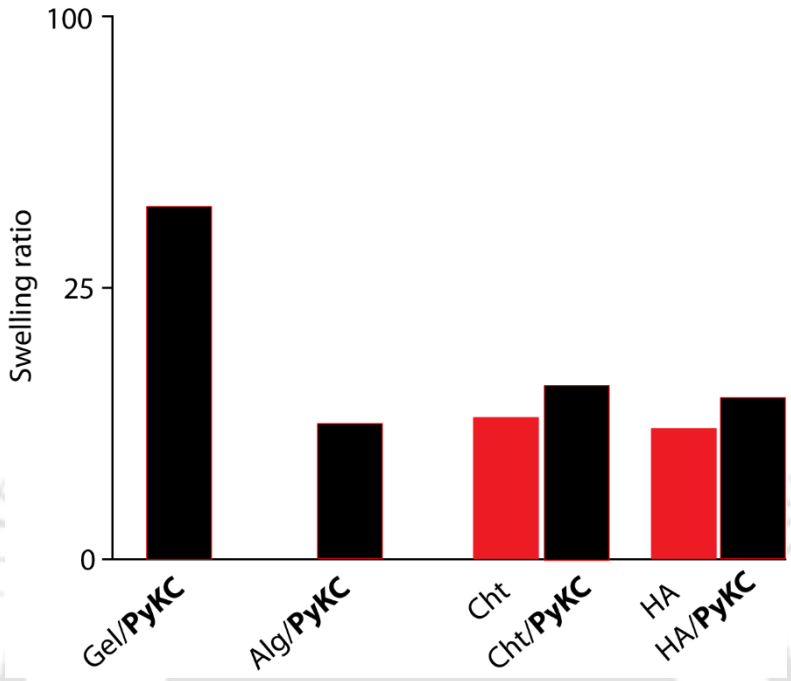

Figure 3.3 Swelling ratio of different hydrogels.

In order to study the kinetics of the hydrogel formation and their mechanical properties, rheological analyses were performed. The composite and the polymer samples under similar conditions were used for both frequency as well as amplitude sweep experiments. The hydrogels were subjected to the application of 0.01–1000% strain at a constant frequency. As expected, in the amplitude sweep experiments, both Alg and Gel samples showed higher G" (loss modulus) values than the corresponding G' (storage modulus) showing the liquid character as they fail to form any hydrogel (Figure 3.4).[201]

Rheological strain sweep resulted in a wide linear viscoelastic region of up to ~10% strain for Cht/PyKC and Gel/PyKC hydrogels while Alg/PyKC hydrogel showed linear viscoelastic region up to 1% starin. Interestingly, HA/PyKC hydrogel displayed strain sustain-ability up to 100%. G' of the polymer/PyKC composite hydrogels obtained from the frequency sweep experiment on the prepared hydrogels by applying the frequency range of 0.01-1000 rad/s, showed the HA/PyKChydrogels to be the strongest (~5000 Pa), followed by Gel/PyKC (~4000 Pa), Alg/PyKC (~2000 Pa), Cht/PyKC (~100 Pa) (Figure 3.5).

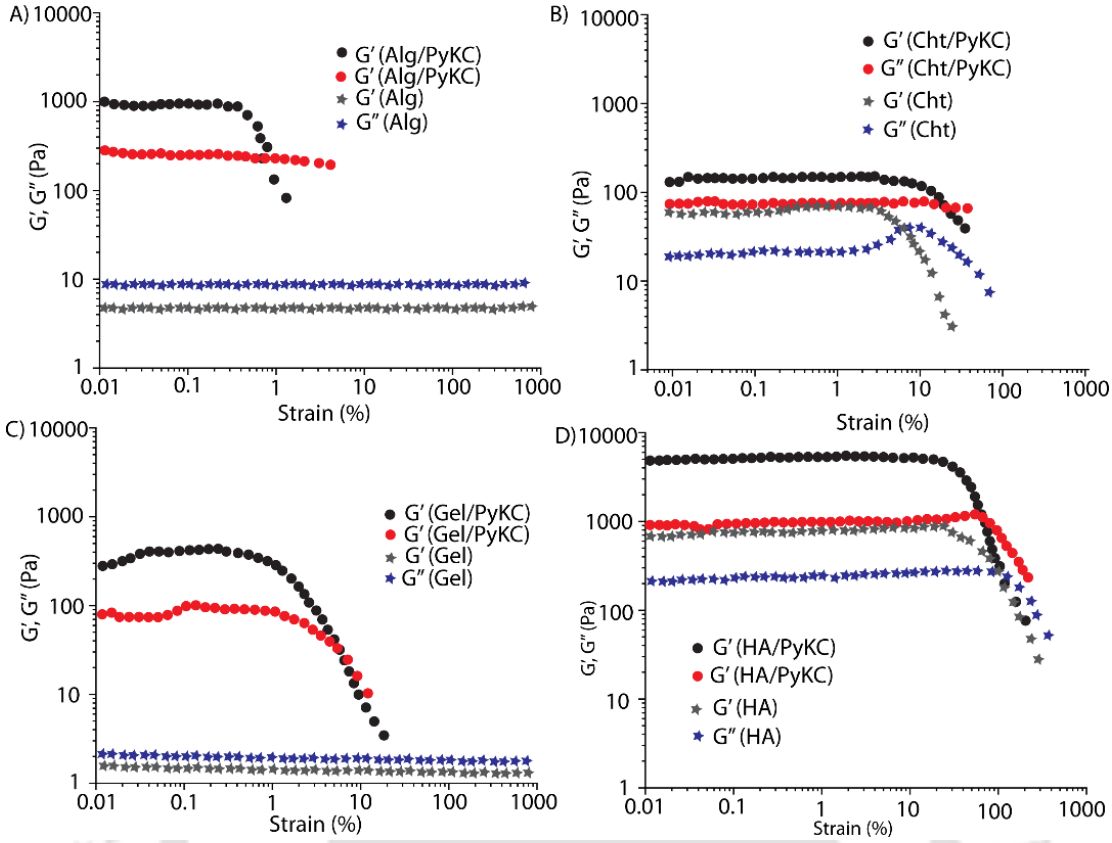

Figure 3.4Changes in storage and loss moduli as a function of shear strain (amplitude sweep at a frequency of 1 rad s^{-1}) for A) Alg and Alg/PyKC, B) Cht and Cht/PyKC, C) Gel and Gel/PyKC and D) HA and HA/PyKC hydrogels measured at room temperature

These results are interesting as Gel and Alg were unable to form any hydrogel under similar experimental condition but the presence of only 1% PyKC resulted in a moderately strong hydrogel. Notably, the presence of PyKC, in all cases enhanced the gel strength considerably. As a good gelator, PyKC probably forms the driving force of the supramolecular organization with these polymers via H-bonding, thus producing a composite hydrogel with high mechanical rigidity. The hydrophilic/lipophilic balance (HLB)[170] of Cht/PyKC hydrogel probably beyond the suitability to form rigid gel.

The standard rheological analyses were followed by thixotropy measurements. Thixotropy of hydrogels is an important property that helps in determining the possibility of bio-medical applications especially in case of localized drug delivery and 3D cell-proliferation. [201, 234] A thixotropic hydrogel shows thinning upon application of a shear strain and on removal of the strain it returns back to the original gel state. In the present cases, all the composite hydrogels showed good thixotropic characters.

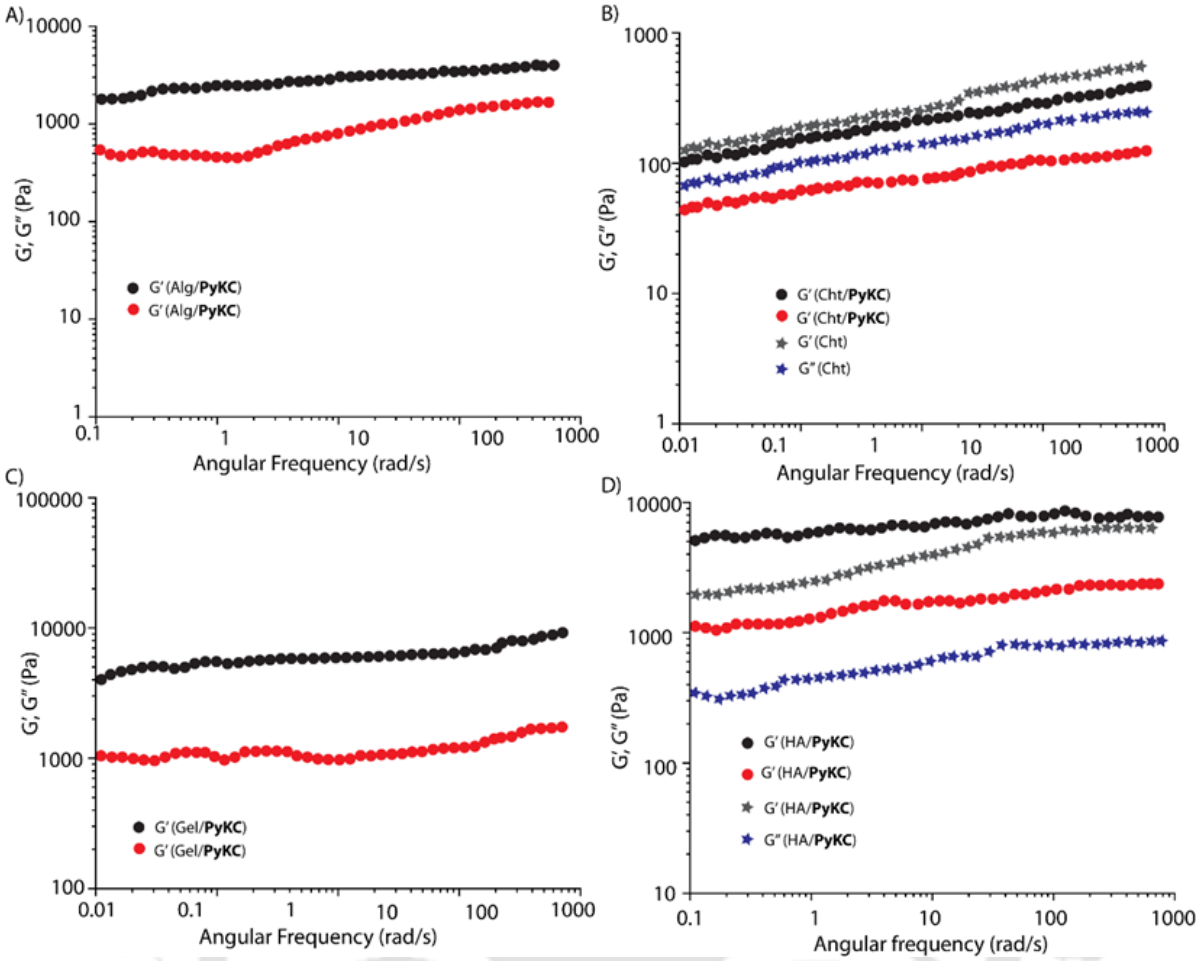

Figure 3.5 Frequency sweep profile of different hydrogels studied at room temperature.

However, the hydrogels formed by 10 wt% HA and Alg did not show thixotropic behavior. Figure 3.4 shows that all the composite hydrogels exhibit yield strain and transform into quasi-liquid, which indicate the start of deformation of the gels and possible thixotropic nature. Time dependent strain sweeps were executed at a fixed angular frequency (1 rad s^{-1}) and alternating the applied strains for each of these composite hydrogels (Figure 3.6). At higher strain, the viscoelastic nature is lost which returned back in every successive step where lower strain is applied. These results confirm that all the hydrogels are thixotropic. The injectability of these composite gels were tested by preparing the hydrogels in a syringe and then injecting them into water. In all cases, the composite hydrogels could easily be injected (Figure 3.7).

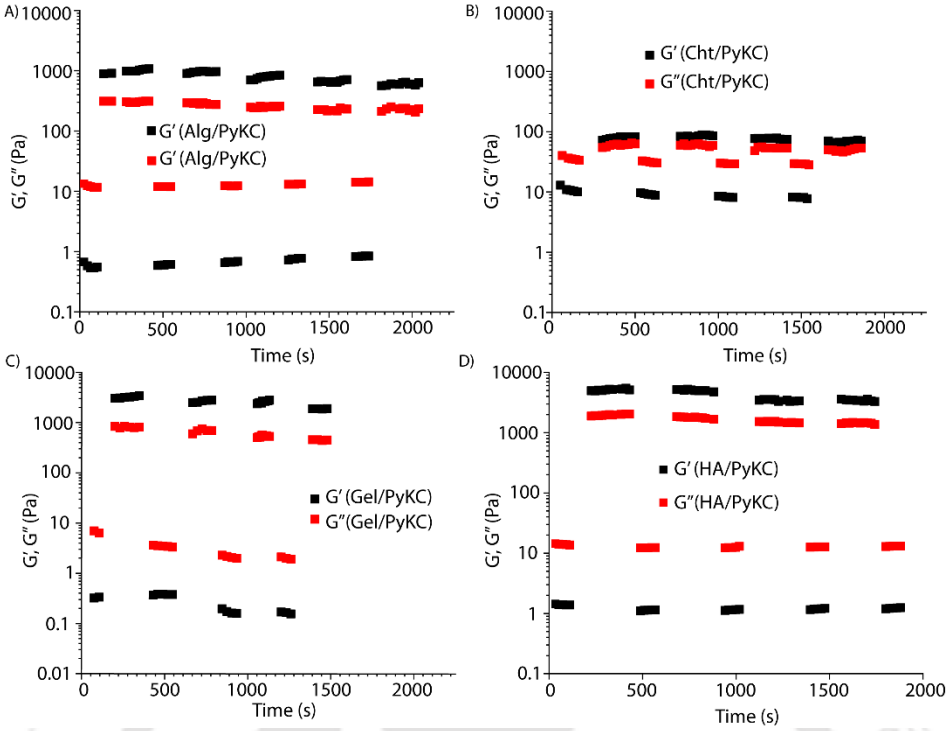

Figure 3.6Thixotropic behavior of the composite hydrogels (A) Alg/PyKC, B) Cht/PyKC, C) Gel/PyKC and D) HA/PyKC) demonstrated by the continuous step strain measurements at room temperature.

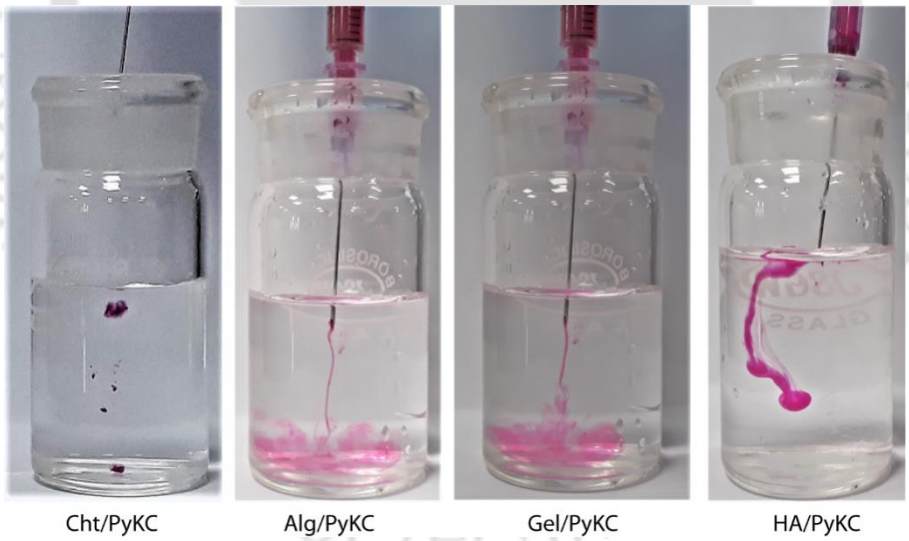

Figure 3.7. Photographs of all the composite hydrogels (rhodamine loaded) during injection in bulk water showing injectability property.

It is clear that the presence of PyKC significantly alters the aggregation property of the polymers. When compared between the polymeric and the corresponding composite hydrogels, significant presence of the PyKC-dimers in the composites, and the fact that Alg and Gel required the presence of PyKC to form hydrogels supports critical role of PyKC toward the hydrogel formation in these composites. Moreover, the presence of PyKC not only enhances the mechanical strength in the composites but also increases the water uptake as well as introduces the thixotropic behaviour.

Next, the temperature dependent rheological analyses of the HA/PyKC and Alg/PyKC systems were performed. The amplitude and frequency sweep experiments were performed at three different temperatures (25, 37 and 50 °C). As can be seen from Figures 3.8 and 3.9, HA/PyKC hydrogel displayed strain sustainability up to 100% at all three temperatures.

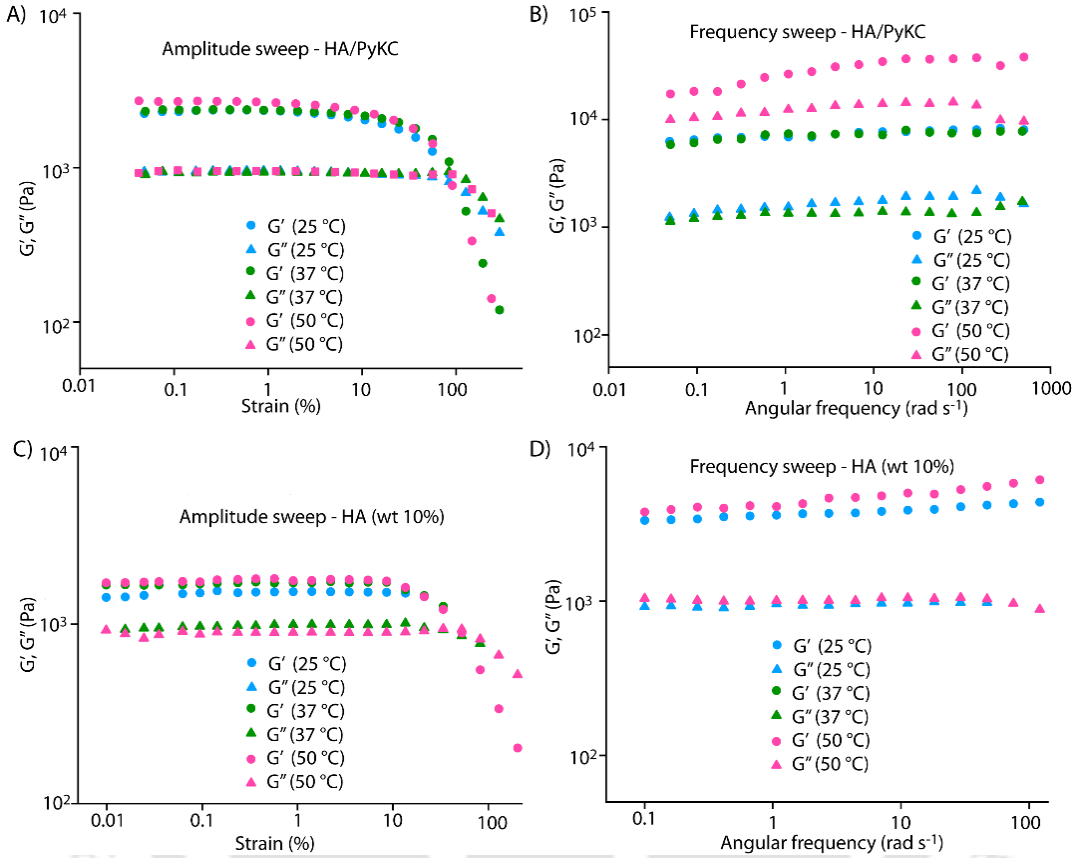

Figure 3.8 Temperature dependent amplitude sweep and frequency sweep of HA/PyKC and HA hydrogels. A) and C) amplitude sweeps and B) and C) frequency sweep data for HA/PyKC and HA respectively.

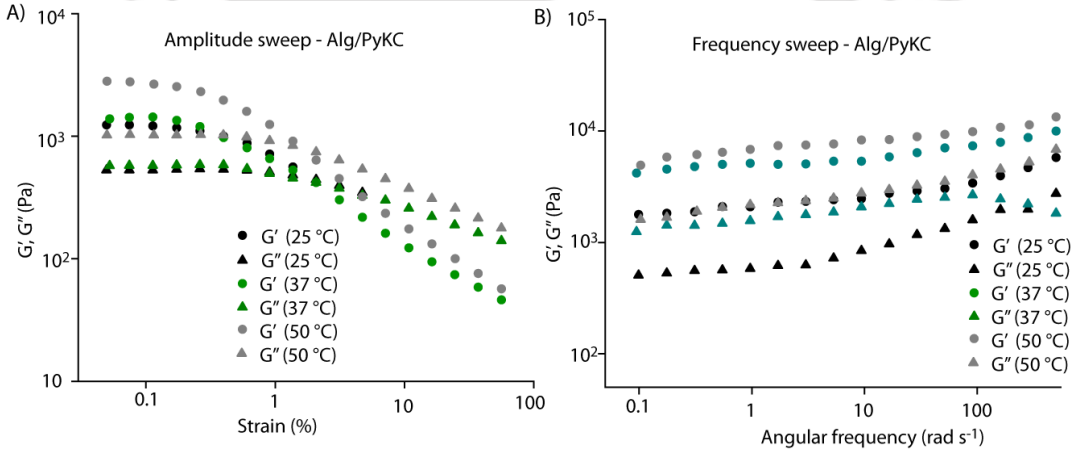

Figure 3.9 Temperature dependent A) amplitude sweep and B) frequency sweep of Alg/PyKC hydrogel.

The G′ values from the frequency sweep experiments indicated that with increase in temperature the gels become stronger and retained their stability at all temperature ranges. However, in case of Alg/PyKC hydrogel, the strain sustainability was found to be up to only 2 % (Figure 3.9). From the

temperature sweep experiments, both the HA/PyKC and 10 % HA hydrogels were found to resist dissolution at higher temperature.

Further, the hysteresis loop obtained in case of HA/PyKC hydrogel clearly indicate that at higher shear rate the hydrogel was not damaged and it comes back to its initial position when the shear rate was lowered (Figure 3.10 A). However, in case of 10 % HA hydrogel, at higher shear rate the hydrogel was damaged but upon rest, the structure reforms and finally meets to the initial position.

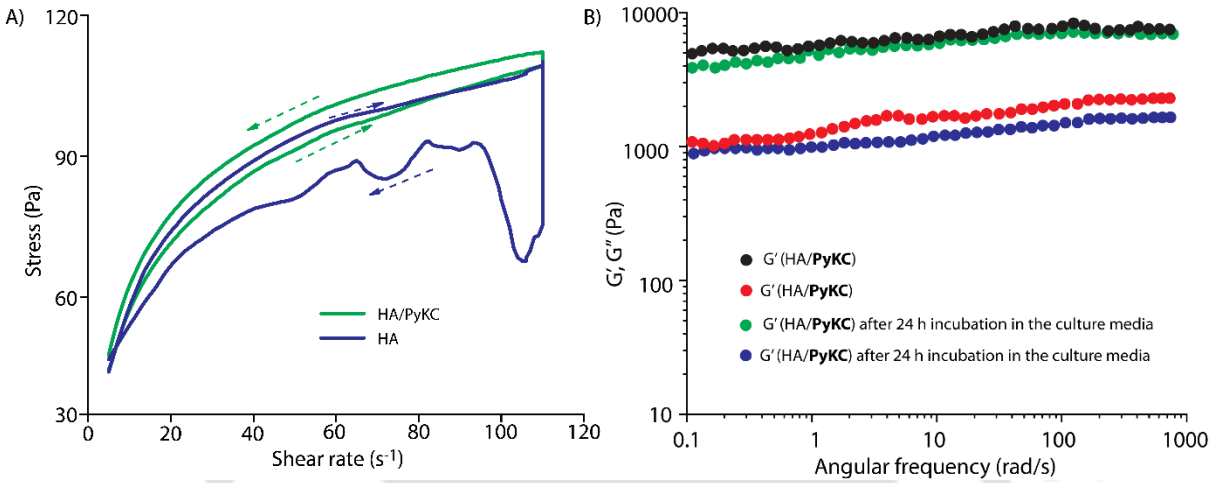

Figure 3.10 A) Hystersis loops of HA/PyKC and HA hydrogels measured at RT. B) Frequency sweep profile HA/PyKC composite hydrogel before and after 24 h incubation in α-MEM supplemented with 10% fetal calf serum, 100 U/mL penicillin, and 100 U/mL streptomycin.

To evaluate the potential of the Polymer/PyKC composite hydrogel as a scaffold for tissue engineering, their biocompatibility was assessed using in vitro cell culture experiments. However, Cht/PyKC hydrogel was too weak to proceed for the cell regeneration study, therefore we decided to proceed with the other three Polymer/PyKC composite hydrogels. MC3T3-E1 preosteoblast cells were seeded on prewashed Alg/PyKC, HA/PyKC and Gel/PyKC composite hydrogels. The viability of the MC3T3-E1 cells, evaluated by MTT assay after 3 days showed high bio-compatibility of 85 – 90% on HA/PyKC hydrogel while Gel/PyKC and Alg/PyKC hydrogels showed 60 – 65% and 37 – 40% cell viability respectively (Figure 3.11 A).

Among all the composite hydrogels tested, HA/PyKC demonstrated superior characters in terms of mechanical properties and also found to be biocompatible. Thus, all further studies were carried out using the HA/PyKC composite hydrogel. Since bio-stability of any hydrogel is a prerequisite for bio-medical applications, we evaluated the stability of the HA/PyKC hydrogel toward proteolytic digestion.[211]

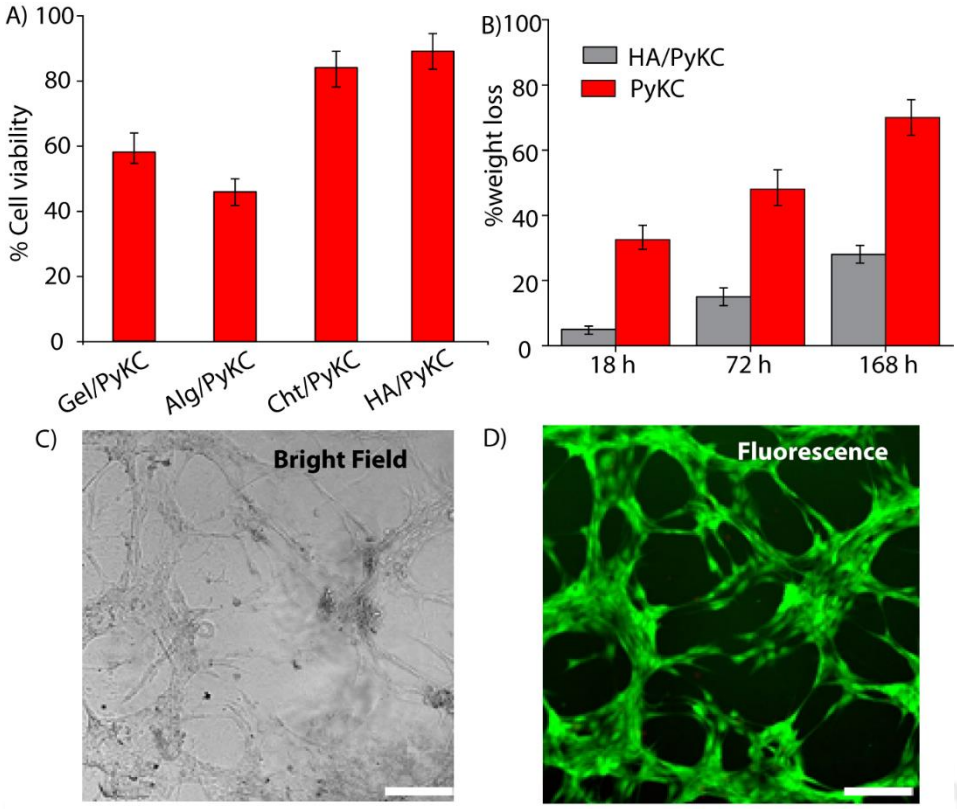

Figure 3.11Cytocompatibility and stability of the composite hydrogels. A) Cytotoxicity profile of different composite hydrogels toward MC3T3-E1 preosteoblast cells after 3 days. B) Stability of the HA/PyKC and PyKC hydrogels against the proteinase K digestion. C) Bright field image of MC3T3-E1 cells on Hyaluronic acid/PyKC composite hydrogel. D) Fluorescence spectroscopic image of live MC3T3-E1 cells on Hyaluronic acid/PyKC composite hydrogel. Scale bar = 100 μm.

Figure 3.11 B shows the enhanced resistance of the composite hydrogel toward proteinase K digestion compared to the PyKC hydrogel. As can be seen, even after 7 days of incubation, only 28% of the composite hydrogel is lost while ~70% amount PyKC hydrogel is lost. These results show a strong resistance of the composite hydrogel toward enzymatic digestion and also provides evidence that the two components mutually enhance the quality of the hydrogel for bio-medical applications.

The stability of the HA/PyKC hydrogel in the culture medium was then tested by incubating the hydrogel in α-MEM supplemented with 10% fetal calf serum, 100 U/mL penicillin, and 100 U/mL streptomycin. Photographs of the hydrogel was then taken at different time interval. It is prominent that with time, the culture medium penetrated inside the hydrogel matrix as the colour of the hydrogel is intensified over time (Figure 3.12). However, the composite hydrogel was observed tobe quite stable after 24 h of incubation as upon inversion of the vial, the gel was found to be intact. Rheological analyses of this hydrogel showed only a nominal decrease in its strength (Figure 3.10 B).

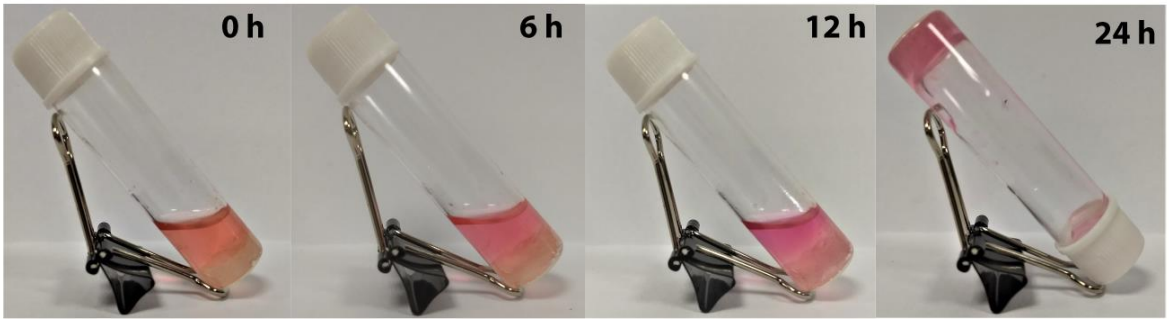

Figure 3.12Photographs of HA/PyKC hydrogel at different time intervals while incubated in αMEM showing stability of the composite hydrogel in the culture medium.

To this end, bone regeneration in artificial scaffold is an important area of research. The HA/PyKC composite hydrogel showed mechanical properties that could be suitable as an artificial scaffold for bone regeneration.[235, 236] First we studied the scaffold ability to supports pre-osteoblast growth, proliferation and differentiation using MC3T3-E1 pre-osteoblast cells. The cytocompatibility analysis of HA/PyKC hydrogel displayed ~90% cell viability. The morphology of the cells on HA/PyKC hydrogel after 3 days were observed Live/Dead staining comprising a cell membrane dye used to indicate live cells (fluorescein diacetate, green), and a DNA stain that indicates dead cells (propidium iodide, red). Most promisingly we observe, highly populated green cells with good shape and morphology (Figure 3.11 C-D) while no propidium iodide staining which further supports the viability of MC3T3-E1 cells on the HA/PyKC hydrogel.

Further, we determined the extent of differentiation and matrix mineralization of the MC3T3-E1 cells on the HA/PyKC composite hydrogel by Alizarin red assay. Extracellular calcium deposits are produced by pre-osteoblasts during mineralization. These deposits can be stained by Alizarin red and can be quantified to determine the extent of mineralization arising from bone nodule formation. The amount can then be normalized to the number of cells. The cellular matrix displayed an in-tense red stain after 14 days of differentiation on HA/PyKC hydrogel compared to that of pre-differentiation (Figure 3.13 A). Quantified alizarin red staining intensity was found to be ~ 4 times higher in case of differentiated cells (Figure 3.13 B) as compared to the pre-differentiated cells.

Further we evaluated early osteogenic differentiation marker of osteoblast progenitor cells MC3T3-E1 by determining the alkaline Phosphatase (ALP) activity of the cells that were grown on the composite hydrogel. MC3T3-E1 preosteoblasts were seeded on prewashed composite hydrogels and differentiated in osteogenic medium for 14 days. Following incubation, ALP activity was measured using an ALP substrate, 4-Methylumbelliferyl Phosphate (4-MUP), to the seeded cells. As can be seen in Figure 3.13 C, the ALP activity was ~ 3.5 times higher in case of the differentiated cells when compared with pre-differentiated cells. The observed elevated ALP activity for the differentiated cells suggests that the

HA/PyKC composite hydrogel is capable of inducing osteogenic response to osteoblast progenitor MC3T3-E1 cells. These results provide convincing evidence that the HA/PyKC hydrogel efficiently induces the differentiation and mineralization of MC3T3-E1 preosteoblast cells and thus meets the pre-requisites of a potential bone regeneration scaffold to be utilized in future.

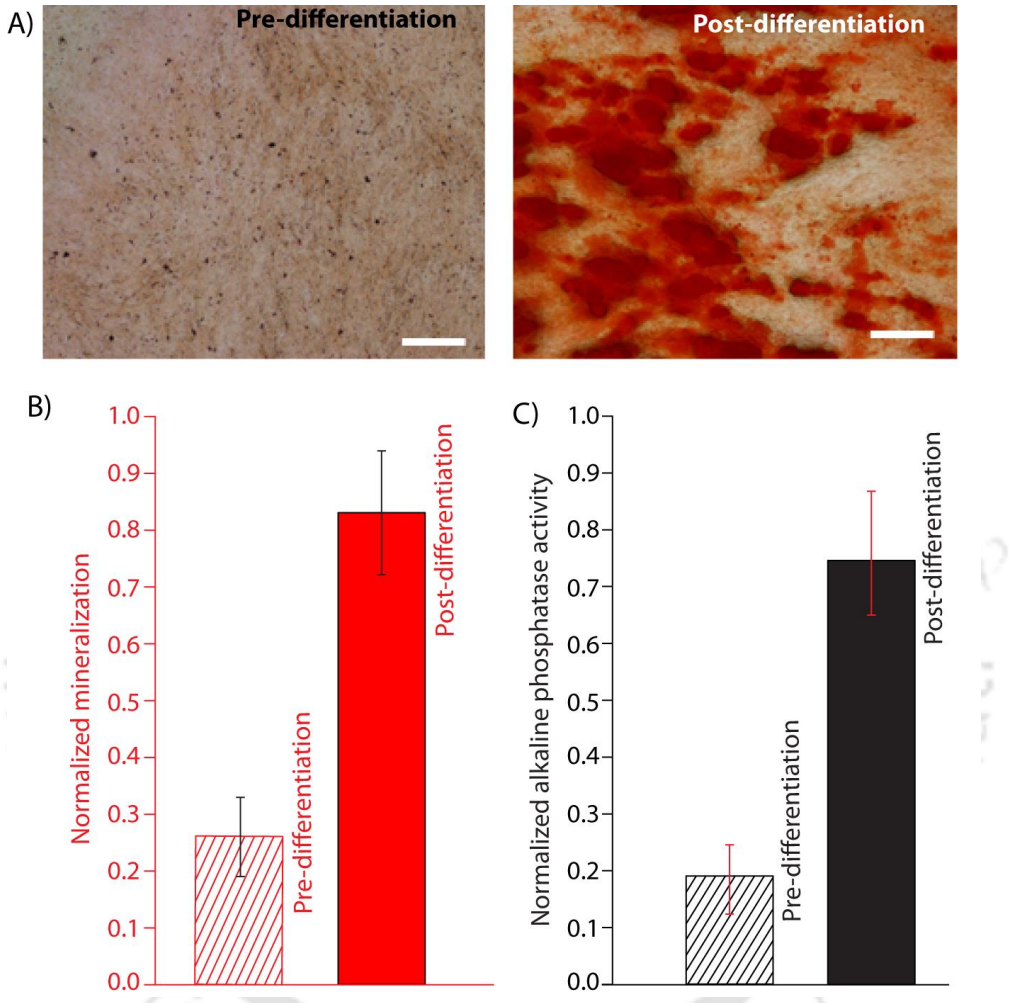

Figure 3.13 Osteogenic response of MC3T3-E1 cellson the HA/PyKC composite hydrogel. A) Microscope images of MC3T3-E1 preosteoblast cells stained with Alizarin red before (pre-differentiation) and after (post-diferentiation) 14 days of osteogenic differentiation on HA/PyKC hydrogel. Scale bar = 500 μm. B) Quantification of calcification by Alizarin red staining of MC3T3-E1 preosteoblast before and after 14 days of osteogenic differentiation on HA/PyKC hydrogel. C) Quantification of Alkaline Phosphatase (ALP) activity of MC3T3-E1 preosteoblast cells before and after 14 days of osteogenic differentiation on HA/PyKC hydrogel. Scale bar = 500 μm.

3.3 Conclusions

We have successfully demonstrated the significant effect of a short peptide, PyKC, on the gelation process and hydrogel properties of different biopolymers. Systematic analyses of the composite hydrogels of PyKC with four different biopolymers show that the presence of PyKC enhances the water content, mechanical strength as well as introduces thixotropic property to these biopolymers. Importantly, all these changes are achieved with only 1% doping of the peptide. The composite

hydrogel of HA/PyKC was found to be the most suitable to serve as a scaffold capable of inducing osteogenic differentiation to osteoblast progenitor cells. Matrix mineralization and high ALP activity displayed by the proliferated pre-osteoblast cells on the composite hydrogel adds to its high potential for future bone tissue engineering applications. Moreover, the thixotropic behavior also opens up the possibility of evaluating this composite hydrogel for the purpose of artificial synovial fluid.

3.4 Experimental section

3.4.1 General information and materials

All the protected amino acids and coupling agents, resin were acquired from GL Biochem, China. Gelatin, Sodium Alginate and Proteinase K (from Tritirachium albumin) and Minimum Essential Medium Eagle (αMEM) were purchased from Sigma Aldrich (USA), Sodium Hyaluronate and Chitosan were procured from TCI Chemicals (India). Triethylsilane (TES), trifluoroacetic acid (TFA), N, N - diisopropylethylamine (DIPEA). HPLC-grade dimethylformamide (DMF), and acetonitrile (ACN) were obtained from Spectrochem (India) and Fisher Scientific (India). Milli-Q water with a conductivity of less than 2 μS cm^{-1} was used for all sample preparations. Electrospray ionization mass spectrometry (ESIMS) were performed with a Q-Tof-Micro Quadrupole mass spectrometer (Micromass) and data were analyzed using the built-in software. MALDI analysis were performed with Bruker Daltonics - autoflex™ speed MALDI-TOF instrument.

3.4.2 Synthesis of PyKC

PyKC was synthesized according to the following Scheme 3.2.

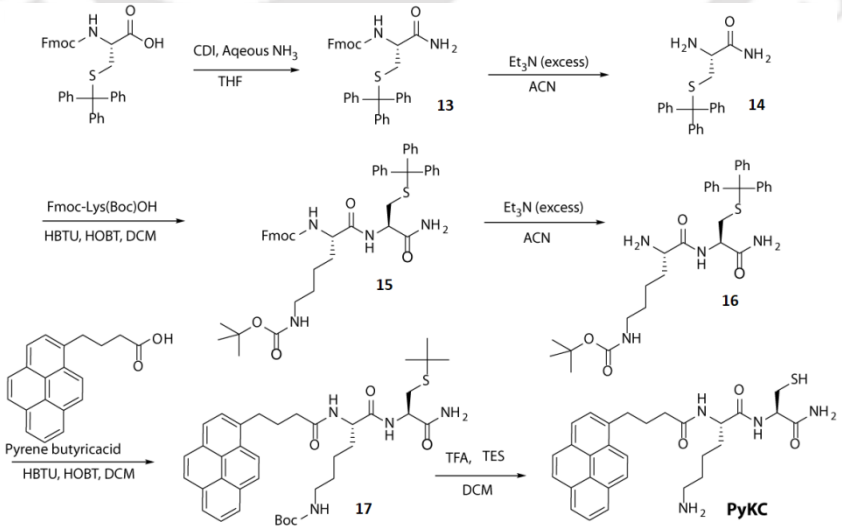

Scheme 3.2 Synthetic route for PyKC

Characterization data

Compound 13

To an ice-cold solutin of Fmoc-Cys(Trt)-OH (2 g, 3.4 mmol) in tetrahydrofuran (THF), Carbonyldiimidazole (CDI, 1.10 g, 6.8 mmol) was charged under nitrogen atmosphere and the mixture was stirred for 3 h. Aqueous ammonia (25%) (1 mL; 13.3 mmol) was added into the reaction mixture and stirred for another 1 h at 0 °C. The reaction was quenched by adding 2N HCl (20 mL). THF was removed under reduced pressure and the aqueous layer was extracted with ethyl acetate. The organic layer was separated, dried over anhydrous Na_2SO_4, filtered and concentrated under reduced pressure. Desired product was purified by column chromatography to obtain the product as a white solid (Yield = 90%) ESI-MS (m/z): calculated, 582.21 for $C_{37}H_{32}N_2O_3S$; found, 605.233 for $[M+Na]^+$; ^1H NMR (400 MHz, $CDCl_3$) δ (ppm) = 7.64 (dd, *J* = 7.6, 5.1 Hz, 2H), 7.45 (d, *J* = 7.6 Hz, 2H), 7.30 (dt, *J* = 8.2, 2.5 Hz, 8H), 7.16 (tdd, *J* = 7.7, 6.3, 2.2 Hz, 9H), 7.12 – 7.06 (m, 3H), 4.32 (dd, *J* = 6.5, 2.8 Hz, 2H), 4.07 (t, *J* = 6.6 Hz, 1H), 3.37 (q, *J* = 7.0 Hz, 1H), 2.62 – 2.46 (m, 2H), 1.10 (t, *J* = 7.0 Hz, 1H). ^{13}C NMR (100 MHz, $CDCl_3$) δ (ppm) = 172.39, 144.43, 129.70, 128.23, 127.93, 127.90, 127.25, 127.22, 127.09, 125.14, 125.09, 120.16, 77.16, 47.33.

Compound 14

Compound **1** (1.7 g, 1 equiv.) was dissolved in acetonitrile (ACN), to which triethylamine (3 mL, excess) was added and stirred for 24 h at room temperature. On disappearance of the starting material, the reaction mixture was extracted with DCM, washed with brine and the organic layer was dried over anhydrous Na_2SO_4. DCM was evaporated and the product was purified by column chromatography to obtain a white solid (yield = 95%). ESI-MS (m/z): calculated, 363.15 for $C_{22}H_{22}N_2OS$; found, 384.776 for $[M+Na]^+$. ^1H NMR (400 MHz, $CDCl_3$) δ (ppm) = 7.34 – 7.27 (m, 6H), 7.15 (dd, *J* = 8.4, 6.7 Hz, 6H), 7.09 (d, *J* = 7.2 Hz, 3H), 6.70 – 6.63 (m, 1H), 5.82 – 5.74 (m, 1H), 2.86 (dd, *J* = 8.5, 4.0 Hz, 1H), 2.58 (dd, *J* = 12.8, 4.0 Hz, 1H), 2.41 (dd, *J* = 12.8, 8.5 Hz, 1H). ^{13}C NMR (150 MHz, $CDCl_3$) δ (ppm) = 176.26, 144.59, 129.62, 128.03, 126.86, 67.04, 53.96, 37.24.

Compound 15

Fmoc-Lys (Boc)-OH (1.07 g, 1 equiv.), HOBT (0.425 g, 1.1 equiv.) HBTU (0.48 g, 1.1 equiv.) and DIPEA (0.43 mL, 1.1 equiv.) were taken in dry DCM under argon atmosphere and stirred for 30 min at 0 °C. A solution of compound **2** (0.9 g, 1 equiv.) in dry DCM, was added to the mixture under cold condition and was allowed to come to room temperature. After 24 h, the reaction mixture was extracted with DCM, washed with brine and the organic layer was dried over anhydrous Na_2SO_4. After evaporating the DCM, the crude mixture was purified using column chromatography. The product obtained was a light-yellow solid (yield = 75 %). MALDI-TOF (m/z): calculated, 812.36 for $C_{48}H_{52}N_4O_6S$; found, 835.43 for $[M+Na]^+$; ^1H NMR (600 MHz, $CDCl_3$) δ (ppm) =7.78 (d, *J* = 7.6 Hz, 2H), 7.59 (dd, *J* = 7.6, 2.9 Hz, 2H), 7.42 (d, *J* = 7.8 Hz, 8H), 7.33 – 7.27 (m, 8H), 7.20 (t, *J* = 7.2 Hz, 3H), 6.66 (s, 1H), 6.35 (s, 1H), 5.83 (s, 1H), 5.57 (s, 1H), 4.39 (d, *J* = 6.9 Hz, 2H), 4.18 (t, *J* = 6.9 Hz, 2H), 4.09 (s, 1H), 3.16 – 2.99 (m, 2H), 2.78 (s, 1H), 2.65 – 2.54 (m, 1H), 1.87

(s, 4H), 1.45 (s, 13H), 1.35 (s, 2H); ^{13}C NMR (150 MHz, $CDCl_3$) δ(ppm) =172.24, 171.89, 144.41, 129.63, 128.19, 127.90, 127.89, 127.25, 127.02, 125.18, 120.12, 67.29, 53.57, 52.02, 47.23, 33.20, 29.78, 28.56, 22.27.

Compound 16

Compound **3** (1.43 g, 1 equiv.) was dissolved in ACN, to which triethylamine (3 mL, excess) was added and stirred for 36 h at room temperature. The reaction mixture was extracted with DCM, washed with brine solution, and the organic layer was dried over anhydrous Na_2SO_4. DCM was evaporated and the product was purified using column chromatography to obtain a white solid (yield = 95%). MALDI-TOF (m/z): calculated, 590.29 for $C_{33}H_{42}N_4O_4S$; found, 613.25 for $[M+Na]^+$; ^{1}H NMR (600 MHz, $CDCl_3$) δ(ppm) =7.73 (s, 1H), 7.40 (d, *J* = 7.8 Hz, 6H), 7.28 (t, *J* = 7.6 Hz, 6H), 7.21 (t, *J* = 7.3 Hz, 3H), 6.25 (s, 1H), 5.56 (s, 1H), 4.62 (s, 1H), 3.99 (s, 1H), 3.35 (s, 1H), 3.11 (s, 1H), 3.05 (s, 1H), 2.67 (dd, *J* = 13.1, 8.1 Hz, 1H), 2.61 (dd, *J* = 13.0, 5.6 Hz, 1H), 1.76 (s, 1H), 1.42 (s, 13H), 1.37 (t, *J* = 7.3 Hz, 2H); ^{13}C NMR (150 MHz, $CDCl_3$) δ(ppm) = 175.56, 172.24, 144.41, 129.60, 128.06, 126.89, 67.15, 54.91, 51.73, 46.11, 34.46, 33.11, 29.85, 28.45, 22.75.

Compound 17

Pyrene butyric acid (0.414 g, 1 equiv.), HOBT (0.202 g, 1.1 equiv.) HBTU (0.567 g, 1.1 equiv.) and DIPEA (0.58 mL, 1.1 equiv.) were taken in dry DCM under argon atmosphere and stirred for 30 min at 0 °C. A solution of compound **4** (0.9 g, 1 equiv.) in dry DCM, was added to the mixture under cold condition and was allowed to room temperature. After 24 h, the reaction mixture was extracted with DCM, washed with brine, and the organic layer was dried over anhydrous Na_2SO_4. After evaporating the DCM, the crude mixture was purified using column chromatography. The product obtained was a light green solid (yield = 65%). MALDI-TOF (m/z): calculated, 860.40 for $C_{53}H_{56}N_4O_5S$; found, 883.541 for $[M+Na]^+$; ^{1}H NMR (400 MHz, $CDCl_3$) δ(ppm)= 8.24 (d, *J* = 9.3 Hz, 1H), 8.16 (d, *J* = 7.6 Hz, 2H), 8.08 (dd, *J* = 8.5, 2.6 Hz, 2H), 8.01 (d, *J* = 4.4 Hz, 2H), 7.98 (d, *J* = 7.6 Hz, 1H), 7.80 (d, *J* = 7.8 Hz, 1H), 7.37 (dd, *J* = 7.6, 1.8 Hz, 6H), 7.23 (t, *J* = 7.6 Hz, 6H), 7.19 – 7.12 (m, 3H), 6.61 (dd, *J* = 22.1, 7.0 Hz, 2H), 6.43 (s, 1H), 5.51 (d, *J* = 6.7 Hz, 1H), 4.73 (d, *J* = 6.4 Hz, 1H), 4.33 – 4.10 (m, 2H), 3.40 – 3.21 (m, 2H), 3.12 – 2.99 (m, 2H), 2.88 – 2.77 (m, 1H), 2.52 (dd, *J* = 13.0, 5.2 Hz, 1H), 2.33 (t, *J* = 7.3 Hz, 2H), 2.24 – 2.09 (m, 3H), 1.69 (s, 6H), 1.65 – 1.53 (m, 2H), 1.36 (s, 12H), 1.28 (d, *J* = 11.8 Hz, 13H), 0.93 – 0.81 (m, 5H). ^{13}C NMR (150 MHz, $CDCl_3$) δ(ppm)= 173,93, 172.45, 172.00, 144.38, 135.84, 131.47, 130.00, 129.60, 128.13, 127.58, 127.48, 127.45, 126.96, 126.77, 125.93, 125.14, 125.04, 124.98, 124.91, 124.87, 123.45, 79.29, 77.37, 77.16, 76.95, 67.18, 53.80, 52.12, 46.09, 39.63, 35.74, 33.41, 32.87, 31.33, 29.79, 29.75, 28.50, 27.33, 22.38.

PyKC

Compound **5** was taken in 80% TFA – DCM containing 1% triethylsilane and stirred at room temperature for 1h. The solvent and TFA were removed under reduced pressure and the crude material was slowly added to cold dry diethyl ether to precipitate PyKC. The solid was washed several times with diethyl ether and the purity of the solid was checked by analytical HPLC. ESI-MS calculated. 518.24 for

$C_{29}H_{34}N_4O_3S$, found: 519.24 (m/z). ^{1}HNMR (DMSO-d_6, 400 MHz): δ (ppm) = 8.39 (d, J = 9.3 Hz, 1H), 8.28 (m, 2H), 8.23 (m, 2H), 8.14 (d, J = 2.0 Hz, 2H), 8.07 (t, J = 7.6 Hz, 1H), 7.97 (t, J = 8.2 Hz, 2H), 7.66 (s, 3H), 7.29 (s, 1H), 7.20 (s, 1H), 4.39 – 4.21 (m, 2H), 2.90 – 2.66 (m, 4H), 2.29 (m, 3H), 2.03 (m, 2H), 1.69 (m, 1H), 1.55 (m, 3H), 1.35 (d, J = 35.3 Hz, 2H). ^{13}C NMR (100 MHz, DMSO-d_6): δ (ppm) = 172.96, 172.31, 171.87, 137.06, 131.36, 130.90, 129.78, 128.06, 127.93, 127.70, 126.99, 126.63, 125.42, 125.26, 124.03, 55.06, 53.19, 39.18, 35.29, 32.71, 31.44, 28.00, 27.10, 26.58, 22.82.

3.4.3 Preparation of the hydrogel

PyKC stock solution (2 wt%) was prepared in Tris buffer and was used immediately to avoid any dimerization before the composite hydrogel preparation. Hyaluronic acid and sodium alginate stock solutions of 20 wt % were prepared by overnight stirring or shaking in ultrapure water. Chitosan stock solution of 20 wt % was prepared in 0.1 M acetic acid solution by overnight stirring. For Gelatin, a readymade 2% solution in water available from Sigma was used directly. For composite hydrogel formation, two components were mixed in 1:1 ratio by volume (to attain a final concentration of 10 wt% for HA, Alg and Cht while the concentration of PyKC remain 1 wt%). The mixing was followed by 30 sec vortexing followed by 24 h incubation at room temperature. For Gel composite hydrogel, the same protocol of mixing was followed while the final concentration of Gel was maintained at 1 wt%. For the hydrogels of pure biopolymers, solutions of the biopolymers were prepared following the above-mentioned protocols and the respective concentrations were maintained in the final solutions before they were incubated for 24 h at room temperature to form the hydrogels. However, Alg and Gel failed to form hydrogels at 10 and 1 wt.% concentrations respectively.

3.4.4 Field emission scanning electron microscopy (FESEM)

Small portions (5 µL) of 24 h matured composite and pure biopolymer hydrogels were cast on silicon wafers and dried under ambient condition for 24 h. Images were taken on a Gemini SEM 300 (Sigma Zeiss; FESEM) instrument.

3.4.5 Swelling property

All the pure and composite biopolymer hydrogels were freeze dried individually and weights of the hydrogels were noted (W_d), and the dried disc shaped materials were immersed in large excess of water at room temperature for a definite time. The dispersion of water-swollen gels was centrifuged, taken out of the bulk water and weighed (W_s). The measurements were performed at different time intervals up to 24 h and repeated three times to get mean values for calculations. The swelling ratio (SR) were calculated following equation (1)

$$SR = \frac{W_s - W_d}{W_d} \times 100\% \quad (1)$$

3.4.6 Stability of Hydrogels toward proteolytic digestion

The enzymatic degradation of the hydrogels were carried out by using proteinase K enzyme assay. To characterize the enzymatic degradation of the hydrogels, a small portion of each hydrogel sample was placed in a 1.5 ml centrifuge tube and incubated with 1 ml of proteinase K solution (3 units/mL) in HEPES buffer (20 mM, pH 7.4). To maintain enzymatic activity, buffer solution was replaced every 24 h. After a predetermined time, the samples were removed from the solution, soaked with the tissue paper and weighed. The experiments were performed in triplicate to get the mean values. The percentage degradation was calculated by the ratio of the final weight to the original weight of the hydrogels.

3.4.7 Stability of hydrogel in cell culture medium

The composite hydrogel, HA/PyKC was prepared in a glass vial. α-MEM supplemented with 10% fetal calf serum, 100 U/mL penicillin, and 100 U/mL streptomycin was then added on top of the hydrogel and incubated at 37 °C. Photographs were taken at different time points.

3.4.8 Rheology

The rheological measurements of the pure biopolymer and composite hydrogels were done with the use of an Anton Paar MCR 102 rheometer equipped with a 20 mm parallel plate (with 0.3 mm zero gap) measuring system at 25 °C. For the oscillatory tests, an amplitude strain sweep was carried out at frequency of 1 Hz and deformation ranging from 0.01 to 1000%. The frequency sweep was made in controlled deformation (fixed from the range of linear viscoelasticity (LVE) determined through amplitude sweep measurements), and in a frequency range from 0.1 to 100 rad/s. Cyclic dynamic strain sweep experiment was performed at a constant angular frequency of 1 rad s^{-1} by altering the applied strain from 0.1 to 1000%. In this experiment, a higher strain (γ = 1000%) and a lower strain (γ = 0.1%) are applied on the gel alternatively over a period of five successive cycles. For temperature dependent rheological experiments, amplitude sweep and frequency sweep experiments were performed at room temperature (25 °C), physiological temperature (37 °C) and at 50 °C. For temperature sweep experiment, samples were allowed to equilibrate on the rheometer at 25 °C for 3 min prior to the temperature-sweep measurements. Following this, the temperature was raised from 25 °C to 50 °C at 1 °C/min at a constant frequency of 1 Hz and constant amplitude of 10 % and the viscosity values were recorded. For Shear stress versus shear rate hysteresis cycles were performed at three stages. At first the shear rate was increased linearly from 5 s^{-1} to 110 s^{-1}. In

the second stage, the shear rate was maintained at 110 s^{-1}. In the final stage, the shear rate was decreased linearly from 110 s^{-1} to 5 s^{-1} and the shear stress was measured accordingly.

3.4.9 Cell Viability on the composite hydrogel

Murine MC3T3-E1 preosteoblast cells were cultured in alpha-minimum essential medium (α-MEM) supplemented with 10% fetal calf serum, 100 U/mL penicillin, and 100 U/mL streptomycin in a petri dish at 37 ^{0}C in a humidified atmosphere in an incubator containing 5% CO_2. Hydrogels formed in 96-well plate were washed with culture medium several times over 2 days followed by UV sterilization for 30 min. Cells were then seeded on the hydrogels and incubated at 37 °C in a humidified atmosphere containing 5% CO_2. Cell viability was finally assessed using MTT assay 3 days after seeding for the non-differentiating cells. MTT stock solution (5 mg/mL) was prepared in phosphate buffer saline (PBS). 20 µL from this solution was added to each well followed by a 4 h incubation. The MTT reduced adduct (Formazan) formed were then extracted by the addition of 100 µL DMSO in each well and shaking for 20 min. Finally, the absorbance from each well were recorded using Tecan Spark plate reader (at 570 nm) while the background correction was done at 680 nm.

The qualitative cell viability assessment of HA-PyKC composite hydrogel was performed using the Live/Dead staining at the same time point as those of MTT studies. Hydrogels were prepared in 24-well plate and rinsed repeatedly with culture medium, followed by UV sterilization, for 2 days. Then, cells were seeded on the hydrogels for 3 days. A solution containing fluorescein diacetate (6.6 µg/mL, for live cells) and propidium iodide (5 µg/mL, for dead cells) was then used for Live/Dead staining. The labelled cells were immediately viewed using a Nikon Eclipse Ti fluorescent microscope and images were captured by a Zyla scMOS camera using Nikon Intensilight C-HGFI fluorescent lamp.

3.4.10 Alkaline phosphatase (ALP) activity

For intracellular ALP activity, hydrogels were formed in a 96-well plate and rinsed repeatedly with culture medium, followed by 30 min UV sterilization, for 2 days. 3000 MC3T3-E1 preosteoblasts were then seeded on the prewashed hydrogels and supplemented with differentiation medium (ascorbic acid and beta-glycerophosphate) every 2 days for a period of 14 days. After that period, the hydrogels were stained with 100 µL ALP substrate solution containing 4-Methylumbelliferyl phosphate (4-MUP) and incubated for 30 min in dark. Finally, fluorescence was measured (λ_{ex} = 360 nm and λ_{em} = 440 nm). Each reading was normalized to the cell count in each hydrogel.

3.4.11 Mineralization assay

Alizarin red staining assay, which quantifies the amount of mineralization arising from bone nodule formation, was used to determine the extent of matrix mineralization of MC3T3-E1 preosteoblasts on the hydrogels. The hydrogels were formed in a 24-well plate and washed repeatedly with culture medium, followed by UV sterilization for 30 min, for 2 days. 3000 MC3T3-E1 preosteoblasts were seeded on the prewashed hydrogels and supplemented with differentiation medium containing ascorbic acid and beta-glycerophosphate every 2 days for a period of 14 days. The amount of induced calcification was quantified by Alizarin red staining. After washing off excessive dyes, optical light images were acquired from each well. The deposited calcium were dissolved in 2:1 MeOH/AcOH buffer the following day and shaken for 45 mins to ensure complete dissolution of the calcified matrix. The percentage of calcification was finally quantified by reading the absorbance of these solutions at 405 nm. Each reading was normalized to the cell count in each hydrogel.

Indian Institute of Technology Guwahati

Chapter 4: Dual Dynamic Covalent Bond Mediated Polymer-Peptide Coacervate

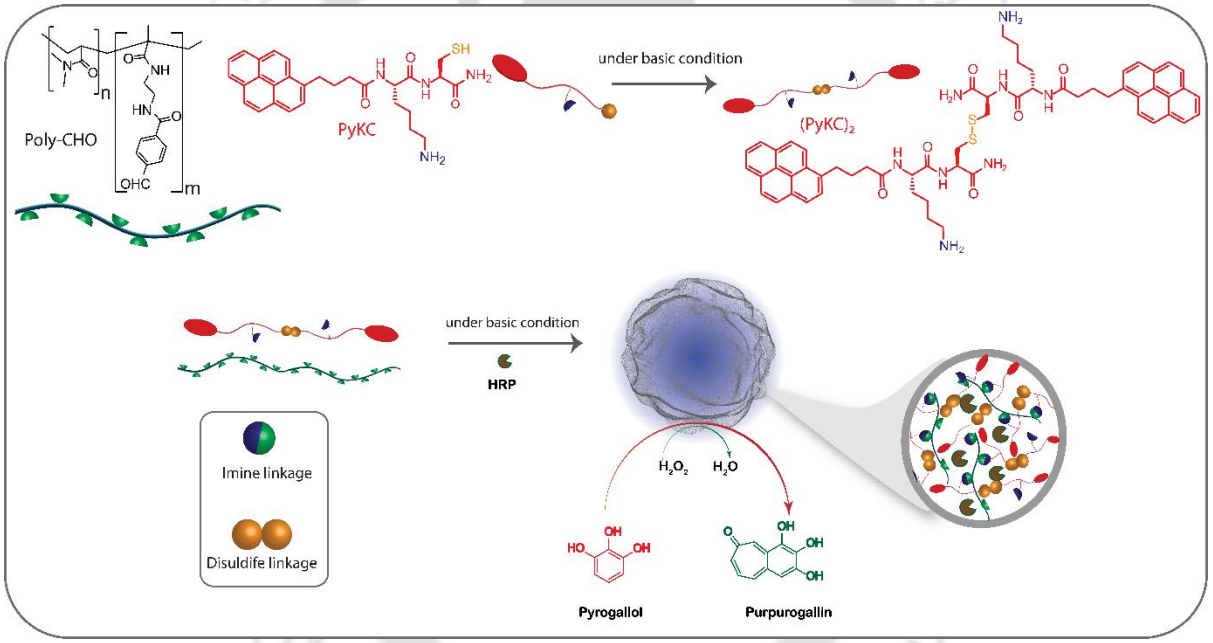

Indian Institute of Technology Guwahati

4.1 Introduction

A variety of functionalities define living systems, including compartmentalization, metabolism, replication, and adaptation[237]. One of science's most fundamental concerns is how such sophisticated, life-like behavior can originate from a collection of molecules. Researchers have been working on creating and building progressively plausible protocells, the most basic compartments from which living cells could have emerged[238]. Liposomes, compartments surrounded by membranes consisting of lipids or fatty acids, have been postulated as clear candidates for protocellular compartments because of their similarities to current cells. Many of these protocells with a membrane shell are difficult to spontaneously develop. Membraneless compartments, such as coacervates, could have created an alternate type of protocell, as hypothesized by Oparin in his study on the origins of life in the 1930s, following Bungenberg-de Jong's introduction of coacervates in 1929. Since the mid-twentieth century, coacervates have been studied primarily in the context of food science research. Coacervates are condensed liquid-like droplets generated by many weak associative contacts between molecules through liquid-liquid phase separation, and they disintegrate in response to biochemical signals in cells after being dynamically formed. The droplets can be nanometers or microns in diameter and resemble an emulsion, but they don't need to contain surfactants or other stabilizing chemicals[239]. Short peptides, as well as lengthy polymers, have recently been discovered to be capable of producing simple and complicated coacervates. Coacervates are intriguing protocell models because the coacervate droplets they form behave as compartments that sequester and concentrate a wide spectrum of solutes[240]. Without the use of a membrane, coacervation is a potent technique for compartmentalization. Natural cellular coacervates include organelles such as stress granules, Cajal bodies, and P granules[241-244]. These naturally occurring membrane-less organelles are thought to be generated via the liquid-liquid phase separation (LLPS) of intrinsically disordered proteins and RNA, and they play an important role in cellular functions such as RNA metabolism[245].

Numerous complex and simple coacervate-based droplets are reported that are used to understand the memebrnane-less organelles.[246-254] Synthetic complex coacervates are commonly prepared via electrostatic attachment of oppositely charged synthetic polymers like polypeptides or polynucleotides.[251, 255-259] Apart from electrostatic interactions, other non-covalent interactions like π–π stacking, cation-π interaction, hydrogen bonding, and hydrophobic interactions also play a crucial role toward the phase separation.[252] However, coacervates based on neutral molecules are rarely reported.[260]

We created a neutral polymer – short peptide based coacervate that forms through two dynamic covalent linkages, imine and disulphide bonds, and these coacervates can sequester a variety of

enzymes, proteins, and dyes. Finally, HRP was encapsulated inside the coacervate and shown to be protected from excess H_2O_2 present in the bulk solution.

4.2 Results and discussion

For this purpose, we planned to synthesize an aldehyde-appended polymer (Poly-CHO, Scheme 4.1) and use Cystamine to crosslink the polymer. We envisioned that when mixed in neutral to basic condition, the aldehyde and the amine groups of Cystamine will form imine bonds and thereby lead to the formation of the coacervates.[261] However, when Poly-CHO was mixed with Cystamine in different weight ratios at pH 8, no phase separation was observed. The turbidity of the systems was measured at 600 nm which did not result in any noticeable enhancement in the optical density. Under electron microscope, we could observe the formation of droplets of ~ 50 nm (Figure 5.6). We anticipated that the lack of hydrophobicity in the system is presumably not allowing LLPS.

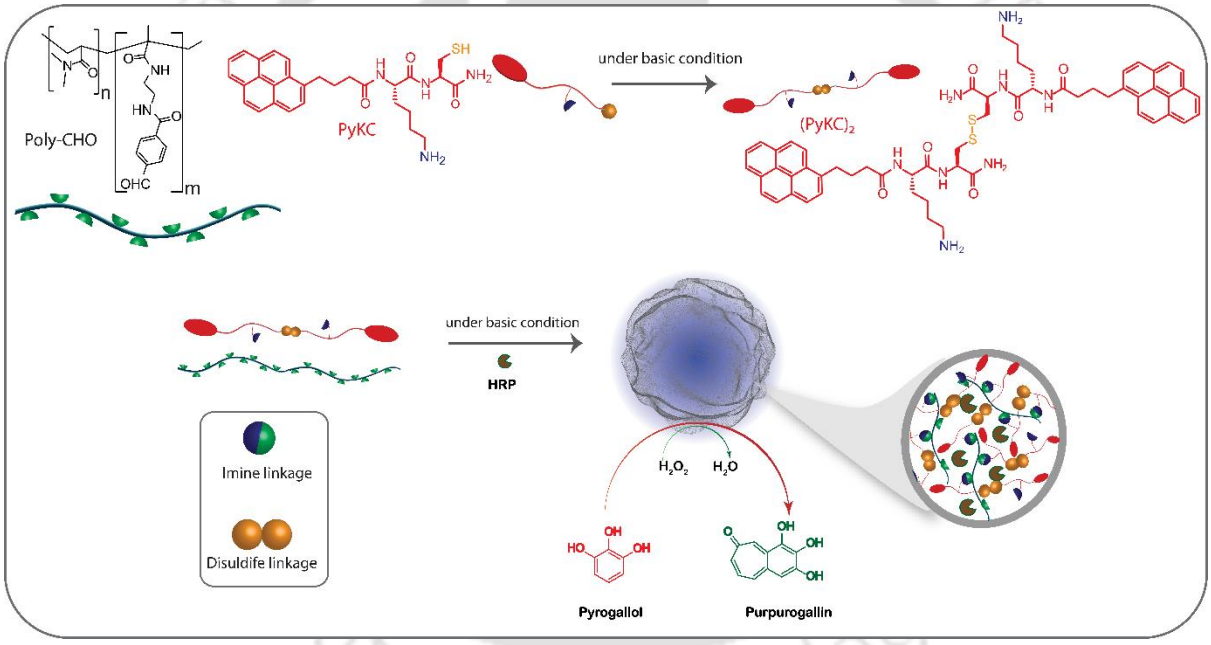

Scheme 4.1 Chemical structures of Poly-CHO, PyKC, and $(PyKC)_2$, and schematic representation of HRP entrapped coacervate with enzymatic reaction.

In order to introduce hydrophobic interaction, Cystamine was replaced with PyKC (Scheme 4.1). PyKC is a well-studied short peptide from our group that is capable of forming supramolecular hydrogel upon disulphide-linked dimerization at a higher concentration (10 mg/mL).[262-264] Under basic condition, PyKC forms the disulphide-linked dimer $(PyKC)_2$ (Scheme 4.1).[262] However, the dimerization process takes ~ 12 h in absence of any oxidizing agent like, H_2O_2. Thus, we decided to use preformed $(PyKC)_2$ for the coacervation tests. $(PyKC)_2$ and Poly-CHO were mixed in different

weight ratios (1:1 – 1:20, with respect to 0.3 mg of PyKC/mL, much lower than the minimum gelation concentration of PyKC (10 mg/mL))[262] at pH 8 (20 mM Tris buffer). The solutions became turbid indicating possible formation of the coacervates (Figure 4.1).

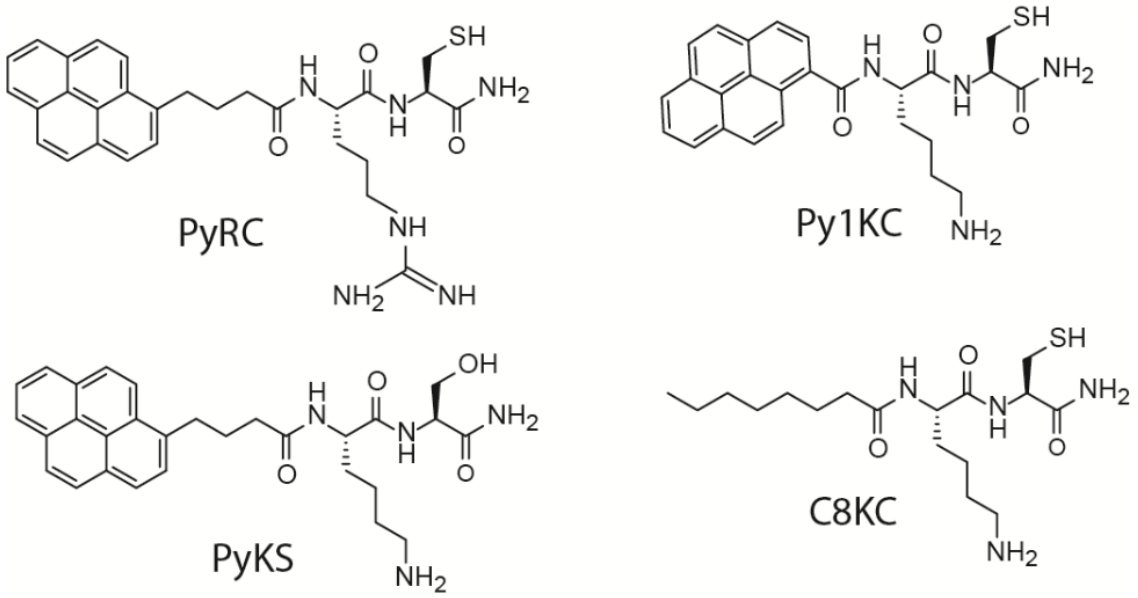

Chart 4.1 Turbidity of different compositions of polymers and peptides.

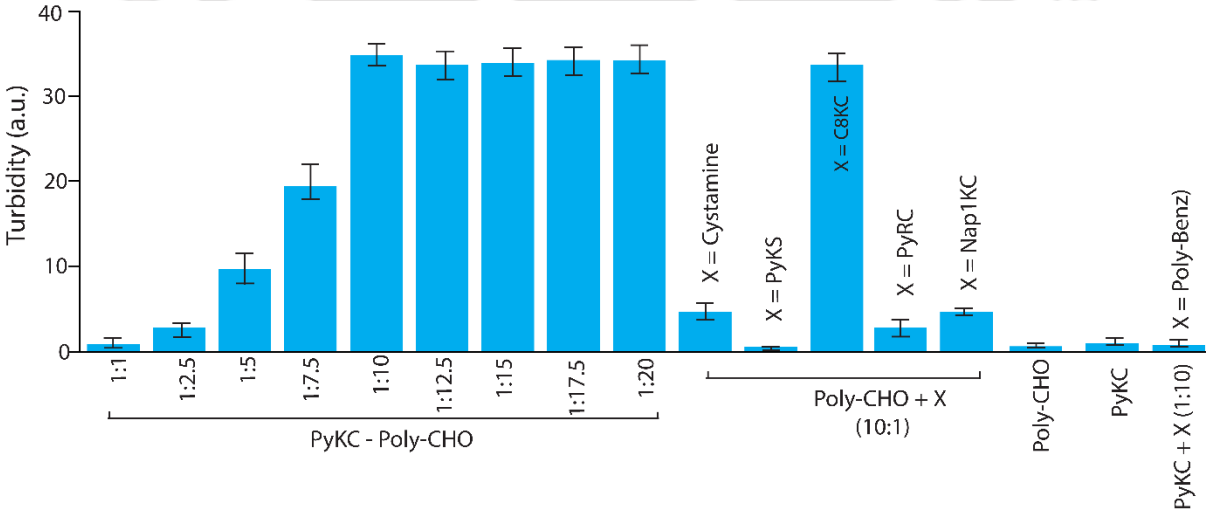

Figure 4.1 Turbidity of different compositions of polymers and peptides.

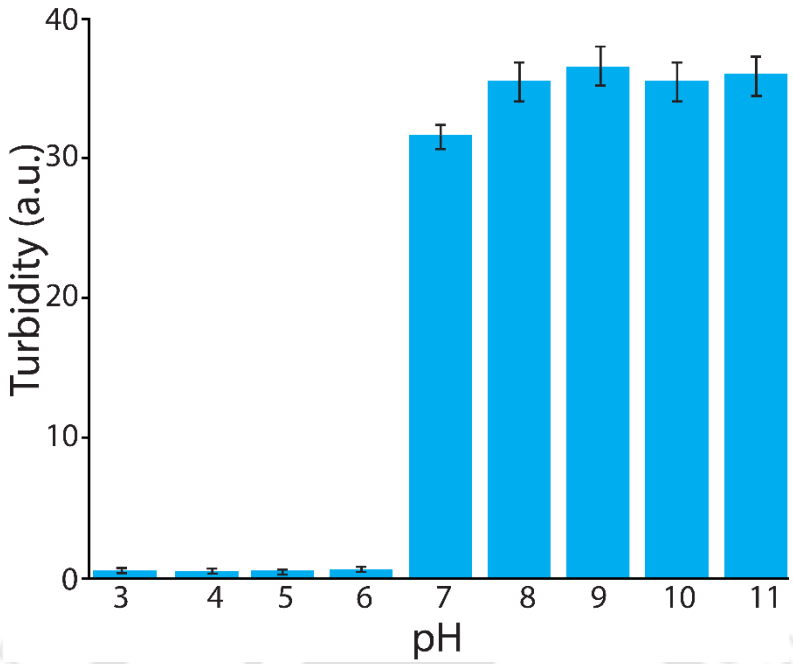

Figure 4.2 Turbidity of $(PyKC)_2$–Poly-CHO (1:10) solutions at different pH.

Importantly, below 1:5 ratios, very little turbidity was noted and droplets of ~ 50-300 nm size were observed. Above this ratio, turbidity enhanced with an increase in Poly-CHO content, and above 1:10, no further increase was observed. Under phase-contrast microscope, homogeneous microdroplets with an average diameter of ~10 μm was observed (Figure 4.5). The obtained morphology is strikingly different than only PyKC or Poly-CHO solutions under similar conditions (Figure 4.5). Based on these observations, the composition of 1:10 PyKC – Poly- CHO was used for further studies. A phase diagram is prepared by measuring the turbidity of solutions with various compositions at different pH (Figure 4.3 A).

Further, we measured the water content[247] of the coacervates formed by this composition at pH 8 and found that the droplets contain high amount of water (77 ± 3%). The coacervates were found to be stable for more than 24h as no change in the turbidity was observed within this period. The coacervates were also found to be stable in presence of high concentration of urea, a well-known chaotropic agent, demonstrating no prominent role of hydrogen bonding (Figure 4.3 B). When the coacervates were subjected to heating, up to 50 °C, no change in the turbidity was observed (Figure 4.3 B). However, above this temperature, the turbidity enhanced indicating possible coalescence of the coacervates.

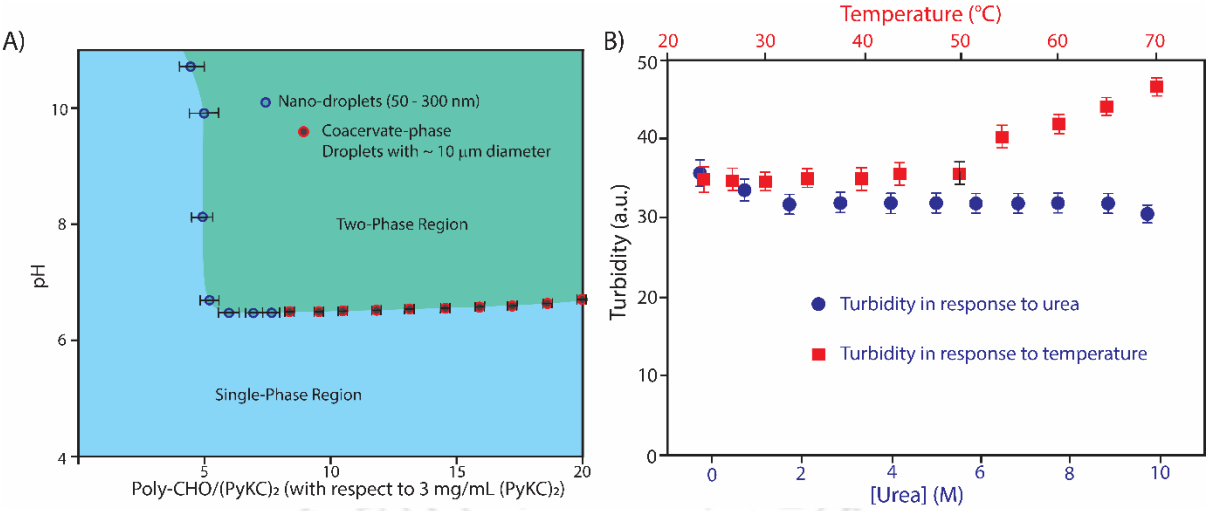

Figure 4.3 A) Phase diagram of PyKC – Poly-CHO measured at room temperature. B) Effect of urea and temperature on the turbidity of coacervates formed by $(PyKC)_2$ – Poly-CHO in 20 mM Tris buffer pH 8.

Next, we monitored the pyrene emission of PyKC during the coacervation. At lower pH, for 1:10 $(PyKC)_2$ – Poly-CHO, along with the characteristic monomeric signals of pyrene (375 – 425 nm), a strong excimer emission centered at 480 nm was observed. However, as we moved to the basic pH, the emission quenched completely (Figure 4.4 B). When, the solution at pH8 was treated with a well-known disulphide bond breaker TCEP (Tris(2-carboxyethyl)phosphine hydrochloride), both, monomeric as well as the excimer emissions returned back. To check whether the quenching of the pyrene emission is associated with the coacervation, the pH dependent turbidity measurements were performed. $(PyKC)_2$ and Poly-CHO (1:10) were taken in buffers of different pH (3 – 11). Extremely low turbidity (< 2) was observed at acidic pH. The turbidity value showed a prominent jump (>30) at and above pH 7 (Figure 5.2). However, with further increase in pH, no change in the turbidity was noticed. The turbidity value perfectly corroborated with the quenching of the pyrene emission. Thus, both techniques can be utilized to evaluate the coacervate formation. The observed quenching of the pyrene emission upon caocervation can be explained by the encapsulation of the pyrene units within the cross-linked polymer. This brings the pyrene units close to the acrylamide groups which are known for their ability to quench pyrene emission especially in aggregated states.[265, 266]

The failure of Cystamine and success of PyKC/$(PyKC)_2$ to form coacervates leads to the assumption that pyrene-butyric acid moiety of PyKC reinforces hydrophobic interaction within the coacervates. To confirm that, Py1KC, and C8KC (Chart 4.1) were tested for coacervation with Poly-CHO. Interestingly, only C8KC (Figures 5.1 and 5.6) showed similar sized coacervates like PyKC confirming the hydrophobic role of pyrene-butyric acid group. However, we continued the work with PyKC as the presence of pyrene unit allows us to monitor the coacervation process using emission spectroscopy.

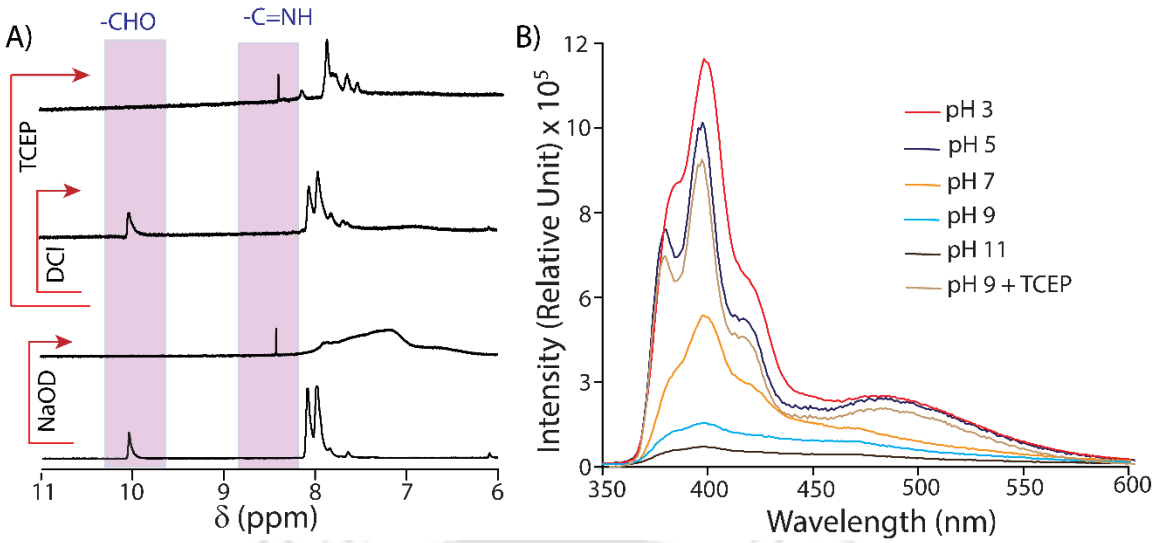

Figure 4.4 A) Partial ^{1}H NMR spectra of $(PyKC)_2$–Poly-CHO (1:10) in D_2O (containing a drop of DCl) before and after sequential addition of NaOD, DCl or TCEP as mentioned in the figure. B) Emission spectra of $(PyKC)_2$–Poly-CHO (1:10) under different conditions.

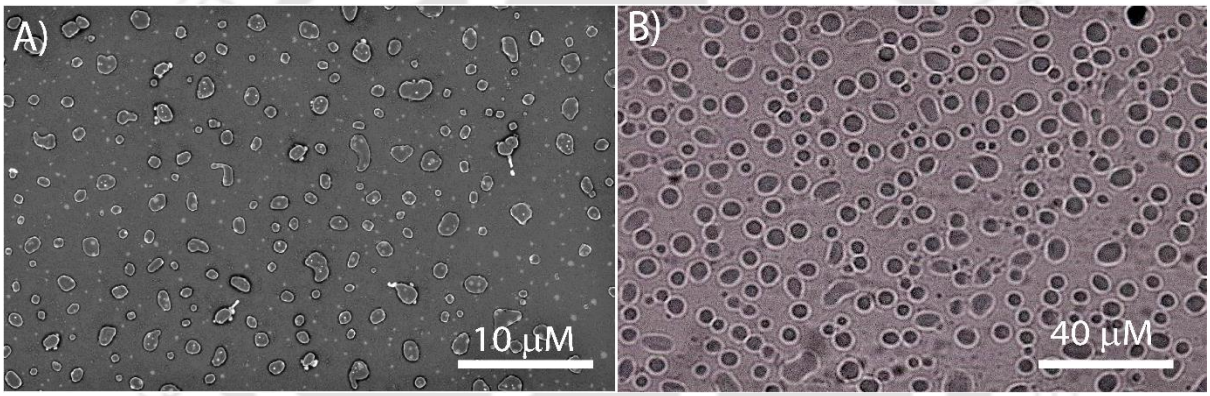

Figure 4.5 A) Optical microscopic image and B) FESEM image of coacervates formed by 1:10 $(PyKC)_2$–Poly-CHO.

The coacervation in the present case is supposed to be driven by two simultaneous dynamic processes, a) formation of imine linkages; and b) disulphide bond formation. Both processes are facilitated in basic condition and lead to cross-linking of the polymer. ^{1}H NMR study of the systemPyKC – Poly-CHO) showed appearance of the imine signal and disappearance of the aldehyde signal in presence of NaOD (Figure 4.4 A).

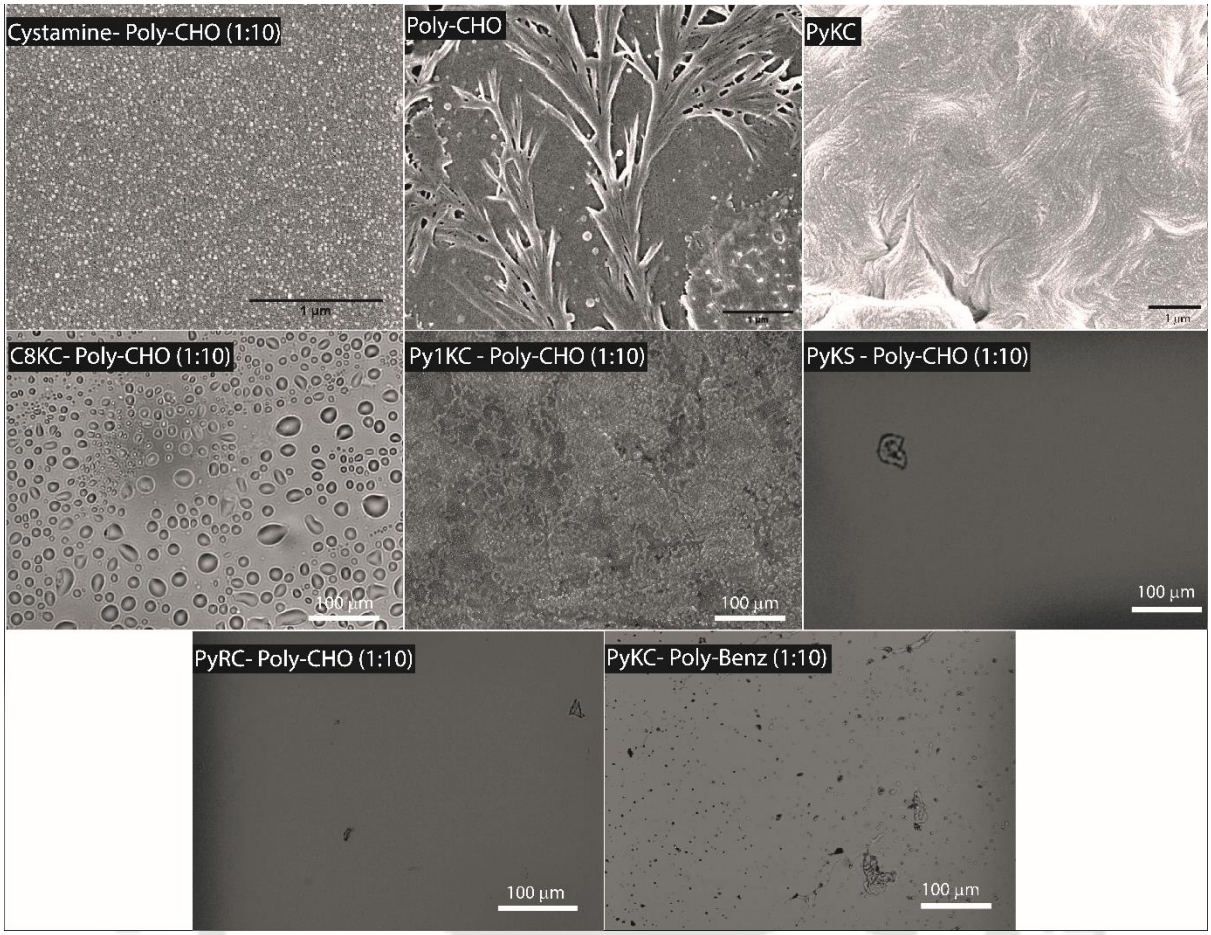

Figure 4.6 FESEM images of Poly-CHO, PyKC and different combinations of peptides and polymers. All solutions were prepared in 20 mM Tris buffer pH 8 at room temperature.

The same solution after treatment with excess DCl resulted into disappearance of the imine proton peak while the aldehyde signal reappeared. All these observations demonstrate the critical role of the imine linkages toward coacervation. Interestingly, in a separate experiment, when the NaOD treated solution was further treated with TCEP, no change in the imine/aldehyde signal was observed. However, the broad peak in the aromatic region (owing to coacervation) became sharp.

The sharpening of the aromatic protons is a result of the dissolution of the coacervates as the disulphide linkages are broken. Moreover, when a mixture of PyKC – Poly-CHO in D_2O was treated with H_2O_2, no noticeable change in the aldehyde peak was observed. Additionally, we have also prepared two similar peptides, PyKS and PyRC, and used them separately with Poly-CHO. Under similarexperimental conditions, both peptides failed to form any coacervate as monitored by turbidity measurements and optical microscopic analysis (Figures 5.1 and 5.5). Moreover, when PyKC was mixed with a similar polymer (Poly-Benz, Scheme 4.1) that lack any aldehyde group, no coacervation was observed (Figure 4.1). All these results confirm the critical role of both dynamic linkages toward coacervation.

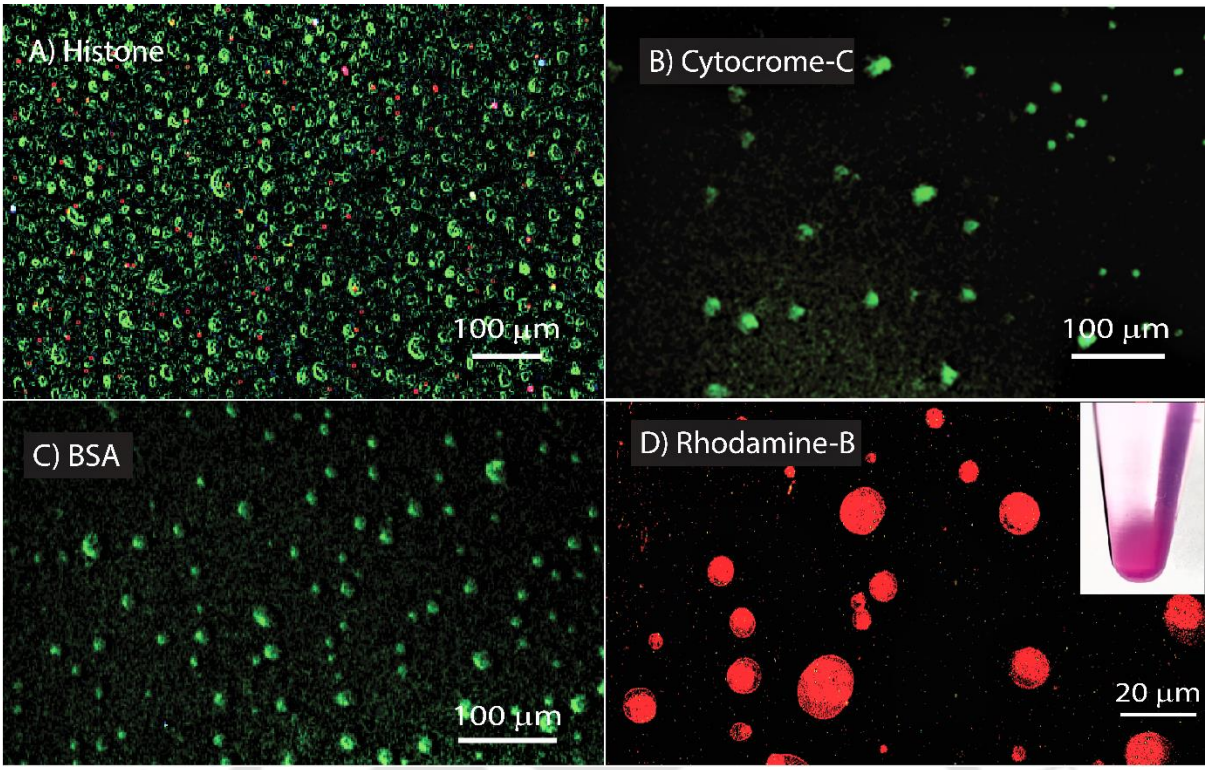

Figure 4.7 A)-C) Optical microscope images of different protein (FITC-labelled) loaded coacervates formed by PyKC – Poly-CHO. **D)** Rho loaded coacervates (Inset: the coacervates after centrifugation).

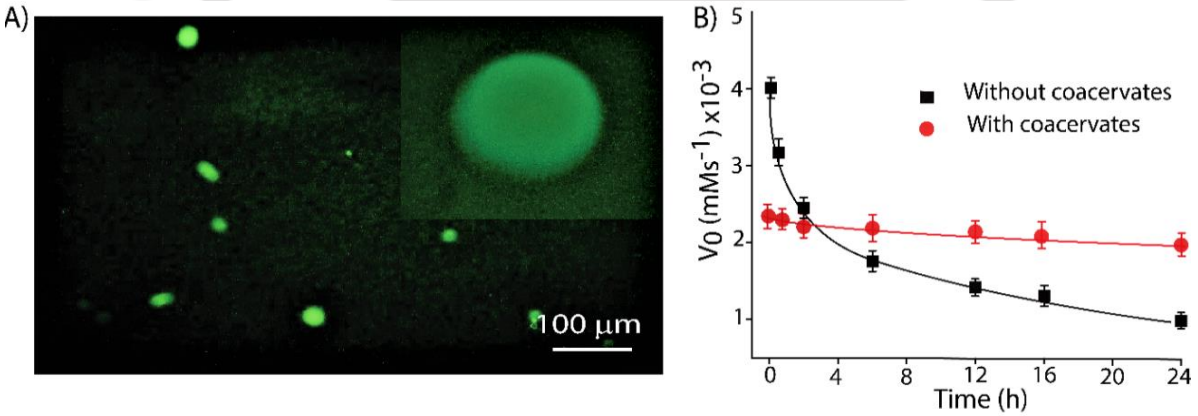

Figure 4.8 A) FITC-HRP loaded coacervates (Inset: magnified image of one of the coacervates). B) Activity profile against time for free and coacervate entrapped FITC-HRP.

The condensates of living systems are known to encapsulate guests (small molecules and proteins) and modulate the activity/property of the guests.[248, 267] Similar to natural condensates, the Poly-CHO – PyKC system could also encapsulate small dye like Rhodamine B (Rho) and different proteins (HRP(horseradish peroxidase), Cytochrome C, histone, BSA (Bovine serum albumin) [Figure 4.7]. When prepared in presence of Rho and FITC-HRP, the condensates showed moderate encapsulation (72 % of Rho and 51% of FITC-HRP) of these two molecules (Figures 4.7 and 4.8). The elemental mapping of FITC-HRP loaded coacervates showed uniform distribution of iron across the coacervates (Figure 4.9).

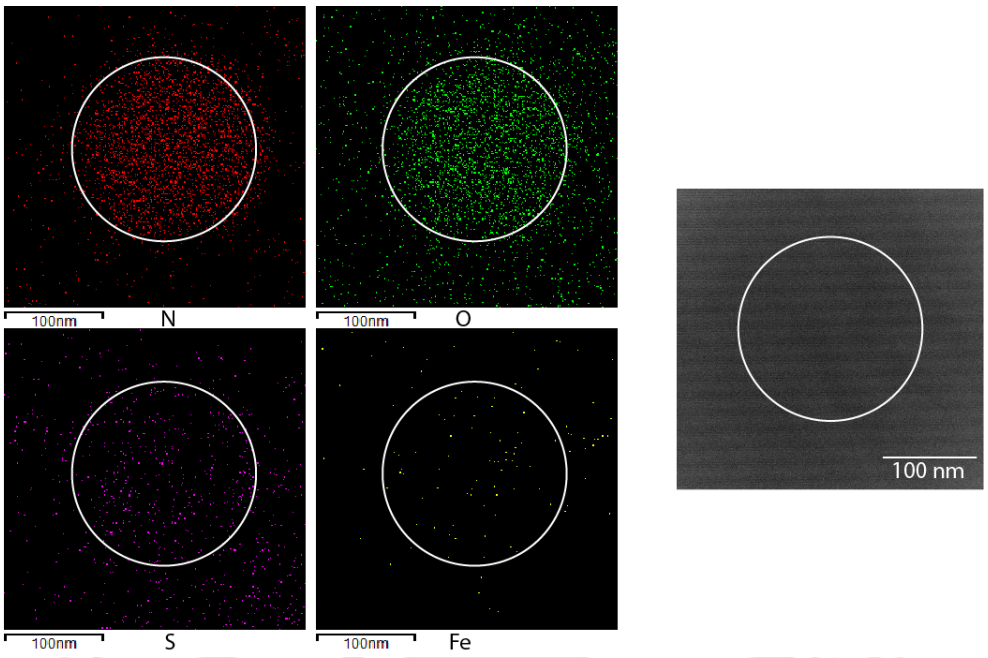

Figure 4.9 Elemental mapping of FITC-HRP encapsulated coacervates formed by PyKC – Poly-CHO (1:10) showing the uniform distribution of iron across the coacervates. One coacervate was chosen under the microscope and zoomed in to 100 nm scale before the elemental mapping was performed.

The encapsulated protein was then tested for its biocatalytic efficiency using H_2O_2 and pyrogallol and the rate of formation of purpurogallin was monitored. The initial velocity (V_0) was found to be lower than that of the free enzyme (without coacervates). However, the activity of the free enzyme decreased rapidly with time in the presence of H_2O_2 and within 24 h the enzyme was almost completely deactivated (Figure 4.8 B). On the other hand, no measurable change in the activity was observed for the coacervate encapsulated HRP within this period. The irreversible deactivation of the enzyme by H_2O_2 is well documented in literature.[268] The lower diffusion of H_2O_2 into the interior of the coacervates allows the entrapped enzyme to remain protected from the deactivation by H_2O_2. However, that also resulted into slower reaction kinetics.

4.3 Conclusion

In conclusion, we have shown the coacervation of a binary mixture of a neutral polymer and a short peptide using two separate dynamic covalent bonds, imine and disulphide linkages. The coacervation process allows for encapsulating and stabilizing various proteins efficiently. Interestingly, the traditional categories of simple and complex coacervation do not apply in this circumstance. The coacervate production is not the result of non-covalent interactions between the two components, hence it cannot be characterised as a complex coacervate. On the other hand, the covalently cross-linked polymer does not go through self-aggregation steps as happens in the case of simple coacervates. As the coacervates are formed through dynamic linkages, we decided to call them as dynamic coacervates.

4.4 Experimental section

4.4.1 General information and materials

Rink amide MBHA resin, protected amino acids, HBTU and HOBT were procured from GL Biochem, China. N, N dimethyl acrylamide and GSH were purchased from TCI Chemicals, India. 1-Pyrenebutyric acid, HRP, BSA, Rhodamine, and Triethylsilane (TES) were procured from Sigma Aldrich, USA. Urea and Urease from Jack beans and Cytochrome C were obtained from SRL, India. All other chemicals, solvents and reagents were purchased from Spectrochem or SRL, India. To prepare samples, Milli-Q water with a conductivity of less than 2 $mScm^{-1}$ was used. Electrospray ionisation mass spectrometry (ESI-MS) is performed with a Q-Tof-Micro quadrupole mass spectrometer (Micromass), and data are analysed using the built-in software. Emission spectra were recorded on a Horiba Flurmax 4+ spectrophotometer. Analytical HPLC were performed on on Ultimate 3000 HPLC from Dionex.

4.4.2 Synthesis of polymers

The monomers for Poly-CHO and Poly-Benz were prepared following the synthetic routes mentioned below.

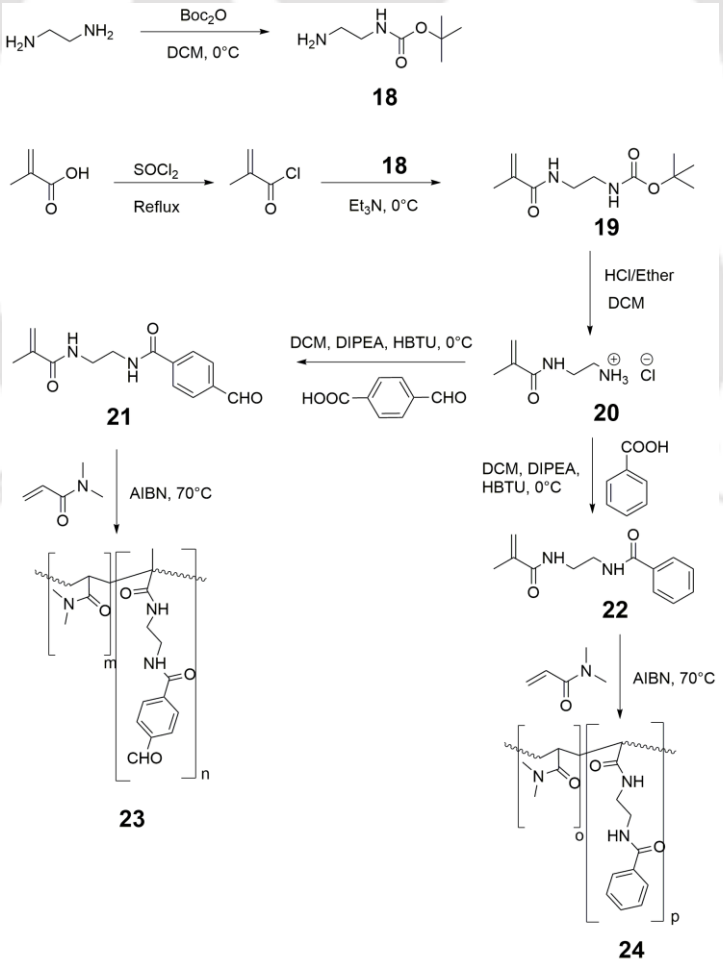

4.4.2.1 Synthesis of Boc-EDA (18)

Ethylenediamine (10 mL, 150 mmol) was dissolved in 100 mL dry dichloromethane (DCM) and was cooled to 0 °C. To this, a solution of Di-tert-butyl dicarbonate (3.7 mL, 16.1 mmol) in DCM (80 mL) was added dropwise under argon atmosphere for 2 h. The reaction mixture was then stirred at room temperature overnight. The reaction mixture was diluted with DCM and washed with saturated solution of sodium carbonate followed by brine solution. The organic phase was dried under sodium sulphate and concentrated under reduced pressure to get a colourless liquid (Yield = 2.28 g, 95%).

4.4.2.2 Synthesis of methacryloyl chloride

1.3 mL (15.5 mmol) of methacrylic acid was dissolved in ~ 5 mL of freshly distilled thionyl chloride and refluxed at 65 °C for 5h under argon atmosphere. It was then cooled and excess thionyl chloride was removed under reduced pressure to get a light-yellow oil of methacryloyl chloride. The Crude product was used without further purification.

4.4.2.3 Synthesis of MA-EDA-Boc (19)

Boc-EDA (2.28 g, 14.25 mmol) was dissolved in DCM (100 mL) and stirred at 0 °C. A solution of methacryloyl chloride in DCM (50 mL) was added to the solution of Boc-EDA at 0 °C under inert atmosphere and stirred for 12h. The reaction mixture was then washed with brine and saturated sodium bicarbonate. The organic phase was dried over Na_2SO_4, and solvent was removed under reduced pressure. The crude product was purified by column chromatography (2 – 5% methanol in DCM) to get a white solid (yield = 2.59 g, 70 %). ^{1}H NMR (600 MHz, $CDCl_3$) δ (ppm) = 6.97 (s, 1H), 5.72 (s, 1H), 5.32 (d, *J* = 12.6 Hz, 1H), 5.28 (s, 1H), 3.32 (d, *J* = 45.8 Hz, 4H), 1.91 (s, 3H), 1.38 (s, 10H). ESI-MS (m/z): calculated 229.155 for $C_{11}H_{20}N_2O_3$ $[M+H]^+$ found, 229.164.

4.4.2.4 Synthesis of MA-EDA.HCl (20)

2M HCl in Ether (15 mL) was added to a stirring solution of MA-EDA-Boc (2.5 g, 10.92 mmol) in DCM (5 mL) at 0 °C. The reaction mixture was stirred at room temperature for 12 h followed by evaporation of the solvents under reduced pressure to get a white residue. (Yield = 1.76 g, 96 %).^{1}H NMR (600 MHz, D_2O) δ (ppm) = 5.77 (s, 1H), 5.51 (s, 1H), 3.58 (t, *J* = 5.9 Hz, 2H), 3.22 – 3.17 (m, 3H), 2.81 (s, 1H), 1.94 (s, 3H). ^{13}C NMR (151 MHz, D_2O) δ (ppm) = 172.40, 138.44, 121.94, 54.36, 39.24, 37.01, 17.53. ESI-MS (m/z): calculated 129.1022 for $C_6H_{13}N_2O$ $[M+H]^+$ found, 129.105.

4.4.2.5 Synthesis of MA-CHO (21)

4-Formyl benzoic acid (987 mg, 6.58 mmol), HBTU (2.74 g, 7.2 mmol), and diisopropylethyl amine (DIPEA, 2.5 mL,14.46 mmol) were dissolved in dry DCM and stirred stirred at 0 °C for 30 min. To this mixture a solution of MA-EDA.HCl (1.2 g, 7.2 mmol in 5 mL dimethylformamide (DMF)) was added dropwise and stirred for 24h. The reaction mixture was washed with cold brine solution and the organic layer was dried under Na_2SO_4 and concentrated under reduced pressure. The crude product was purified by column chromatography (5 – 7% methanol in DCM) to yield a white solid (yield: 1.19 g, 72 %).

^{1}H NMR (600 MHz, $CDCl_3$) δ (ppm) = 10.10 (s, 1H), 8.03 – 7.95 (m, 4H), 7.72 – 7.62 (m, 1H), 6.61 (t, *J* = 5.7 Hz, 1H), 5.80 (s, 1H), 5.40 (d, *J* = 1.5 Hz, 1H), 3.70 – 3.61 (m, 4H), 1.99 (t, *J* = 1.3 Hz, 3H). ^{13}C NMR (151 MHz, $CDCl_3$) δ (ppm) = 191.80, 175.44, 170.36, 167.33, 167.24, 139.26, 139.23, 139.21, 138.31, 129.97, 129.95, 129.92, 127.94, 120.91, 41.72, 40.16, 39.68, 18.69. ESI-MS (m/z): calculated 261.1239 for $C_{14}H_{16}N_2O_3^+$ $[M+H]^+$ found, 261.134.

4.4.2.6 Synthesis of MA-Benz (22)

Benzoic acid (200 mg, 1.63 mmol) and HBTU (744 mg, 1.96 mmol) were dissolved in 10 mL dry DCM at 0 °C. To this mixture, DIPEA (0.67 mL, 3.92 mmol) was added and was stirred at 0 °C for half 1h. A solution of MA-EDA.HCl (0.3 g, 1.82 mmol dissolved in 3 mL DMF) was added dropwise into the mixture and stirred for 24 h. The reaction mixture was washed with cold brine solution and the organic layer was dried under Na_2SO_4 and concentrated under reduced pressure. The crude product was purified by column chromatography (5 – 7% methanol in DCM) to yield a white solid (yield = 286 mg, 76 %).^{1}H NMR (600 MHz, $CDCl_3$) δ (ppm) = 7.81 – 7.77 (m, 2H), 7.46 – 7.43 (m, 1H), 7.37 (td, *J* = 8.0, 2.7 Hz, 2H), 5.75 – 5.72 (m, 1H), 5.31 – 5.29 (m, 1H), 3.58 (dd, *J* = 7.4, 4.4 Hz, 2H), 3.51 (dd, *J* = 8.2, 3.3 Hz, 2H), 1.92 (s, 2H). ^{13}C NMR (151 MHz, $CDCl_3$) δ (ppm) = 168.81, 168.65, 139.40, 134.00, 133.99, 131.76, 128.73, 128.70, 127.17, 120.63, 41.07, 41.06, 40.61, 18.70. ESI-MS (m/z): calculated 233.13 for $C_{13}H_{16}N_2O_2^+$ $[M+H]^+$ found, 233.16.

4.4.2.7 Syntheses of Poly-CHO (23) and Poly-Benz (24)

Both polymers were prepared by copolymerization of the monomers MA-CHOor MA-Benz (1.02 mmol) and *N*, *N* dimethyl acrylamide (10.2 mmol) by radial polymerization using 2,2'-azobis(2-methylpropionitrile) (AIBN) (2 mg) as radical initiator at 65 °C under argon atmosphere in DMF for 24 h. The resulting mixture was cooled to room temperature and was added dropwise into diethylether to get a white precipitation. The precipitate was dissolved in minimum volume of DCM and was further precipitated from ether. Finally, the precipitate was dissolved in distilled water and dialyzed using a 12 Kda dialysis membrane across distilled water. The copolymerization ratio was calculated from the integration ratio of ^{1}H NMR signals.

Characterization of Poly-CHO: ^{1}H NMR (600 MHz, D_2O) δ (ppm) = 10.05 (s, 1H), 8.02 (d, *J* = 62.5 Hz, 4H), 3.56 (s, 5H), 3.20 – 3.08 (m, 10H), 3.07 – 2.98 (m, 23H), 2.93 (s, 55H), 2.64 (s, 15H), 1.81 – 1.21 (m, 32H), 0.94 (s, 3H).

Characterization of Poly-Benz: ^{1}H NMR (600 MHz, D_2O) δ (ppm) = 7.85 – 7.45 (m, 5H), 3.49 (d, *J* = 59.8 Hz, 4H), 3.20 – 2.80 (m, 65H), 2.63 (s, 11H), 1.51 (d, *J* = 160.8 Hz, 24H), 0.96 (d, *J* = 41.5 Hz, 3H).

Table 4.1 Determination of molecular weight of polymers

Molecular weights of the Poly-CHO and Poly-Benz polymers were determined using Gel Permeation Chromatography (GPC, Waters Corporation, USA) equipped with UV/Visible Detector, Refractive Index Detector, HPLC Pump.THF was used as a mobile phase and analysis was done by using PLgel MIXED-C columns (particle size: 5 µm; dimensions: 7.5 × 300 mm) and EMPOWER-2 software.

Polymer	N, N dimethyl acrylamide	MA-CHO (4)	MA-Benz (5)	M_n (GPC)	M_w (GPC)	Refactive index (D)
Poly-CHO	46	3.07	-	5357	5655	1.0556
Poly-Benz	42.57	-	3.87	5116	5451	1.0654

4.4.3 Syntheses of Peptides

All the peptides (PyKC, PyRC, PyKS, C8KC and Py1KC (Scheme 4.1 and Chart 4.1) were synthesized on Rink amide MBHA resin using standard Fmoc (9-fluorenylmethoxycarbonyl) solid-phase peptide synthesis (SPPS) method. The amino acids used are, Fmoc-Cys(Trt)OH (For PyKC, PyRC, Py1KC, and C8KC), Fmoc-Lys(Boc)OH (For PyKC, PyKS, Py1KC, and C8KC), Fmoc-Arg(Pbf)OH (for PyRC), Fmoc-Ser(Otbu)OH (for PyKS), 1-Pyrene carboxylic acid (for Py1KC), 1-Pyrene butyric acid (for PyKC, PyRC, and PyKS), and Octylamine (for C8KC). In a typical coupling, 3 equiv. of protected amino acid (with respect to the loading of the resin), 3 equiv. of HBTU, and 6 equiv. of DIPEA were taken in 5 mL of DMF (for 0.1 mmol scale with respect to the resin loading) and stirred for 5 minutes prior to addition of the mixture to the resin. The reaction mixture was shaken for 60 min and the resin was washed several times with DMF. The Fmoc-deprotection was achieved by treatment of the resin with 20% piperidine (5 mL, 5 minutes, three times) followed by thorough washing of the resin with DMF. The Fmoc-deprotection and coupling steps were repeated until the designed peptide sequence was obtained. After the final Fmoc-deprotection, the peptide loaded resin was washed several times with DMF followed by DCM and dried under reduced pressure. The dried resin was then treated with a mixture of 95% trifluoroacetic acid (TFA) in DCM containing 1% triethylsilane (TES) and stirred for 1 h. The resin was finally washed with DCM several times. The cleavage cocktail and the washings were combined and concentrated to a minimum volume on a rotary evaporator. The cleaved peptide was then precipitated from cold dry ether, centrifuged and lyophilized to get the crude peptide. Purification was done in a semi-preparative HPLC using a Luna 5 µm (C18) column (Phenomenex) with a programme of acetonitrile and water starting at 5% acetonitrile to reach 30% after 5 min and continued to reach 100% at 40 min.

Characterization of PyKC: ^{1}HNMR (DMSO-d_6, 400 MHz): δ(ppm) = 8.39 (d, *J* = 9.3 Hz, 1H), 8.28 (m, 2H), 8.23 (m, 2H), 8.14 (d, *J* = 2.0 Hz, 2H), 8.07 (t, *J* = 7.6 Hz, 1H), 7.97 (t, *J* = 8.2 Hz, 2H), 7.66 (s, 3H), 7.29 (s, 1H), 7.20 (s, 1H), 4.39 – 4.21 (m, 2H), 2.90 – 2.66 (m, 4H), 2.29 (m, 3H), 2.03 (p, *J* = 7.3 Hz, 2H), 1.69 (m, 1H), 1.55 (m, 3H), 1.35 (d, *J* = 35.3 Hz, 2H). ^{13}C NMR (100 MHz, DMSO-d_6): δ(ppm) = 172.96, 172.31, 171.87, 137.06, 131.36, 130.90, 129.78, 128.06, 127.93, 127.70, 126.99, 126.63, 125.42, 125.26, 124.03, 55.06, 53.19, 39.18, 35.29, 32.71, 31.44, 28.00, 27.10, 26.58, 22.82. ESI-MS calcd. for $[M+H]^+$, $C_{29}H_{34}N_4O_3S$: 519.24, found: 519.24 (m/z).

Characterization of Py1KC: ^{1}H NMR (400 MHz, DMSO-d_6): δ(ppm) = 8.92 (d, *J* = 7.5 Hz, 1H), 8.54 (d, *J* = 9.3 Hz, 1H), 8.42 (s, 1H), 8.36 (dd, *J* = 7.7, 4.1 Hz, 3H), 8.31 – 8.21 (m, 3H), 8.20 (d, *J* = 7.9 Hz, 1H), 8.14 (m, 2H), 7.70 (s, 3H), 7.53 (s, 1H), 7.29 (s, 1H), 4.68 – 4.58 (m, 1H), 4.46 (m, 1H), 2.93 (dd, *J* = 13.5, 5.0 Hz, 1H), 2.88 – 2.79 (m, 3H), 1.85 (s, 2H), 1.72 – 1.48 (m, 2H), 1.54 (s, 2H).

Characterization of PyRC: ^{1}H NMR (600 MHz, DMSO-d_6) δ(ppm) = 8.35 (d, *J* = 9.3 Hz, 1H), 8.25 (d, *J* = 7.7 Hz, 2H), 8.19 (dd, *J* = 8.5, 5.7 Hz, 2H), 8.16 – 8.12 (m, 2H), 8.04 (s, 1H), 7.91 (d, *J* = 7.8 Hz, 1H), 7.53 (s, 1H), 7.39 (s, 1H), 7.25 (s, 1H), 4.45 (d, *J* = 5.0 Hz, 1H), 4.31 – 4.25 (m, 1H), 3.35 – 3.27 (m, 2H), 3.08 (dd, *J* = 6.3, 3.4 Hz, 2H), 2.31 (d, *J* = 7.3 Hz, 2H), 2.00 (s, 2H), 1.69 (ddq, *J* = 12.3, 9.1, 5.4 Hz, 1H). ^{13}C NMR (151 MHz, DMSO-d_6) δ(ppm) = 171.73, 136.51, 130.88, 130.41, 129.30, 128.14, 127.58, 127.44, 127.23, 126.52, 126.15, 124.94, 124.78, 124.23, 124.14, 123.51, 52.54, 51.88, 34.79, 32.24, 28.86, 27.45, 25.07. ESI-MS (m/z): calculated 547.249 for $C_{29}H_{34}N_6O_3S$ $[M+H]^+$ found, 547.084.

Characterization of PyKS: ^{1}H NMR (600 MHz, DMSO-d_6) δ(ppm) = 8.38 (d, *J* = 9.2 Hz, 1H), 8.30 – 8.25 (m, 2H), 8.22 (dd, *J* = 8.5, 5.7 Hz, 2H), 8.12 (dd, *J* = 12.1, 6.0 Hz, 3H), 8.06 (t, *J* = 7.6 Hz, 1H), 7.95 (d, *J* = 7.8 Hz, 1H), 7.81 (d, *J* = 7.8 Hz, 1H), 4.91 (t, *J* = 5.5 Hz, 1H), 4.32 – 4.27 (m, 1H), 4.22 – 4.16 (m, 1H), 3.62 (dt, *J* = 10.9, 5.5 Hz, 1H), 3.56 (dt, *J* = 10.5, 5.0 Hz, 1H), 2.74 (d, *J* = 7.3 Hz, 2H), 2.32 (d, *J* = 7.3 Hz, 2H), 2.06 – 1.96 (m, 2H), 1.68 (dd, *J* = 10.2, 5.2 Hz, 1H), 1.58 – 1.47 (m, 4H), 1.34 (q, *J* = 7.3, 6.9 Hz, 3H). ^{13}C NMR (151 MHz, DMSO-d_6) δ(ppm) = 172.47, 171.95, 171.68, 136.61, 130.91, 130.46, 129.33, 128.19, 127.61, 127.48, 127.26, 126.54, 126.18, 124.98, 124.82, 124.26, 124.17, 123.57, 61.61, 54.93, 52.60, 34.86, 32.26, 31.16, 27.55, 26.62, 22.34. ESI-MS (m/z): calculated 503.27 for $C_{29}H_{34}N_4O_4$ $[M+H]^+$ found, 503.2858.

Characterization of C8KC: ^{1}H NMR (600 MHz, D_2O) δ(ppm) = 4.52 (dd, *J* = 7.2, 5.3 Hz, 1H), 4.32 (dd, *J* = 8.6, 5.9 Hz, 1H), 3.00 (t, *J* = 7.8 Hz, 3H), 2.31 (t, *J* = 7.3 Hz, 2H), 1.90 – 1.81 (m, 1H), 1.77 (dd, *J* = 9.4, 4.9 Hz, 1H), 1.74 – 1.67 (m, 3H), 1.61 (d, *J* = 7.1 Hz, 2H), 1.54 – 1.40 (m, 3H), 1.32 – 1.23 (m, 9H), 0.86 (t, *J* = 6.9 Hz, 3H). ^{13}C NMR (151 MHz, D_2O) δ(ppm) = 177.68, 174.19, 174.08, 55.15, 53.60, 39.14, 35.34, 30.94, 30.18, 28.13, 28.04, 26.23, 25.27, 25.21, 22.07, 21.91, 21.88, 13.34.ESI-MS (m/z): calculated 261.1239 for $C_{17}H_{34}N_4O_3S[M+H]^+$ found, 374.914.

4.4.4 Optical microscopy

Optical microscopic studies were performed using an inverted optical Olympus IX81 epifluorescence microscope. Typically, 10 μL of solutions were placed on a glass slide with a coverslip and placed under the microscope to capture the bright field, and fluorescence images.

4.4.5 Field Emission Scanning Electron Microscopy (FESEM)

Small portions (5 μL) of sample solutions were casted on silicon wafers and the samples were immediately dipped into liquid nitrogen followed by freeze drying. Images were taken using a Gemini SEM 300 (Sigma Zeiss; FESEM) instrument.

4.4.6 Transmission Electron Microscopy (TEM)

TEM samples were prepared by casting 10 μL sample on copper grids (300 mesh with thick carbon film from Pacific Grid Tech, USA) and it was then allowed to adsorb for 1 min. The excess samples were wiped out with tissue paper and dried for few hours before analysing it using a JEOL JEM-2100F (FETEM) electron microscope.

4.4.7 Turbidity measurement

The turbidity of the solutions was measured by using a UV-vis spectrophotometer at 600 nm, where none of the components absorbed the light. The turbidity was calculated using the below given formula, Turbidity = 100 - %T, where %T is transmittance.

4.4.8 ^{1}H-NMR analysis showing the reversible formation of imine linkage

The reversible formation of imine linkage between the aldehyde groups of Poly-CHO and the amine group of PyKC was monitored by the changes in the ^{1}H-NMR peak for the imine and aldehyde protons in response to the NaOD and DCl and TCEP. Briefly, a solution containing Poly-CHO (10 mg) and PyKC (1 mg) was prepared in D_2O and NMR was recorded immediately. To this solution, 2 μL of NaOD was added the ^{1}H NMR spectrum was recorded after 30 minutes. The disappearance of the aldehyde peak (10 ppm) and the appearance of the imine peak (8.2 ppm) indicated the formation of imine linkages. To this solution, 5 mL of DCl was added and the ^{1}H NMR spectrum was recorded after 30 min to show the disappearance of the imine signal and reappearance of the aldehyde peak. The same experiment was repeated where after NaOD addition, TCEP was added and after 30 min the ^{1}H NMR spectrum was recorded. In this case, sharpening of the aromatic peaks was observed but the imine signal remained unchanged.

4.4.9 Preparation of coacervates using PolyCHO and PyKC

Required volumes of stock solutions of Poly-CHO and PyKC were mixed and the volume was made up to 1 mL by using a Tris buffer (20 mM, pH 8) to get the final concentrations of Poly-CHO and PyKC as 3 and 0.3 mg/mL respectively. The solution was incubated for 24 h and coacervation was checked by using optical microscopy, turbidity and emission quenching experiments. The morphology was checked by using FESEM. Similar procedure was followed for Poly-CHO – PyKC ratio optimization, coacervation

by other combinations of polymer (Poly-CHO, Poly-Benz) and peptides (Cystamine, PyRS, PyKS, Py1KC, C_8KC). For pH dependent coacervation, similar procedure was followed. However, in place of Tris buffer, different buffers of varying pH were used.

4.4.10 Estimation of water content

Water content in the coacervates was measured following a literature procedure.[247] A solution (6 mL) of $(PyKC)_2$ – Poly-CHO (1:10 with 0.3 mg $(PyKC)_2$/mL) was prepared at pH 5. This solution (5 mL) was transferred to a clean and weighed (W_{empty}) glass tube. The solution was then treated with 0.2 M NaOH to adjust the pH to 8 and incubated for 1 h to ensure complete formation of the coacervates. The glass tube was then placed in a 15 mL falcon tube and centrifuged at 3000 rpm for 30 min. The supernatant was pipetted out and the last droplets of supernatant were blotted with a filter paper. The tube with the coacervates was weighed again ($W_{Coacervate}$). The glass tube was placed inside a vacuum oven at 120 °C for 48 h to dry to a constant weight. Finally, the dried tube was weighed (W_{dry}) to calculate the weight loss. The water content was calculated as,

$$Water\ content = \frac{W_{Coacervate} - W_{dry}}{W_{Coacervate} - W_{empty}} \times 100\%$$

4.4.11 Fluorophore labelling of proteins

In a typical procedure, 5 mg of the protein was dissolved in 1 ml of 100 mM $NaHCO_3$-Na_2CO_3 buffer solution (pH 9). The required amount (3-5 mg) of FITC was dissolved in 50 µL anhydrous DMF and transferred into the stirred solution of the protein. The stirring was further continued for 3 hours in the dark. Then, the reaction mixtures were taken in an activated dialysis membrane (cut-off: 10,000 Da). The mixture was dialyzed against cold buffer solution with proper time to time refilling until the green emission of the unreacted FITC was fully diminished. Lastly, the mixture was dialyzed against the cold milli-Q water for the complete removal of the salts. The tagged proteins were obtained after freeze-drying the dialyzed protein solution. MALDI, UV-Visible, Fluorescence measurements confirmed the attachment of the fluorophore.

4.4.12 Preparation of protein and dye entrapped coacervates

All the dye and protein-trapped coacervates were prepared following a similar protocol. The process with HRP is mentioned below.

For the preparation of FITC-HRP sequestered Coacervates, the coacervates were prepared by addition of appropriate amounts of stock solutions of Poly-CHO and PyKC to a 10 mL solution of FITC-HRP (62 units) prepared in Tris buffer (20 mM, pH 8). It was then incubated at room temperature for 1 h before centrifugation at 10,000 rpm for 15 min. The supernatant solution was collected to determine the extent of entrapment of FITC-HRP using UV-Visible spectrophotometer. Briefly, the absorbance of known concentrations of HRP was measured, and the calibration curve was plotted. Then the absorbance of

the supernatant was measured, and using the calibration curve the amount of HRP trapped inside the coacervate was determined (2.8 ± 0.2 units/mL). The residue from the centrifugation was further dispersed in 10 mL of Tris buffer (20 mM, pH 8) and used for time dependent enzyme activity experiment described below. All measurements were done in triplicates.

4.4.13 Enzyme activity measurements

Stock solutions of Pyrogallol (100 mM) and H_2O_2 (100 mM) were prepared in acetonitrile and Milli-Q water respectively. To analyse the peroxidase activity of the entrapped HRP enzyme, 30 μl of H_2O_2 (0.3 mM) was added to the previously prepared HRP entrapped coacervate dispersion. Thereafter, 1 mL aliquots of the above-prepared solution were taken at different time points, and the activity of entrapped HRP was assessed. Typically, 0.5 μl pyrogallol stock solution was added to these aliquots to maintain a concentration of 0.05 mM. The oxidation of pyrogallol to purpurogallin (λ_{max} = 420 nm, ε_{420nm} = 2640 $M^{-1}cm^{-1}$ in water) was monitored over a period of 5 min by using UV-Visible spectroscopy. The initial velocity (V_o, change in concentration within the first 100 s) were plotted against time (Figure 4.8 B). Similarly, the control experiment was performed for free HRP (maintaining the enzyme concentration similar to the trapped amount) in the absence of the coacervates. All measurements were done in triplicates.

4.4.14 Phase diagram

To estimate the phase diagram, a 30 mL stock solution of $(PyKC)_2$ at a concentration of 3 mg/mL was prepared in Milli-Q water and incubated at room temperature for 48 h. This solution was then divided into several 1 mL portion. To these portions, HCl or NaOH stocks were added to attain different target pH. Once the respective pH values were attained, these solutions were separately titrated with a stock solution of Poly-CHO in water. After every addition of the polymer, the solutions were incubated for 10 min before the turbidity of the solutions were measured. As observed before, solutions showing turbidity values above ~15 only showed the formation of coacervates under optical microscope. Thus, all solutions showing highest turbidity value below 15 were tested for FESEM imaging. Interestingly, solutions with turbidity value in the range of 8 – 15 showed very small droplets with diameters of 50 – 300 nm. Any solution with turbidity value above 15 were considered as coacervates. It is to be noted that more-emphasis was given to pH range 5-7 and composition range 1: 2.5 – 1:5 ($(PyKC)_2$ – Poly-CHO) as we realized that the phase boundary lies in these two regions based on our initial results. The turbidity measurements were performed in triplicate and the average compositions where the coacervates or nano-droplets were formed were plotted against the pH value to obtain the phase diagram. All measurements were performed at room temperature.

4.4.15 Effect of H_2O_2 on the aldehyde groups of the polymer.

To check, the effect of H_2O_2 on the aldehyde groups present in the polymer, 600 μL D_2O solution (3 mg/mL) of the polymer was treated with H_2O_2 (6 μL of the stock) and the sample was incubated for 12 h. The ^1H NMR spectra showed no prominent change in the aldehyde peak. However, due to the presence of H_2O, a broad peak of *H*OD appeared which masked most of the aliphatic region.

Indian Institute of Technology Guwahati

Chapter 5: Creating Multimodal Transience in Polymer-Peptide Composite Coacervate.

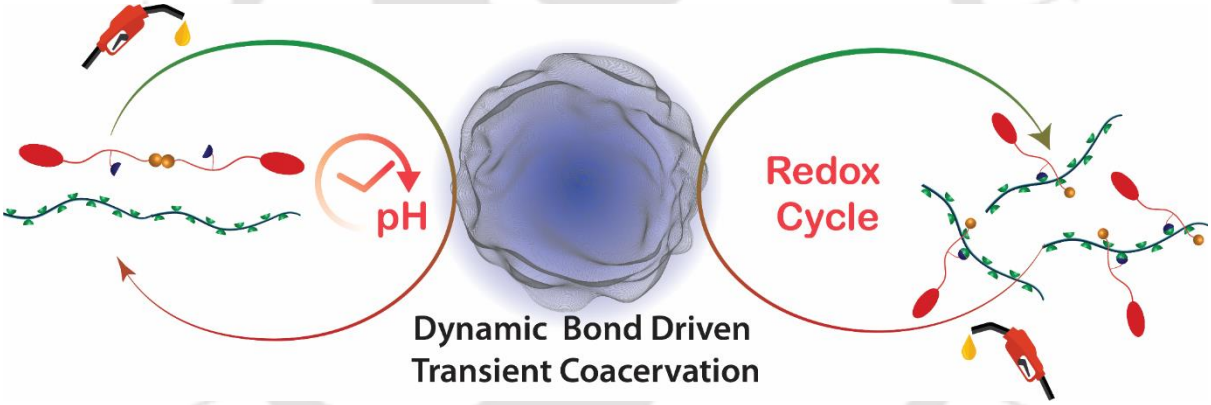

Indian Institute of Technology Guwahati

5.1 Introduction

The ability of self-assembled structures in living systems to adapt to changes in environmental conditions is one of their most intriguing aspects. Creating similar capabilities in synthetic self-assemblies offers a lot of promise for developing smart systems. Supramolecular chemistry has almost mastered the self-assembly of structures of any complexity[269], but these structures are static and lack the rich functionality found in cellular structures. Many synthetic materials have been designed to switch between equilibrium states upon reaction with the desired signal, for example, micelles, and vesicles transitioning from assembled to disassembled states for site-specific cargo release.[270, 271] In contrast to this, nature often utilizes fuel-driven processes which achieve non-equilibrium structures with features including spatiotemporal control, responsiveness, and auto-configuration. These features allow for complex cellular functions such as division, motility, and intracellular transport[270]. There are numerous synthetic coacervate-based droplets[272-274] that are utilized to study the properties of membrane-less organelles. Reversible complex coacervate droplets that form or dissolve in response to a change in pH,[275] temperature,[276] salt or polymer concentration,[276] or UV light[277] or an enzymatic reaction[278, 279] have been observed. In response to a change in their surroundings, these droplets evolve from one equilibrium state to another (e.g., from droplets to solution). A model such as this could give information about how chemical reactions control droplet growth or how kinetics can control the size of droplets.[280-282]Successful execution of such synthetic systems, on the other hand, leads to the formation of smart systems that sense and react to changes in the environment's spatiotemporal composition. Natural self-assembling systems are notable for their far-from-equilibrium transient nature[283, 284]. Importantly, the majority of natural coacervates are extremely dynamic and only persist for a short period of time[285-287]. These droplets' transient existence is governed by non-equilibrium biological reactions[288]. Fuel-driven transitory self-assemblies of synthetic molecules have been successfully shown on multiple occasions in recent years[289-294]. There have also been some attempts to make transient coacervates[280, 295-297]. However, there are no known systems that can be generated transiently under the impact of multiple non-equilibrium reactions.

We wanted to investigate if coacervates could be generated transiently using multiple fuel-driven processes. We thought that systems with many dynamic bonds would be a suitable foundation for developing such a system.Herein, we utilized the coacervates described in Chapter 4 for the same.The coacervates mentioned in Chapter 4 are formed through two dynamic covalent linkages namely, imine and disulphide bonds. Thus, under the influence of a pH clock and redox cycle, the coacervates can be created transiently. Notably, the transient existence of the coacervates can be executed multiple times by applying the triggers sequentially within the same system.

5.2 Results and discussion

As discussed in the previous chapter, we used an aldehyde-appended polymer (Poly-CHO) and a Pyrene capped dipeptide (PyKC) to create coacervate. Because the formation of coacervate is primarily caused by the formation of imine, which is pH sensitive, as well as disulphide, which is redox sensitive, we first demonstrated the response of coacervate in the presence of various stimuli.

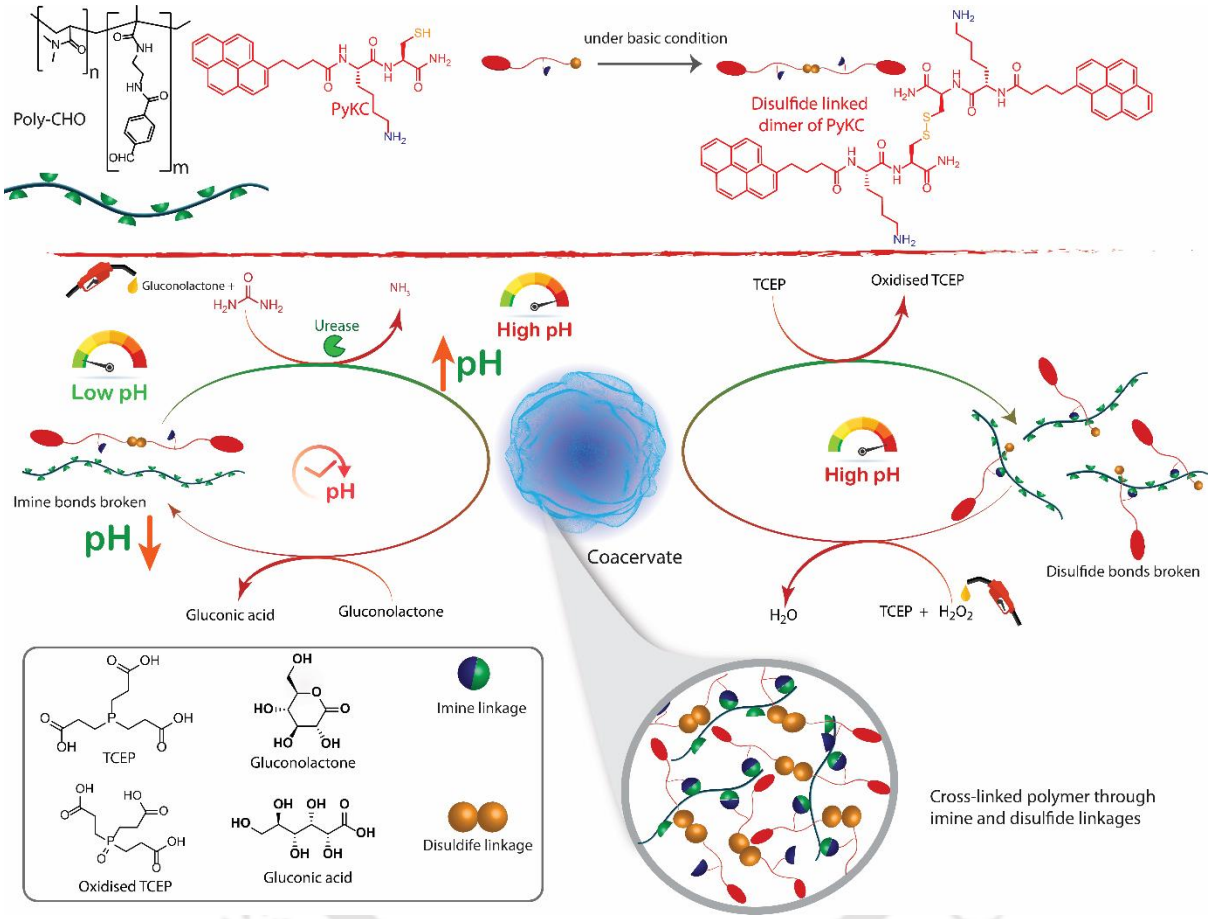

Scheme 5.1A) Chemical structures of Poly-CHO, PyKC and $(PyKC)_2$. B) Graphical presentation of the pH and redox cycle induced transient formation of the coacervates.

Initially, the responsiveness of the coacervates toward acid/base and oxidizing/reducing agents was evaluated. An aqueous mixture of $(PyKC)_2$ and Poly-CHO (1:1) was treated with NaOH to increase the pH to 8. The emission intensity measured at 376 dropped significantly (Figure 5.1 B) while the turbidity enhanced (Figure 5.1A) drastically indicating the formation of the coacervates. It was then treated with TCEP to break the disulphide bonds.[247] As a result, emission intensity enhanced while the turbidity decreased. These observations point toward the disassembly of the coacervates. Similarly, the system was further sequentially treated with H_2O_2, HCl, NaOH and TCEP. In each case, the corresponding

emission intensity/turbidity followed the expected pattern of assembly or disassembly of the coacervates.

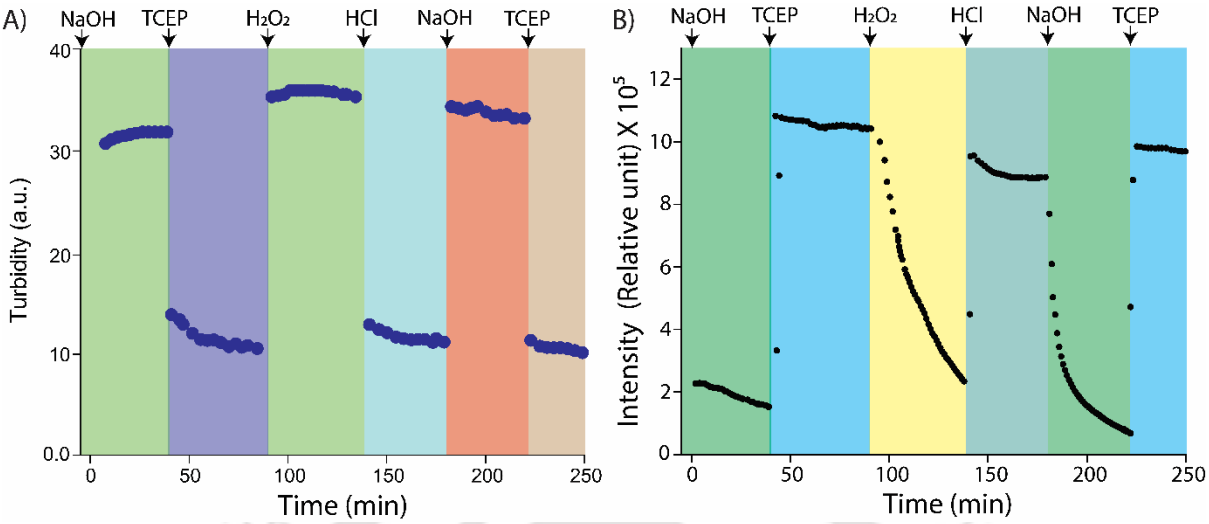

Figure 5.1 Responsiveness of the coacervates toward base/acid and H_2O_2/TCEP. A solution of $(PyKC)_2$ – Poly-CHO (1:10) at pH 5 was first basified with NaOH to pH 8 and the change in A) turbidity of the system, B) emission of pyrene at 376 nm (λ_{ex} = 337 nm) were monitored as various triggers were added sequentially at different time points.

These results clearly demonstrate the dual responsiveness and adaptability of the coacervates. is produced, the hydrolysis of GdL to gluconic acid works in the background as it is a much slower process compared to that of ammonia generation. Once urea is consumed and the basic condition is reached, the deactivating effect of GdL becomes prominent and thereby decreases the pH of the system. To establish the right composition, different ratios of urea/GdL were used keeping 0.4 mM urea and 0.02 mg/mL urease in the system. As can be seen from Figure 5.2 A, a combination of 1:5 urea-GdL allows an initial jump of pH from 5.5 to 8.4 within 3 mins (Figure 5.2 A). After that, the pH drops slowly due to the GdL hydrolysis and reaches the initial value of 5.1 within 100 min. As the lifetime of the pH clock for this composition is considerably lower than the others, for further studies, we used this particular ratio.

The activator/deactivator driven transient formation of the coacervates was monitored using turbidity and pyrene emission. Initially, $(PyKC)_2$ - Poly-CHO (1:10) and urease (0.02 mg/mL) was dissolved in water and pH was maintained at 5.1 followed by the addition of urea – GdL (0.4 mM – 2 mM) and the solution was subjected to time dependent analyses. As can be seen from Figure 5.2 B-C and S8, with the addition of urea/GdL, within 8 min, turbidity enhanced to 35 and the emission dropped significantly. The change in the pH of the medium was also monitored and it shows a rise in the pH to 8.5 (Figure 5.7 A). The enhancement in turbidity and drop in pyrene emission suggest the formation of coacervates at this pH. The turbidity/emission remained almost unchanged for ~ 50 min before the values started going back to the initial state. Following the pH clock (Figure 5.7 A), it is clear that the pH of the system remains basic to neutral for up to ~50 min and then it enters the acidic range. As the imine bonds

remain stable under neutral to basic condition,[261] the coacervates exist for this particular period and as the pH drops to acidic range, the hydrolysis of imine linkages leads to the disassembly. The optical microscopic images of the sample prior to the addition of urea-GdL (-5 min), during (15 min) and at the end (120 min) of one transient cycle along with the photographs of the samples are shown in Figure 5.2 D.

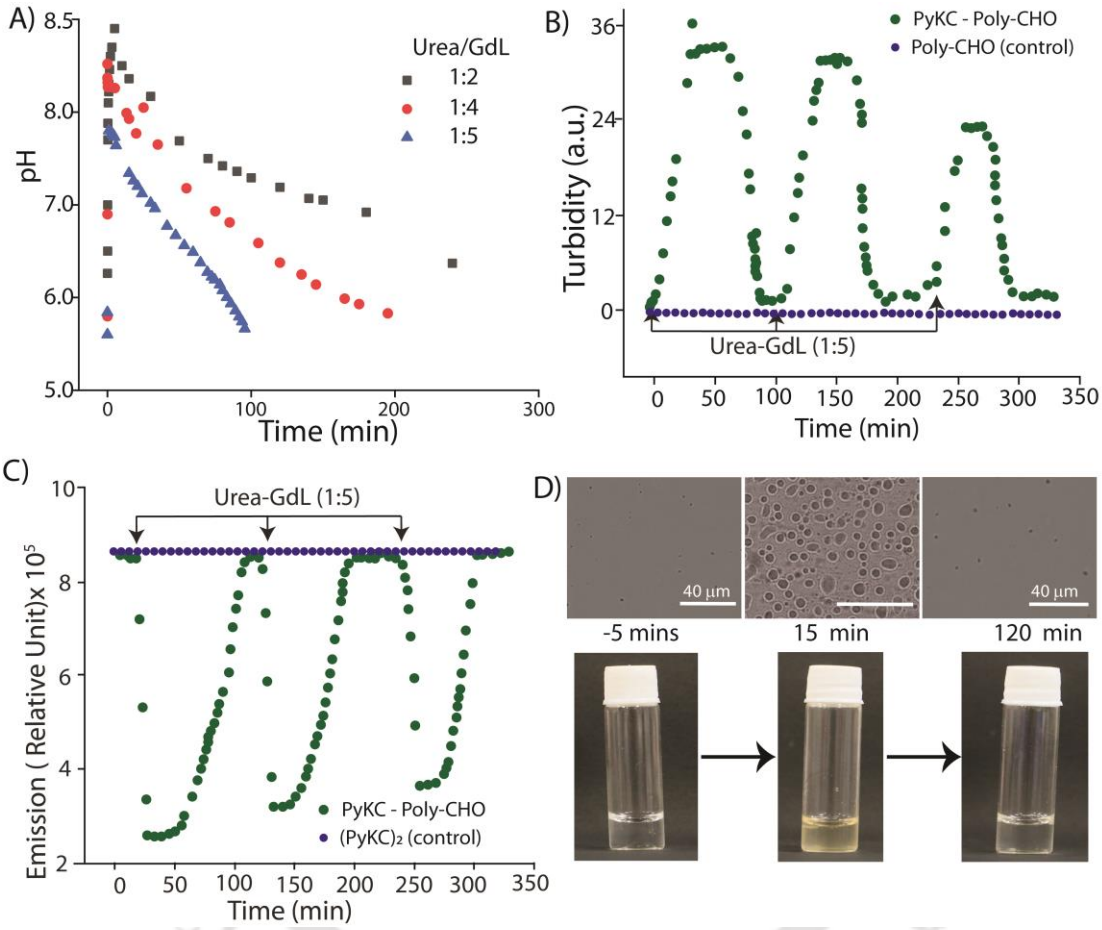

Figure 5.2 A) Optimization of pH clock by varying the urea (0.4 mM) – GdL ratio in presence of 0.02 mg/mL urease. B) Turbidity and C) emission at 376 nm (λ_{ex} = 337 nm) of a $(PyKC)_2$ – Poly-CHO (1:10) solution when subjected to consecutive pH cycles. D) Optical microscopic images and the corresponding pictures of the sample from B and C at different time during the first cycle.

The transient existence of the coacervates under the influence of the pH clock was thus established. However, it is important to evaluate the possibility to recreate the temporal existence when the system is refueled for multiple cycles. Thus, at the end of the first cycle, the system was refueled with urea – GdL (1:5) for two more cycles and similar transient cycles were observed. However, a minor dampening in the lifetime was observed owing to the dilution factor and presence of unused GdL after every cycle. Next, the redox cycle was applied to create the coacervates transiently. As both the dynamic bond formation is facilitated at basic condition, changing the pH of the system to 8 and addition of TCEP (the deactivator) could result in the formation of the coacervates transiently. A combination of NaOH and

TCEP was added to the solution of PyKC – Poly-CHO and the pH was maintained ~ 8. A sharp increase followed by a sharp decline in the turbidity was observed Figure 5.4). However, it is to be noted that the turbidity was found to be much lower than the coacervates. The addition of NaOH triggered very fast formation of the imine bonds. However, the simultaneous reduction by TCEP did not allow the coacervates to be formed. In a separate experiment, we did try the same by adding Tris buffer pH 8 and TCEP. However, in that case, as the imine bond formation was slower compared to theTCEP induced reduction, very small change in the turbidity was observed.

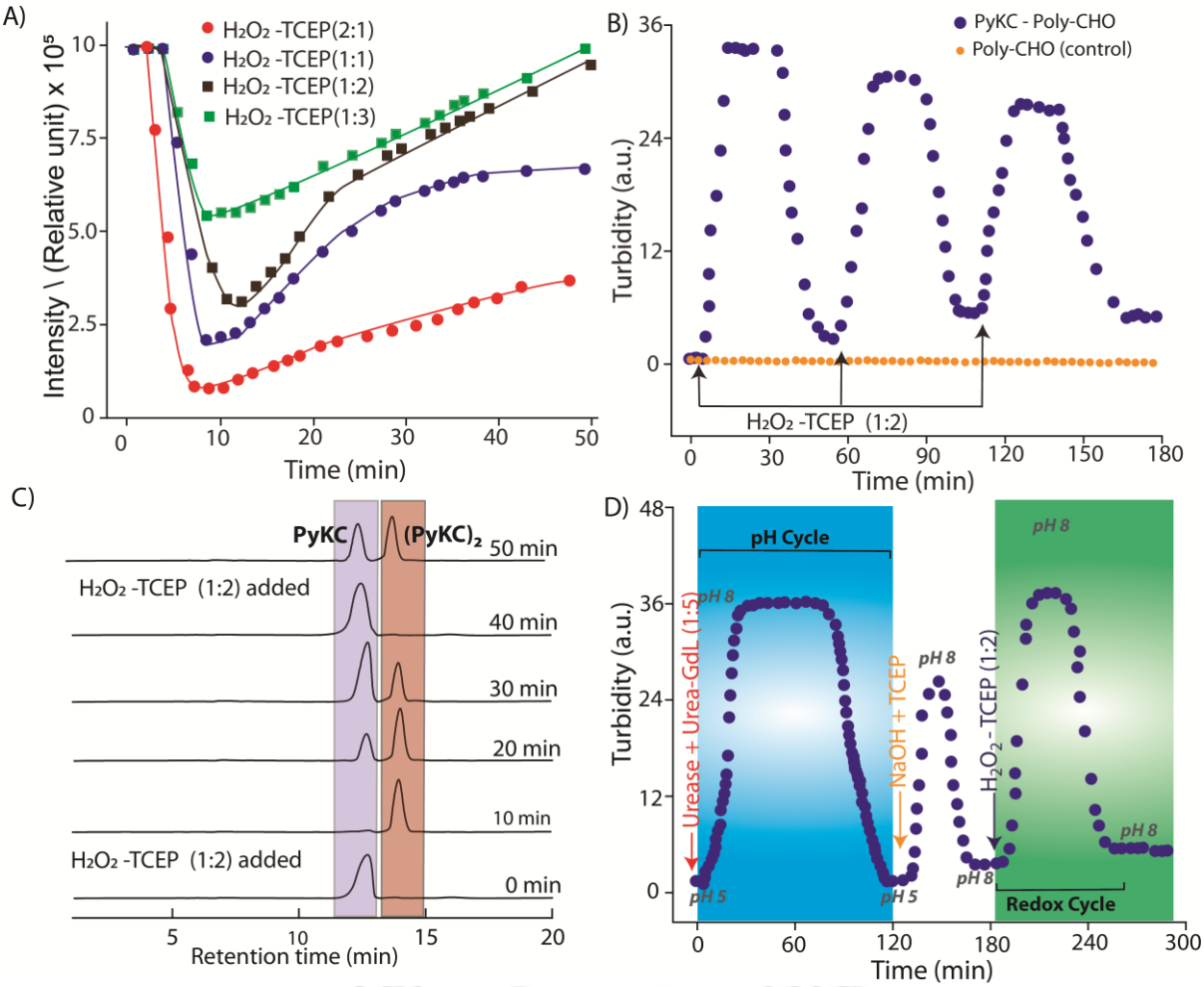

Figure 5.3 A) Optimization of the redox reaction cycle by monitoring the change in pyrene emission in PyKC – Poly-CHO (1:10) solutions in presence of different compositions of TCEP – H_2O_2. B) Change in the turbidity of a PyKC – Poly-CHO (1:10) solution when subjected to three consecutive redox reaction cycles. C) HPLC chromatograms showing the presence of PyKC and $(PyKC)_2$ in the solution at different times during the transient formation of the coacervates under redox chemical cycle as shown in B. D) Turbidity profile of PyKC – Poly-CHO (1:10) solution when a pH cycle is applied followed by a redox reaction cycle.

We realized that to create a redox cycle, the pH should be maintained in the basic region while a strong oxidizing agent (activator) like H_2O_2 should be used along with TCEP. To optimize the composition of the activator/deactivator, different compositions of H_2O_2– TCEP were tested (Figure 5.3 A).[298-300] Since, a strong oxidizing agent H_2O_2 is used, in place of $(PyKC)_2$, PyKC was used to start the cycle. PyKC – Poly-CHO (1:10) was dissolved in Tris buffer (20 mM, pH 8).

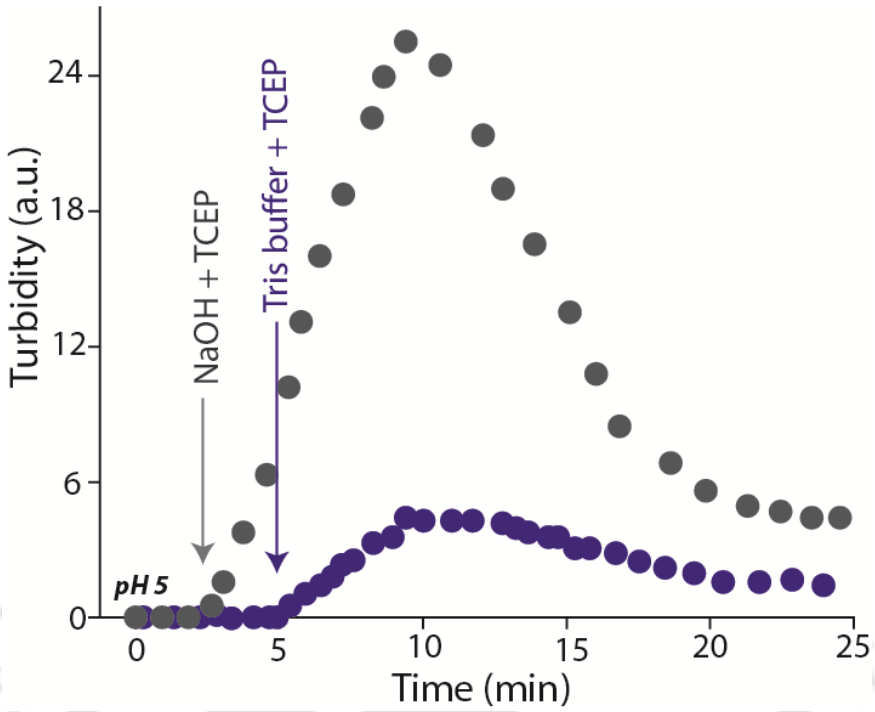

Figure 5.4 Change in turbidity when a pH 5 solution of PyKC – Poly-CHO (1:10) was treated with either NaOH – TCEP or Tris buffer (pH 8) – TCEP mixture.

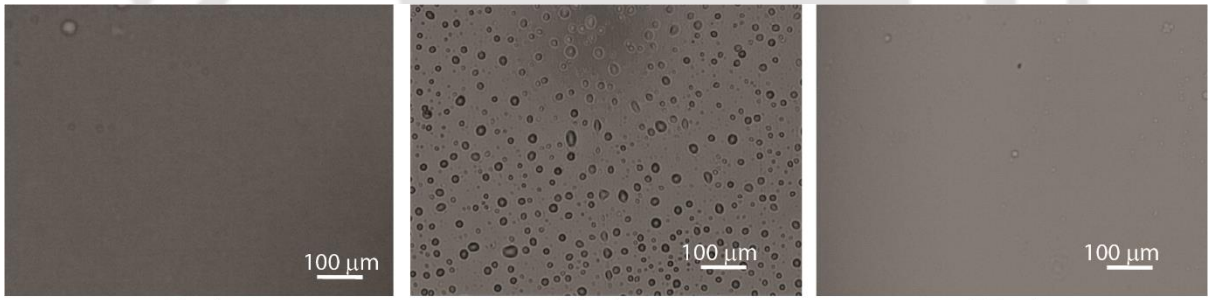

Figure 5.5 Optical microscopic images of the solutions at different times during the first cycle of redox cycle (Figure 5.3 B) induced transient formation of the coacervates of PyKC – Poly-CHO (1:10) in 20 mM Tris buffer pH 8.

To this, different amounts of H_2O_2 – TCEP were added and the change in the pyrene emission at 376 nm was monitored. Among the five different compositions tested, 1:2 H_2O_2 – TCEP was found to be the most suitable for the transient cycle. For this particular ratio, not only a significant decrease in the emission was observed but also the value returned back to its original position at the end of the cycle (~40 min).

Based on this observation, we subjected the system (PyKC – Poly-CHO (1:10) in Tris buffer (20 mM, pH 9) to the redox cycle by adding H_2O_2 – TCEP (1:2) and monitored the turbidity (Figure 5.1 A) and emission at 376 nm (Figure 5.1 B). Upon addition of the activator (H_2O_2), the turbidity enhanced from 7 to 34 within 7 min and remained unchanged for ~ 20 min. After that a decline in the turbidity was observed. Within next 10 min the value dropped to 8 indicating the disassembly of the coacervates. Two

more cycles of the redox couple induced transient coacervation was successfully executed and that too showed similar life time. The emission behaviour and the microscopic images also corroborated well with the turbidity results (Figure 5.3 B, 5.5 and 5.6 A).

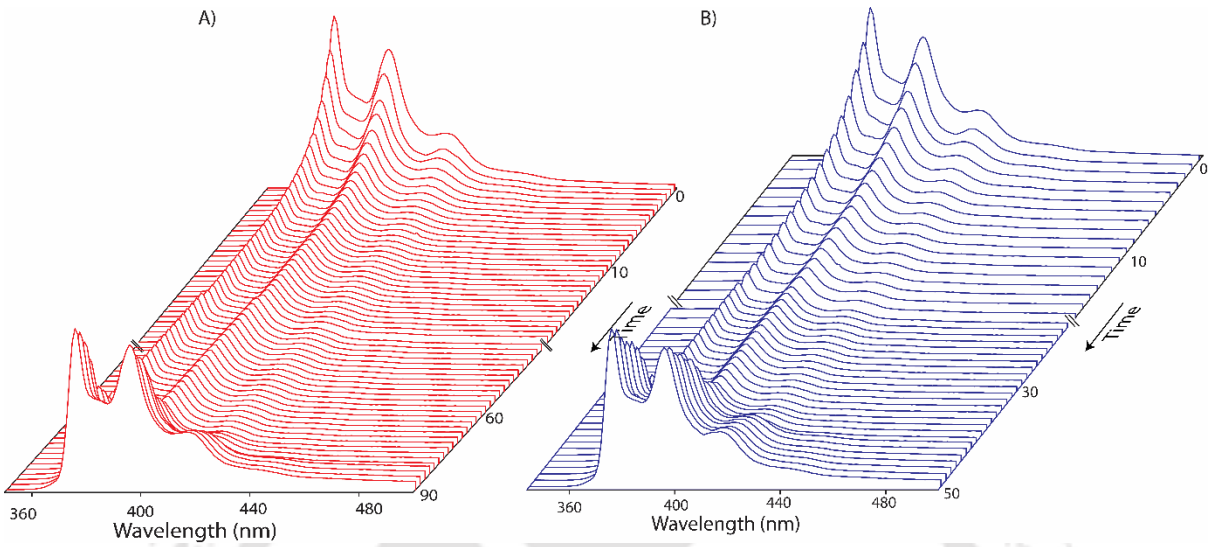

Figure 5.6 Full wavelength emission spectra during the first transientA) redox cycle (Figure 5.3 B) andB) pH cycle (Figure 5.2 C), while exciting the system at 337 nm.

The formation/breakage of the disulphide linkages during these redox cycles were then investigated. At different time interval of the transient cycle, aliquots were withdrawn and immediately acidified with HCl in order to break the imine linkages. These samples were analysed through HPLC to find the formation PyKC – $(PyKC)_2$ ratio which is an indicator of the disulphide bond formation/breakage. As can be seen from Figure 5.3 C, initially, only a minoramount of $(PyKC)_2$ was present in the system. However, once H_2O_2 – TCEP was added, most of the PyKC was dimerized within 10 min. As the cycle progressed, the dimeric PyKC slowly gets converted to monomeric PyKC and at 40^{th} min. (end of thecycle), full conversion was observed. Around this time (45^{th} min.), the second cycle was initiated and at 50^{th} min., both the species were found in almost equal proportion.

As the coacervates can be formed transiently under two different triggers, it would be extremely useful if both the triggers can be applied sequentially to create the coacervates transiently. To check that possibility, we started with $(PyKC)_2$ – Poly-CHO (1:10) in water maintained at pH 5. The pH cycle was initiated using urease, urea – GdL (1:5). The transient cycle followed the usual pattern (Figure 5.3 D) and the system returned back to the original homogeneous solution phase as well as pH 5 within 120 min. As the redox cycle can operate only in basic condition, a combination of NaOH – TCEP wasadded. A sharp enhancement in the turbidity (up to ~25) followed by a fast decline was observed.

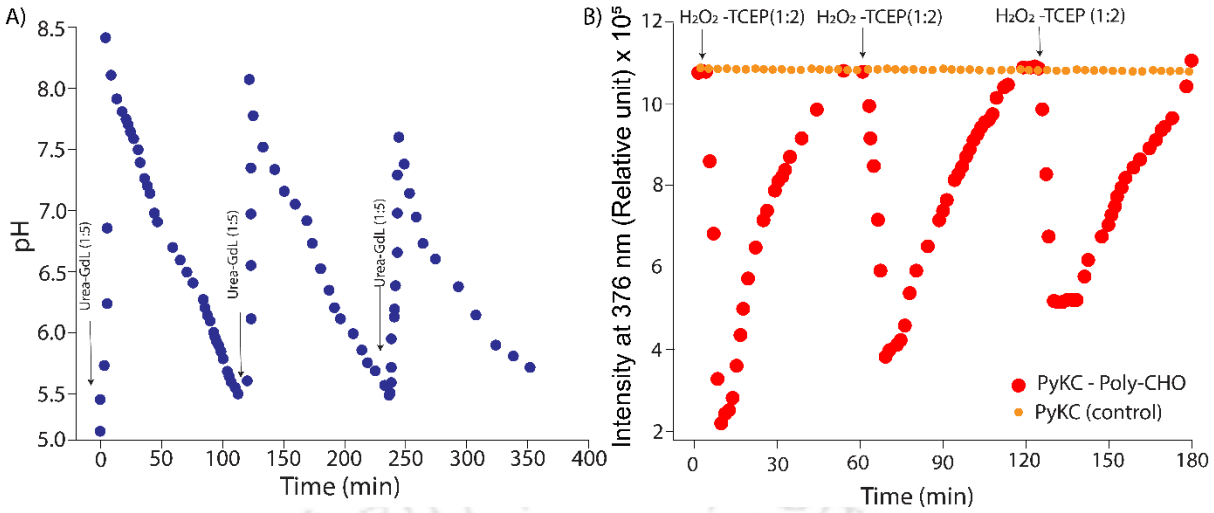

Figure 5.7A) The change in pH during the pH clock assisted transient formation of coacervates as shown in Figure 5.2 B and C of the main manuscript. B) Transient formation of the coacervates (PyKC – Poly-CHO 1:10 in 20 mM Tris buffer pH 8) under the influence of redox cycle as monitored using fluorescence quenching of pyrene at 376 nm (λ_{ex} = 337 nm).

The sudden change in the pH of the system led to the formation of some aggregates which eventually collapsed due to the presence of TCEP. The redox triggered transient cycle was then commenced by the addition of 1:2 H_2O_2 – TCEP. The turbidity enhanced to the maxima and remained there for ~ 30 min as the coacervates are formed. After that, the turbidity returned back to the original lower value indicating the dissolution of the coacervates. These results unequivocally demonstrate the adaptability of the system.

5.3 conclusion

In summary, we have demonstrated the coacervation of a polymer and a short peptide through two different dynamic covalent bonds. The coacervates are responsive to the change in pH of the medium as well as toward reducing agents. Utilizing the dynamic imine bonds and disulphide linkages, the coacervates were transiently formed under the influence of a pH cycle and a redox cycle respectively. Importantly, the system showed adaptability as the transient formation of the coacervates can be achieved within the same solution when both the triggers (pH and redox cycles) are applied sequentially.

5.4 Experimental section

5.4.1 Optical microscopy

Optical microscopic studies were performed using an inverted optical Olympus IX81 epifluorescence microscope. Typically, 10 mL of solutions were placed on a glass slide with a coverslip and placed under the microscope to capture the bright field, and fluorescence images.

5.4.2 Turbidity measurement

The turbidity of the solutions was measured by using a UV-vis spectrophotometer at 600 nm, where none of the components absorbed the light. The turbidity was calculated using the below given formula,

Turbidity = 100 - %T, where %T is transmittance.

5.4.3 Stock Solutions for Different Experiments

Stock solutions of Poly-CHO (30 mg/mL) and PyKC (3 mg/mL) were prepared in Milli-Q water and were incubated for minimum 48 h to ensure complete dimerization of the PyKC ($(PyKC)_2$, checked by analytical HPLC) before using the solutions for further experiments. However, for transient formation of the coacervates under the influence of redox cycle, freshly prepared stock solution of PyKC (3 mg/mL) in Tris buffer (20 mM, pH 8) was used to ensure the presence of only the monomeric species. Similarly, for these cases, Poly-CHO (30 mg/mL) stock solution was also prepared in Tris buffer (20 mM, pH 8).

Below is the list of stock solutions used for different studies,

Urease: 2 mg/mL in Milli-Q water and stored at 4 °C.

Urea: 20 mM in Milli-Q water.

GdL: 20 mM in DMSO.

H_2O_2: 100 mM in Milli-Q water.

TCEP: 100 mM in Milli-Q water.

NaOH: 1 M in Milli-Q water.

HCl: 1 M in Milli-Q water.

5.4.4 Preparation of Coacervates using PolyCHO and PyKC

Required volumes of stock solutions of Poly-CHO and PyKC were mixed and the volume was made up to 1 mL by using a Tris buffer (20 mM, pH 8) to get the final concentrations of Poly-CHO and PyKC as 3 and 0.3 mg/mL respectively. The solution was incubated for 24 h and coacervation was checked by using optical microscopy, turbidity and emission quenching experiments. The morphology was checked by using FESEM.

Similar procedure was followed for Poly-CHO – PyKC ratio optimization, coacervation by other combinations of polymer (Poly-CHO, Poly-Benz) and peptides (Cystamine, PyRS, PyKS, Py1KC, C_8KC).

For pH dependent coacervation, similar procedure was followed. However, in place of Tris buffer, different buffers of varying pH were used.

5.4.5 Transient pH Cycle:

The required amount of urease (final concentration: 0.02 mg/mL) was added to 1 mL Milli-Q water and the pH of the solution was adjusted to ~5 using 1 M HCl solution. Appropriate volumes of urea and GdL stock solutions in the required ratio were added to the solution. The change in pH was then monitored over time at 298K on a Hanna HI 2210 pH meter equipped with HI1131 pH probe from Hanna.

Once the optimization was done, to form the coacervates transiently, similar procedure was applied where the initial solution contained $(PyKC)_2$ (0.3 mg/mL using the 48 h matured stock solution of PyKC) and Poly-CHO (3 mg/mL, using the stock solution). To this, required amount of urease (to attain a final concentration of 0.02 mg/mL) was added. The pH cycle was initiated by addition of the stock solutions of urea and GdL (1:5) and either the turbidity or the

change in the emission intensity of the 376 nm peak (λ_{ex} = 337 nm) was monitored against time.

5.4.6 Transient Redox Cycle

For redox responsive transient coacervation, required volume of stock solutions of PyKC and Poly-CHO were mixed in Tris buffer (20 mM, pH 8) to maintain the overall concentrations of 0.3 and 3 mg/mL. Required volume of H_2O_2 and TCEP stock solutions were added to this solution to attain a certain H_2O_2 – TCEP ratio (where H_2O_2 concentration was maintained at 0.2 mM). The change in the emission intensity of the 376 nm peak was monitored against time while the sample was excited at 337 nm.

Once the optimization was done, the coacervate formation using the optimized H_2O_2 – TCEP ratio (1:2) were monitored by either turbidity or the change in the emission intensity of the 376 nm peak (λ_{ex} = 337 nm) against time.

5.4.7 Response of the Coacervates Toward Different Stimuli

To evaluate the responsiveness of the coacervates toward different stimuli, initially 1 mL solution of Poly-CHO (3 mg/mL) and $(PyKC)_2$ (0.3 mg/mL) was prepared in Milli-Q water using the respective stock solutions. The pH of the system was adjusted to 5 by adding required amount of 1 M HCl solution. Either turbidity or the change in the emission intensity of the 376 nm peak (λ_{ex} = 337 nm) of the solution was then monitored as different stimuli were added sequentially. The order of the addition of stimuli is as given below,

NaOH (50 mL of stock) → TCEP (10 mL of stock) →H_2O_2 (10 mL of stock) → HCl (50 mL of stock) → NaOH (50 mL of stock) → TCEP (10 mL of stock)

5.4.8 Transient Formation of the Coacervates Under the Influence of Two Different Triggers

To check whether the coacervates can be formed transiently within the same solution using two different cycles one after the other, we started with $(PyKC)_2$ (0.3 mg/mL) and Poly-CHO (3 mg/mL) in 1 mL Milli-Q water and adjusted the pH to 5 by addition of required amount of 1 M HCl solution. To this, 10 mL of urease stock solution (to attain a final concentration of 0.02 mg/mL) was added. The pH cycle was initiated by addition of the stock solutions of urea (20 mL of stock solution) and GdL (100 mL of stock solution) and the turbidity was monitored against time. After the completion of the pH cycle, to bring the pH to basic medium and break the disulphide linkages, a combination of NaOH (50 mL of stock solution) – TCEP (20 mL of stock solution) was added. The turbidity increased initially and then

decreased to the bottom. At this point, H_2O_2(10 mL of stock solution) – TCEP (10 mL of stock) was added to initiate the redox cycle. The pH of the system was also monitored at different time points during the experiment.

5.4.9 Estimation of PyKC and $(PyKC)_2$ during Transient Redox Cycle

A solution of PyKC – Poly-CHO (1:10, with 0.3 mg/mL PyKC) was prepared in1 mL 20 mM Tris buffer pH 8. The redox cycle was initiated by adding H_2O_2 (20 mL of stock solution)– TCEP (10 mL of stock solution). At different time interval, 50 mL aliquots were withdrawn and to them 5 mL of 1 M HCl solution were added immediately. It is to be noted that one aliquot was taken immediately after the dissolution of PyKC – Poly-CHO. All the samples were then analysed by analytical HPLC using a Luna 5 mm (C18) column.

6. References

1. Lehn, J. M., Supramolecular chemistry—scope and perspectives molecules, supermolecules, and molecular devices (Nobel Lecture). *Angew. Chem. Int. Ed.* **1988,***27* (1), 89-112.

2. Lehn, J. M., Perspectives in supramolecular chemistry—from molecular recognition towards molecular information processing and self-organization. *Angew. Chem. Int. Ed.* **1990,***29* (11), 1304-1319.

3. Whitesides, G. M.; Mathias, J. P.; Seto, C. T., Molecular self-assembly and nanochemistry: a chemical strategy for the synthesis of nanostructures. *Science* **1991,***254* (5036), 1312-9.

4. Grenningloh, G.; Rehm, E. J.; Goodman, C. S., Genetic analysis of growth cone guidance in Drosophila: fasciclin II functions as a neuronal recognition molecule. *Cell***1991,***67* (1), 45-57.

5. Desiraju, G. R., Chemistry beyond the molecule. *Nature* **2001,***412* (6845), 397-400.

6. Subramani, K.; Ahmed, W., Self-Assembly of Proteins and Peptides and Their Applications in Bionanotechnology and Dentistry. In *Emerging Nanotechnologies in Dentistry*, Elsevier: 2012; pp 209-224.

7. Dasgupta, A.; Mondal, J. H.; Das, D., Peptide hydrogels. *RSC Adv.* **2013,***3* (24), 9117-9149.

8. Li, J.; Mooney, D. J., Designing hydrogels for controlled drug delivery. *Nat. Rev. Mater.* **2016,***1* (12), 1-17.

9. Dan, N., Core–shell drug carriers: liposomes, polymersomes, and niosomes. In*Nanostructures for drug delivery*, Elsevier: 2017; pp 63-105.

10. Löwik, D. W.; van Hest, J. C., Peptide based amphiphiles. *Chem. Soc. Rev.* **2004,***33* (4), 234-245.

11. Edwards-Gayle, C. J. C.; Hamley, I. W., Self-assembly of bioactive peptides, peptide conjugates, and peptide mimetic materials. *Org. Biomol. Chem.* **2017,***15* (28), 5867-5876.

12. Löwik, D. W.; van Hest, J. C., Peptide based amphiphiles. *Chem. Soc. Rev.***2004,***33* (4), 234-245.

13. Schneider, J. P.; Pochan, D. J.; Ozbas, B.; Rajagopal, K.; Pakstis, L.; Kretsinger, J., Responsive hydrogels from the intramolecular folding and self-assembly of a designed peptide. *J. Am. Chem. Soc.* **2002,***124* (50), 15030-7.

14. Doig, A. J., Recent advances in helix-coil theory. *Biophys. Chem.***2002,***101*, 281-293.

15. Reches, M.; Gazit, E., Controlled patterning of aligned self-assembled peptide nanotubes. *Nat. Nanotechnol.* **2006,***1* (3), 195-200.

16. Sathaye, S.; Zhang, H.; Sonmez, C.; Schneider, J. P.; MacDermaid, C. M.; Von Bargen, C. D.; Saven, J. G.; Pochan, D. J., Engineering complementary hydrophobic interactions to control beta-hairpin peptide self-assembly, network branching, and hydrogel properties. *Biomacromolecules* **2014,***15* (11), 3891-900.

17. Dasgupta, A.; Das, D., Designer Peptide Amphiphiles: Self-Assembly to Applications. *Langmuir* **2019,***35* (33), 10704-10724.

18. Fleming, S.; Ulijn, R. V., Design of nanostructures based on aromatic peptide amphiphiles. *Chem. Soc. Rev.* **2014,***43* (23), 8150-77.

19. Liebmann, T.; Rydholm, S.; Akpe, V.; Brismar, H., Self-assembling Fmoc dipeptide hydrogel for in situ 3D cell culturing. *BMC Biotechnol.* **2007,***7* (1), 88.

20. Tang, C.; Ulijn, R. V.; Saiani, A., Effect of Glycine Substitution on Fmoc-Diphenylalanine Self-Assembly and Gelation Properties. *Langmuir* **2011,***27* (23), 14438-14449.

21. Shi, J. F.; Gao, Y. A.; Yang, Z. M.; Xu, B., Exceptionally small supramolecular hydrogelators based on aromatic-aromatic interactions. *Beilstein J. Org. Chem.***2011,***7* (1), 167-172.

22. Sánchez-Iglesias, A.; Grzelczak, M.; Altantzis, T.; Goris, B.; Perez-Juste, J.; Bals, S.; Van Tendeloo, G.; Donaldson Jr, S. H.; Chmelka, B. F.; Israelachvili, J. N., Hydrophobic interactions modulate self-assembly of nanoparticles. *ACS Nano* **2012,***6* (12), 11059-11065.
23. Ta, S., Micellar solutions as reaction media. *Tetrahedron* **1996,***52* (34), 11113-11152.
24. Das, D.; Roy, S.; Das, P. K., Efficient and simple NaBH4 reduction of esters at cationic micellar surface. *Org. Lett.* **2004,***6* (22), 4133-4136.
25. Pileni, M. P., Nanosized particles made in colloidal assemblies. *Langmuir* **1997,***13* (13), 3266-3276.
26. Carvalho, C. M. L.; Cabral, J. M. S., Reverse micelles as reaction media for lipases. *Biochimie* **2000,***82* (11), 1063-1085.
27. Savsunenko, O.; Matondo, H.; Franceschi-Messant, S.; Perez, E.; Popov, A. F.; Rico-Lattes, I.; Lattes, A.; Karpichev, Y., Functionalized vesicles based on amphiphilic boronic acids: a system for recognizing biologically important polyols. *Langmuir* **2013,***29* (10), 3207-13.
28. Weiss, R. G.; Terech, P., Molecular gels. **2006,***Materials with Self-Assembled Fibrillar Networks*

29. Patterson, J.; Siew, R.; Herring, S. W.; Lin, A. S.; Guldberg, R.; Stayton, P. S., Hyaluronic acid hydrogels with controlled degradation properties for oriented bone regeneration. *Biomaterials* **2010,***31* (26), 6772-81.
30. Priftis, D.; Laugel, N.; Tirrell, M., Thermodynamic characterization of polypeptide complex coacervation. *Langmuir* **2012,***28* (45), 15947-57.
31. Sarkar, S.; Choudhury, P.; Dinda, S.; Das, P. K., Tailor-Made Self-Assemblies from Functionalized Amphiphiles: Diversity and Applications. *Langmuir* **2018,***34* (36), 10449-10468.
32. Gortner, R.; Hoffman, W., An interesting colloidal gel. *J. Am. Chem. Soc***1921,***43*, 2199-2202.

33. Li, Y.; Qin, M.; Cao, Y.; Wang, W., Designing the mechanical properties of peptide-based supramolecular hydrogels for biomedical applications. *Sci China Phys Mech* **2014,***57* (5), 849-858.
34. Du, X.; Zhou, J.; Shi, J.; Xu, B., Supramolecular Hydrogelators and Hydrogels: From Soft Matter to Molecular Biomaterials. *Chem. Rev.* **2015,***115* (24), 13165-307.
35. Lim, J. Y. C.; Lin, Q.; Xue, K.; Loh, X. J., Recent advances in supramolecular hydrogels for biomedical applications. *Mater. Today Adv.***2019,***3*, 100021.
36. Dong, R. J.; Pang, Y.; Su, Y.; Zhu, X. Y., Supramolecular hydrogels: synthesis, properties and their biomedical applications. *Biomater Sci-Uk* **2015,***3* (7), 937-954.
37. Appel, E. A.; del Barrio, J.; Loh, X. J.; Scherman, O. A., Supramolecular polymeric hydrogels. *Chem. Soc. Rev.* **2012,***41* (18), 6195-214.
38. Li, J., Self-assembled supramolecular hydrogels based on polymer–cyclodextrin inclusion complexes for drug delivery. NPG Asia Mater 2: 112–118. *Small***2010,***10* (7), 1387-1393.

39. Stuart, M. A. C.; Hofs, B.; Voets, I. K.; de Keizer, A., Assembly of polyelectrolyte-containing block copolymers in aqueous media. *Curr. Opin. Colloid Interface Sci.***2005,***10* (1-2), 30-36.
40. Sangeetha, N. M.; Maitra, U., Supramolecular gels: functions and uses. *Chem. Soc. Rev.* **2005,***34* (10), 821-36.
41. Ayabe, M.; Kishida, T.; Fujita, N.; Sada, K.; Shinkai, S., Binary organogelators which show light and temperature responsiveness. *Org. Biomol. Chem.***2003,***1* (15), 2744-2747.
42. Ulijn, R. V.; Smith, A. M., Designing peptide based nanomaterials. *Chem. Soc. Rev.* **2008,***37* (4), 664-75.
43. Adams, D. J.; Topham, P. D., Peptide conjugate hydrogelators. *Soft Matter* **2010,***6* (16), 3707-3721.

44. Paramonov, S. E.; Jun, H. W.; Hartgerink, J. D., Self-assembly of peptide-amphiphile nanofibers: the roles of hydrogen bonding and amphiphilic packing. *J. Am. Chem. Soc.* **2006,***128* (22), 7291-8.
45. Liu, X.; Zhao, L.; Liu, F. F.; Astruc, D.; Gu, H. B., Supramolecular redox-responsive ferrocene hydrogels and microgels. *Coordin. Chem. Rev.***2020,***419*, 213406.
46. Das, S.; Das, D., Rational Design of Peptide-based Smart Hydrogels for Therapeutic Applications. *Front. Chem.* **2021,***9*, 770102.
47. Rajagopal, K.; Lamm, M. S.; Haines-Butterick, L. A.; Pochan, D. J.; Schneider, J. P., Tuning the pH responsiveness of beta-hairpin peptide folding, self-assembly, and hydrogel material formation. *Biomacromolecules* **2009,***10* (9), 2619-25.
48. Fletcher, N. L.; Lockett, C. V.; Dexter, A. F., A pH-responsive coiled-coil peptide hydrogel. *Soft Matter* **2011,***7* (21), 10210-10218.
49. Zhao, Y.; Yokoi, H.; Tanaka, M.; Kinoshita, T.; Tan, T., Self-assembled pH-responsive hydrogels composed of the RATEA16 peptide. *Biomacromolecules* **2008,***9* (6), 1511-8.
50. Ghosh, G.; Barman, R.; Sarkar, J.; Ghosh, S., pH-Responsive Biocompatible Supramolecular Peptide Hydrogel. *J. Phys. Chem. B* **2019,***123* (27), 5909-5915.
51. D'Souza, A.; Marshall, L. R.; Yoon, J.; Kulesha, A.; Edirisinghe, D. I.; Chandrasekaran, S.; Rathee, P.; Prabhakar, R.; Makhlynets, O. V., Peptide hydrogel with self-healing and redox-responsive properties. *Nano Converg.* **2022,***9* (1), 1-8.
52. Sun, Z.; Li, Z.; He, Y.; Shen, R.; Deng, L.; Yang, M.; Liang, Y.; Zhang, Y., Ferrocenoyl phenylalanine: a new strategy toward supramolecular hydrogels with multistimuli responsive properties. *J. Am. Chem. Soc.* **2013,***135* (36), 13379-86.
53. Bowerman, C. J.; Nilsson, B. L., A reductive trigger for peptide self-assembly and hydrogelation. *J. Am. Chem. Soc.* **2010,***132* (28), 9526-7.
54. Qiu, Y.; Park, K., Environment-sensitive hydrogels for drug delivery. *Adv. Drug Deliv. Rev.* **2001,***53* (3), 321-39.
55. Mailra, N., Supramolecular gels: Function and uses. *Chem. Soc. Rev.* **2005,***34*, 821-836.
56. Jiang, Y.; Chen, J.; Deng, C.; Suuronen, E. J.; Zhong, Z., Click hydrogels, microgels and nanogels: emerging platforms for drug delivery and tissue engineering. *Biomaterials* **2014,***35* (18), 4969-85.
57. Madl, C. M.; Heilshorn, S. C., Bioorthogonal Strategies for Engineering Extracellular Matrices. *Adv. Funct. Mater.* **2018,***28* (11), 1706046.
58. Sun Han Chang, R.; Lee, J. C.; Pedron, S.; Harley, B. A. C.; Rogers, S. A., Rheological Analysis of the Gelation Kinetics of an Enzyme Cross-linked PEG Hydrogel. *Biomacromolecules* **2019,***20* (6), 2198-2206.
59. Rydholm, A. E.; Bowman, C. N.; Anseth, K. S., Degradable thiol-acrylate photopolymers: polymerization and degradation behavior of an in situ forming biomaterial. *Biomaterials* **2005,***26* (22), 4495-506.
60. Hoffman, A. S., Hydrogels for biomedical applications. *Adv Drug Deliver Rev* **2012,***64*, 18-23.
61. Laftah, W. A.; Hashim, S.; Ibrahim, A. N., Polymer Hydrogels: A Review. *Polym-Plast Technol* **2011,***50* (14), 1475-1486.
62. Naficy, S.; Brown, H. R.; Razal, J. M.; Spinks, G. M.; Whitten, P. G., Progress Toward Robust Polymer Hydrogels. *Aust. J. Chem.***2011,***64* (8), 1007-1025.
63. Naficy, S.; Kawakami, S.; Sadegholvaad, S.; Wakisaka, M.; Spinks, G. M., Mechanical properties of interpenetrating polymer network hydrogels based on hybrid ionically and covalently crosslinked networks. *J. Appl. Polym. Sci.***2013,***130* (4), 2504-2513.

64. Chakraborty, P.; Ghosh, M.; Schnaider, L.; Adadi, N.; Ji, W.; Bychenko, D.; Dvir, T.; Adler-Abramovich, L.; Gazit, E., Composite of Peptide-Supramolecular Polymer and Covalent Polymer Comprises a New Multifunctional, Bio-Inspired Soft Material. *Macromol. Rapid Commun.* **2019,***40* (18), e1900175.
65. Lin, C. Y.; Battistoni, C. M.; Liu, J. C., Redox-Responsive Hydrogels with Decoupled Initial Stiffness and Degradation. *Biomacromolecules* **2021,***22* (12), 5270-5280.
66. Cao, Y.; Yao, Y.; Li, Y.; Yang, X.; Cao, Z.; Yang, G., Tunable keratin hydrogel based on disulphide shuffling strategy for drug delivery and tissue engineering. *J. Colloid Interface Sci.* **2019,***544*, 121-129.
67. Das, B. K.; Pramanik, B.; Chowdhuri, S.; Scherman, O. A.; Das, D., Light-triggered syneresis of a water insoluble peptide-hydrogel effectively removes small molecule waste contaminants. *Chem. Commun.* **2020,***56* (23), 3393-3396.
68. Boekhoven, J.; Hendriksen, W. E.; Koper, G. J.; Eelkema, R.; van Esch, J. H., Transient assembly of active materials fueled by a chemical reaction. *Science* **2015,***349* (6252), 1075-9.
69. van Rossum, S. A. P.; Tena-Solsona, M.; van Esch, J. H.; Eelkema, R.; Boekhoven, J., Dissipative out-of-equilibrium assembly of man-made supramolecular materials. *Chem. Soc. Rev.* **2017,***46* (18), 5519-5535.
70. Kariyawasam, L. S.; Hartley, C. S., Dissipative Assembly of Aqueous Carboxylic Acid Anhydrides Fueled by Carbodiimides. *J. Am. Chem. Soc.* **2017,***139* (34), 11949-11955.
71. Wojciechowski, J. P.; Martin, A. D.; Thordarson, P., Kinetically Controlled Lifetimes in Redox-Responsive Transient Supramolecular Hydrogels. *J. Am. Chem. Soc.* **2018,***140* (8), 2869-2874.
72. Pappas, C. G.; Sasselli, I. R.; Ulijn, R. V., Biocatalytic Pathway Selection in Transient Tripeptide Nanostructures. *Angew. Chem. Int. Ed.* **2015,***54* (28), 8119-23.
73. Li, J. L.; Wang, A. H.; Zhao, L. Y.; Dong, Q. Q.; Wang, M. Y.; Xu, H. L.; Yan, X. H.; Bai, S., Self-Assembly of Monomeric Hydrophobic Photosensitizers with Short Peptides Forming Photodynamic Nanoparticles with Real-Time Tracking Property and without the Need of Release in Vivo. *Acs Appl. Mater. Inter.***2018,***10* (34), 28420-28427.
74. Wang, H.; Wang, Y.; Shen, B.; Liu, X.; Lee, M., Substrate-Driven Transient Self-Assembly and Spontaneous Disassembly Directed by Chemical Reaction with Product Release. *J. Am. Chem. Soc.* **2019,***141* (10), 4182-4185.
75. Liu, Y.; Winter, H. H.; Perry, S. L., Linear viscoelasticity of complex coacervates. *Adv. Colloid Interface Sci.* **2017,***239*, 46-60.
76. Abbas, M.; Lipin, W. P.; Wang, J.; Spruijt, E., Peptide-based coacervates as biomimetic protocells. *Chem. Soc. Rev* **2021,***50* (6), 3690-3705.
77. Aumiller, W. M.; Keating, C. D., Phosphorylation-mediated RNA/peptide complex coacervation as a model for intracellular liquid organelles. *Nat. Chem.***2016,***8* (2), 129-137.
78. Nakashima, K. K.; Baaij, J. F.; Spruijt, E., Reversible generation of coacervate droplets in an enzymatic network. *Soft Matter* **2018,***14* (3), 361-367.
79. Abbas, M.; Lipinski, W. P.; Nakashima, K. K.; Huck, W. T. S.; Spruijt, E., A short peptide synthon for liquid-liquid phase separation. *Nat. Chem.***2021,***13* (11), 1046-+.
80. Shen, Y.; Ruggeri, F. S.; Vigolo, D.; Kamada, A.; Qamar, S.; Levin, A.; Iserman, C.; Alberti, S.; George-Hyslop, P. S.; Knowles, T. P. J., Biomolecular condensates undergo a generic shear-mediated liquid-to-solid transition. *Nat. Nanotechnol.* **2020,***15* (10), 841-847.
81. van Esch, J. H.; Klajn, R.; Otto, S., Chemical systems out of equilibrium. *Chem. Soc. Rev.* **2017,***46* (18), 5474-5475.
82. Mukhopadhyay, S., Catalytic coacervate crucibles. *Nat. Chem.* **2021,***13* (11), 1028-1030.

83. Weiβ, G.; Knoch, A.; Laicher, A.; Stanislaus, F.; Daniels, R., Simple coacervation of hydroxypropyl methylcellulose phthalate (HPMCP) I. Temperature and pH dependency of coacervate formation. *Int. J. Pharm.* **1995,***124* (1), 87-96.
84. Mohanty, B.; Bohidar, H. B., Microscopic structure of gelatin coacervates. *Int. J. Biol. Macromol.* **2005,***36* (1-2), 39-46.
85. Merindol, R.; Loescher, S.; Samanta, A.; Walther, A., Pathway-controlled formation of mesostructured all-DNA colloids and superstructures. *Nat. Nanotechnol.* **2018,***13* (8), 730-738.
86. Imura, T.; Yanagishita, H.; Kitamoto, D., Coacervate formation from natural glycolipid: one acetyl group on the headgroup triggers coacervate-to-vesicle transition. *J. Am. Chem. Soc.* **2004,***126* (35), 10804-5.
87. Deng, N. N., Complex coacervates as artificial membraneless organelles and protocells. *Biomicrofluidics* **2020,***14* (5), 051301.
88. Tiebackx, F., Gleichzeitige ausflockung zweier kolloide. *Zeitschrift für Chemie und Industrie der Kolloide***1911,***8* (4), 198-201.
89. Priftis, D.; Tirrell, M., Phase behaviour and complex coacervation of aqueous polypeptide solutions. *Soft Matter* **2012,***8* (36), 9396-9405.
90. McCall, P. M.; Srivastava, S.; Perry, S. L.; Kovar, D. R.; Gardel, M. L.; Tirrell, M. V., Partitioning and Enhanced Self-Assembly of Actin in Polypeptide Coacervates. *Biophys. J.* **2018,***114* (7), 1636-1645.
91. Lu, T. M.; Nakashima, K. K.; Spruijt, E., Temperature-Responsive Peptide-Nucleotide Coacervates. *J. Phys. Chem. B* **2021,***125* (12), 3080-3091.
92. De Kruif, C. G.; Weinbreck, F.; de Vries, R., Complex coacervation of proteins and anionic polysaccharides. *Curr. Opin. Colloid Interface Sci.***2004,***9* (5), 340-349.
93. Dompé, M.; Cedano-Serrano, F. J.; Heckert, O.; van den Heuvel, N.; van der Gucht, J.; Tran, Y.; Hourdet, D.; Creton, C.; Kamperman, M., Thermoresponsive Complex Coacervate-Based Underwater Adhesive. *Adv. Mater.* **2019,***31* (21), 1808179.
94. Jeon, O.; Wolfson, D. W.; Alsberg, E., In-situ formation of growth-factor-loaded coacervate microparticle-embedded hydrogels for directing encapsulated stem cell fate. *Adv. Mater.* **2015,***27* (13), 2216-23.
95. Sun, Y.; Lau, S. Y.; Lim, Z. W.; Chang, S. C.; Ghadessy, F.; Partridge, A.; Miserez, A., Phase-separating peptides for direct cytosolic delivery and redox-activated release of macromolecular therapeutics. *Nat. Chem.* **2022,***14* (3), 274-283.
96. Te Brinke, E.; Groen, J.; Herrmann, A.; Heus, H. A.; Rivas, G.; Spruijt, E.; Huck, W. T. S., Dissipative adaptation in driven self-assembly leading to self-dividing fibrils. *Nat. Nanotechnol.* **2018,***13* (9), 849-855.
97. Donau, C.; Spath, F.; Sosson, M.; Kriebisch, B. A. K.; Schnitter, F.; Tena-Solsona, M.; Kang, H. S.; Salibi, E.; Sattler, M.; Mutschler, H.; Boekhoven, J., Active coacervate droplets as a model for membraneless organelles and protocells. *Nat. Commun.***2020,***11* (1), 1-10.
98. Karoui, H.; Seck, M. J.; Martin, N., Self-programmed enzyme phase separation and multiphase coacervate droplet organization. *Chem. Sci.* **2021,***12* (8), 2794-2802.
99. Lewis, R. W.; Klemm, B.; Macchione, M.; Eelkema, R., Fuel-driven macromolecular coacervation in complex coacervate core micelles. *Chem. Sci.* **2022,***13* (16), 4533-4544.
100. Singha, N.; Srivastava, A.; Pramanik, B.; Ahmed, S.; Dowari, P.; Chowdhuri, S.; Das, B. K.; Debnath, A.; Das, D., Unusual confinement properties of a water insoluble small peptide hydrogel. *Chem. Sci.* **2019,***10* (23), 5920-5928.

101. Zhang, H.; Fei, J.; Yan, X.; Wang, A.; Li, J., Enzyme-responsive release of doxorubicin from monodisperse dipeptide-based nanocarriers for highly efficient cancer treatment in vitro. *Adv. Funct. Mater.* **2015,***25* (8), 1193-1204.
102. Wang, H.; Yang, Z., Short-peptide-based molecular hydrogels: novel gelation strategies and applications for tissue engineering and drug delivery. *Nanoscale* **2012,***4* (17), 5259-67.
103. Wan, S.; Borland, S.; Richardson, S. M.; Merry, C. L. R.; Saiani, A.; Gough, J. E., Self-assembling peptide hydrogel for intervertebral disc tissue engineering. *Acta Biomater.* **2016,***46*, 29-40.
104. Takeuchi, T.; Bizenjima, T.; Ishii, Y.; Imamura, K.; Suzuki, E.; Seshima, F.; Saito, A., Enhanced healing of surgical periodontal defects in rats following application of a self-assembling peptide nanofibre hydrogel. *J. Clin. Periodontol.* **2016,***43* (3), 279-88.
105. Paladini, F.; Meikle, S. T.; Cooper, I. R.; Lacey, J.; Perugini, V.; Santin, M., Silver-doped self-assembling di-phenylalanine hydrogels as wound dressing biomaterials. *J. Mater. Sci.: Mater. Med.***2013,***24* (10), 2461-2472.
106. Zou, Q. L.; Abbas, M.; Zhao, L. Y.; Li, S. K.; Shen, G. Z.; Yan, X. H., Biological Photothermal Nanodots Based on Self-Assembly of Peptide Porphyrin Conjugates for Antitumor Therapy. *J. Am. Chem. Soc.* **2017,***139* (5), 1921-1927.
107. Liu, K.; Xing, R.; Zou, Q.; Ma, G.; Mohwald, H.; Yan, X., Simple Peptide-Tuned Self-Assembly of Photosensitizers towards Anticancer Photodynamic Therapy. *Angew. Chem. Int. Ed.* **2016,***55* (9), 3036-9.
108. Li, S.; Zou, Q.; Li, Y.; Yuan, C.; Xing, R.; Yan, X., Smart Peptide-Based Supramolecular Photodynamic Metallo-Nanodrugs Designed by Multicomponent Coordination Self-Assembly. *J. Am. Chem. Soc.* **2018,***140* (34), 10794-10802.
109. Kapałczyńska, M.; Kolenda, T.; Przybyła, W.; Zajączkowska, M.; Teresiak, A.; Filas, V.; Ibbs, M.; Bliźniak, R.; Łuczewski, Ł.; Lamperska, K., 2D and 3D cell cultures–a comparison of different types of cancer cell cultures. *Arch. Med. Sci.***2018,***14* (4), 910.

110. Jayawarna, V.; Ali, M.; Jowitt, T. A.; Miller, A. F.; Saiani, A.; Gough, J. E.; Ulijn, R. V., Nanostructured hydrogels for three-dimensional cell culture through self-assembly of fluorenylmethoxycarbonyl–dipeptides. *Adv. mater.* **2006,***18* (5), 611-614.

111. Liu, X.; Wang, X.; Wang, X.; Ren, H.; He, J.; Qiao, L.; Cui, F. Z., Functionalized self-assembling peptide nanofiber hydrogels mimic stem cell niche to control human adipose stem cell behavior in vitro. *Acta Biomater.* **2013,***9* (6), 6798-805.
112. Seow, W. Y.; Kandasamy, K.; Purnamawati, K.; Sun, W.; Hauser, C. A. E., Thin peptide hydrogel membranes suitable as scaffolds for engineering layered biostructures. *Acta Biomater.***2019,***88*, 293-300.
113. Song, R.; Murphy, M.; Li, C.; Ting, K.; Soo, C.; Zheng, Z., Current development of biodegradable polymeric materials for biomedical applications. *Drug Des. Devel. Ther.* **2018,***12*, 3117-3145.
114. Nonoyama, T., Robust hydrogel-bioceramics composite and its osteoconductive properties. *Polym J.* **2020,***52* (7), 709-716.
115. Okumura, Y.; Ito, K., The polyrotaxane gel: A topological gel by figure-of-eight cross-links. *Adv. Mater.* **2001,***13* (7), 485-487.
116. Sakai, T.; Matsunaga, T.; Yamamoto, Y.; Ito, C.; Yoshida, R.; Suzuki, S.; Sasaki, N.; Shibayama, M.; Chung, U. I., Design and fabrication of a high-strength hydrogel with ideally homogeneous network structure from tetrahedron-like macromonomers. *Macromolecules* **2008,***41* (14), 5379-5384.

117. Gong, J. P.; Katsuyama, Y.; Kurokawa, T.; Osada, Y., Double-network hydrogels with extremely high mechanical strength. *Adv. mater.***2003,***15* (14), 1155-1158.

118. Akagawa, Y.; Kubo, T.; Koretake, K.; Hayashi, K.; Doi, K.; Matsuura, A.; Morita, K.; Takeshita, R.; Yuan, Q.; Tabata, Y., Initial bone regeneration around fenestrated implants in Beagle dogs using basic fibroblast growth factor-gelatin hydrogel complex with varying biodegradation rates. *J. Prosthodont. Res.* **2009,***53* (1), 41-47.

119. Asamura, S.; Mochizuki, Y.; Yamamoto, M.; Tabata, Y.; Isogai, N., Bone Regeneration Using a Bone Morphogenetic Protein-2 Saturated Slow-Release Gelatin Hydrogel Sheet Evaluation in a Canine Orbital Floor Fracture Model. *Ann. Plast. Surg.* **2010,***64* (4), 496-502.

120. Boontheekul, T.; Kong, H. J.; Mooney, D. J., Controlling alginate gel degradation utilizing partial oxidation and bimodal molecular weight distribution. *Biomaterials* **2005,***26* (15), 2455-65.

121. Kim, J.; Kim, I. S.; Cho, T. H.; Lee, K. B.; Hwang, S. J.; Tae, G.; Noh, I.; Lee, S. H.; Park, Y.; Sun, K., Bone regeneration using hyaluronic acid-based hydrogel with bone morphogenic protein-2 and human mesenchymal stem cells. *Biomaterials* **2007,***28* (10), 1830-1837.

122. Martínez-Sanz, E.; Ossipov, D. A.; Hilborn, J.; Larsson, S.; Jonsson, K. B.; Varghese, O. P., Bone reservoir: Injectable hyaluronic acid hydrogel for minimal invasive bone augmentation. *J. Control. Release* **2011,***152* (2), 232-240.

123. Jo, S.; Kim, S.; Cho, T. H.; Shin, E.; Hwang, S. J.; Noh, I., Effects of recombinant human bone morphogenic protein-2 and human bone marrow-derived stromal cells on in vivo bone regeneration of chitosan–poly (ethylene oxide) hydrogel. *J. Biomed. Mater. Res. A***2013,***101* (3), 892-901.

124. Fini, M.; Motta, A.; Torricelli, P.; Giavaresi, G.; Nicoli Aldini, N.; Tschon, M.; Giardino, R.; Migliaresi, C., The healing of confined critical size cancellous defects in the presence of silk fibroin hydrogel. *Biomaterials* **2005,***26* (17), 3527-36.

125. Wang, X.; Kluge, J. A.; Leisk, G. G.; Kaplan, D. L., Sonication-induced gelation of silk fibroin for cell encapsulation. *Biomaterials* **2008,***29* (8), 1054-64.

126. Fu, S.; Ni, P.; Wang, B.; Chu, B.; Zheng, L.; Luo, F.; Luo, J.; Qian, Z., Injectable and thermo-sensitive PEG-PCL-PEG copolymer/collagen/n-HA hydrogel composite for guided bone regeneration. *Biomaterials* **2012,***33* (19), 4801-9.

127. Holloway, J. L.; Ma, H.; Rai, R.; Burdick, J. A., Modulating hydrogel crosslink density and degradation to control bone morphogenetic protein delivery and in vivo bone formation. *J. Control Release* **2014,***191*, 63-70.

128. Watson, B. M.; Vo, T. N.; Engel, P. S.; Mikos, A. G., Biodegradable, in Situ-Forming Cell-Laden Hydrogel Composites of Hydroxyapatite Nanoparticles for Bone Regeneration. *Ind. En.g Chem. Res.***2015,***54* (42), 10206-10211.

129. Gilmore, K. A.; Lampley, M. W.; Boyer, C.; Harth, E., Matrices for combined delivery of proteins and synthetic molecules. *Adv. Drug Deliv. Rev.* **2016,***98*, 77-85.

130. Nel, A.; Xia, T.; Madler, L.; Li, N., Toxic potential of materials at the nanolevel. *Science* **2006,***311* (5761), 622-627.

131. Hansen, M. B.; van Gaal, E.; Minten, I.; Storm, G.; van Hest, J. C.; Lowik, D. W., Constrained and UV-activatable cell-penetrating peptides for intracellular delivery of liposomes. *J. Control Release* **2012,***164* (1), 87-94.

132. Abbas, M.; Zou, Q.; Li, S.; Yan, X., Self-Assembled Peptide- and Protein-Based Nanomaterials for Antitumor Photodynamic and Photothermal Therapy. *Adv. Mater.* **2017,***29* (12), 1605021.

133. Slowing, I. I.; Vivero-Escoto, J. L.; Wu, C. W.; Lin, V. S. Y., Mesoporous silica nanoparticles as controlled release drug delivery and gene transfection carriers. *Adv. Drug Deliv. Rev.***2008,***60* (11), 1278-1288.

134. Ghosh, P.; Han, G.; De, M.; Kim, C. K.; Rotello, V. M., Gold nanoparticles in delivery applications. *Adv. Drug Deliv. Rev.* **2008,***60* (11), 1307-1315.
135. Lammers, T., Aime S. Hennink WE Storm G. Kiessling F. *Acc. Chem. Res* **2011,***44*, 1029-1038.
136. Torchilin, V. P., Multifunctional nanocarriers. *Adv. Drug Deliv. Rev.* **2006,***58* (14), 1532-55.
137. Song, Z.; Chen, X.; You, X.; Huang, K.; Dhinakar, A.; Gu, Z.; Wu, J., Self-assembly of peptide amphiphiles for drug delivery: the role of peptide primary and secondary structures. *Biomater. Sci.* **2017,***5* (12), 2369-2380.
138. Vashist, A.; Vashist, A.; Gupta, Y. K.; Ahmad, S., Recent advances in hydrogel based drug delivery systems for the human body. *J. Mater. Chem. B* **2014,***2* (2), 147-166.
139. Vegners, R.; Shestakova, I.; Kalvinsh, I.; Ezzell, R. M.; Janmey, P. A., Use of a gel-forming dipeptide derivative as a carrier for antigen presentation. *J. Pept. Sci.* **1995,***1* (6), 371-378.
140. Nagai, Y.; Unsworth, L. D.; Koutsopoulos, S.; Zhang, S., Slow release of molecules in self-assembling peptide nanofiber scaffold. *J. Control Release***2006,***115* (1), 18-25.
141. Yang, C. B.; Li, D. X.; FengZhao, Q. Q.; Wang, L. Y.; Wang, L.; Yang, Z. M., Disulphide bond reduction-triggered molecular hydrogels of folic acid Taxol conjugates. *Org. Biomol. Chem.***2013,***11* (40), 6946-6951.
142. Chen, J.; Zou, X., Self-assemble peptide biomaterials and their biomedical applications. *Bioact. Mater.* **2019,***4*, 120-131.
143. Lampel, A.; Ulijn, R. V.; Tuttle, T., Guiding principles for peptide nanotechnology through directed discovery. *Chem. Soc. Rev.* **2018,***47*, 3737-3758.
144. Dasgupta, A.; Mondal, J. H.; Das, D., Peptide hydrogels. *RSC Advances* **2013,***3*, 9117-9149.
145. Seow, W. Y.; Hauser, C. A. E., Short to ultrashort peptide hydrogels for biomedical uses. *Mater. Today***2014,***17*, 381-388.
146. Sis, M. J.; Webber, M. J., Drug Delivery with Designed Peptide Assemblies. *Trends Pharmacol. Sci.* **2019,***40*, 747-762.
147. Altunbas, A.; Lee, S. J.; Rajasekaran, S. A.; Schneider, J. P.; Pochan, D. J., Encapsulation of curcumin in self-assembling peptide hydrogels as injectable drug delivery vehicles. *Biomaterials* **2011,***32*, 5906-5914.
148. Worthington, P.; Pochan, D. J.; Langhans, S. A., Peptide Hydrogels – Versatile Matrices for 3D Cell Culture in Cancer Medicine. *Front. Oncol.* **2015,***5*.
149. Dowari, P.; Saha, S.; Pramanik, B.; Ahmed, S.; Singha, N.; Ukil, A.; Das, D., Multiple Cross-Linking of a Small Peptide to Form a Size Tunable Biopolymer with Efficient Cell Adhesion and Proliferation Property. *Biomacromolecules* **2018,***19*, 3994-4002.
150. Singha, N.; Srivastava, A.; Pramanik, B.; Ahmed, S.; Dowari, P.; Chowdhuri, S.; Das, B. K.; Debnath, A.; Das, D., Unusual confinement properties of a water insoluble small peptide hydrogel. *Chem. Sci.* **2019,***10*, 5920-5928.
151. Singha, N.; Neogi, S.; Pramanik, B.; Das, S.; Dasgupta, A.; Ghosh, R.; Das, D., Ultrafast, Highly Sensitive, and Selective Detection of p-Xylene at Room Temperature by Peptide-Hydrogel-Based Composite Material. *ACS Appl. Polym. Mater.* **2019,***1*, 2267-2272.
152. Chakraborty, P.; Guterman, T.; Adadi, N.; Yadid, M.; Brosh, T.; Adler-Abramovich, L.; Dvir, T.; Gazit, E., A Self-Healing, All-Organic, Conducting, Composite Peptide Hydrogel as Pressure Sensor and Electrogenic Cell Soft Substrate. *ACS Nano* **2019,***13*, 163-175.
153. Makam, P.; Gazit, E., Minimalistic peptide supramolecular co-assembly: expanding the conformational space for nanotechnology. *Chem. Soc. Rev.* **2018,***47*, 3406-3420.
154. Ulijn, R. V.; Smith, A. M., Designing peptide based nanomaterials. *Chem. Soc. Rev.* **2008,***37*, 664-675.

155. Reithofer, M. R.; Lakshmanan, A.; Ping, A. T. K.; Chin, J. M.; Hauser, C. A. E., In situ synthesis of size-controlled, stable silver nanoparticles within ultrashort peptide hydrogels and their anti-bacterial properties. *Biomaterials* **2014,***35*, 7535-7542.
156. Singha, N.; Das, B. K.; Pramanik, B.; Das, S.; Das, D., Freeze the dynamicity: charge transfer complexation assisted control over the reaction pathway. *Chem. Sci.* **2019,***10*, 10035-10039.
157. Sarkhel, B.; Chatterjee, A.; Das, D., Covalent Catalysis by Cross β Amyloid Nanotubes. *J. Am. Chem. Soc.* **2020,***142*, 4098-4103.
158. Ahmed, S.; Pramanik, B.; Sankar, K. N. A.; Srivastava, A.; Singha, N.; Dowari, P.; Srivastava, A.; Mohanta, K.; Debnath, A.; Das, D., Solvent Assisted Tuning of Morphology of a Peptide-Perylenediimide Conjugate: Helical Fibers to Nano-Rings and their Differential Semiconductivity. *Sci. Rep.* **2017,***7*, 9485.
159. Du, X.; Zhou, J.; Shi, J.; Xu, B., Supramolecular Hydrogelators and Hydrogels: From Soft Matter to Molecular Biomaterials. *Chem. Rev.* **2015,***115*, 13165-13307.
160. Dasgupta, A.; Das, D., Designer Peptide Amphiphiles: Self-Assembly to Applications. *Langmuir* **2019,***35*, 10704-10724.
161. Tang, J. D.; Mura, C.; Lampe, K. J., Stimuli-Responsive, Pentapeptide, Nanofiber Hydrogel for Tissue Engineering. *J. Am. Chem. Soc.* **2019,***141*, 4886-4899.
162. Ulijn, R. V.; Bibi, N.; Jayawarna, V.; Thornton, P. D.; Todd, S. J.; Mart, R. J.; Smith, A. M.; Gough, J. E., Bioresponsive hydrogels. *Mater. Today* **2007,***10*, 40-48.
163. Zheng, D.; Gao, Z.; Xu, T.; Liang, C.; Shi, Y.; Wang, L.; Yang, Z., Responsive peptide-based supramolecular hydrogels constructed by self-immolative chemistry. *Nanoscale* **2018,***10*, 21459-21465.
164. Yang, X.; Wang, Y.; Qi, W.; Xing, R.; Yang, X.; Xing, Q.; Su, R.; He, Z., Disulphide crosslinking and helical coiling of peptide micelles facilitate the formation of a printable hydrogel. *J. Mater. Chem. B* **2019,***7*, 2981-2988.
165. Bowerman, C. J.; Nilsson, B. L., A Reductive Trigger for Peptide Self-Assembly and Hydrogelation. *J. Am. Chem. Soc.* **2010,***132*, 9526-9527.
166. Song, S.; Wang, J.; Cheng, Z.; Yang, Z.; Shi, L.; Yu, Z., Directional molecular sliding movement in peptide hydrogels accelerates cell proliferation. *Chem. Sci.* **2020,***11*, 1383-1393.
167. Seow, W. Y.; Salgado, G.; Lane, E. B.; Hauser, C. A. E., Transparent crosslinked ultrashort peptide hydrogel dressing with high shape-fidelity accelerates healing of full-thickness excision wounds. *Sci. Rep.* **2016,***6*, 32670.
168. Seow, W. Y.; Hauser, C. A. E., Tunable Mechanical Properties of Ultrasmall Peptide Hydrogels by Crosslinking and Functionalization to Achieve the 3D Distribution of Cells. *Ad. Healthcare Mater.* **2013,***2*, 1219-1223.
169. Das, B. K.; Pramanik, B.; Chowdhuri, S.; Scherman, O. A.; Das, D., Light-triggered syneresis of a water insoluble peptide-hydrogel effectively removes small molecule waste contaminants. *Chem. Commun.* **2020,***56*, 3393-3396.
170. Mondal, J. H.; Ahmed, S.; Das, D., Physicochemical Analysis of Mixed Micelles of a Viologen Surfactant: Extended to Water-in-Oil (w/o) Microemulsion and Cucurbit[8]uril-Assisted Vesicle Formation. *Langmuir* **2014,***30*, 8290-8299.
171. Michelini, E.; Cevenini, L.; Mezzanotte, L.; Coppa, A.; Roda, A., Cell-based assays: fuelling drug discovery. *Anal. Bioanal. Chem.* **2010,***398*, 227-238.
172. Edmondson, R.; Broglie, J. J.; Adcock, A. F.; Yang, L., Three-Dimensional Cell Culture Systems and Their Applications in Drug Discovery and Cell-Based Biosensors. *Assay Drug Dev. Techn.* **2014,***12*, 207-218.

173. Hinderer, S.; Layland, S. L.; Schenke-Layland, K., ECM and ECM-like materials — Biomaterials for applications in regenerative medicine and cancer therapy. *Adv. Drug Deliv. Rev.* **2016,***97*, 260-269.
174. Kyburz, K. A.; Anseth, K. S., Synthetic Mimics of the Extracellular Matrix: How Simple is Complex Enough? *Ann. Biomed. Eng.* **2015,***43*, 489-500.
175. Zhan, H.; Löwik, D. W. P. M., A Hybrid Peptide Amphiphile Fiber PEG Hydrogel Matrix for 3D Cell Culture. *Adv. Funct. Mater.* **2019,***29*, 1808505.
176. Alakpa, Enateri V.; Jayawarna, V.; Lampel, A.; Burgess, Karl V.; West, Christopher C.; Bakker, Sanne C. J.; Roy, S.; Javid, N.; Fleming, S.; Lamprou, Dimitris A.; Yang, J.; Miller, A.; Urquhart, Andrew J.; Frederix, Pim W. J. M.; Hunt, Neil T.; Péault, B.; Ulijn, Rein V.; Dalby, Matthew J., Tunable Supramolecular Hydrogels for Selection of Lineage-Guiding Metabolites in Stem Cell Cultures. *Chem* **2016,***1*, 298-319.
177. Geckil, H.; Xu, F.; Zhang, X.; Moon, S.; Demirci, U., Engineering hydrogels as extracellular matrix mimics. *Nanomedicine* **2010,***5*, 469-484.
178. Gough, J. E.; Saiani, A.; Miller, A. F., Peptide hydrogels: mimicking the extracellular matrix. *Bioinspir. Biomim. Nanobiomater.* **2012,***1* (1), 4-12.
179. Hellmund, K. S.; Koksch, B., Self-Assembling Peptides as Extracellular Matrix Mimics to Influence Stem Cell's Fate. *Front. Chem.* **2019,***7*.
180. Kumar, D.; Workman, V. L.; O'Brien, M.; McLaren, J.; White, L.; Ragunath, K.; Rose, F.; Saiani, A.; Gough, J. E., Peptide Hydrogels—A Tissue Engineering Strategy for the Prevention of Oesophageal Strictures. *Adv. Funct. Mater.* **2017,***27*, 1702424.
181. Adak, A.; Das, G.; Khan, J.; Mukherjee, N.; Gupta, V.; Mallesh, R.; Ghosh, S., Extracellular Matrix (ECM)-Mimicking Neuroprotective Injectable Sulfo-Functionalized Peptide Hydrogel for Repairing Brain Injury. *ACS Biomater. Sci. Eng.* **2020,** (6), 2287–2296.
182. Kim, S.-H.; Lee, S.-H.; Lee, J.-E.; Park, S. J.; Kim, K.; Kim, I. S.; Lee, Y.-S.; Hwang, N. S.; Kim, B.-G., Tissue adhesive, rapid forming, and sprayable ECM hydrogel via recombinant tyrosinase crosslinking. *Biomaterials* **2018,***178*, 401-412.
183. Tao, K.; Wang, J.; Zhou, P.; Wang, C.; Xu, H.; Zhao, X.; Lu, J. R., Self-Assembly of Short Aβ(16−22) Peptides: Effect of Terminal Capping and the Role of Electrostatic Interaction. *Langmuir* **2011,***27*, 2723-2730.
184. Castelletto, V.; Hamley, I. W.; Cenker, Ç.; Olsson, U.; Adamcik, J.; Mezzenga, R.; Miravet, J. F.; Escuder, B.; Rodríguez-Llansola, F., Influence of End-Capping on the Self-Assembly of Model Amyloid Peptide Fragments. *J. Phys. Chem. B* **2011,***115*, 2107-2116.
185. Reches, M.; Gazit, E., Self-assembly of peptide nanotubes and amyloid-like structures by charged-termini-capped diphenylalanine peptide analogues. *Isr. J. Chem.* **2005,***45*, 363-371.
186. Andreasen, M.; Skeby, K. K.; Zhang, S.; Nielsen, E. H.; Klausen, L. H.; Frahm, H.; Christiansen, G.; Skrydstrup, T.; Dong, M.; Schiøtt, B.; Otzen, D., The Importance of Being Capped: Terminal Capping of an Amyloidogenic Peptide Affects Fibrillation Propensity and Fibril Morphology. *Biochemistry* **2014,***53*, 6968-6980.
187. De Leon Rodriguez, L. M.; Hemar, Y.; Cornish, J.; Brimble, M. A., Structure–mechanical property correlations of hydrogel forming β-sheet peptides. *Chem. Soc. Rev.* **2016,***45*, 4797-4824.
188. Ihsan, A. B.; Nargis, M.; Koyama, Y., Effects of the Hydrophilic-Lipophilic Balance of Alternating Peptides on Self-Assembly and Thermo-Responsive Behaviors. *Int. J. Mol. Sci.* **2019,***20*, 4604.
189. Chen, C.; Gu, Y.; Deng, L.; Han, S.; Sun, X.; Chen, Y.; Lu, J. R.; Xu, H., Tuning Gelation Kinetics and Mechanical Rigidity of β-Hairpin Peptide Hydrogels via Hydrophobic Amino Acid Substitutions. *ACS Appl. Mater. Interfaces* **2014,***6*, 14360-14368.

190. Lehninger, A. L.; Cox, M. M. N.; L., D., *Lehninger principles of biochemistry*. W. H. Freeman: New York, 2008.
191. Schnaider, L.; Brahmachari, S.; Schmidt, N. W.; Mensa, B.; Shaham-Niv, S.; Bychenko, D.; Adler-Abramovich, L.; Shimon, L. J. W.; Kolusheva, S.; DeGrado, W. F.; Gazit, E., Self-assembling dipeptide antibacterial nanostructures with membrane disrupting activity. *Nat. Commun.* **2017,***8*, 1365.
192. Reches, M.; Gazit, E., Casting Metal Nanowires Within Discrete Self-Assembled Peptide Nanotubes. *Science* **2003,***300*, 625-627.
193. Na, N.; Mu, X.; Liu, Q.; Wen, J.; Wang, F.; Ouyang, J., Self-assembly of diphenylalanine peptides into microtubes with "turn on" fluorescence using an aggregation-induced emission molecule. *Chem. Commun.* **2013,***49*, 10076-10078.
194. Shlomo, Z.; Vinod, T. P.; Jelinek, R.; Rapaport, H., Stacking interactions by two Phe side chains stabilize and orient assemblies of even the minimal amphiphilic β-sheet motif. *Chem. Commun.***2015,***51*, 3154-3157.
195. Adler-Abramovich, L.; Reches, M.; Sedman, V. L.; Allen, S.; Tendler, S. J. B.; Gazit, E., Thermal and Chemical Stability of Diphenylalanine Peptide Nanotubes: Implications for Nanotechnological Applications. *Langmuir* **2006,***22*, 1313-1320.
196. Kralj, S.; Bellotto, O.; Parisi, E.; Garcia, A. M.; Iglesias, D.; Semeraro, S.; Deganutti, C.; D'Andrea, P.; Vargiu, A. V.; Geremia, S.; De Zorzi, R.; Marchesan, S., Heterochirality and Halogenation Control Phe-Phe Hierarchical Assembly. *ACS Nano* **2020**, 14 (12), 16951–16961.
197. Singha, N.; Gupta, P.; Pramanik, B.; Ahmed, S.; Dasgupta, A.; Ukil, A.; Das, D., Hydrogelation of a Naphthalene Diimide Appended Peptide Amphiphile and Its Application in Cell Imaging and Intracellular pH Sensing. *Biomacromolecules* **2017,***18*, 3630-3641.
198. Pramanik, B.; Singha, N.; Das, D., Sol-, Gel-, and Paper-Based Detection of Picric Acid at Femtogram Level by a Short Peptide Gelator. *ACS Appl. Polym. Mater.* **2019,***1*, 833-843.
199. Mears, L. L. E.; Draper, E. R.; Castilla, A. M.; Su, H.; Zhuola; Dietrich, B.; Nolan, M. C.; Smith, G. N.; Doutch, J.; Rogers, S.; Akhtar, R.; Cui, H.; Adams, D. J., Drying Affects the Fiber Network in Low Molecular Weight Hydrogels. *Biomacromolecules* **2017,***18*, 3531-3540.
200. Adams, D. J., Does Drying Affect Gel Networks? . *Gels* **2018,** *4*, 32.
201. Yan, C.; Pochan, D. J., Rheological properties of peptide-based hydrogels for biomedical and other applications. *Chem. Soc. Rev.* **2010,***39*, 3528-3540.
202. Lim, J. Y. C.; Lin, Q.; Xue, K.; Loh, X. J., Recent advances in supramolecular hydrogels for biomedical applications. *Mater. Today Adv.* **2019,***3*, 100021.
203. Pramanik, B.; Ahmed, S.; Singha, N.; Das, B. K.; Dowari, P.; Das, D., Unorthodox Combination of Cation−π and Charge-Transfer Interactions within a Donor–Acceptor Pair. *Langmuir* **2019,***35*, 478-488.
204. Koons, G. L.; Diba, M.; Mikos, A. G., Materials design for bone-tissue engineering. *Nat. Rev. Mater.* **2020,***5*, 584-603.
205. Liu, L.; Li, C.; Jiao, Y.; Jiang, G.; Mao, J.; Wang, F.; Wang, L., Homogeneous organic/inorganic hybrid scaffolds with high osteoinductive activity for bone tissue engineering. *Polym. Test.* **2020,***91*, 106798.
206. Li, X.; Liu, W.; Sun, L.; Fan, Y.; Feng, Q., The Application of Inorganic Nanomaterials in Bone Tissue Engineering. *J. Biomater. Tissue Eng.* **2014,***4*, 994-1003.
207. Ghosh, M.; Halperin-Sternfeld, M.; Grinberg, I.; Adler-Abramovich, L., Injectable Alginate-Peptide Composite Hydrogel as a Scaffold for Bone Tissue Regeneration. *Nanomaterials* **2019,***9*.
208. Mandal, B. B.; Grinberg, A.; Seok Gil, E.; Panilaitis, B.; Kaplan, D. L., High-strength silk protein scaffolds for bone repair. *Proc. Natl. Acad. Sci.* **2012,***109*, 7699-7704.

209. Van Vlierberghe, S.; Dubruel, P.; Schacht, E., Biopolymer-Based Hydrogels As Scaffolds for Tissue Engineering Applications: A Review. *Biomacromolecules* **2011,***12* (5), 1387-1408.
210. Liu, M.; Zeng, X.; Ma, C.; Yi, H.; Ali, Z.; Mou, X.; Li, S.; Deng, Y.; He, N., Injectable hydrogels for cartilage and bone tissue engineering. *Bone Res.* **2017,***5*, 17014.
211. Zazakowny, K.; Lewandowska-Łańcucka, J.; Mastalska-Popławska, J.; Kamiński, K.; Kusior, A.; Radecka, M.; Nowakowska, M., Biopolymeric hydrogels − nanostructured TiO2 hybrid materials as potential injectable scaffolds for bone regeneration. *Colloids Surf. B: Biointerfaces* **2016,***148*, 607-614.
212. Thambi, T.; Phan, V. H. G.; Lee, D. S., Stimuli-Sensitive Injectable Hydrogels Based on Polysaccharides and Their Biomedical Applications. *Macromol. Rapid Commun.* **2016,***37*, 1881-1896.
213. Xue, X.; Hu, Y.; Deng, Y.; Su, J., Recent Advances in Design of Functional Biocompatible Hydrogels for Bone Tissue Engineering. *Adv. Funct. Mater.* **2021,***31*, 2009432.
214. Cui, H.; Zhu, W.; Nowicki, M.; Zhou, X.; Khademhosseini, A.; Zhang, L. G., Hierarchical Fabrication of Engineered Vascularized Bone Biphasic Constructs via Dual 3D Bioprinting: Integrating Regional Bioactive Factors into Architectural Design. *Adv. Healthcare Mater.* **2016,***5*, 2174-2181.
215. Che, L.; Lei, Z.; Wu, P.; Song, D., A 3D Printable and Bioactive Hydrogel Scaffold to Treat Traumatic Brain Injury. *Adv. Funct. Mater.* **2019,***29*, 1904450.
216. Wu, J.; Zheng, K.; Huang, X.; Liu, J.; Liu, H.; Boccaccini, A. R.; Wan, Y.; Guo, X.; Shao, Z., Thermally triggered injectable chitosan/silk fibroin/bioactive glass nanoparticle hydrogels for in-situ bone formation in rat calvarial bone defects. *Acta Biomater.***2019,***91*, 60-71.
217. Makvandi, P.; Ali, G. W.; Della Sala, F.; Abdel-Fattah, W. I.; Borzacchiello, A., Hyaluronic acid/corn silk extract based injectable nanocomposite: A biomimetic antibacterial scaffold for bone tissue regeneration. *Mater. Sci. Eng.: C* **2020,***107*, 110195.
218. Naumenko, E. A.; Guryanov, I. D.; Yendluri, R.; Lvov, Y. M.; Fakhrullin, R. F., Clay nanotube–biopolymer composite scaffolds for tissue engineering. *Nanoscale* **2016,***8* (13), 7257-7271.
219. Maisani, M.; Ziane, S.; Ehret, C.; Levesque, L.; Siadous, R.; Le Meins, J.-F.; Chevallier, P.; Barthélémy, P.; De Oliveira, H.; Amédée, J.; Mantovani, D.; Chassande, O., A new composite hydrogel combining the biological properties of collagen with the mechanical properties of a supramolecular scaffold for bone tissue engineering. *J. Tissue Eng. Regenerative Med.* **2018,***12*, e1489-e1500.
220. Li, L.; Li, J.; Guo, J.; Zhang, H.; Zhang, X.; Yin, C.; Wang, L.; Zhu, Y.; Yao, Q., 3D Molecularly Functionalized Cell-Free Biomimetic Scaffolds for Osteochondral Regeneration. *Adv. Funct. Mater.* **2019,***29*, 1807356.
221. Seow, W. Y.; Hauser, C. A. E., Short to ultrashort peptide hydrogels for biomedical uses. *Mater. Today* **2014,***17*, 381-388.
222. Fichman, G.; Gazit, E., Self-assembly of short peptides to form hydrogels: design of building blocks, physical properties and technological applications. *Acta Biomater.* **2014,***10*, 1671-82.
223. Diaferia, C.; Ghosh, M.; Sibillano, T.; Gallo, E.; Stornaiuolo, M.; Giannini, C.; Morelli, G.; Adler-Abramovich, L.; Accardo, A., Fmoc-FF and hexapeptide-based multicomponent hydrogels as scaffold materials. *Soft Matter* **2019,***15*, 487-496.
224. Deidda, G.; Jonnalagadda, S. V. R.; Spies, J. W.; Ranella, A.; Mossou, E.; Forsyth, V. T.; Mitchell, E. P.; Bowler, M. W.; Tamamis, P.; Mitraki, A., Self-Assembled Amyloid Peptides with Arg-Gly-Asp (RGD) Motifs As Scaffolds for Tissue Engineering. *ACS Biomater. Sci. Eng.* **2017,***3*, 1404-1416.
225. Halperin-Sternfeld, M.; Ghosh, M.; Sevostianov, R.; Grigoriants, I.; Adler-Abramovich, L., Molecular co-assembly as a strategy for synergistic improvement of the mechanical properties of hydrogels. *Chem. Commun.* **2017,***53*, 9586-9589.

226. Ghosh, M.; Halperin-Sternfeld, M.; Grigoriants, I.; Lee, J.; Nam, K. T.; Adler-Abramovich, L., Arginine-Presenting Peptide Hydrogels Decorated with Hydroxyapatite as Biomimetic Scaffolds for Bone Regeneration. *Biomacromolecules* **2017,***18*, 3541-3550.
227. Ghosh, M.; Bera, S.; Schiffmann, S.; Shimon, L. J. W.; Adler-Abramovich, L., Collagen-Inspired Helical Peptide Coassembly Forms a Rigid Hydrogel with Twisted Polyproline II Architecture. *ACS Nano* **2020,***14*, 9990-10000.
228. Aviv, M.; Halperin-Sternfeld, M.; Grigoriants, I.; Buzhansky, L.; Mironi-Harpaz, I.; Seliktar, D.; Einav, S.; Nevo, Z.; Adler-Abramovich, L., Improving the Mechanical Rigidity of Hyaluronic Acid by Integration of a Supramolecular Peptide Matrix. *Acs Appl. Mater. Inter.***2018,***10*, 41883-41891.
229. Lin, J.; Yao, L.; Li, Z.; Zhang, P.; Zhong, W.; Yuan, Q.; Deng, L., Hybrid hollow spheres of carbon@CoxNi1−xMoO4 as advanced electrodes for high-performance asymmetric supercapacitors. *Nanoscale* **2019,***11*, 3281-3291.
230. Nikoloudakis, E.; Karikis, K.; Han, J.; Kokotidou, C.; Charisiadis, A.; Folias, F.; Douvas, A. M.; Mitraki, A.; Charalambidis, G.; Yan, X.; Coutsolelos, A. G., A self-assembly study of PNA–porphyrin and PNA–BODIPY hybrids in mixed solvent systems. *Nanoscale* **2019,***11*, 3557-3566.
231. Chowdhuri, S.; Saha, A.; Pramanik, B.; Das, S.; Dowari, P.; Ukil, A.; Das, D., Smart Thixotropic Hydrogels by Disulphide-Linked Short Peptides for Effective Three-Dimensional Cell Proliferation. *Langmuir* **2020,***36*, 15450-15462.
232. Kim, B.-S.; Park, I.-K.; Hoshiba, T.; Jiang, H.-L.; Choi, Y.-J.; Akaike, T.; Cho, C.-S., Design of artificial extracellular matrices for tissue engineering. *Progr. Polym. Sci.* **2011,***36*, 238-268.
233. Tang, J.; Katashima, T.; Li, X.; Mitsukami, Y.; Yokoyama, Y.; Sakumichi, N.; Chung, U.-i.; Shibayama, M.; Sakai, T., Swelling Behaviors of Hydrogels with Alternating Neutral/Highly Charged Sequences. *Macromolecules* **2020,***53*, 8244-8254.
234. Chen, M. H.; Wang, L. L.; Chung, J. J.; Kim, Y.-H.; Atluri, P.; Burdick, J. A., Methods To Assess Shear-Thinning Hydrogels for Application As Injectable Biomaterials. *ACS Biomater. Sci. Eng.* **2017,***3*, 3146-3160.
235. Dang, M.; Saunders, L.; Niu, X.; Fan, Y.; Ma, P. X., Biomimetic delivery of signals for bone tissue engineering. *Bone Res.* **2018,***6*, 25.
236. Hao, Z.; Song, Z.; Huang, J.; Huang, K.; Panetta, A.; Gu, Z.; Wu, J., The scaffold microenvironment for stem cell based bone tissue engineering. *Biomater. Sci.* **2017,***5*, 1382-1392.
237. Buddingh', B. C.; van Hest, J. C. J. A. o. c. r., Artificial cells: synthetic compartments with life-like functionality and adaptivity. *Acc. Chem. Res.***2017,***50* (4), 769-777.
238. Dzieciol, A. J.; Mann, S., Designs for life: protocell models in the laboratory. *Chem. Soc. Rev.***2012,***41* (1), 79-85.
239. Johnson, N. R.; Wang, Y., Coacervate delivery systems for proteins and small molecule drugs. *Expert Opin. Drug. Deliv.***2014,***11* (12), 1829-32.
240. Abbas, M.; Lipinski, W. P.; Wang, J.; Spruijt, E., Peptide-based coacervates as biomimetic protocells. *Chem.Soc. Rev.***2021,***50* (6), 3690-3705.
241. Shin, Y.; Brangwynne, C. P., Liquid phase condensation in cell physiology and disease. *Science* **2017,***357* (6357), eaaf4382.
242. Jain, S.; Wheeler, J. R.; Walters, R. W.; Agrawal, A.; Barsic, A.; Parker, R., ATPase-Modulated Stress Granules Contain a Diverse Proteome and Substructure. *Cell* **2016,***164* (3), 487-98.
243. Wu, H., Higher-order assemblies in a new paradigm of signal transduction. *Cell* **2013,***153* (2), 287-92.
244. Brangwynne, C. P.; Eckmann, C. R.; Courson, D. S.; Rybarska, A.; Hoege, C.; Gharakhani, J.; Julicher, F.; Hyman, A. A., Germline P granules are liquid droplets that localize by controlled dissolution/condensation. *Science* **2009,***324* (5935), 1729-32.

245. Banani, S. F.; Lee, H. O.; Hyman, A. A.; Rosen, M. K., Biomolecular condensates: organizers of cellular biochemistry. *Nat. Rev. Mol. Cell Biol.***2017,***18* (5), 285-298.
246. Matsuo, M.; Kurihara, K., Proliferating coacervate droplets as the missing link between chemistry and biology in the origins of life. *Nat. Commun.* **2021,***12* (1), 5487.
247. Abbas, M.; Lipiński, W. P.; Nakashima, K. K.; Huck, W. T. S.; Spruijt, E., A short peptide synthon for liquid–liquid phase separation. *Nat. Chem.* **2021,***13* (11), 1046-1054.
248. Saha, B.; Chatterjee, A.; Reja, A.; Das, D., Condensates of short peptides and ATP for the temporal regulation of cytochrome c activity. *Chem. Commun.* **2019,***55* (94), 14194-14197.
249. Deng, N. N.; Huck, W. T. S., Microfluidic Formation of Monodisperse Coacervate Organelles in Liposomes. *Angew.Chem. Int. Ed. Engl.***2017,***56* (33), 9736-9740.
250. Donau, C.; Späth, F.; Sosson, M.; Kriebisch, B. A. K.; Schnitter, F.; Tena-Solsona, M.; Kang, H.-S.; Salibi, E.; Sattler, M.; Mutschler, H.; Boekhoven, J., Active coacervate droplets as a model for membraneless organelles and protocells. *Nat. Commun.* **2020,***11* (1), 5167.
251. Nakashima, K. K.; van Haren, M. H. I.; André, A. A. M.; Robu, I.; Spruijt, E., Active coacervate droplets are protocells that grow and resist Ostwald ripening. *Nat. Commun.* **2021,***12* (1), 3819.
252. Abbas, M.; Lipiński, W. P.; Wang, J.; Spruijt, E., Peptide-based coacervates as biomimetic protocells. *Chem. Soc. Rev.* **2021,***50* (6), 3690-3705.
253. Chen, X.; Chen, E.-Q.; Shi, A.-C.; Yang, S., Multiphase Coacervates Driven by Electrostatic Correlations. *ACS Macro Lett.* **2021,***10* (8), 1041-1047.
254. Scott, W. A.; Gharakhanian, E. G.; Bell, A. G.; Evans, D.; Barun, E.; Houk, K. N.; Deming, T. J., Active Controlled and Tunable Coacervation Using Side-Chain Functional α-Helical Homopolypeptides. *J. Am. Chem. Soc.* **2021,***143* (43), 18196-18203.
255. Altenburg, W. J.; Yewdall, N. A.; Vervoort, D. F. M.; van Stevendaal, M. H. M. E.; Mason, A. F.; van Hest, J. C. M., Programmed spatial organization of biomacromolecules into discrete, coacervate-based protocells. *Nat. Commun.* **2020,***11* (1), 6282.
256. Deng, N.-N.; Huck, W. T. S., Microfluidic Formation of Monodisperse Coacervate Organelles in Liposomes. *Angw. Chem. Int. Ed. Engl.* **2017,***56* (33), 9736-9740.
257. Magdalena Estirado, E.; Mason, A. F.; Alemán García, M. Á.; van Hest, J. C. M.; Brunsveld, L., Supramolecular Nanoscaffolds within Cytomimetic Protocells as Signal Localization Hubs. *J. Am. Chem. Soc.* **2020,***142* (20), 9106-9111.
258. Zhang, Y.; Chen, Y.; Yang, X.; He, X.; Li, M.; Liu, S.; Wang, K.; Liu, J.; Mann, S., Giant Coacervate Vesicles As an Integrated Approach to Cytomimetic Modeling. *J. Am. Chem. Soc.* **2021,***143* (7), 2866-2874.
259. Mason, A. F.; Buddingh', B. C.; Williams, D. S.; van Hest, J. C. M., Hierarchical Self-Assembly of a Copolymer-Stabilized Coacervate Protocell. *J. Am. Chem. Soc.* **2017,***139* (48), 17309-17312.
260. Imura, T.; Yanagishita, H.; Kitamoto, D., Coacervate Formation from Natural Glycolipid: One Acetyl Group on the Headgroup Triggers Coacervate-to-Vesicle Transition. *J. Am. Chem. Soc.* **2004,***126* (35), 10804-10805.
261. Pramanik, B.; Das, D., Aggregation-Induced Emission or Hydrolysis by Water? The Case of Schiff Bases in Aqueous Organic Solvents. *J. Pys. Chem. C* **2018,***122* (6), 3655-3661.
262. Singha, N.; Srivastava, A.; Pramanik, B.; Ahmed, S.; Dowari, P.; Chowdhuri, S.; Das, B. K.; Debnath, A.; Das, D., Unusual confinement properties of a water insoluble small peptide hydrogel. *Chem. Sci.* **2019,***10* (23), 5920-5928.
263. Singha, N.; Das, B. K.; Pramanik, B.; Das, S.; Das, D., Freeze the dynamicity: charge transfer complexation assisted control over the reaction pathway. *Chem. Sci.* **2019,***10* (43), 10035-10039.

264. Chowdhuri, S.; Ghosh, M.; Adler-Abramovich, L.; Das, D., The Effects of a Short Self-Assembling Peptide on the Physical and Biological Properties of Biopolymer Hydrogels. *Pharmaceutics* **2021,***13* (10), 1602.
265. Miller, E.; Jóźwik-Styczyńska, D., The mechanism of pyrene fluorescence quenching by selective and nonselective quenchers during sol–gel transition. *Colloid Polym. Sci.* **2007,***285* (14), 1561-1571.
266. Loran, C. P.; von Wandruszka, R., Acrylamide quenching of fluorescence in micellar environments. *Anal. Chim. Acta***1992,***258* (2), 335-339.
267. Deshpande, S.; Brandenburg, F.; Lau, A.; Last, M. G. F.; Spoelstra, W. K.; Reese, L.; Wunnava, S.; Dogterom, M.; Dekker, C., Spatiotemporal control of coacervate formation within liposomes. *Nat. Commun.* **2019,***10* (1), 1800.
268. Baynton, K. J.; Bewtra, J. K.; Biswas, N.; Taylor, K. E., Inactivation of horseradish peroxidase by phenol and hydrogen peroxide: a kinetic investigation. *Biochim. Biophys. Acta* **1994,***1206* (2), 272-8.
269. Whitesides, G. M.; Grzybowski, B. J. S., Self-assembly at all scales. Science **2002,***295* (5564), 2418-2421.
270. Singh, N.; Formon, G. J.; De Piccoli, S.; Hermans, T. M. J. A. M., Devising synthetic reaction cycles for dissipative nonequilibrium self-assembly. *Adv. Mater.* **2020,***32* (20), 1906834.
271. Dowari, P.; Das, S.; Pramanik, B.; Das, D. J. C. C., pH clock instructed transient supramolecular peptide amphiphile and its vesicular assembly.*Chem. Commun.* **2019,***55* (94), 14119-14122.
272. Te Brinke, E.; Groen, J.; Herrmann, A.; Heus, H. A.; Rivas, G.; Spruijt, E.; Huck, W., Dissipative adaptation in driven self-assembly leading to self-dividing fibrils. *Nat. Nanotechnol.* **2018,***13* (9), 849-855.
273. Drobot, B.; Iglesias-Artola, J. M.; Le Vay, K.; Mayr, V.; Kar, M.; Kreysing, M.; Mutschler, H.; Tang, T. Compartmentalised RNA catalysis in membrane-free coacervate protocells. *Nat. Commun.* **2018,***9* (1), 1-9.
274. Poudyal, R. R.; Guth-Metzler, R. M.; Veenis, A. J.; Frankel, E. A.; Keating, C. D.; Bevilacqua, P., Template-directed RNA polymerization and enhanced ribozyme catalysis inside membraneless compartments formed by coacervates.*Nat. Commun.***2019,***10* (1), 1-13.
275. Cingil, H. E.; Meertens, N. C.; Voets, I., Temporally programmed disassembly and reassembly of C3Ms.*Small***2018,***14* (46), 1802089.
276. Aumiller Jr, W. M.; Pir Cakmak, F.; Davis, B. W.; Keating, C., RNA-based coacervates as a model for membraneless organelles: formation, properties, and interfacial liposome assembly. Langmuir**2016,***32* (39), 10042-10053.
277. Martin, N.; Tian, L.; Spencer, D.; Coutable-Pennarun, A.; Anderson, J. R.; Mann, S., Photoswitchable phase separation and oligonucleotide trafficking in DNA coacervate microdroplets. *Angw. Chem. Int. Ed.***2019,***131* (41), 14736-14740.
278. Nakashima, K. K.; Baaij, J. F.; Spruijt, E., Reversible generation of coacervate droplets in an enzymatic network. *Soft Matter***2018,***14* (3), 361-367.
279. Semenov, S. N.; Wong, A. S.; Van Der Made, R. M.; Postma, S. G.; Groen, J.; Van Roekel, H. W.; De Greef, T. F.; Huck, W., Rational design of functional and tunable oscillating enzymatic networks. *Nat. Chem.***2015,***7* (2), 160-165.
280. Donau, C.; Späth, F.; Sosson, M.; Kriebisch, B. A.; Schnitter, F.; Tena-Solsona, M.; Kang, H.-S.; Salibi, E.; Sattler, M.; Mutschler, H., Active coacervate droplets as a model for membraneless organelles and protocells. Nat. commun.**2020,***11* (1), 1-10.

281. Zwicker, D.; Decker, M.; Jaensch, S.; Hyman, A. A.; Jülicher, F., Centrosomes are autocatalytic droplets of pericentriolar material organized by centrioles.*PNAS***2014,***111* (26), E2636-E2645.
282. Tena-Solsona, M.; Janssen, J.; Wanzke, C.; Schnitter, F.; Park, H.; Rieß, B.; Gibbs, J. M.; Weber, C. A.; Boekhoven, J., Kinetic Control over droplet ripening in fuel-driven active emulsions. **2020**.
283. Kasai, M.; Asakura, S.; Oosawa, F., The cooperative nature of GF transformation of actin.*Biochim. Biophys. Acta***1962,***57* (1), 22-31.
284. Epstein, I. R.; Xu, B. J. N. n., Reaction–diffusion processes at the nano-and microscales. *Nat. Nanotechnol.***2016,***11* (4), 312-319.
285. Linsenmeier, M.; Kopp, M. R.; Grigolato, F.; Emmanoulidis, L.; Liu, D.; Zürcher, D.; Hondele, M.; Weis, K.; Capasso Palmiero, U.; Arosio, P., Dynamics of synthetic membraneless organelles in microfluidic droplets.*Angw. Chem. Int. Ed.***2019,***131* (41), 14631-14636.
286. Brangwynne, C. P.; Eckmann, C. R.; Courson, D. S.; Rybarska, A.; Hoege, C.; Gharakhani, J.; Jülicher, F.; Hyman, A., Germline P granules are liquid droplets that localize by controlled dissolution/condensation. *Science***2009,***324* (5935), 1729-1732.
287. Banani, S. F.; Lee, H. O.; Hyman, A. A.; Rosen, M., Biomolecular condensates: organizers of cellular biochemistry.*Nat. Rev. Mol. Cell Biol.***2017,***18* (5), 285-298.
288. Rai, A. K.; Chen, J.-X.; Selbach, M.; Pelkmans, L., Kinase-controlled phase transition of membraneless organelles in mitosis. *Nature***2018,***559* (7713), 211-216.
289. Bal, S.; Das, K.; Ahmed, S.; Das, D., Chemically Fueled Dissipative Self-Assembly that Exploits Cooperative Catalysis.*Angew. Chemie.* **2019,***131* (1), 250-253.
290. De, S.; Klajn, R., Dissipative self-assembly driven by the consumption of chemical fuels. *Adv. Matter.* **2018,***30* (41), 1706750.
291. Boekhoven, J.; Hendriksen, W. E.; Koper, G. J.; Eelkema, R.; van Esch, J., Transient assembly of active materials fueled by a chemical reaction. *Science***2015,***349* (6252), 1075-1079.
292. Das, S.; Das, T.; Das, P.; Das, D., Controlling the lifetime of cucurbit [8] uril based self-abolishing nanozymes. *Chem. Sci.***2022,***13* (14), 4050-4057.
293. Das, S.; Das, P.; Dowari, P.; Das, B. K.; Das, D., Bi-directional feedback controlled transience in Cucurbituril based tandem nanozyme.*J. Colloid Interface Sci.***2022,***614*, 172-180.
294. Maiti, S.; Fortunati, I.; Ferrante, C.; Scrimin, P.; Prins, L., Dissipative self-assembly of vesicular nanoreactors. *Nat. chem.* **2016,***8* (7), 725-731.
295. Song, S.; Mason, A. F.; Post, R. A.; De Corato, M.; Mestre, R.; Yewdall, N. A.; Cao, S.; Van Der Hofstad, R. W.; Sanchez, S.; Abdelmohsen, L., Engineering transient dynamics of artificial cells by stochastic distribution of enzymes. *Nat. commun.***2021,***12* (1), 1-9.
296. Späth, F.; Donau, C.; Bergmann, A. M.; Kränzlein, M.; Synatschke, C. V.; Rieger, B.; Boekhoven, J.,Molecular design of chemically fueled peptide–polyelectrolyte coacervate-based assemblies. *J.Am. Chem. Soc.***2021,***143* (12), 4782-4789.
297. Saha, B.; Chatterjee, A.; Reja, A.; Das, D., Condensates of short peptides and ATP for the temporal regulation of cytochrome c activity.*Chem. commun.***2019,***55* (94), 14194-14197.
298. Del Grosso, E.; Prins, L. J.; Ricci, F., Transient DNA-Based Nanostructures Controlled by Redox Inputs. *Angew. Chem. Int. Ed. Engl.* **2020,***59* (32), 13238-13245.
299. Facciotti, C.; Saggiomo, V.; Bunschoten, A.; ten Hove, J. B.; Rood, M. T. M.; van Leeuwen, F. W. B.; Velders, A. H., Assembly, Disassembly and Reassembly of Complex Coacervate Core Micelles with Redox-Responsive Supramolecular Cross-Linkers. *ChemSystemsChem* **2020,***2* (4), e1900032.
300. Ogden, W. A.; Guan, Z., Redox Chemical-Fueled Dissipative Self-Assembly of Active Materials. *ChemSystemsChem* **2020,***2* (4), e1900030.

301. Gao, Y.; Peng, K.; and Mitragotri, S., Covalently Crosslinked Hydrogels via Step-Growth Reactions: Crosslinking Chemistries, Polymers, and Clinical Impact. *Adv. Mater.* **2021**, *33*(25), 2006362.

7. Characterisation Data

Chapter 2

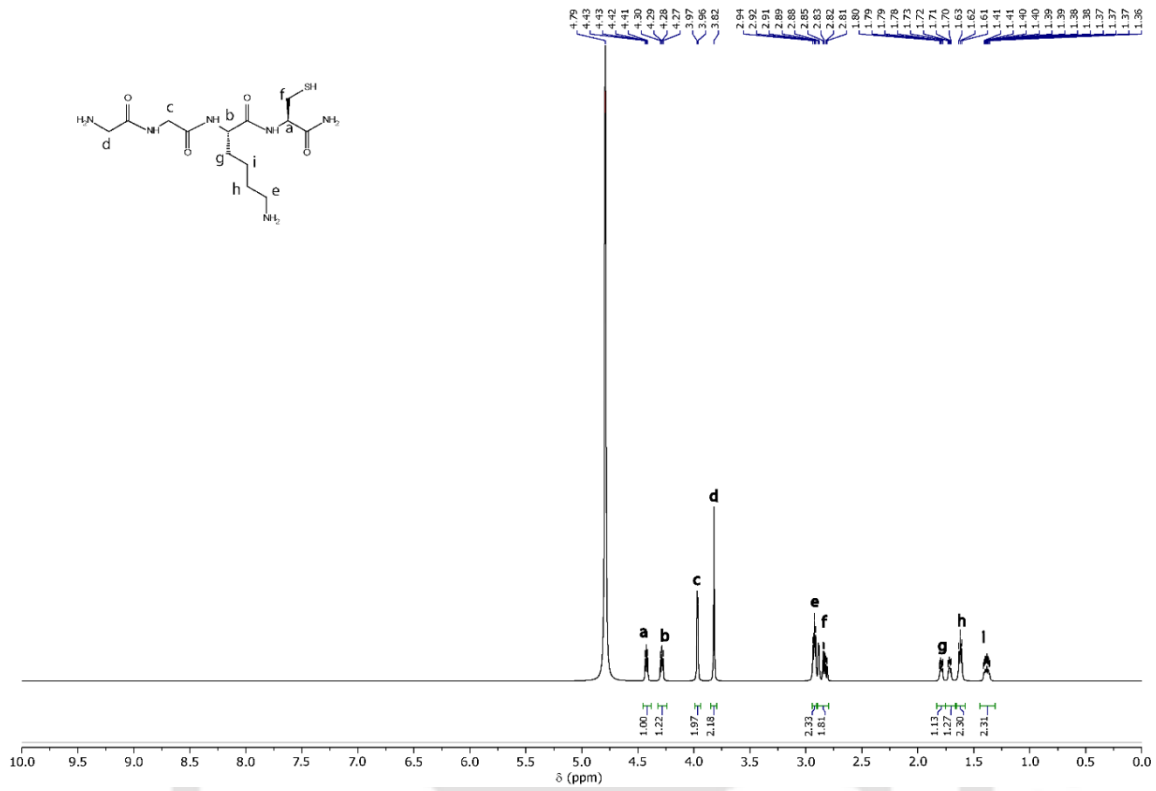

Figure 7.1 ^{1}H NMR Spectrum of Compound **1** in D_2O.

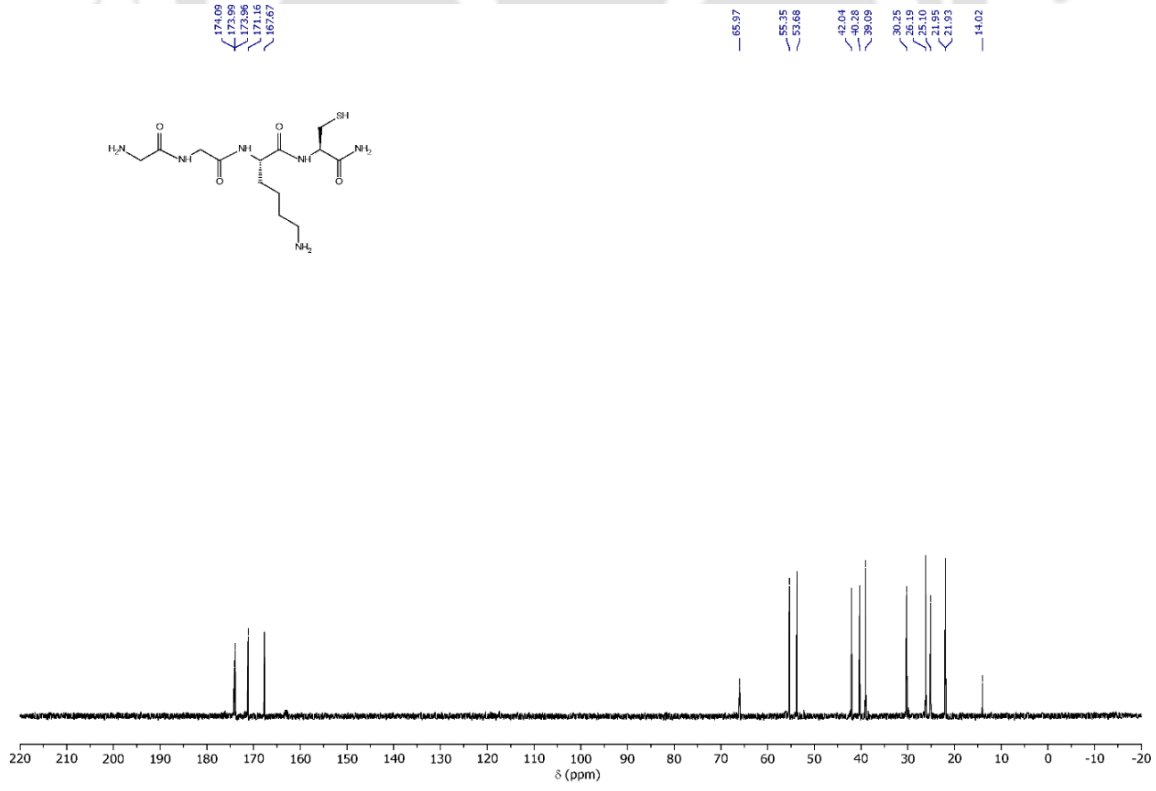

Figure 7.2 ^{13}C NMR Spectrum of Compound **1** in D_2O.

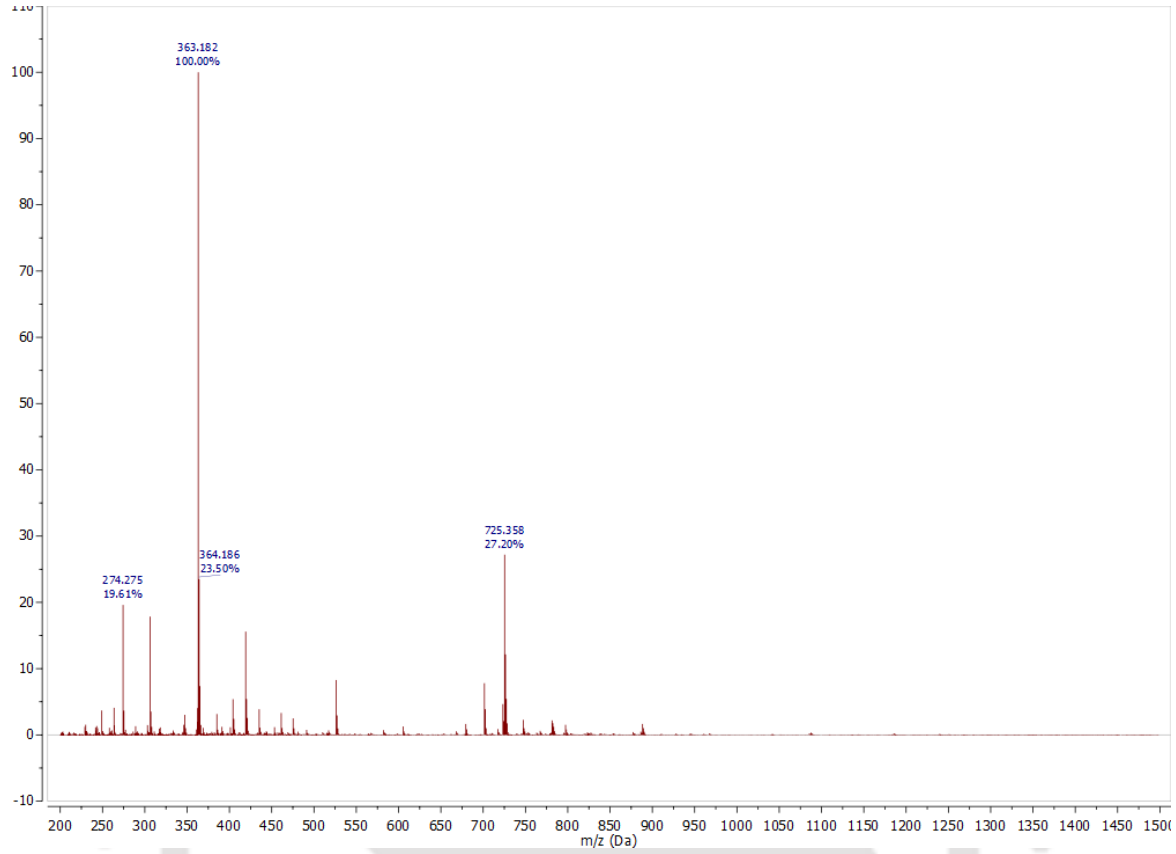

Figure 7.3 ESI-MS Spectrum ofCompound **1**.

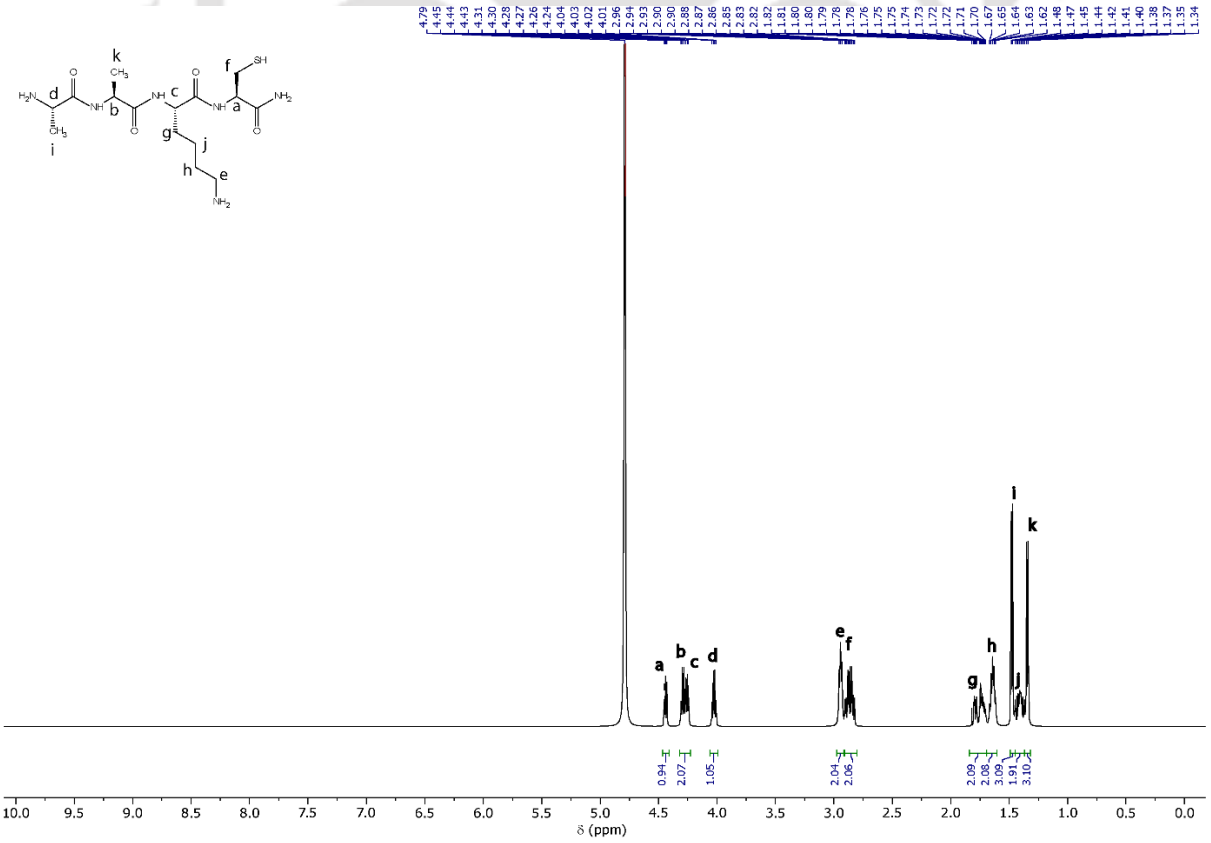

Figure 7.4 ^{1}H NMR Spectrum of Compound **2** in D_2O.

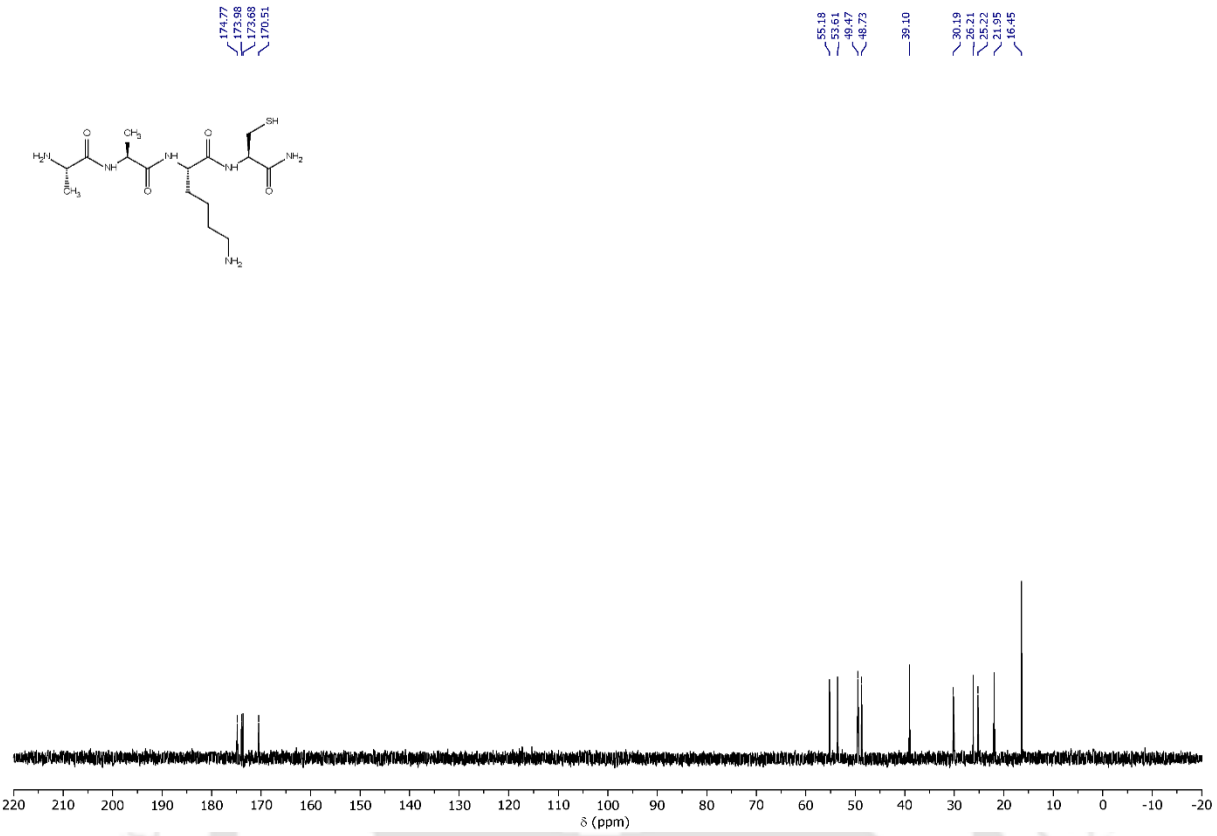

Figure 7.5 ^{13}C NMR Spectrum of Compound **2** in D_2O.

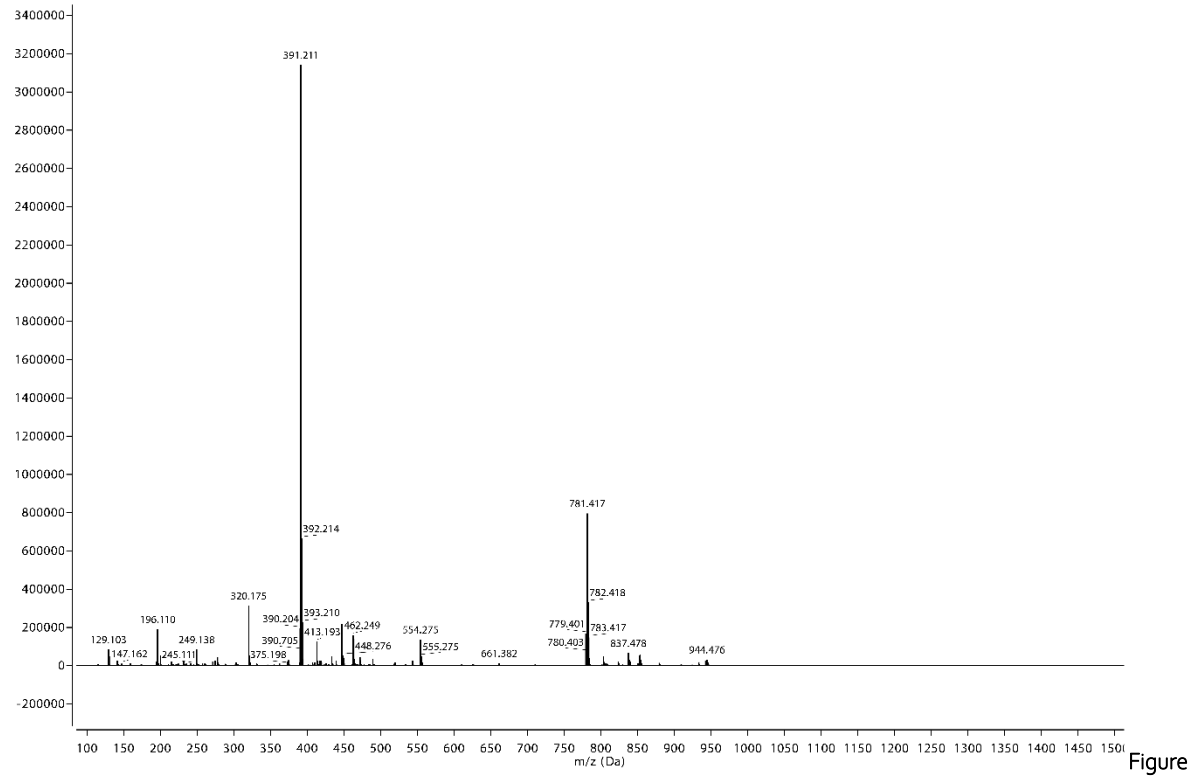

Figure 7.6 ESI-MS Spectrum of Compound **2**.

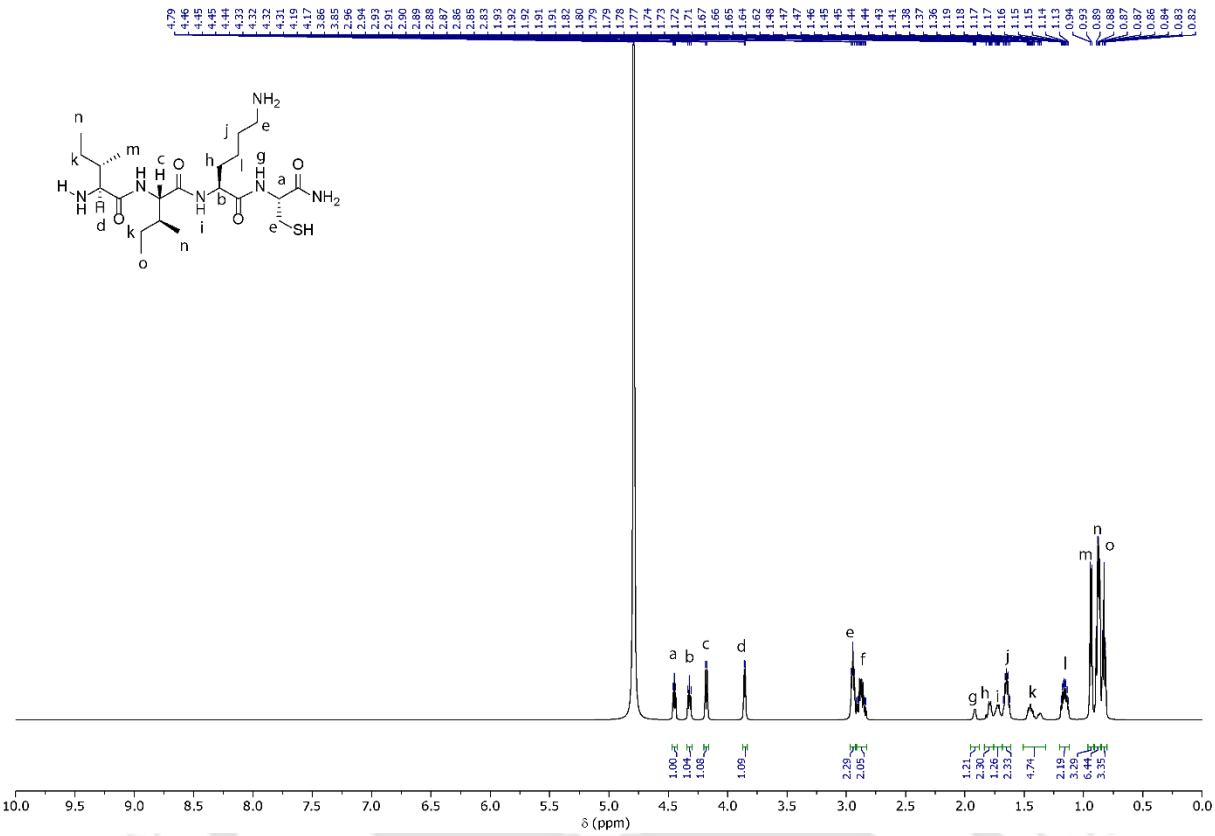

Figure7.7 ^{1}H NMR Spectrum of Compound **3** in D_2O.

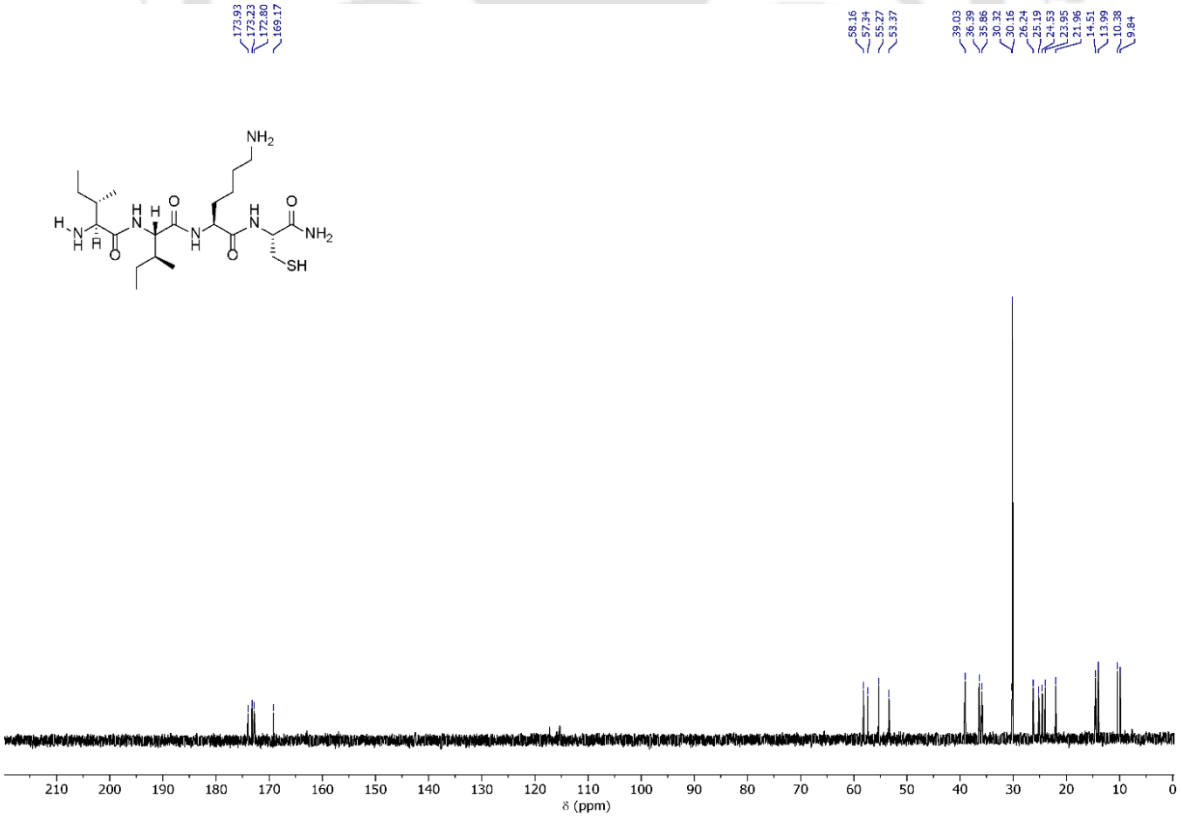

Figure 7.8 ^{13}C NMR Spectrum of Compound **3** in D_2O.

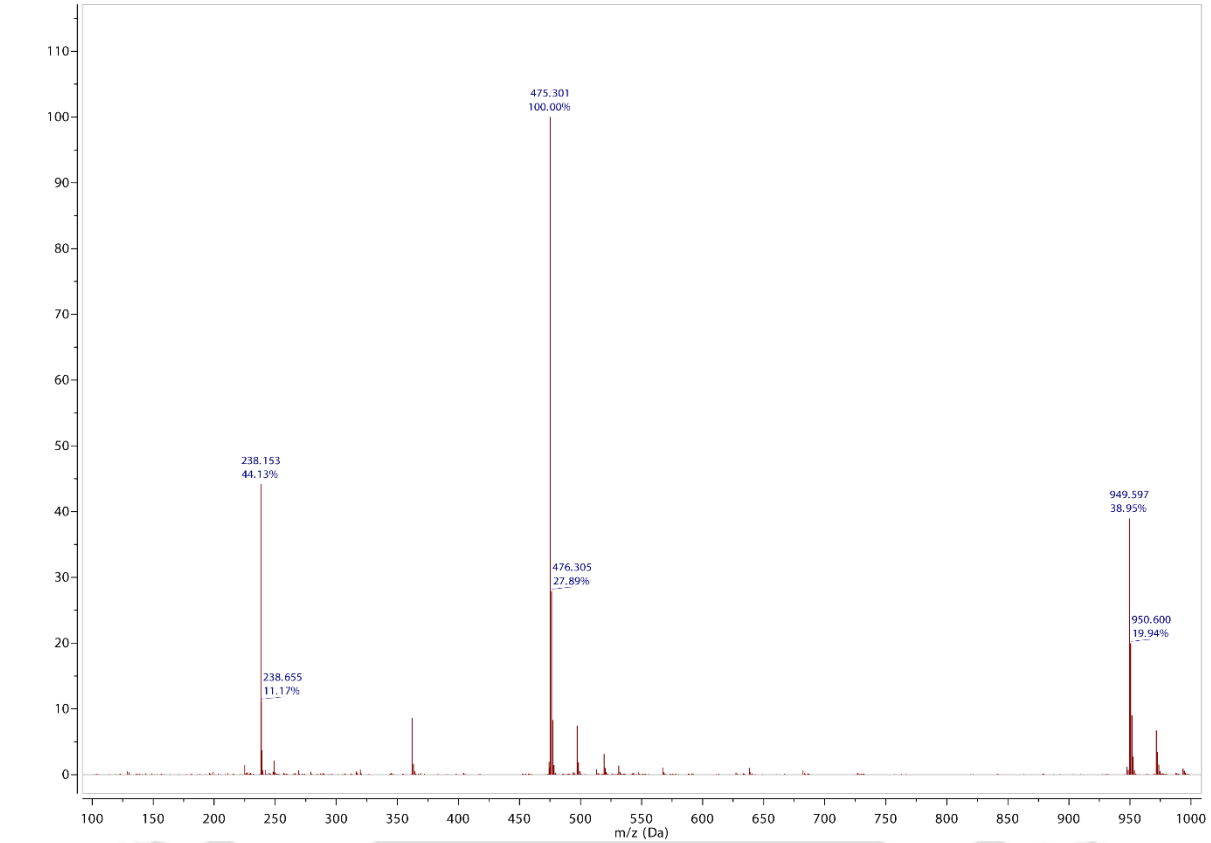

Figure7.9ESI-MSSpectrum of Compound 3.

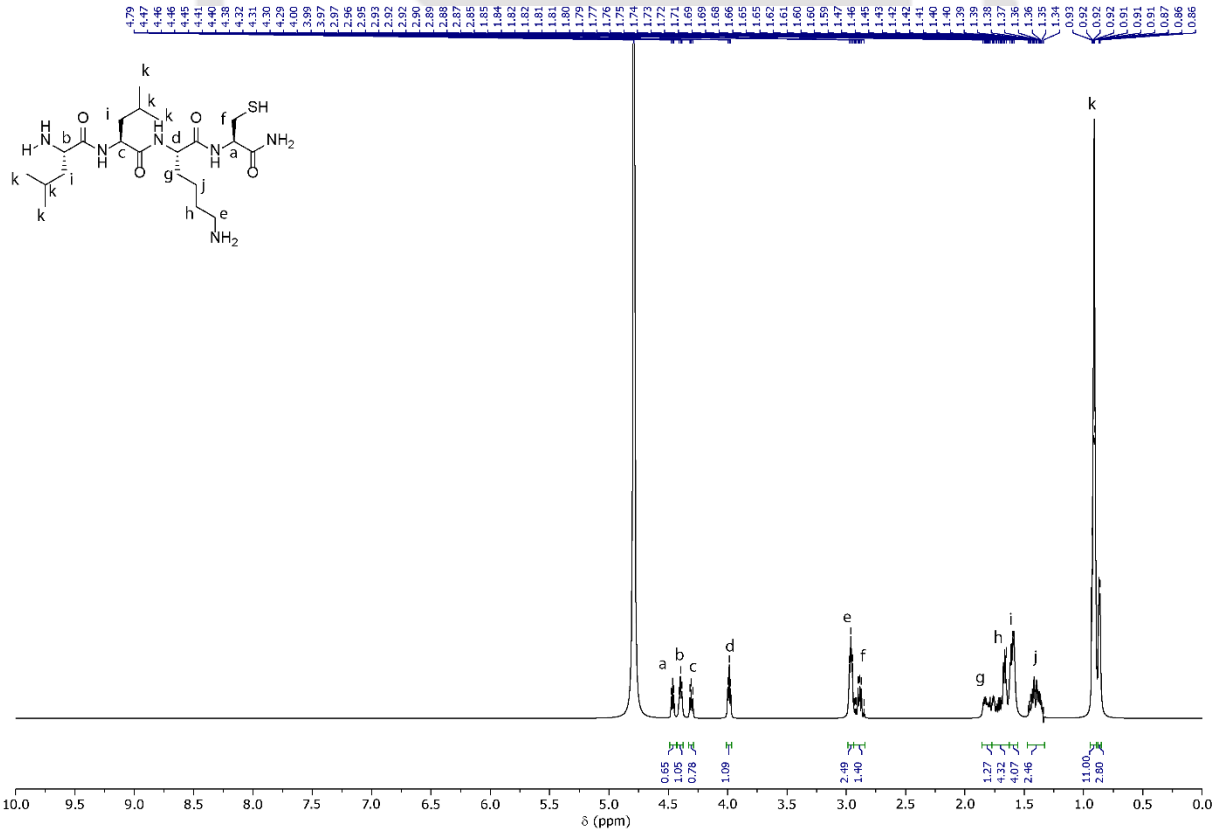

Figure 7.10^{1}H NMR Spectrum of Compound 4in D_2O.

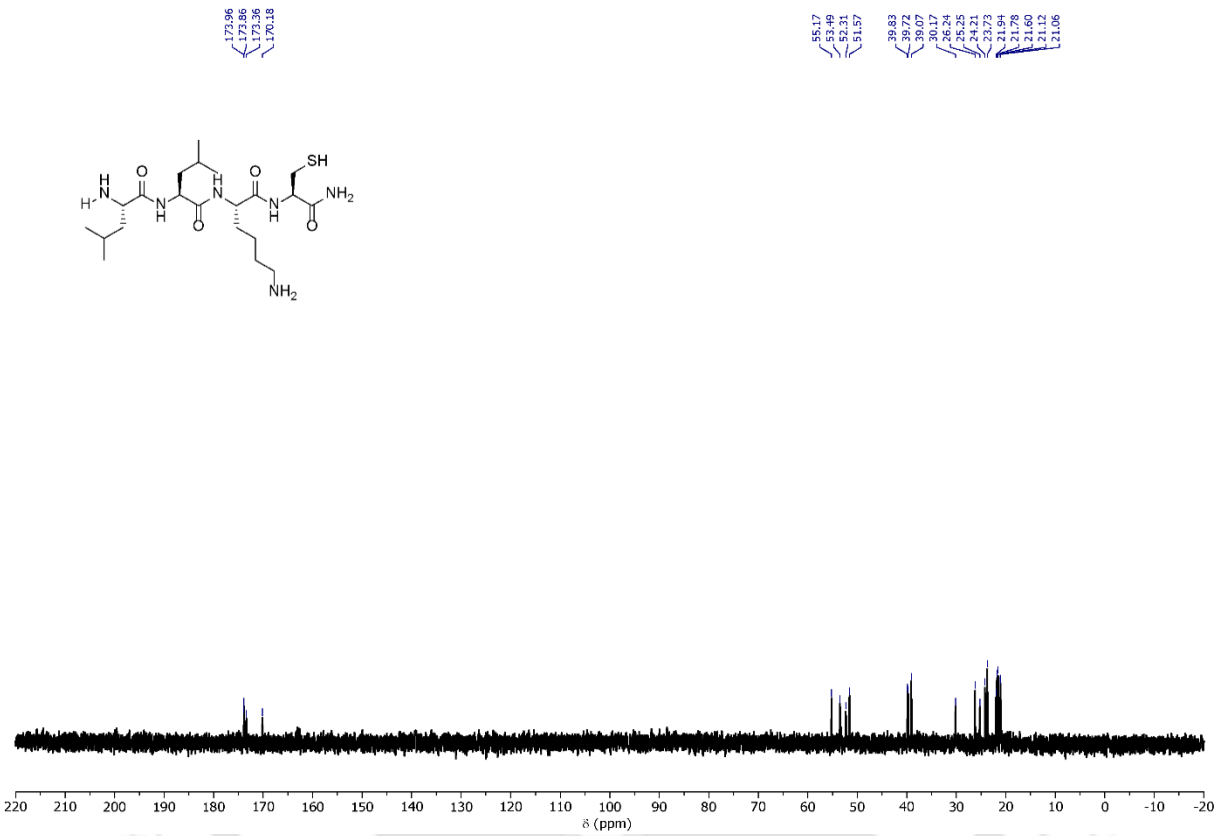

Figure7.11^{13}C NMR Spectrum of Compound 4in D_2O.

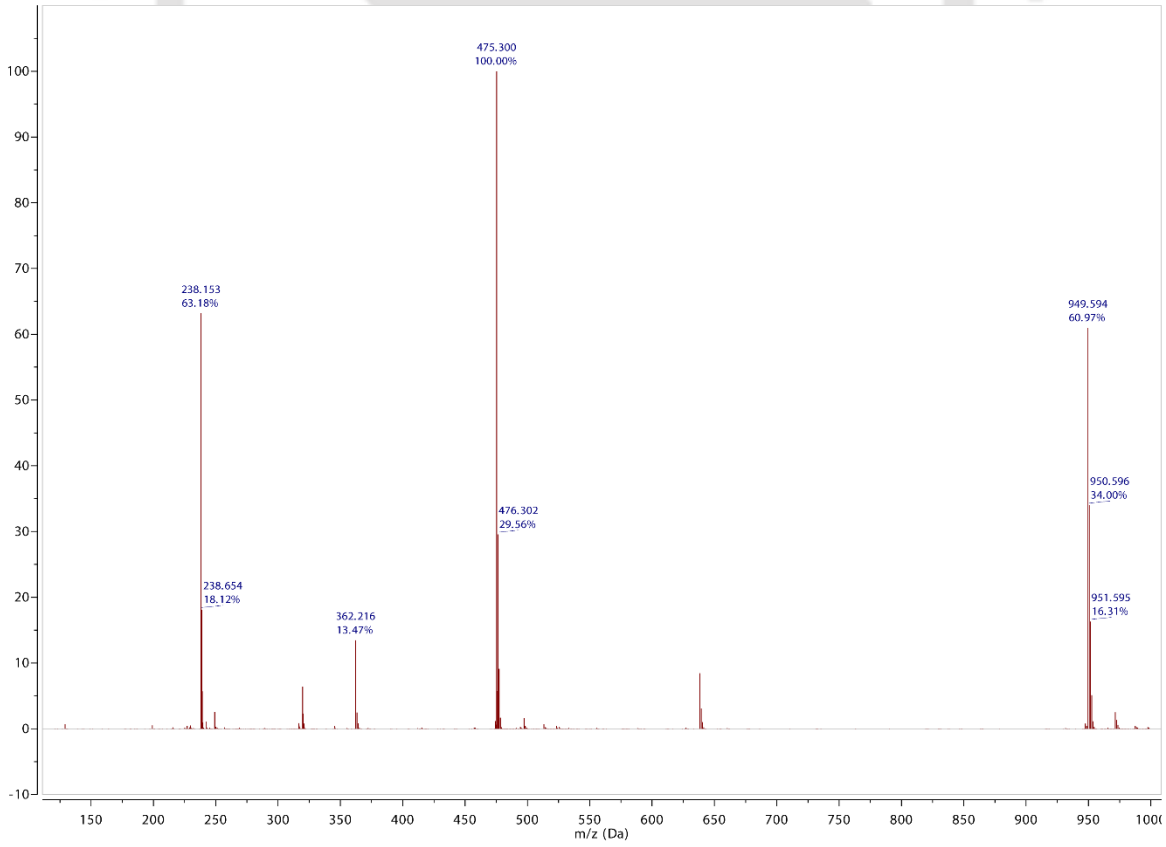

Figure 7.12ESI-MS Spectrum of Compound 4.

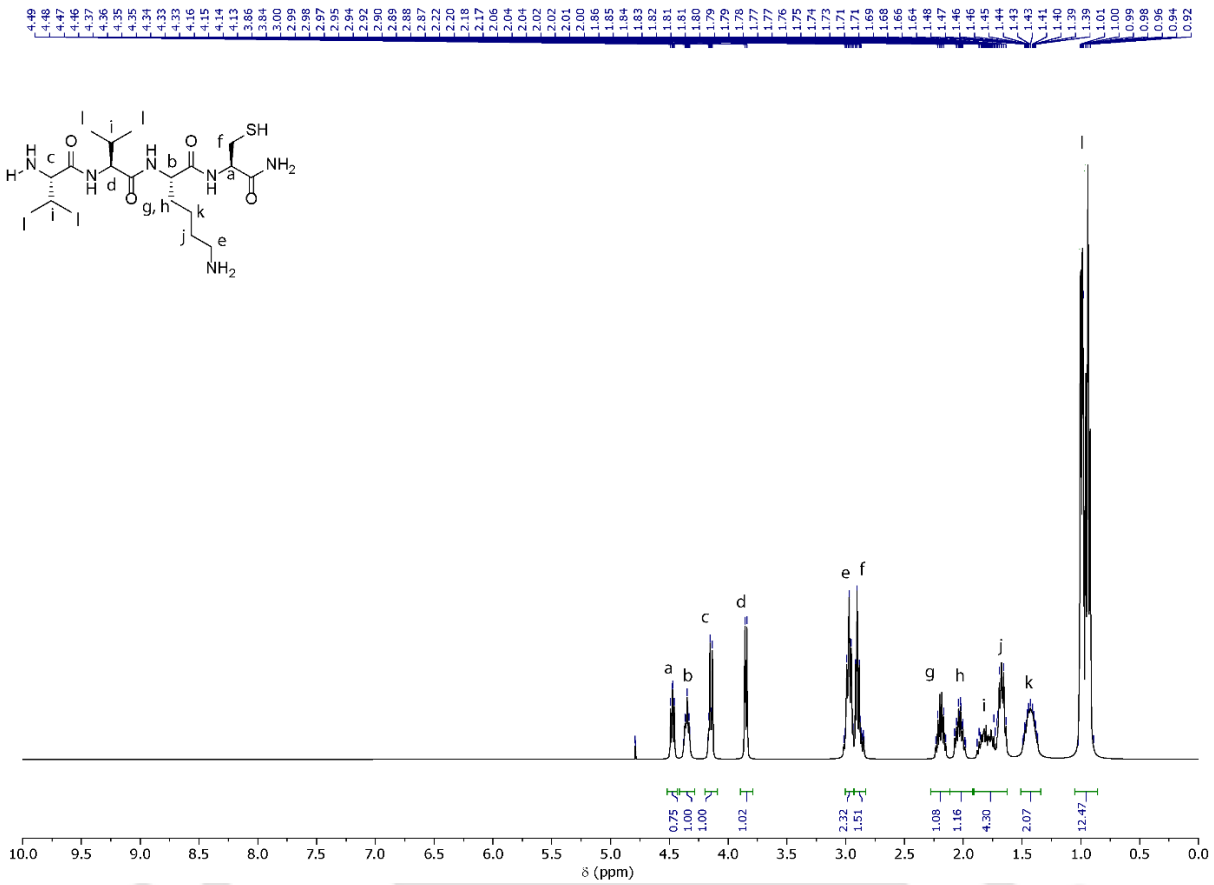

Figure 7.13 ^{1}H NMR Spectrum of Compound 5 in D_2O.

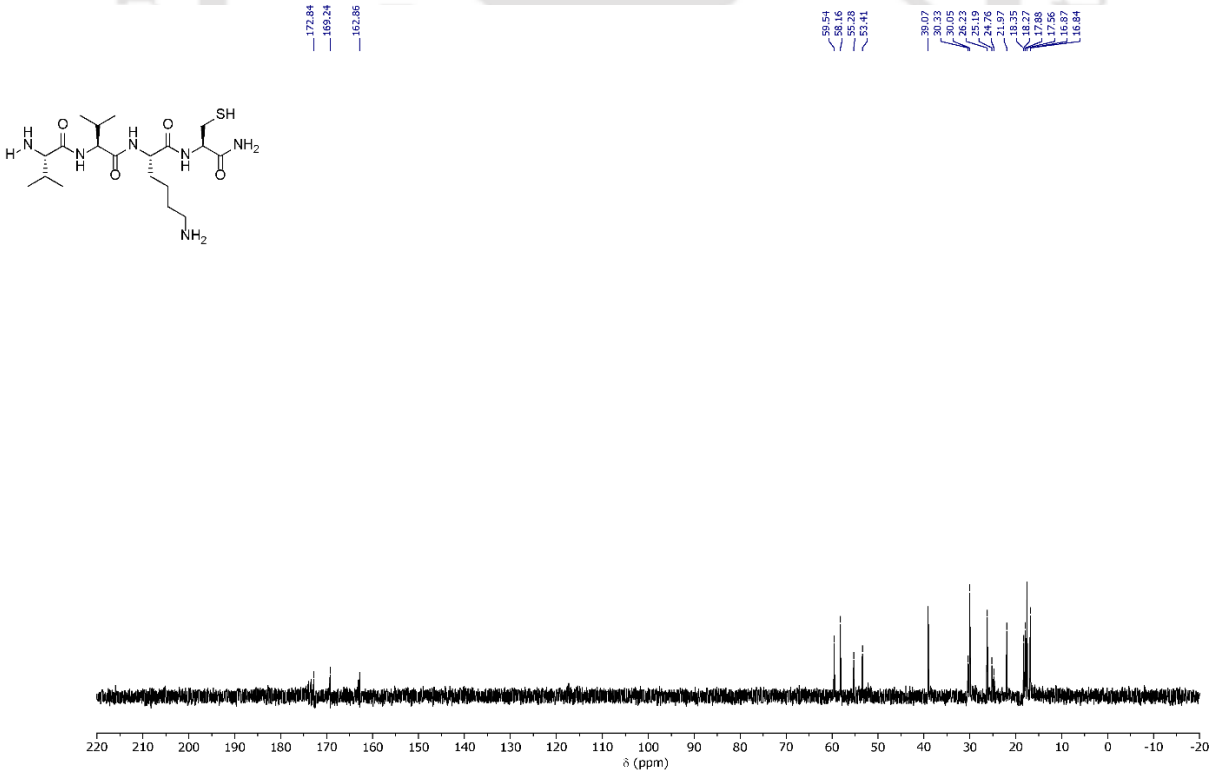

Figure 7.14 ^{13}C NMR Spectrum of Compound 5 in D_2O.

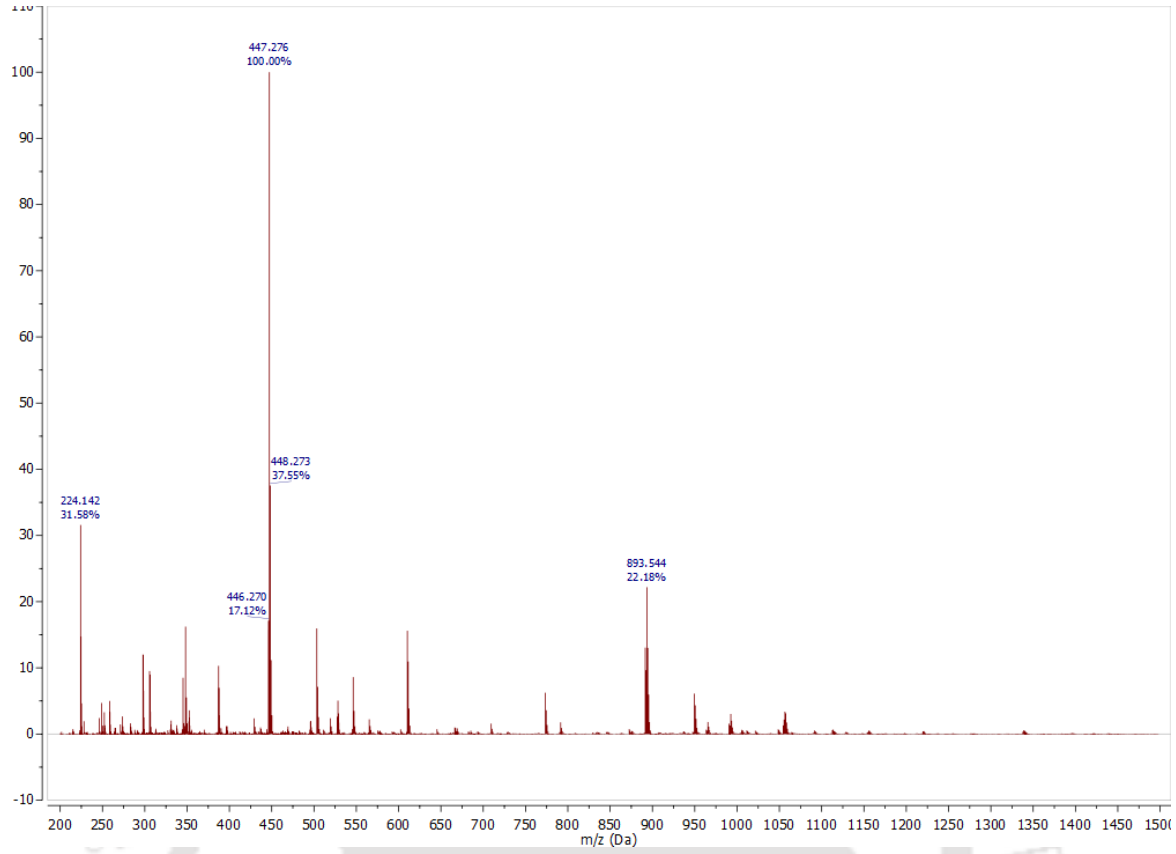

Figure7.15ESI-MS Spectrum of Compound 5.

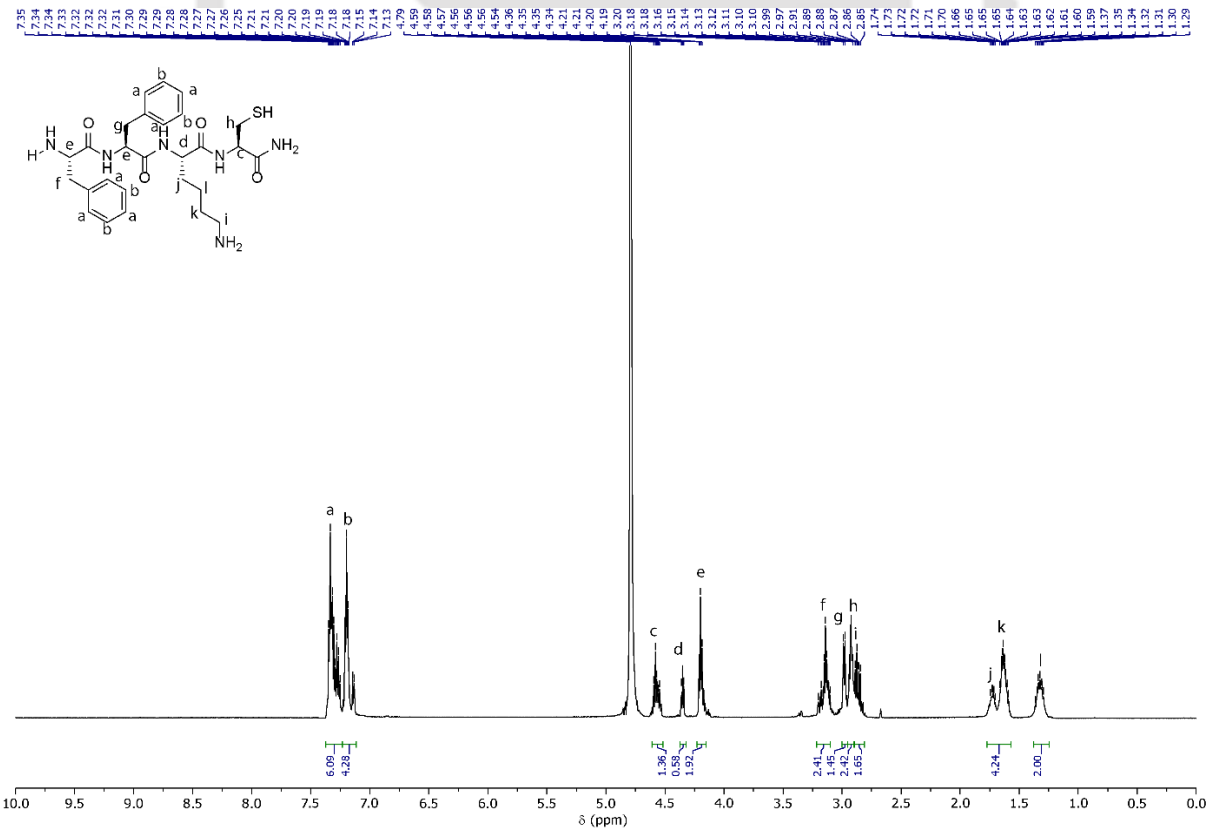

Figure 7.16^{1}H NMR Spectrum of Compound 6in D_2O.

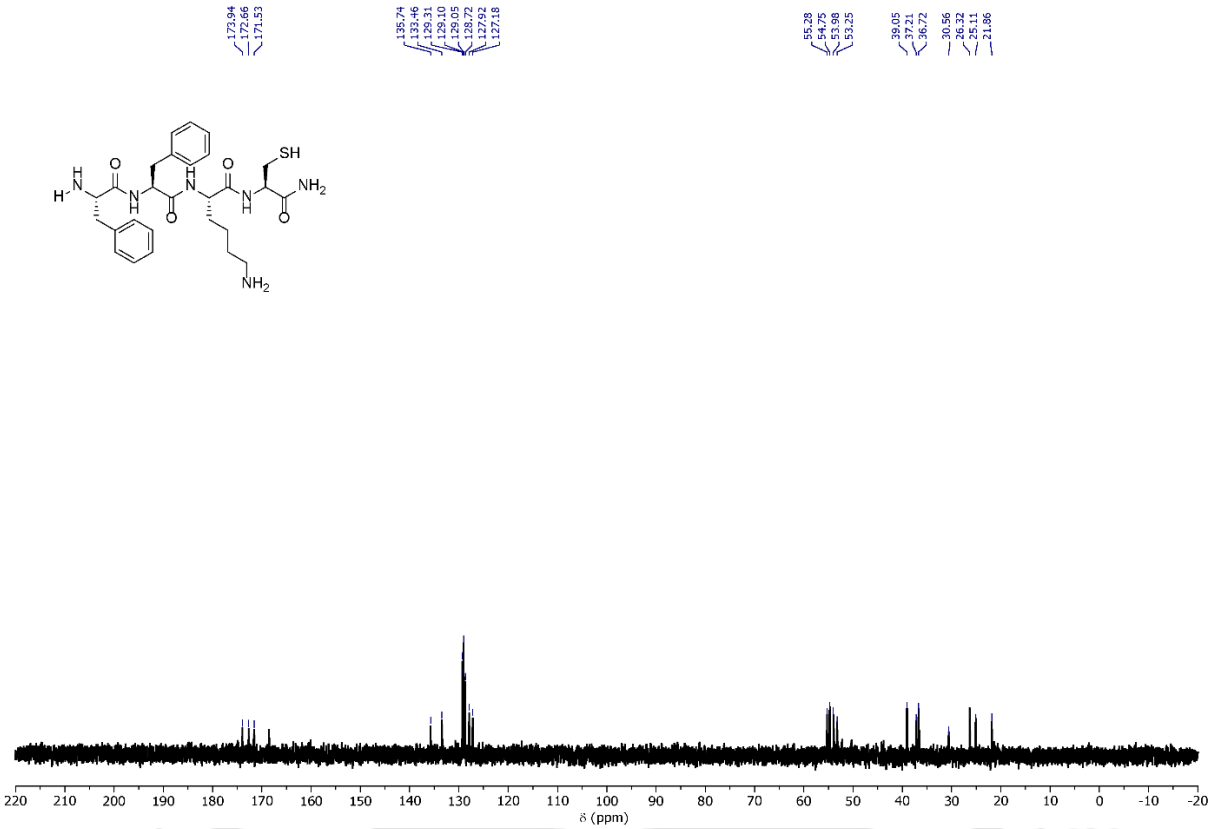

Figure7.17^{13}C NMR Spectrum of Compound **6**in D_2O.

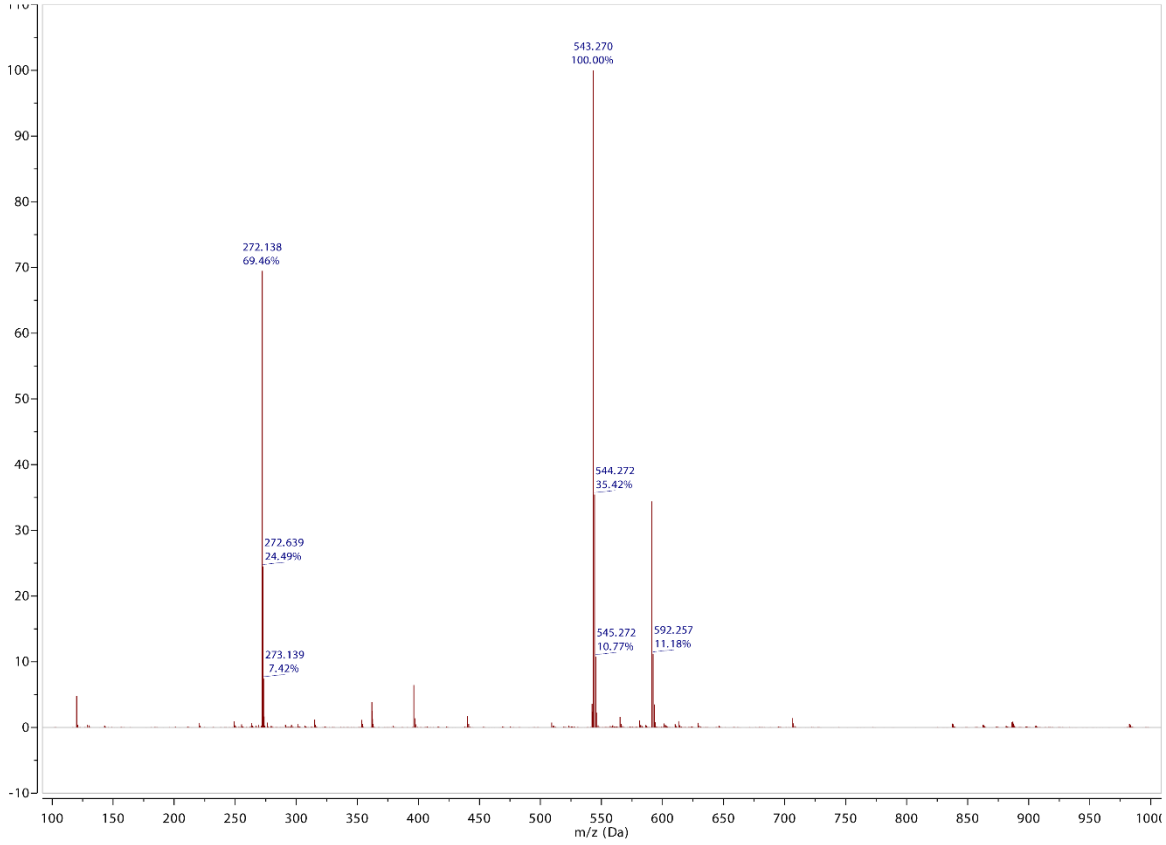

7.18ESI-MS Spectrum of Compound **6**.

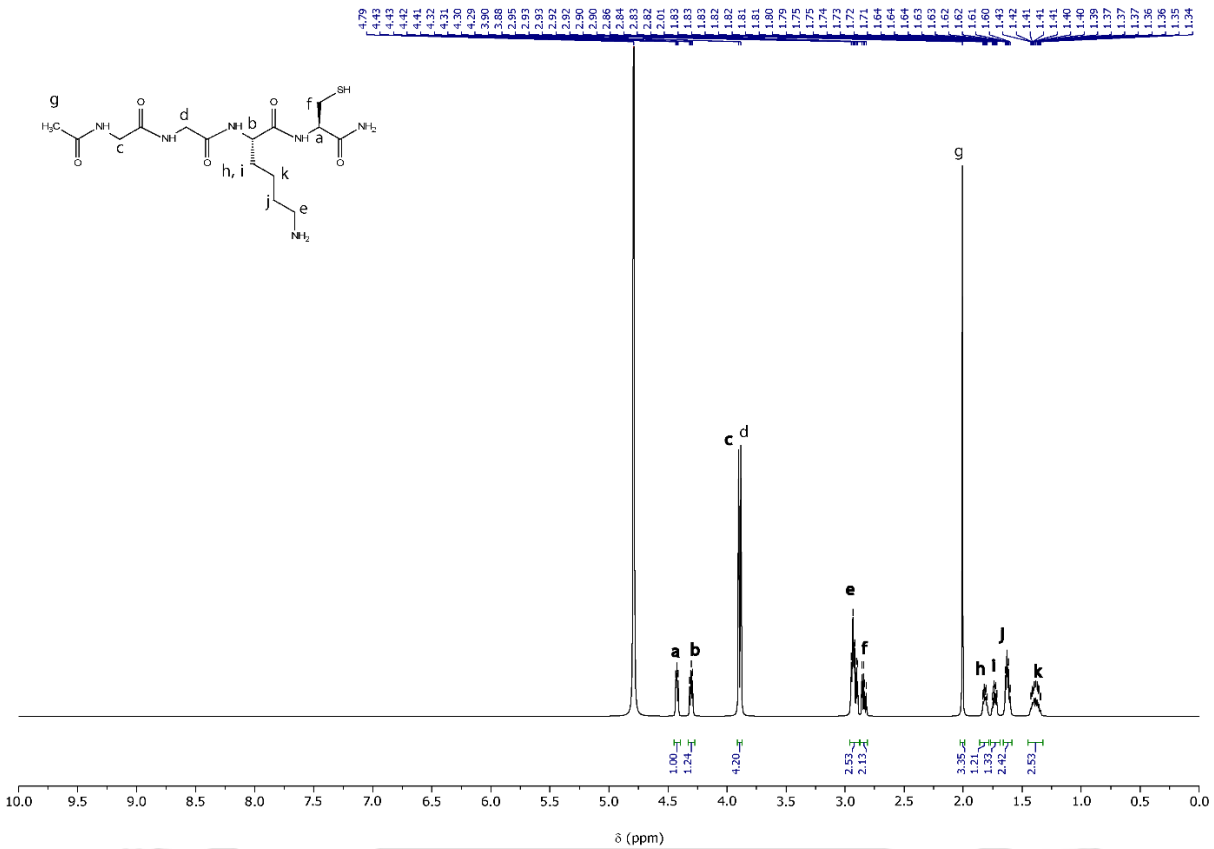

Figure7.19 ^{1}H NMR Spectrum of Compound **7** in D_2O.

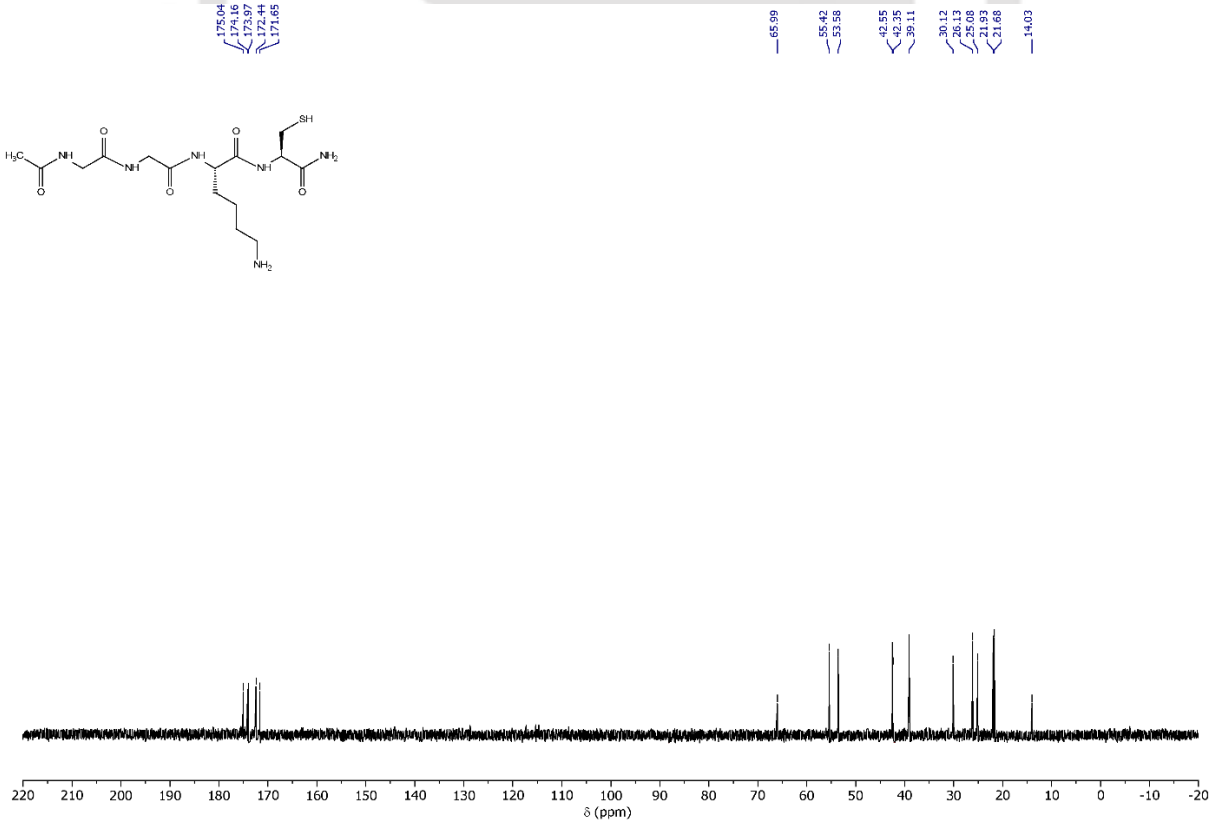

Figure 7.20 ^{13}C NMR Spectrum of Compound **7** in D_2O.

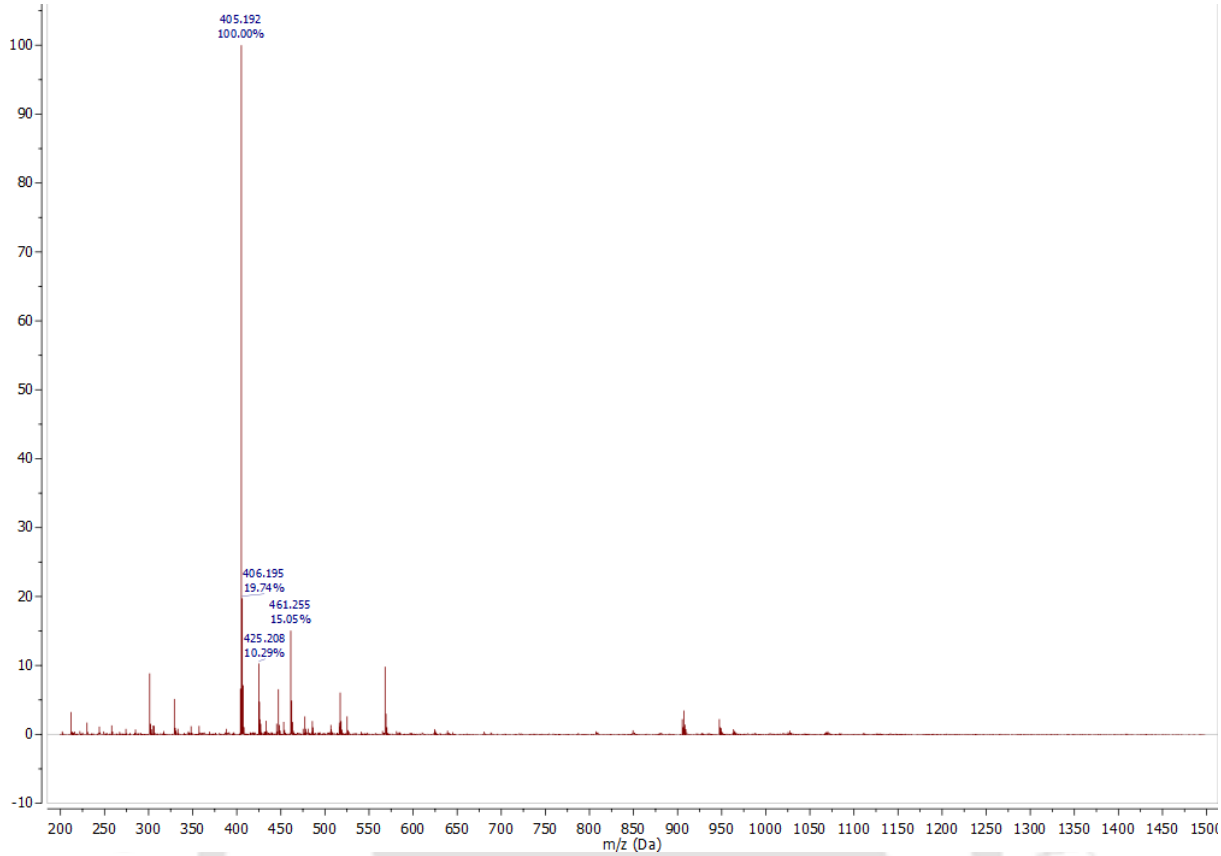

Figure7.21ESI-MS Spectrum of Compound 7.

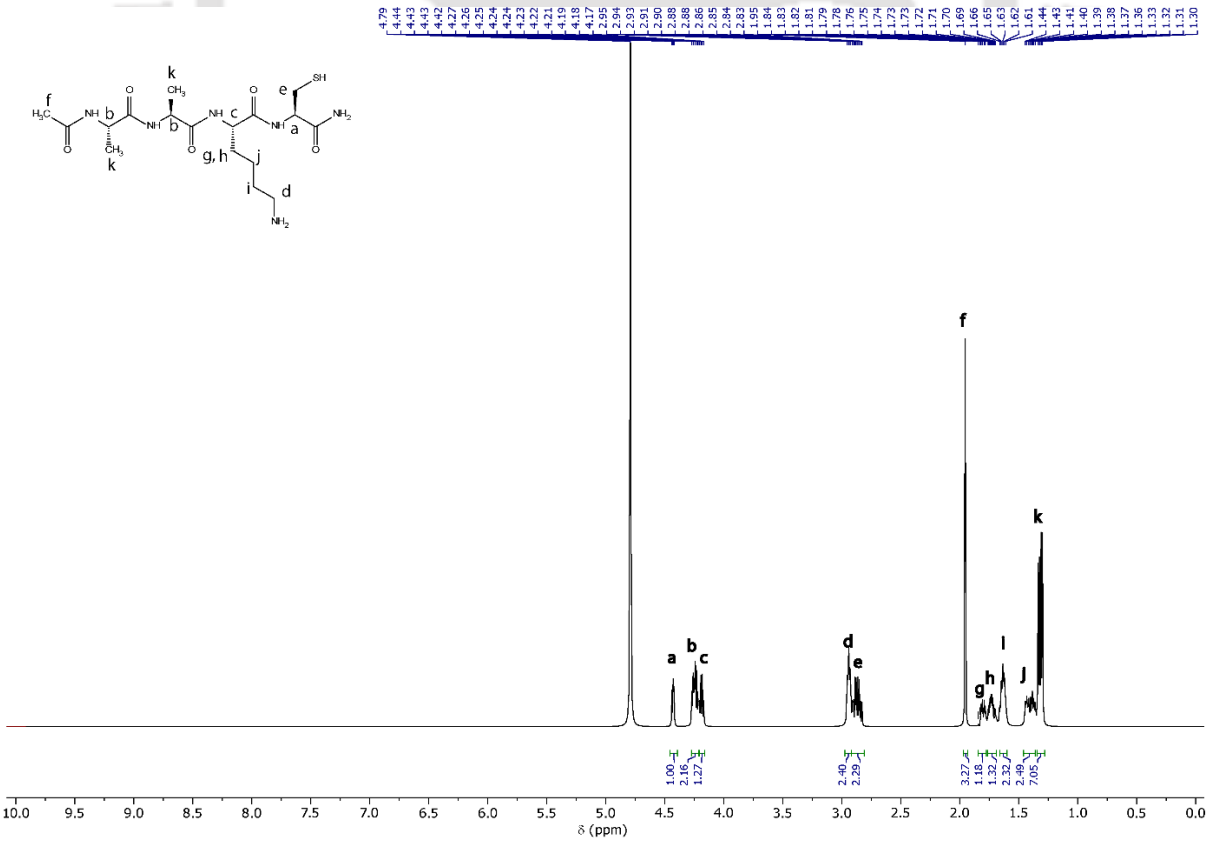

Figure 7.22^{1}H NMR Spectrum of Compound 8in D_2O.

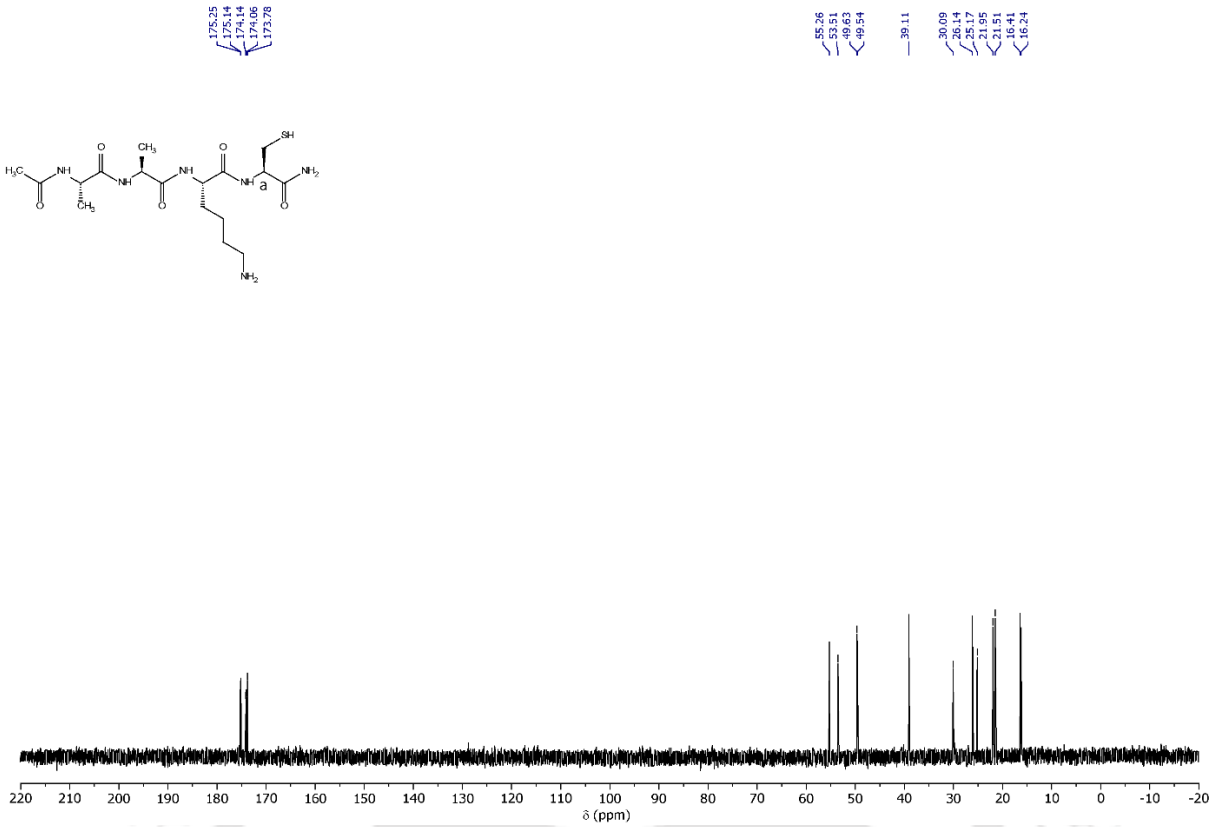

Figure7.23[13] NMR Spectrum of Compound 8in D_2O.

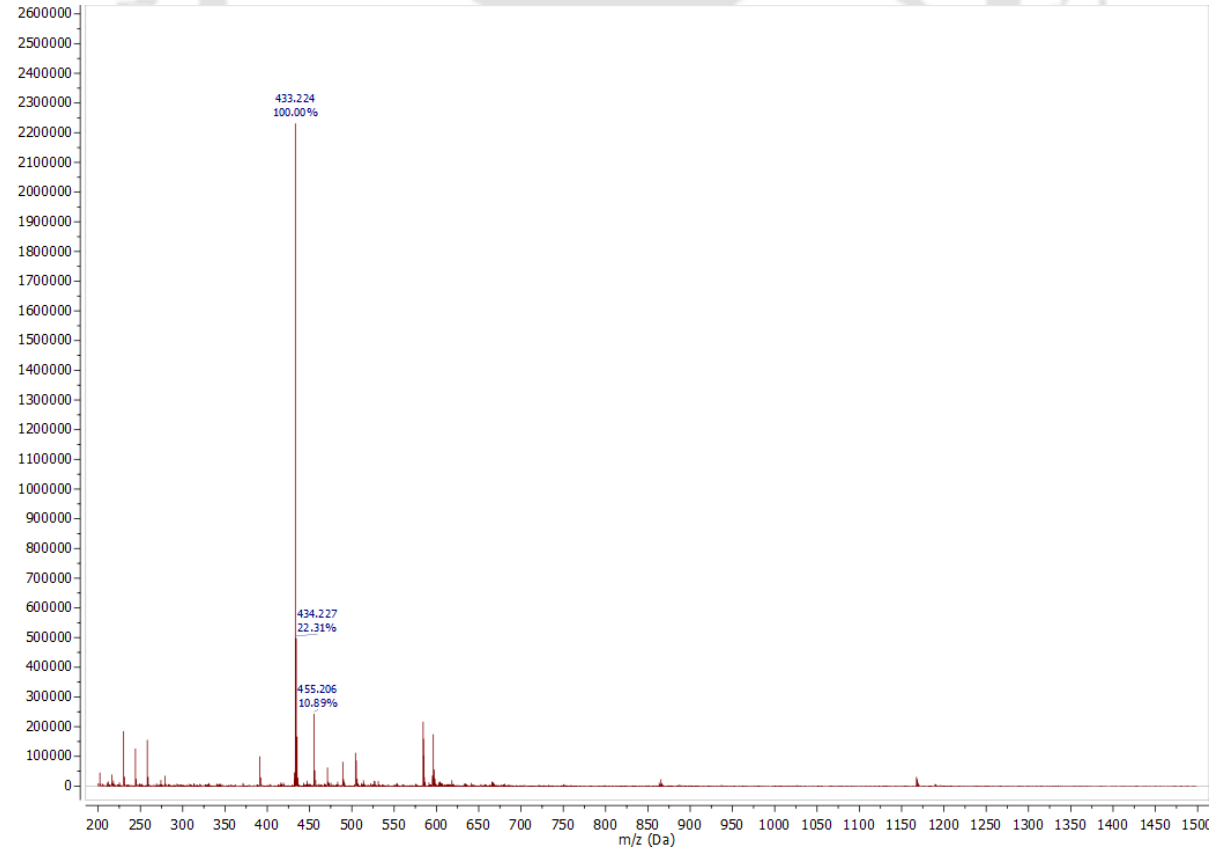

Figure 7.24ESI-MS Spectrum of Compound 8.

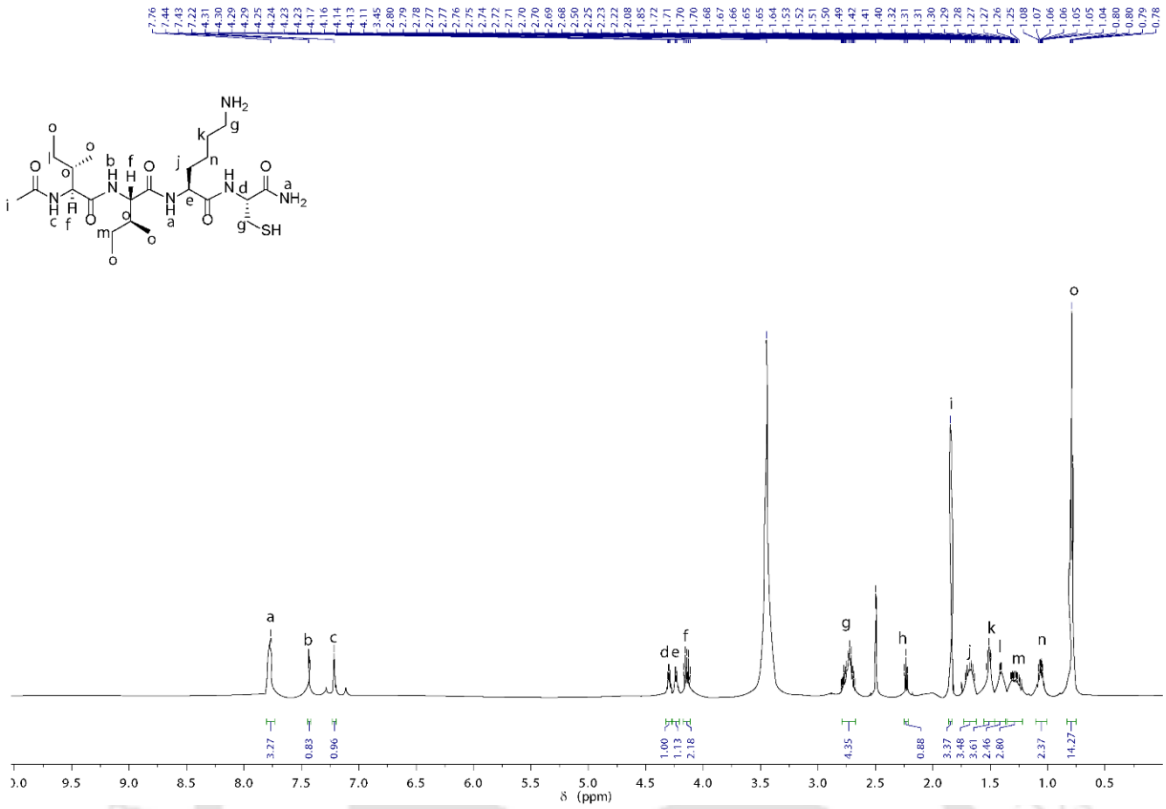

Figure7.25 ^{1}H NMR Spectrum of Compound **9** in DMSO-D_6.

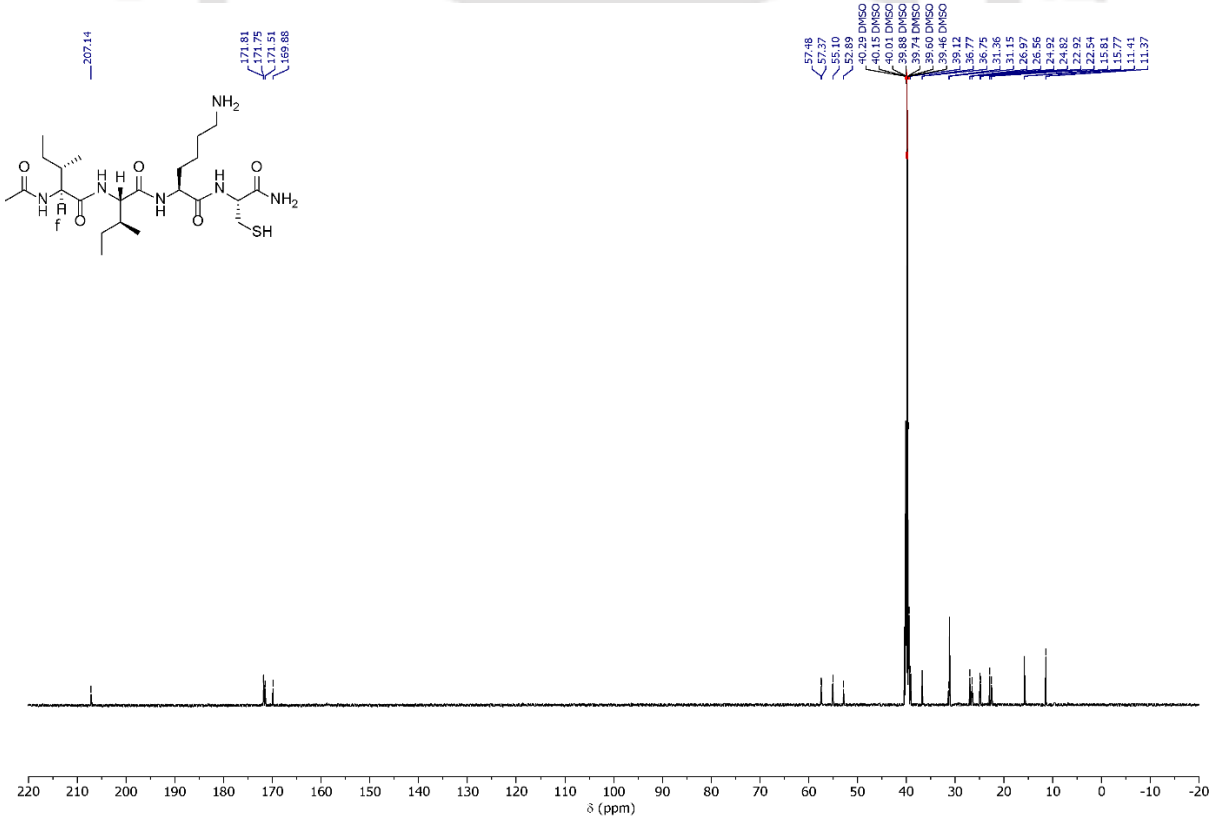

Figure 7.26 ^{1}H NMR Spectrum of Compound **9** in DMSO-D_6.

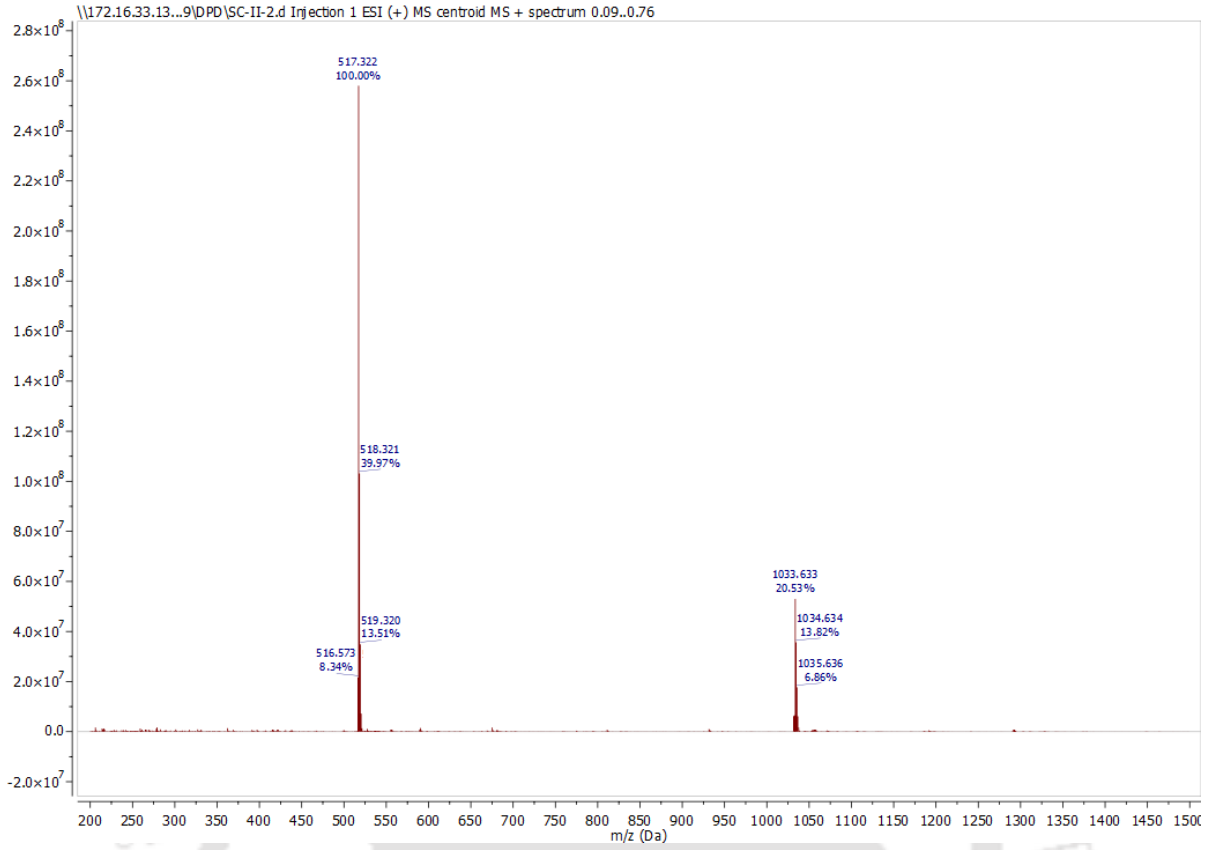

Figure7.27ESI-MS Spectrum of Compound 9.

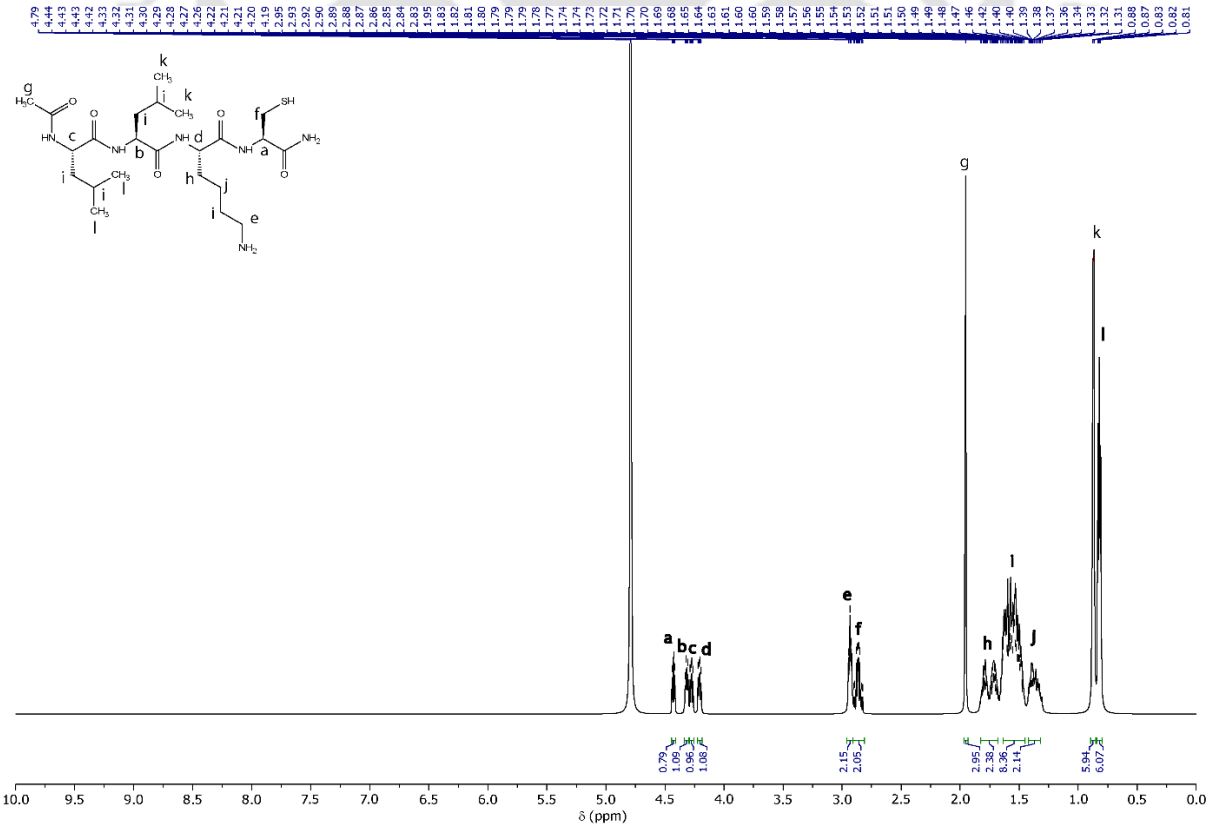

Figure 7.28 ^{1}H NMR Spectrum of Compound 10in D_2O.

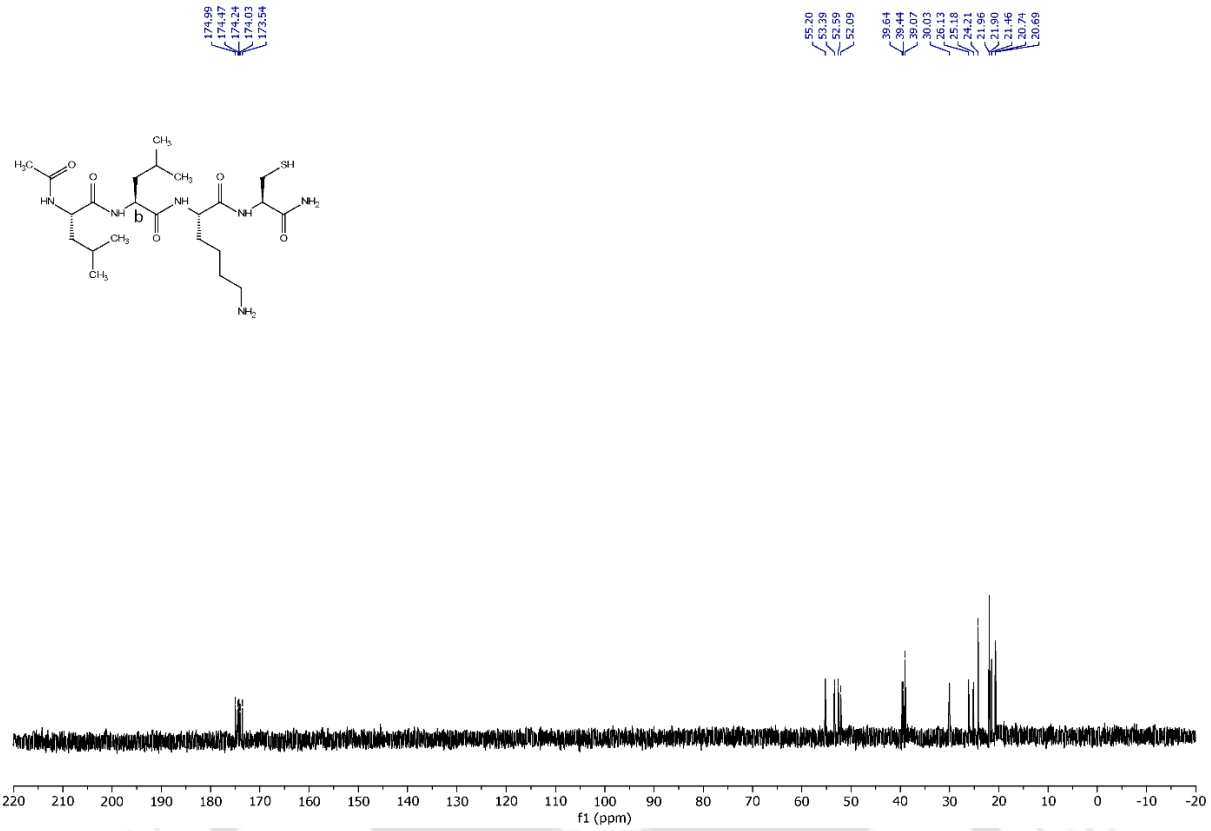

Figure7.29^{13}C NMR Spectrum of Compound **10**in D_2O.

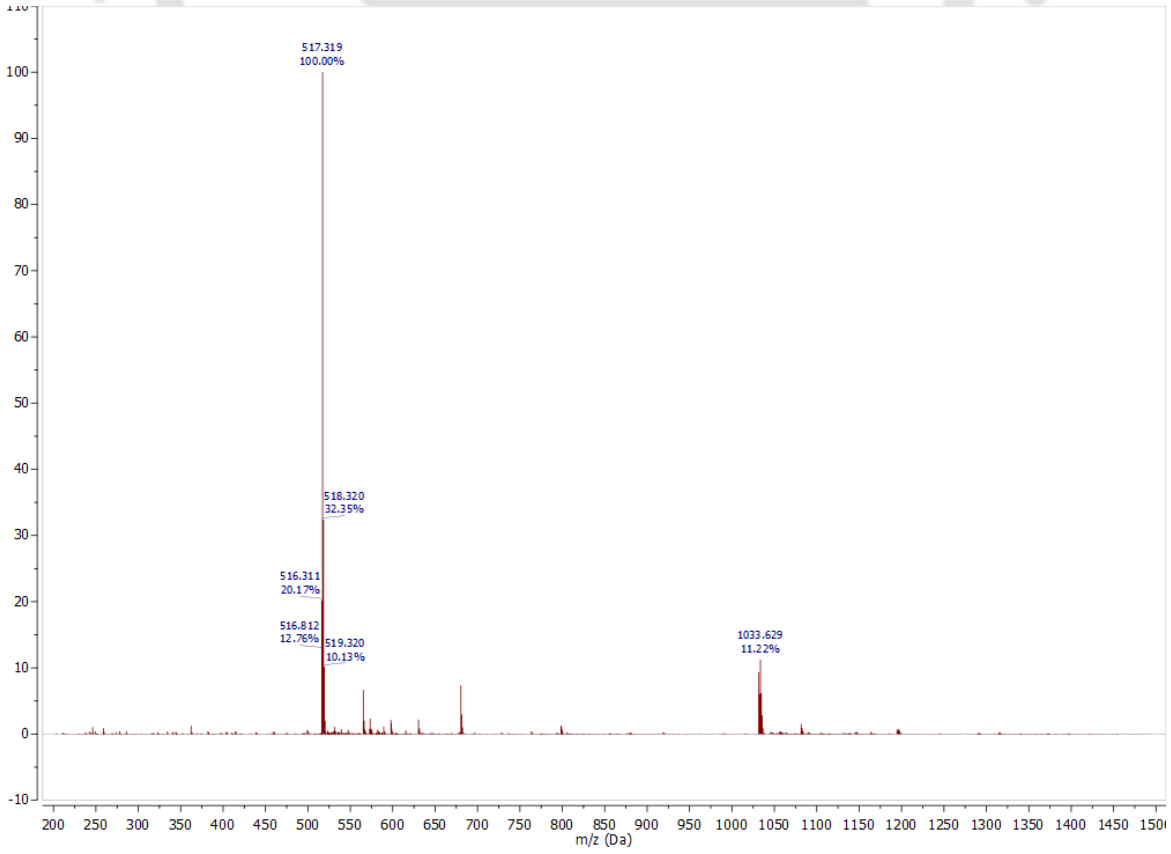

Figure 7.30ESI-MS Spectrum of Compound **10**.

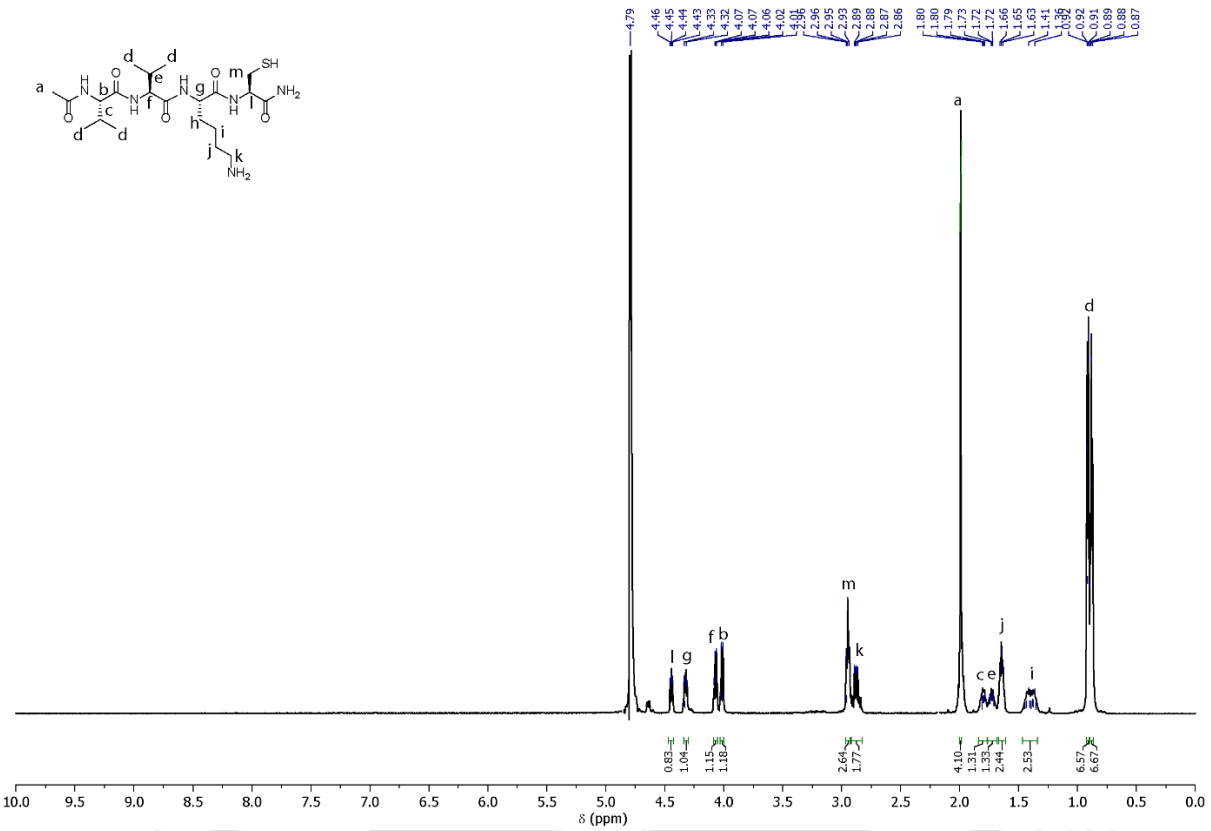

Figure7.31 ^{1}H NMR Spectrum of Compound **11** in D_2O.

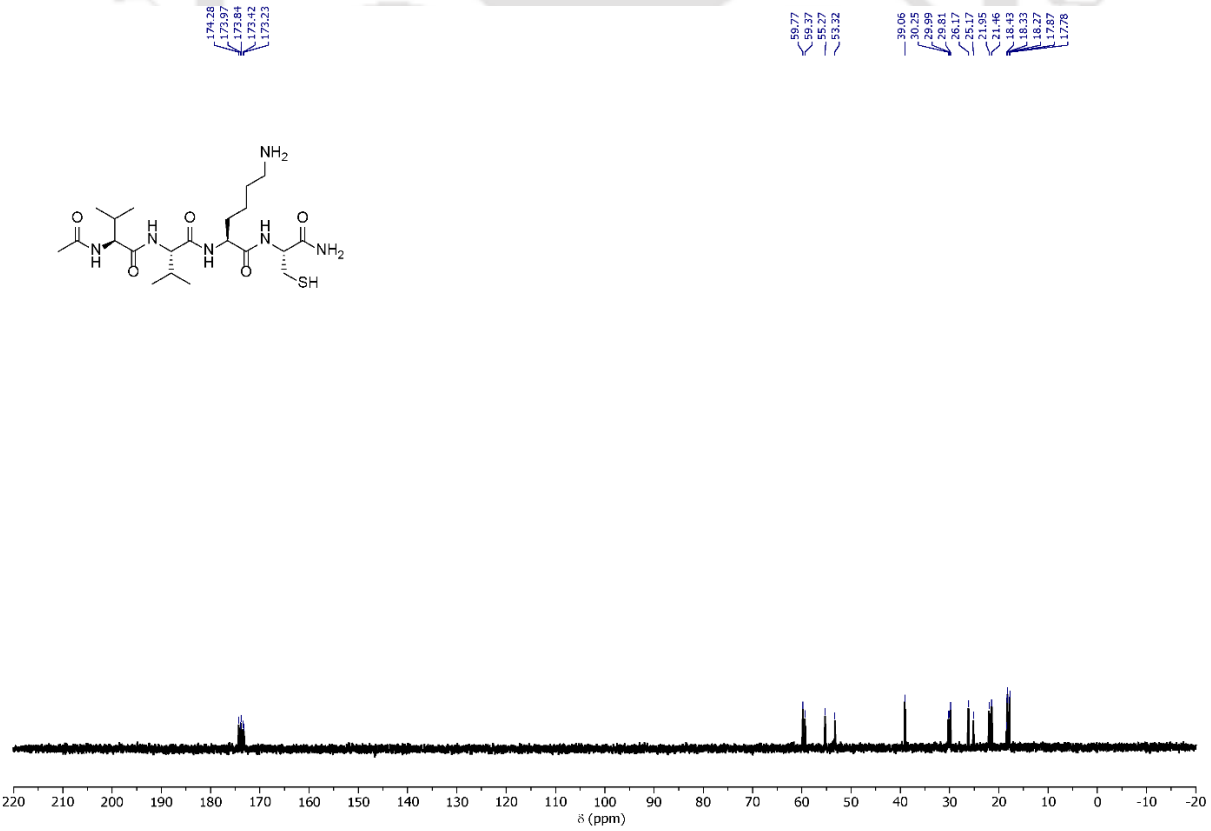

Figure 7.32 ^{13}C NMR Spectrum of Compound **11** in D_2O.

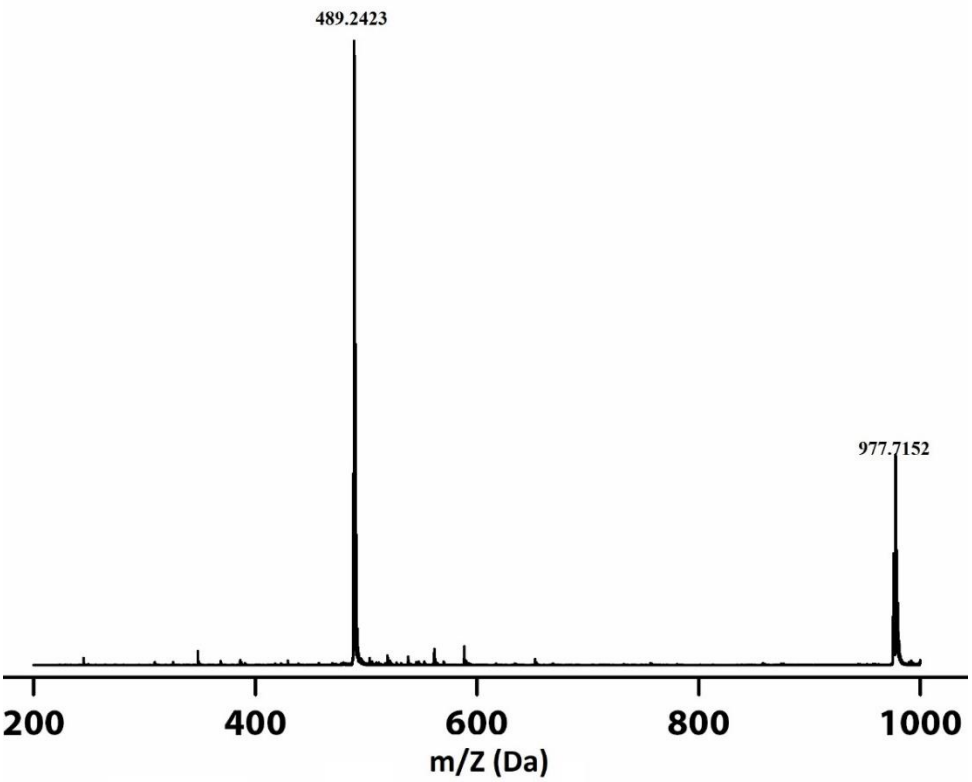

Figure7.33ESI-MS Spectrum of Compound **11**.

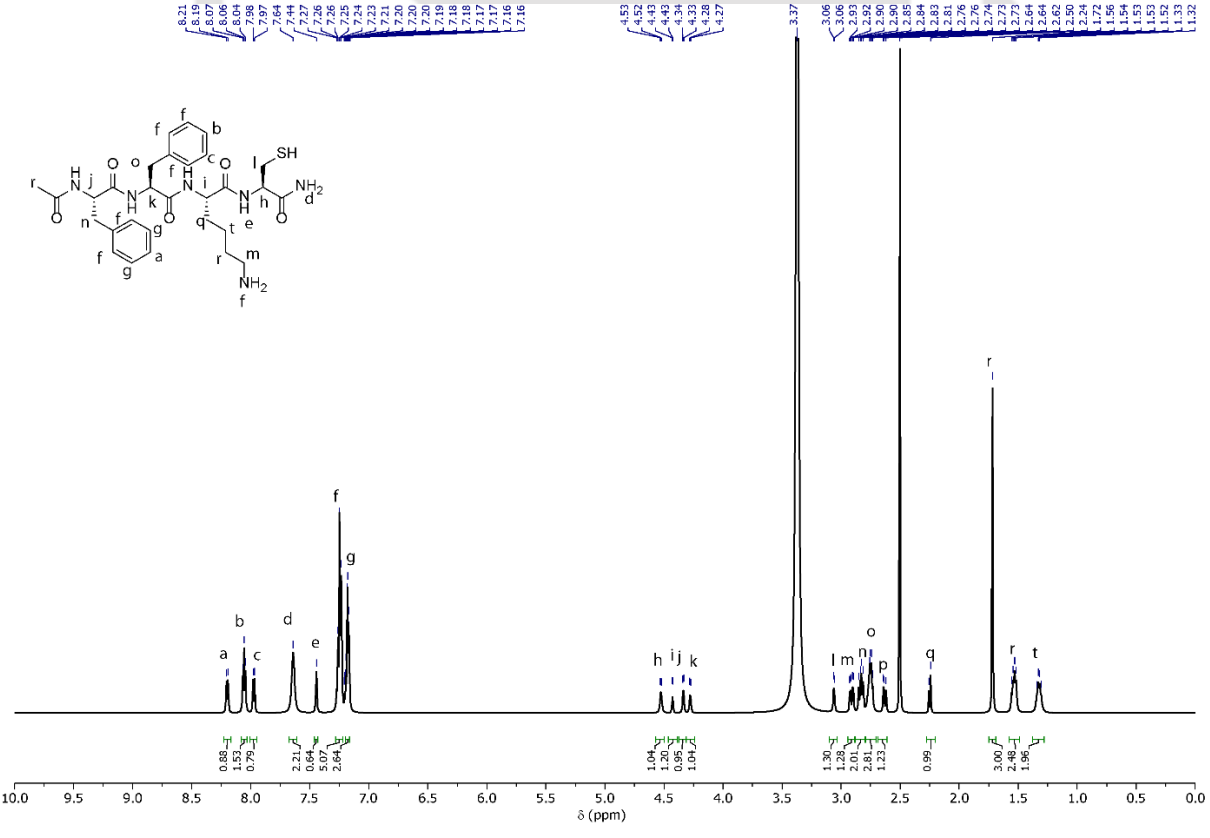

Figure 7.34^{1}H NMR Spectrum of Compound **12**in D_2O.

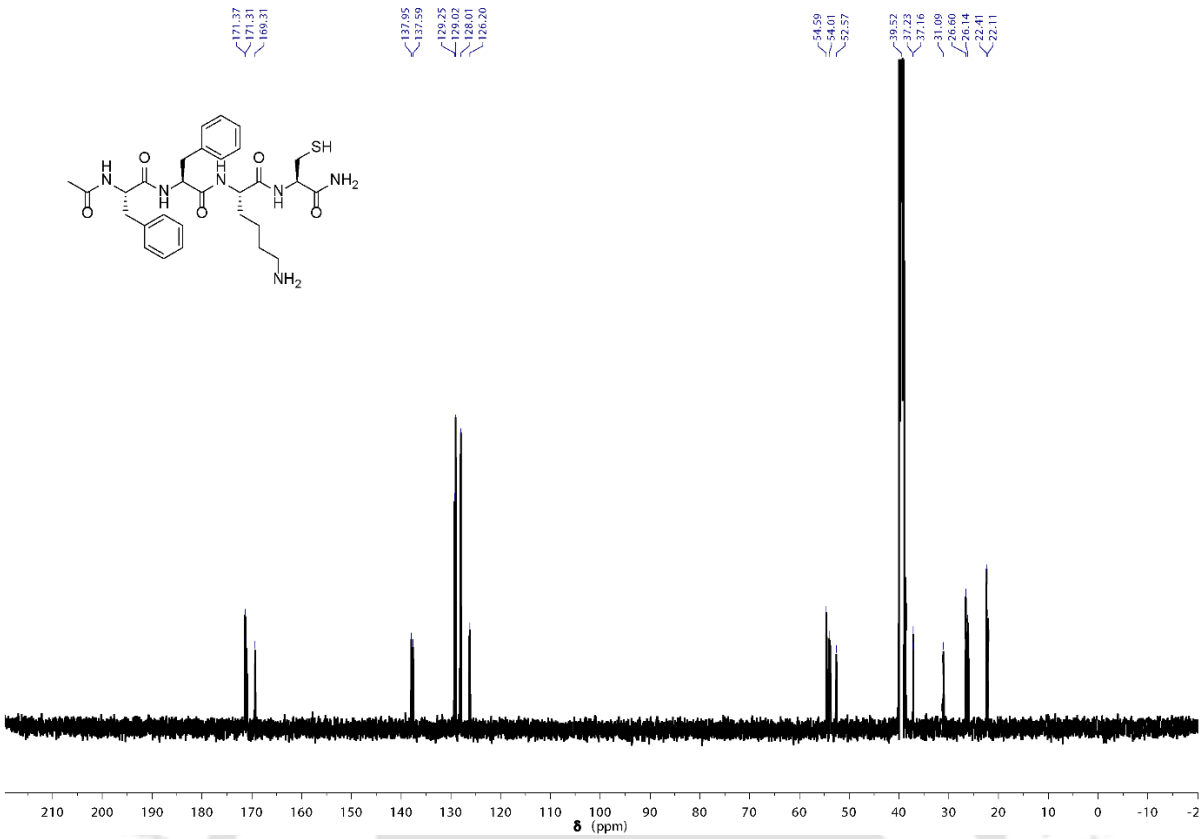

Figure7.35^{1}H NMR Spectrum of Compound **12**in D_2O.

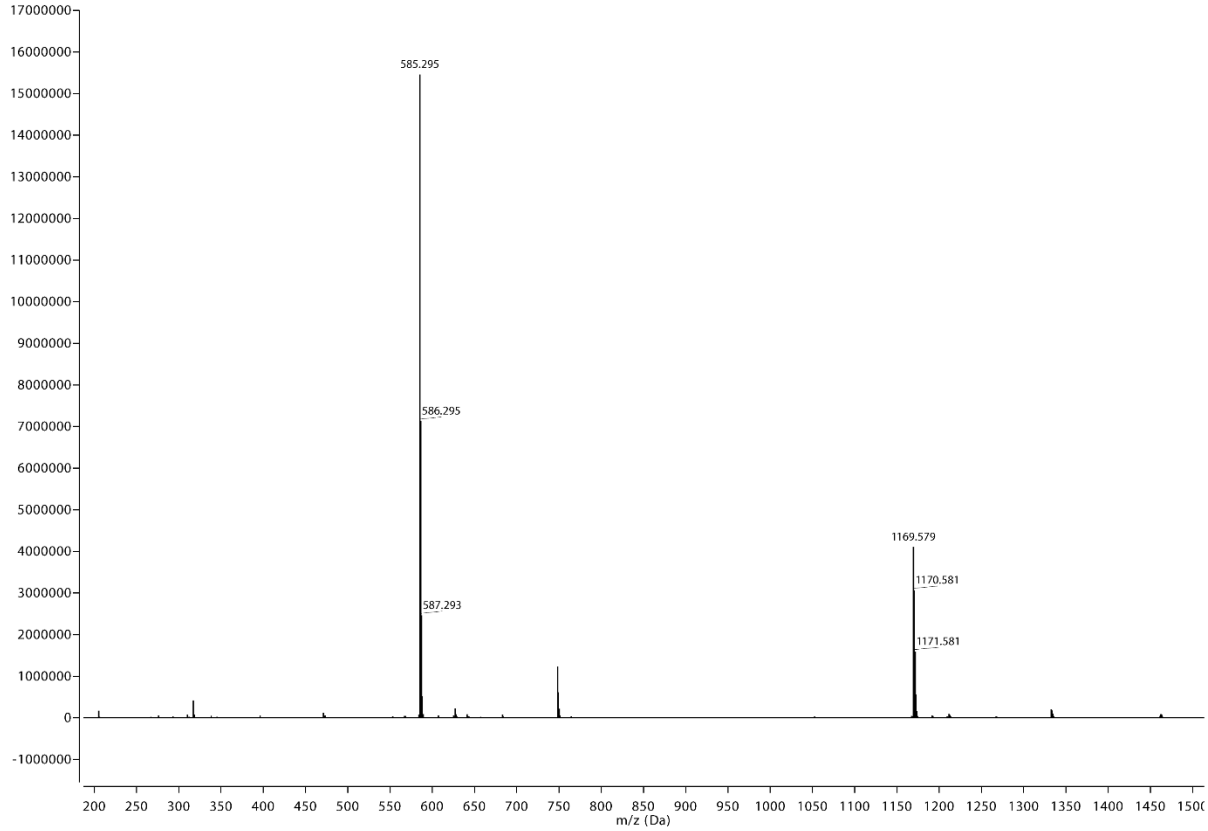

Figure 7.36ESI-MS Spectrum of Compound **12**.

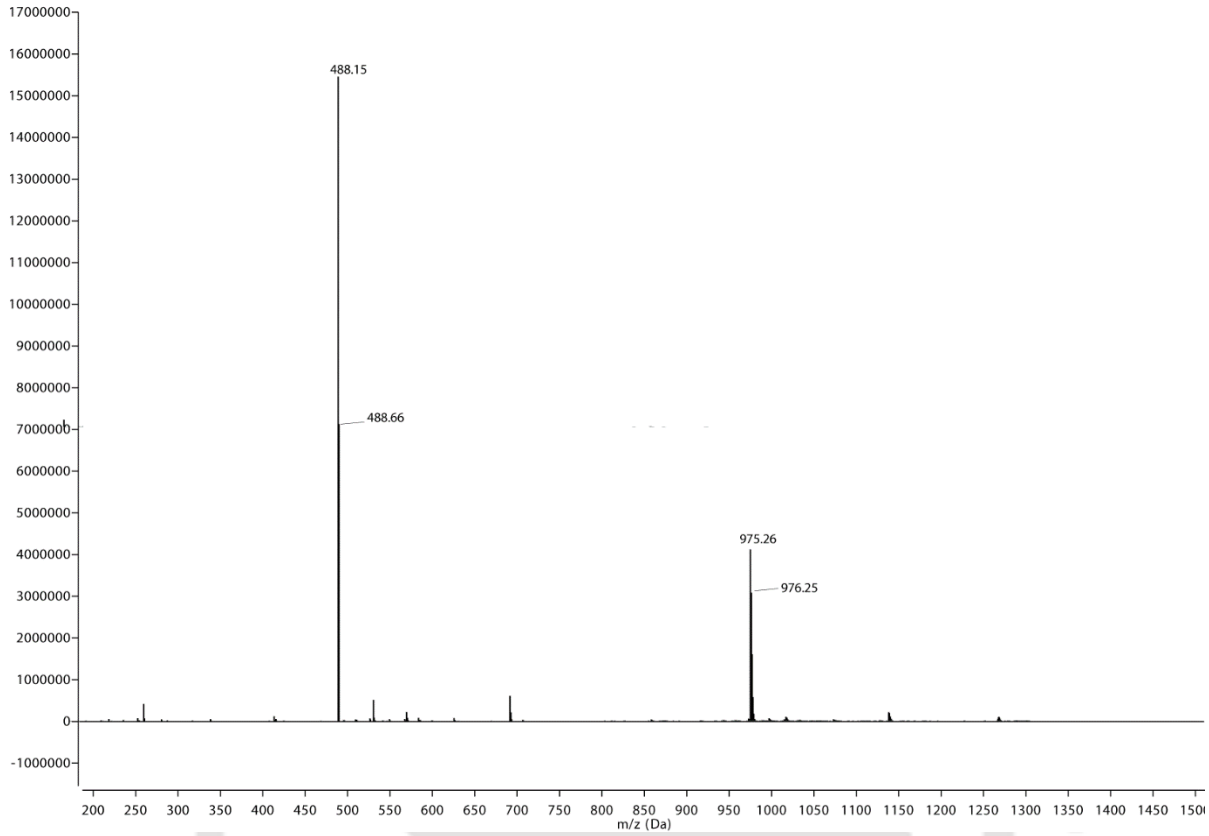

Figure 7.36ESI-MS Spectrum of dimer of Compound **11**.

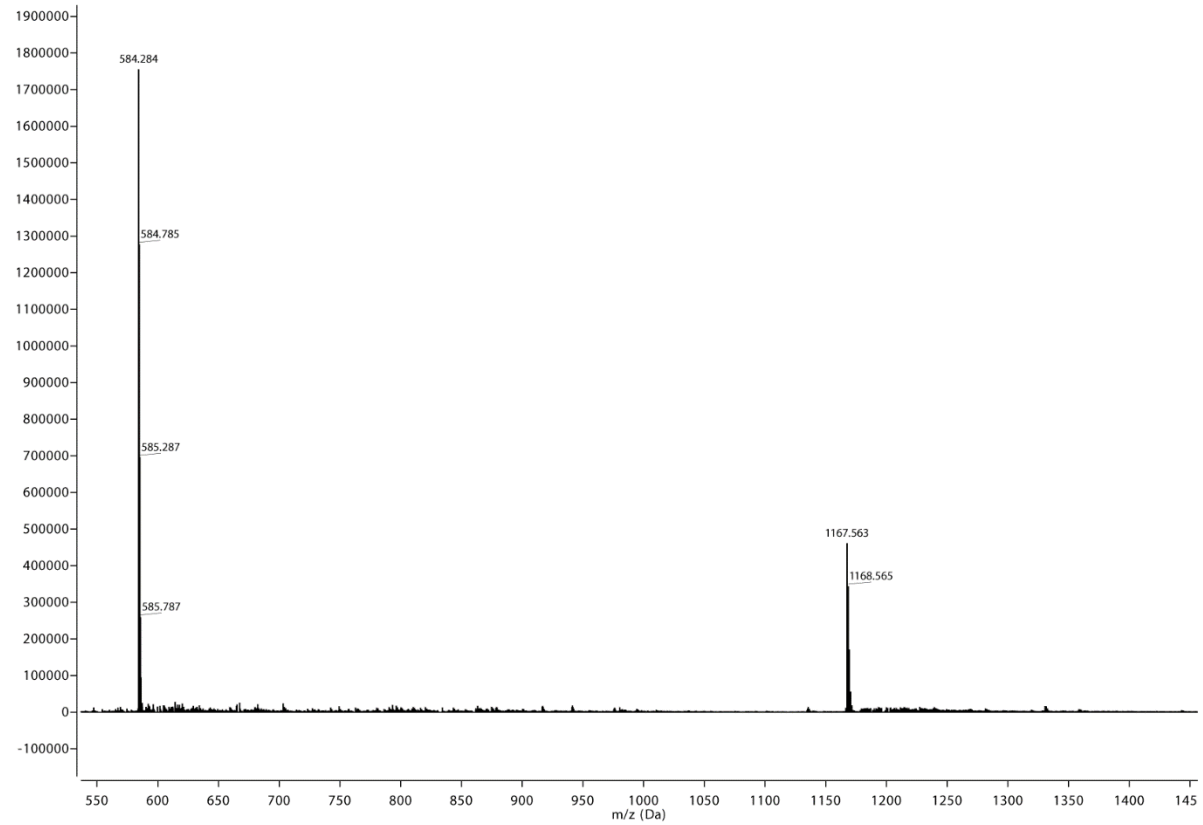

Figure 7.36ESI-MS Spectrum of dimer of Compound **12**.

Chapter 3

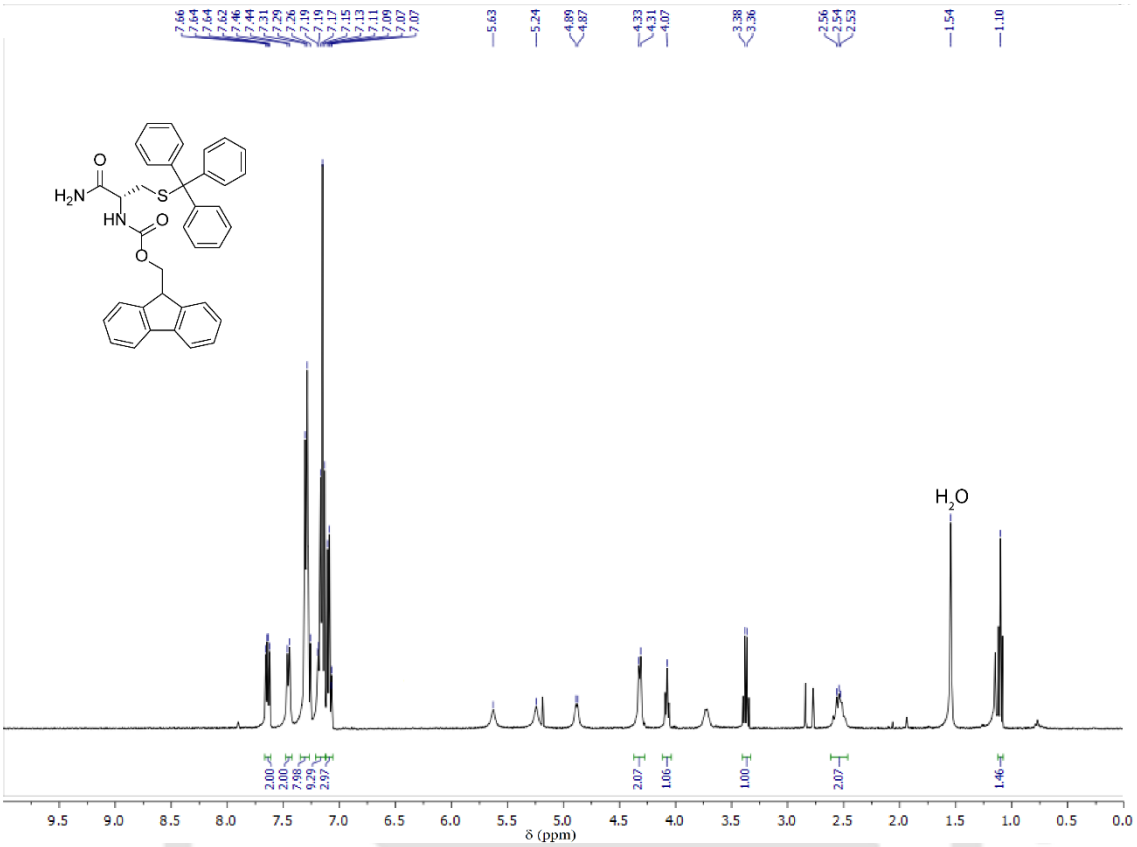

Figure 7.37 ^{1}H NMR Spectrum of **Compound 13** in $CDCl_3$.

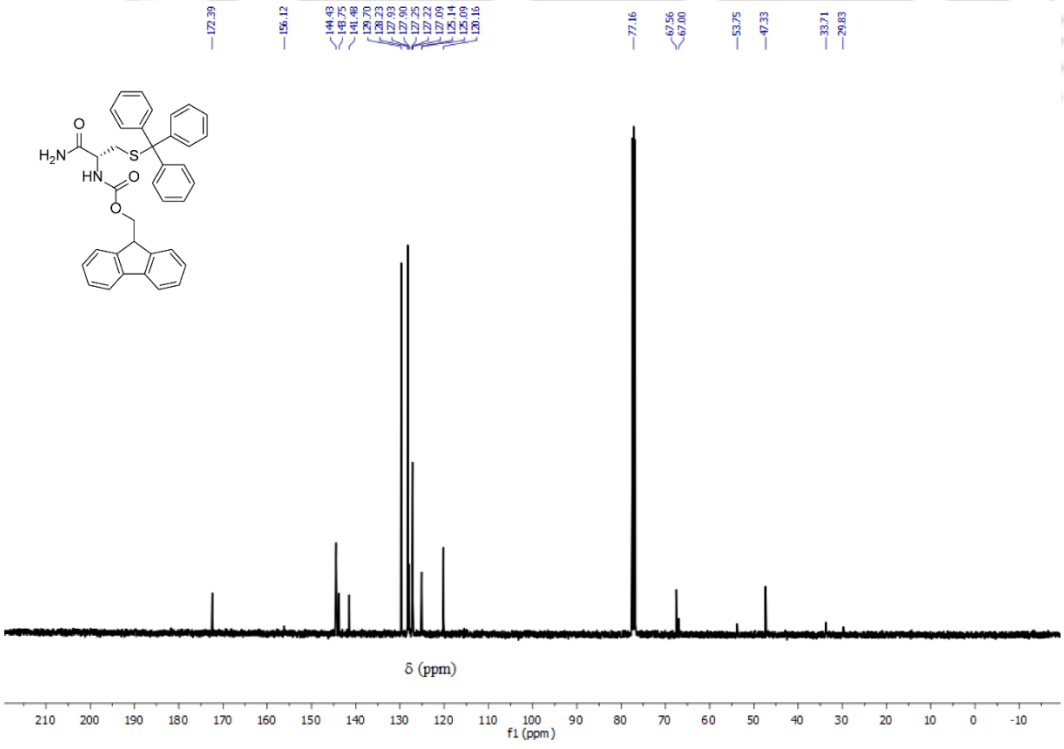

Figure 7.38 ^{13}C NMR Spectrum of **Compound 13** in $CDCl_3$

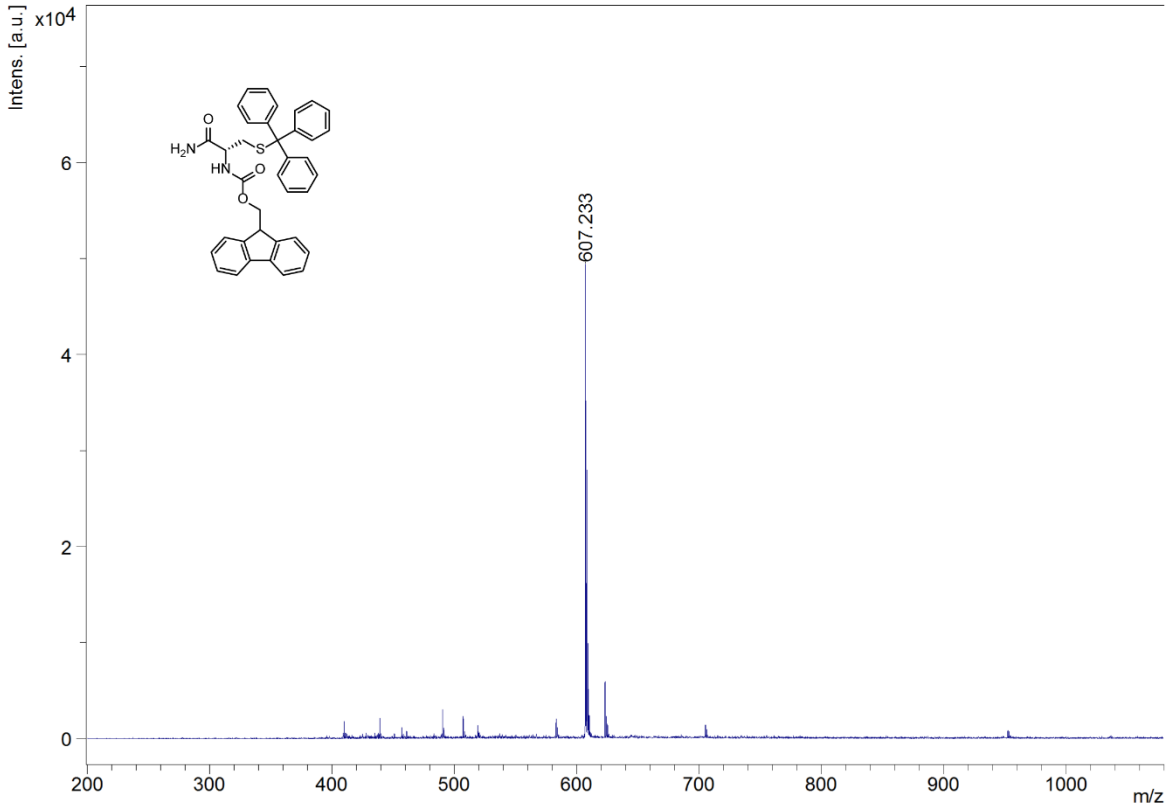

Figure 7.39 MALDI-TOF of **Compound 13**.

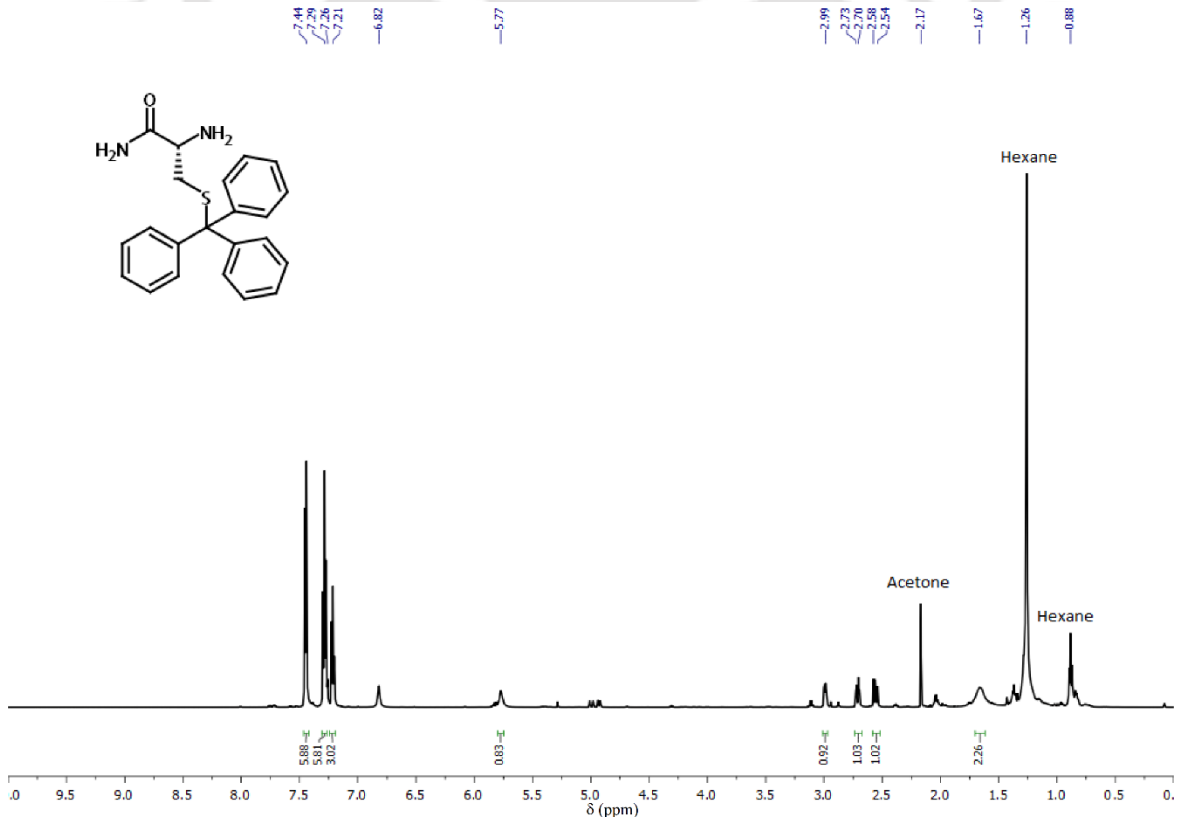

Figure 7.40 ^{1}H NMR Spectrum of **Compound 14** in $CDCl_3$.

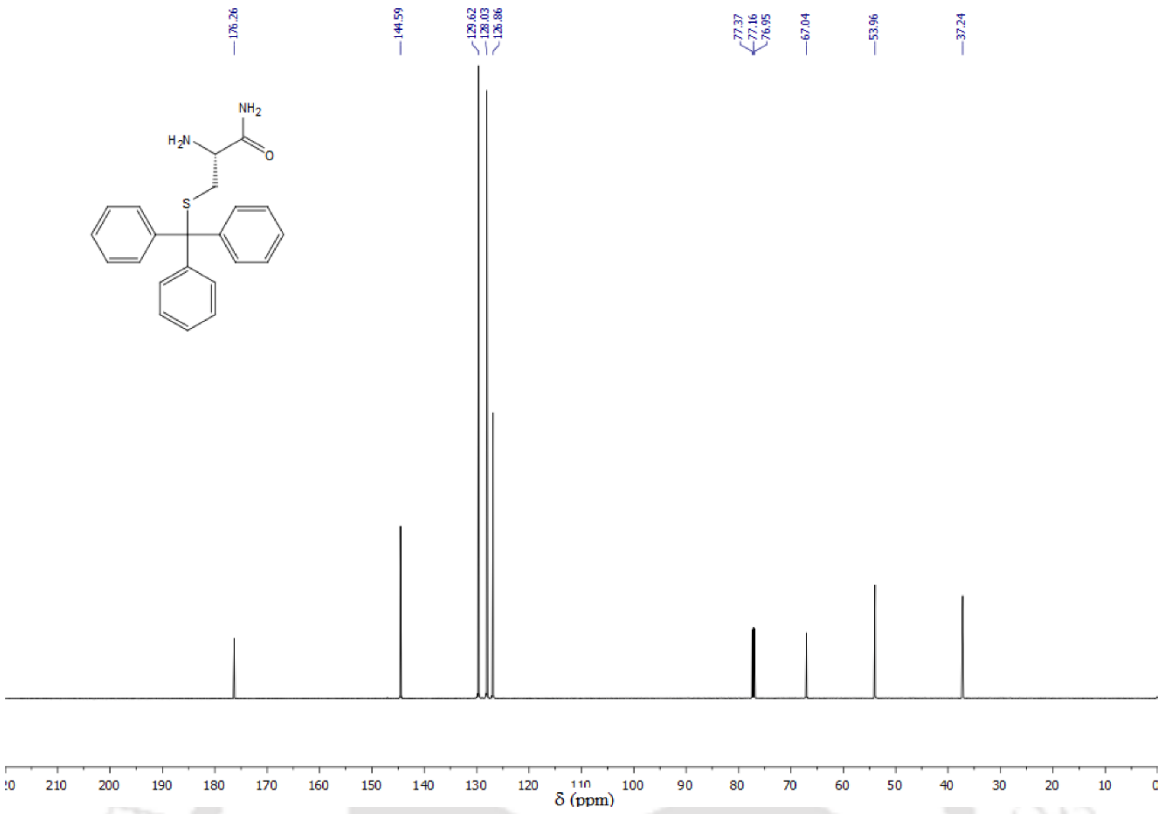

Figure 7.41 ^{13}C NMR Spectrum of **Compound 14** in $CDCl_3$.

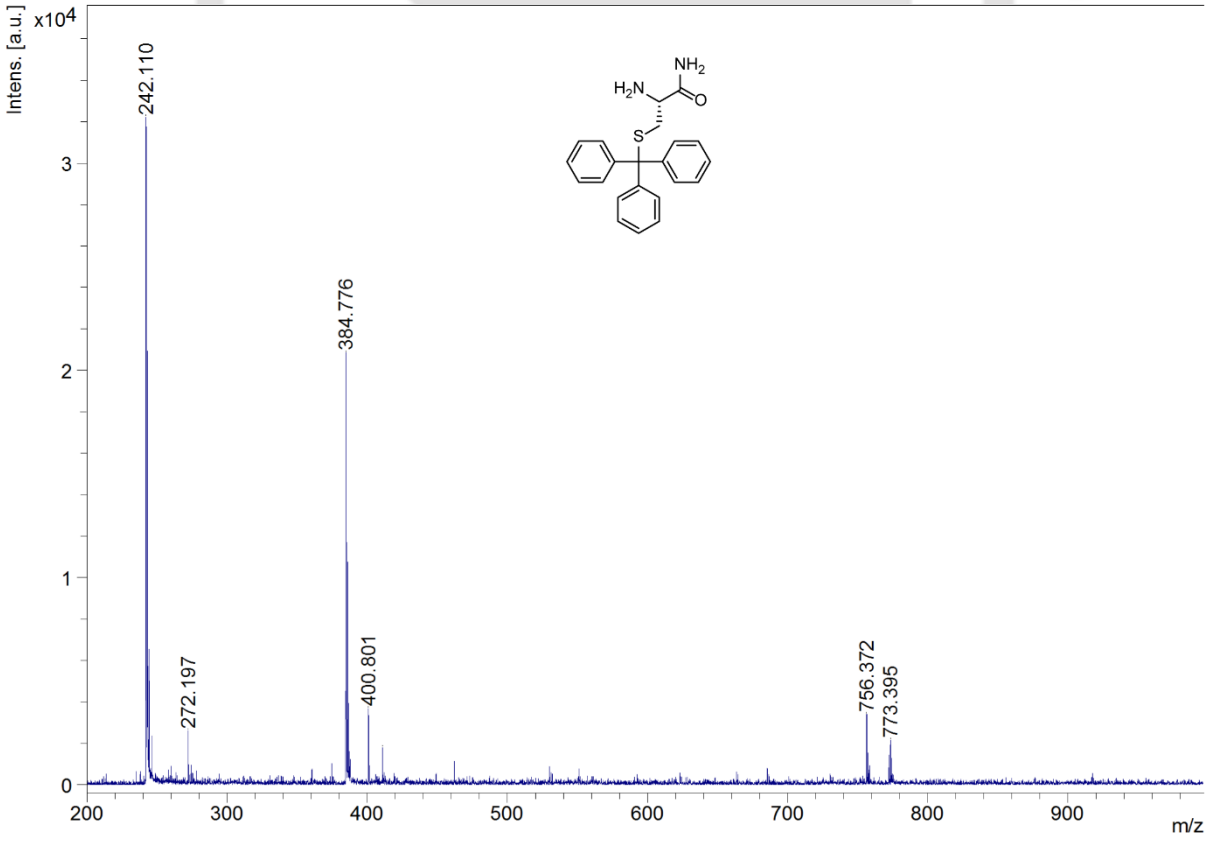

Figure 7.42 MALDI-TOF of Compound **14**.

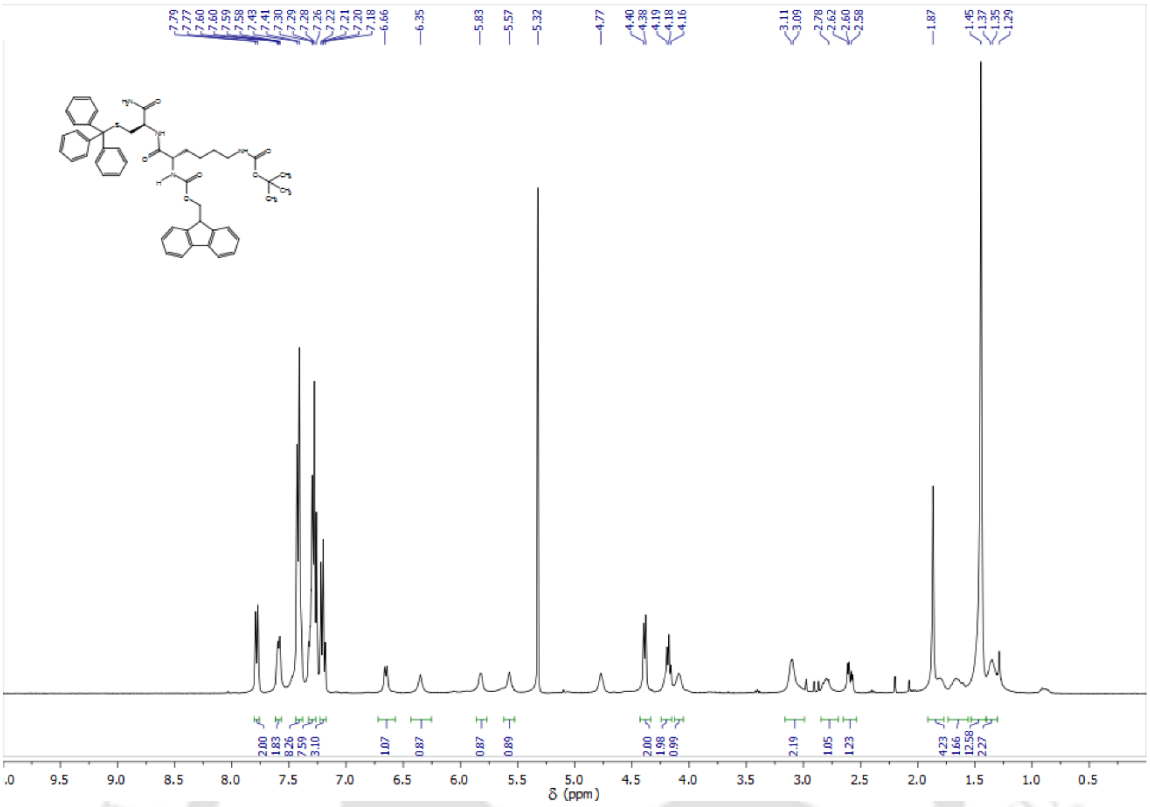

Figure 7.43 ^{1}H NMR Spectrum of Compound **15** in $CDCl_3$.

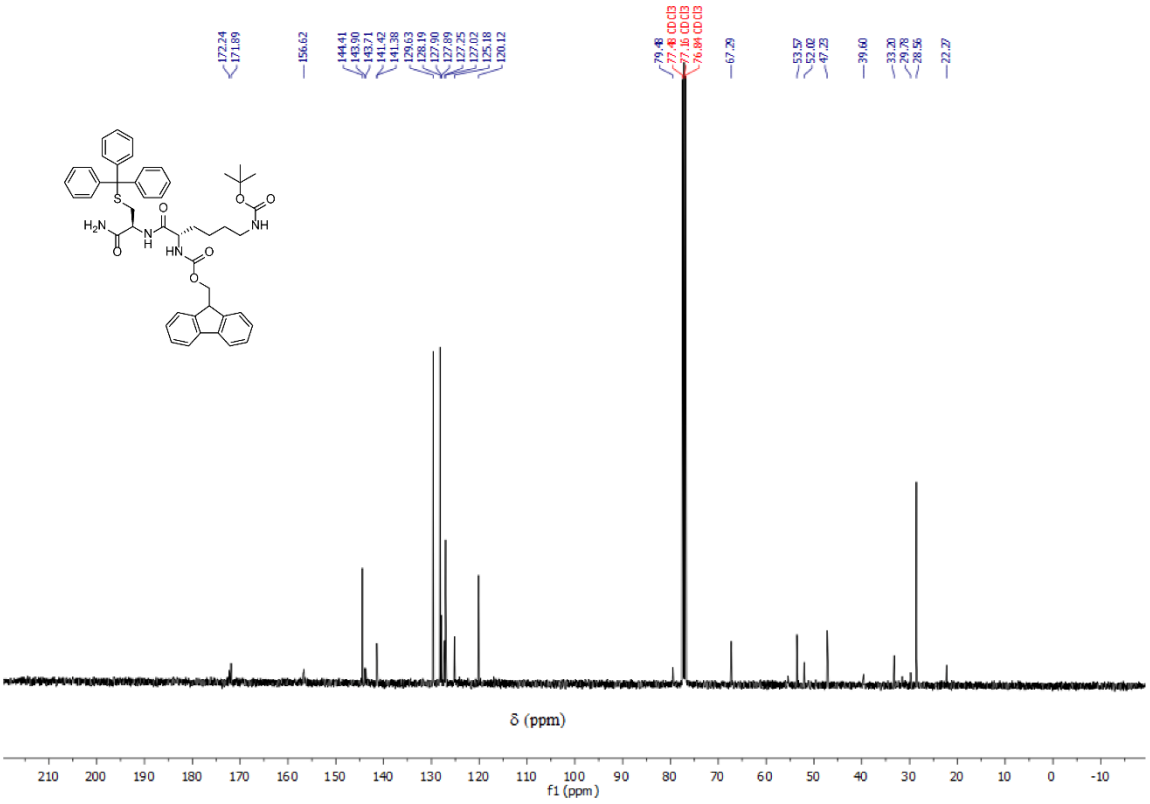

Figure 7.44 ^{13}C NMR Spectrum of Compound **15** in $CDCl_3$.

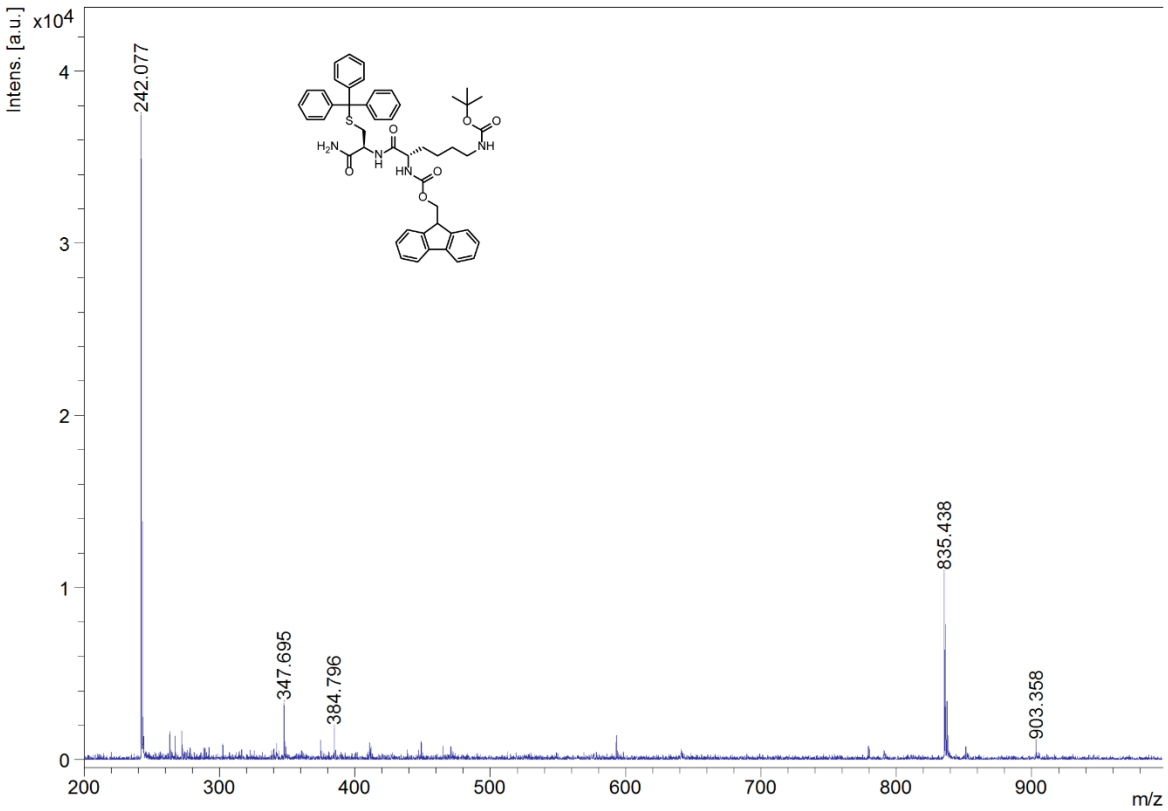

Figure 7.45 MALDI-TOF of Compound **15**.

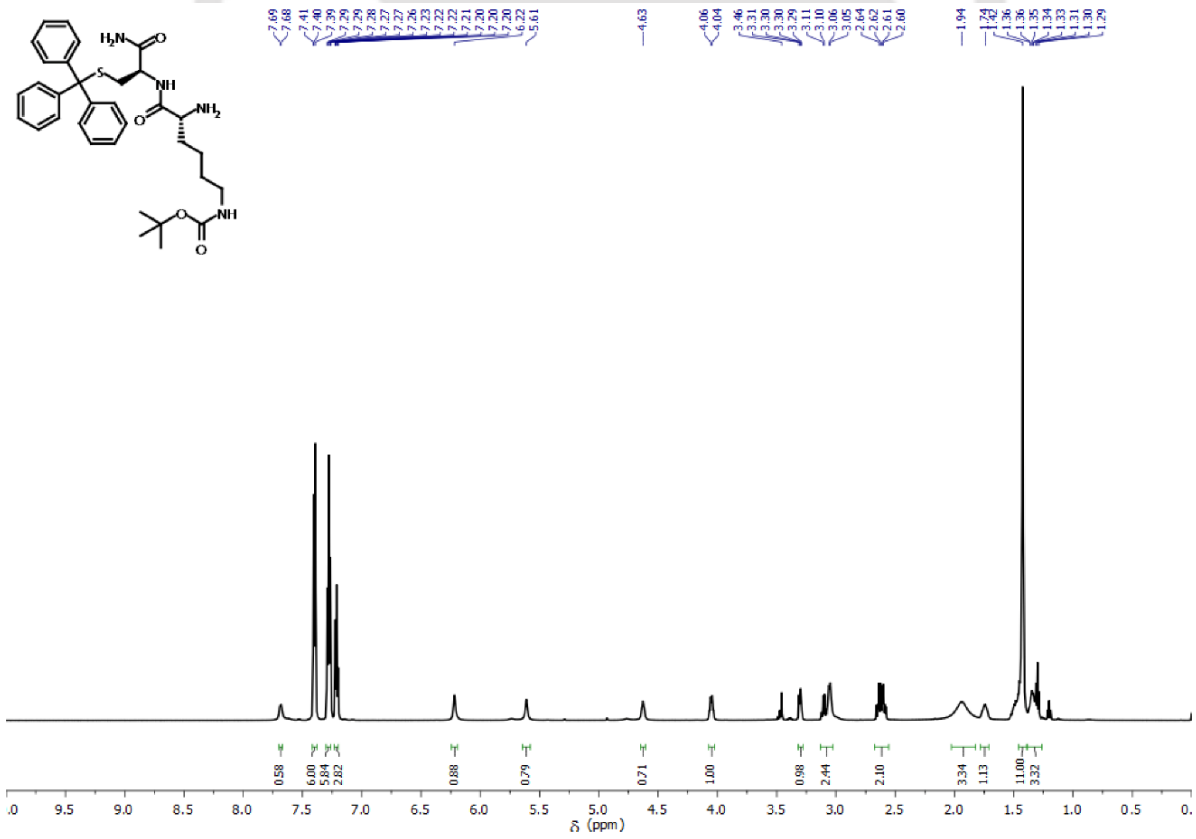

Figure 7.46 ^{1}H NMR Spectrum of Compound **16** in $CDCl_3$.

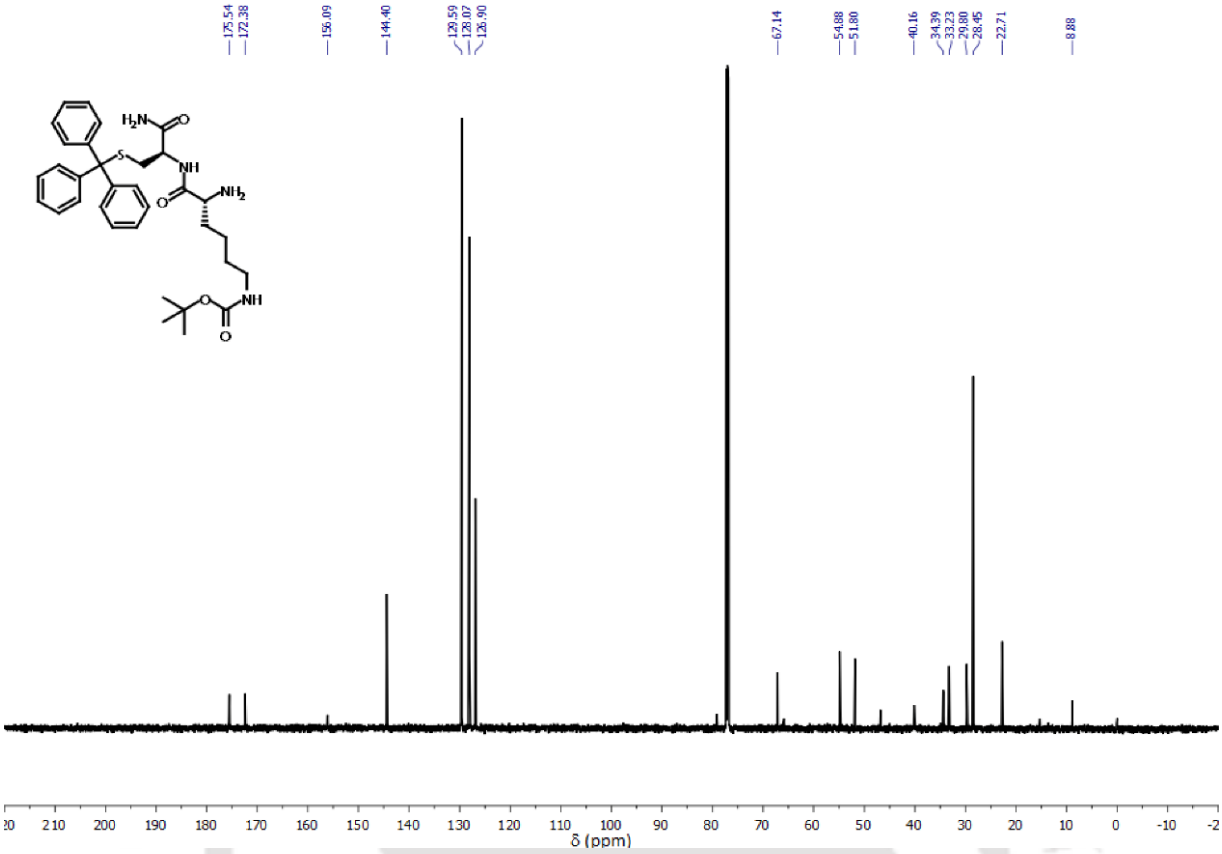

Figure 7.47 ^{13}C NMR Spectrum of Compound **16** in $CDCl_3$.

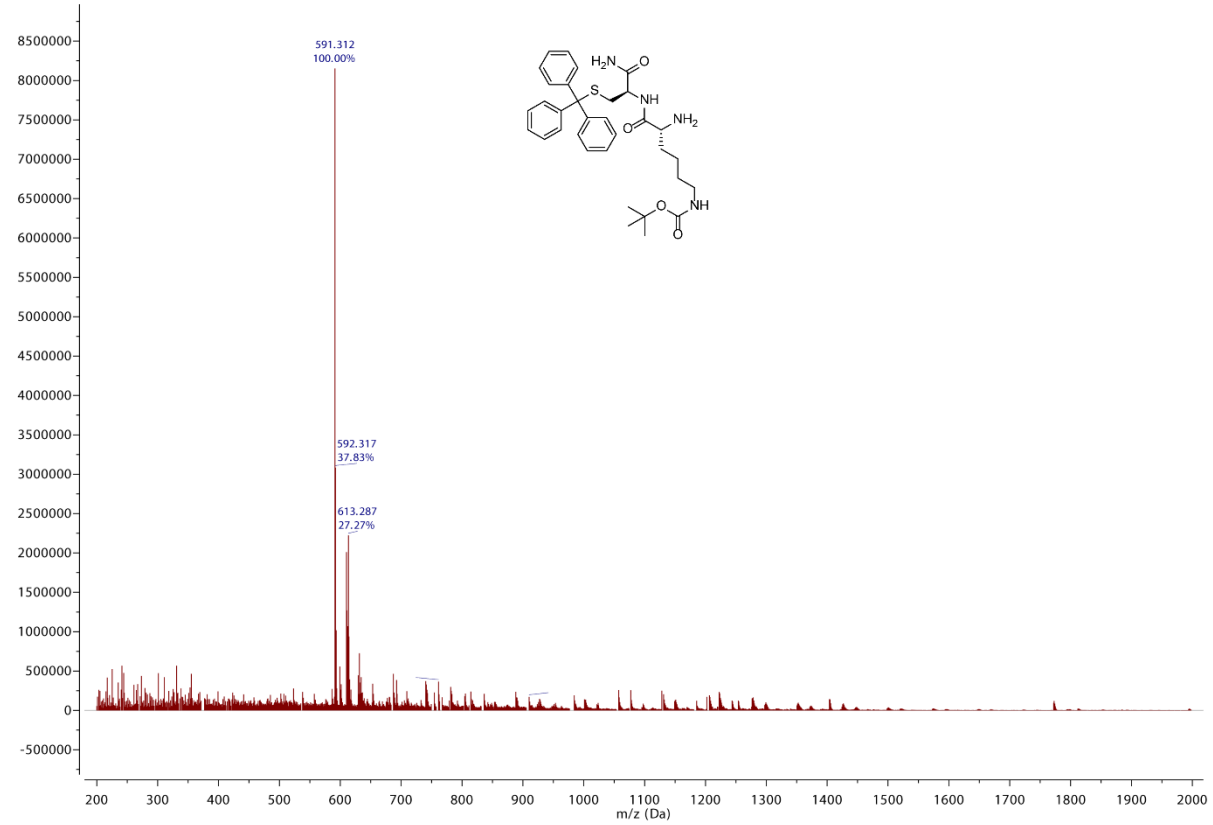

Figure 7.48 ESI-MS Spectrum of Compound **16**.

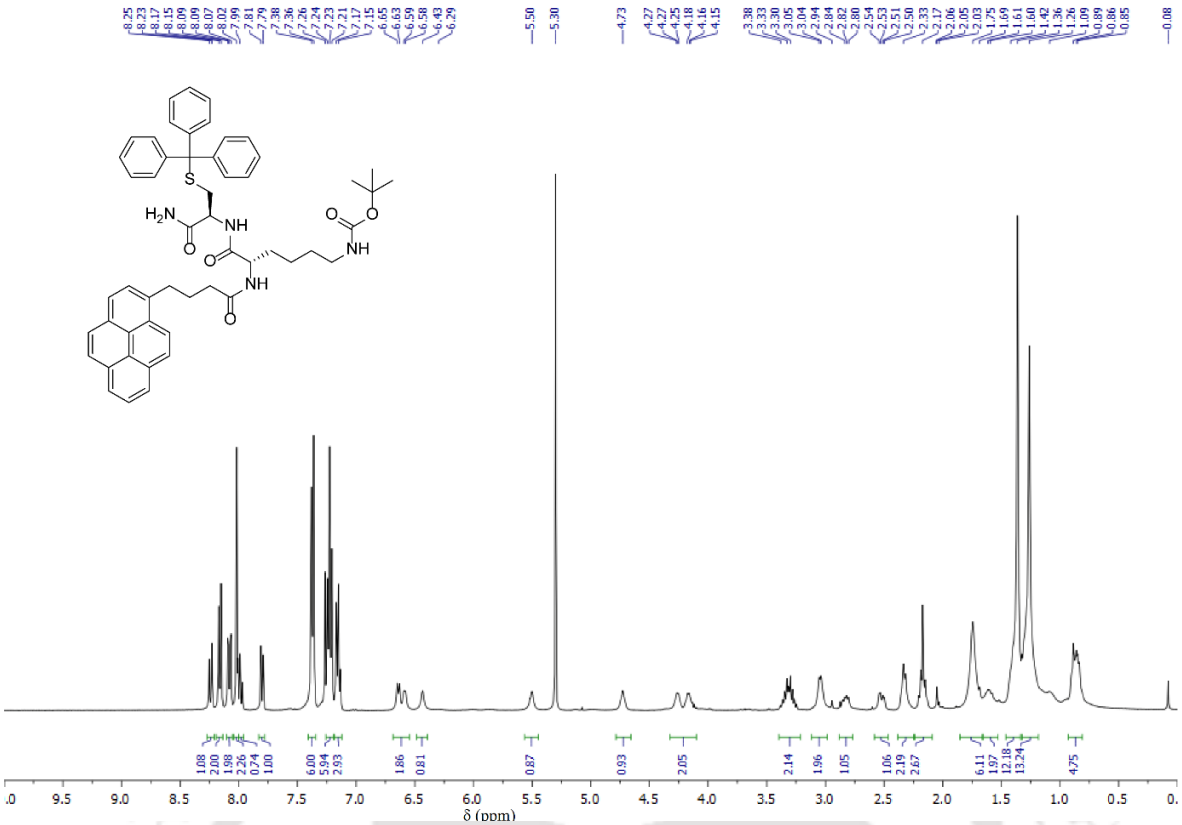

Figure 7.49 ^{1}H NMR Spectrum of Compound **17** in $CDCl_3$.

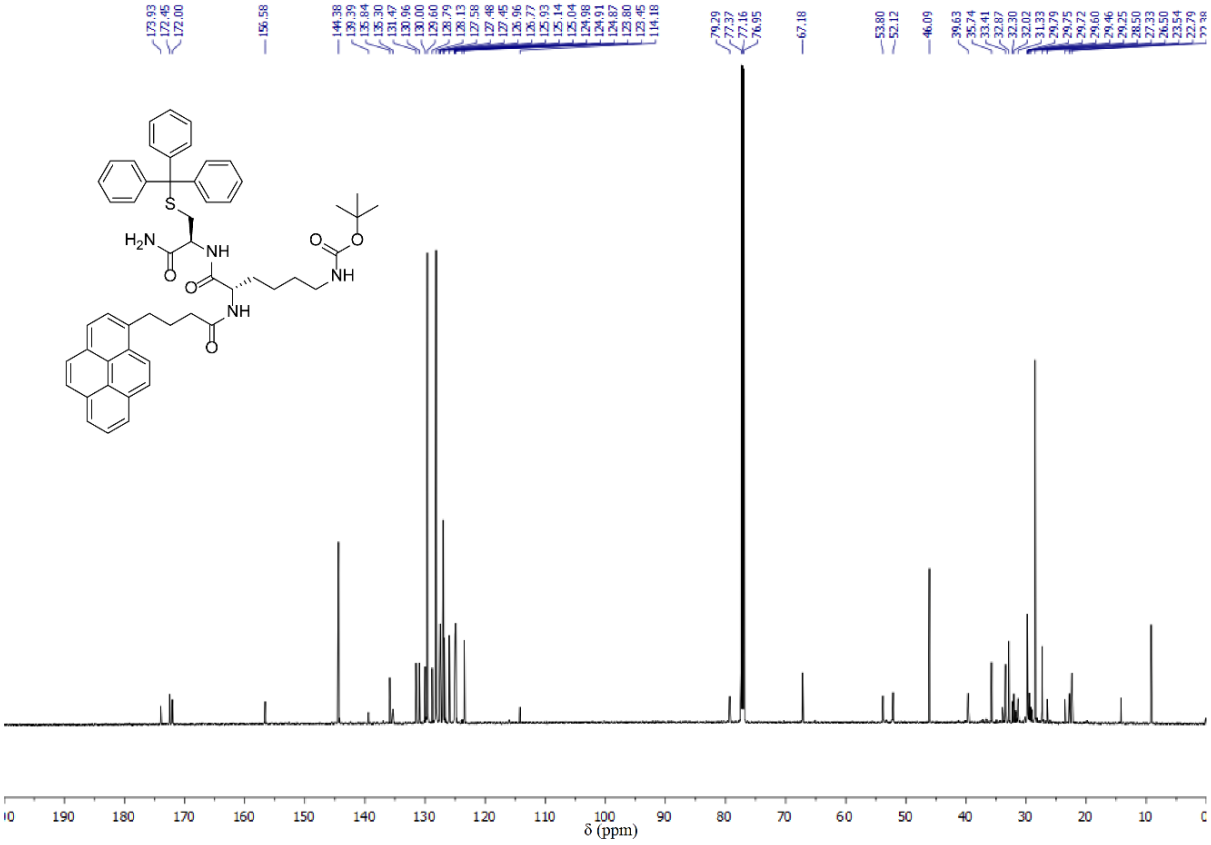

Figure 7.50 ^{13}C NMR Spectrum of Compound **17** in $CDCl_3$.

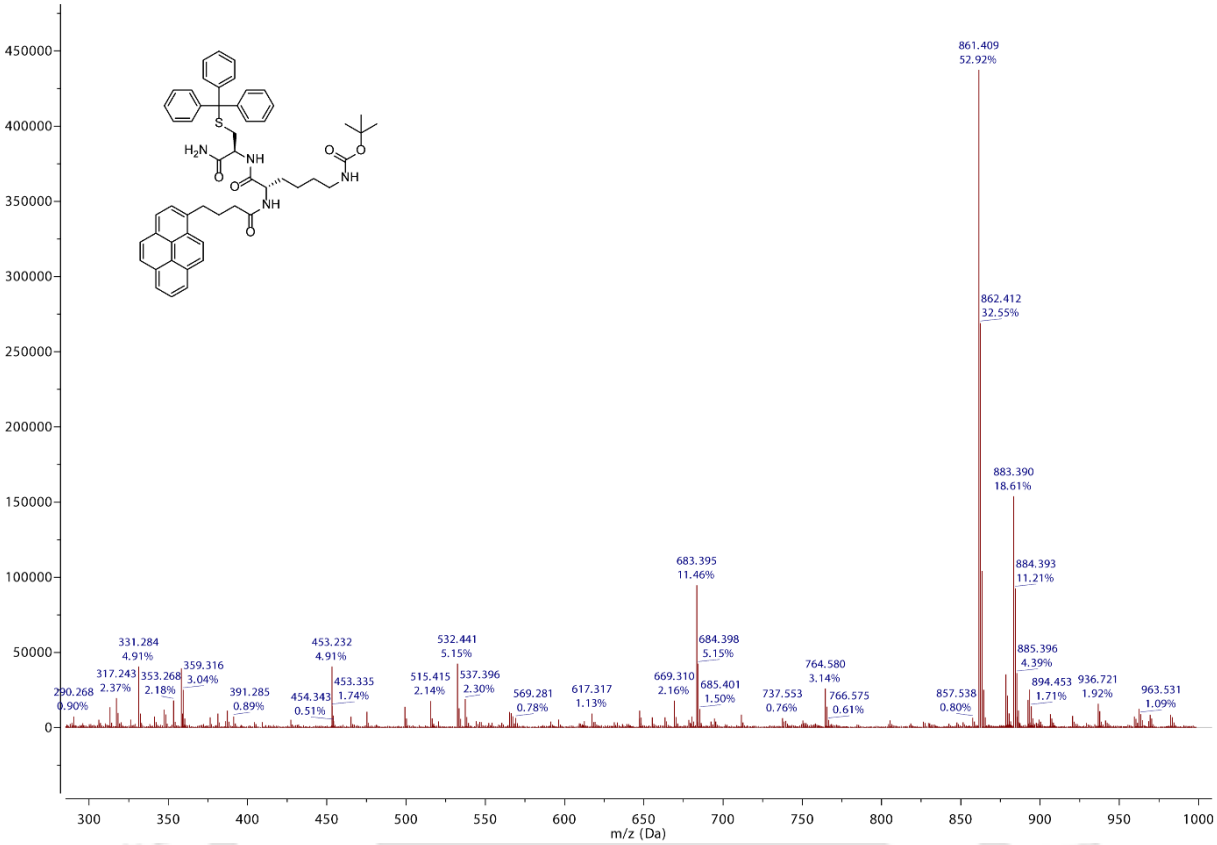

Figure 7.51ESI-MS Spectrum of Compound **17**.

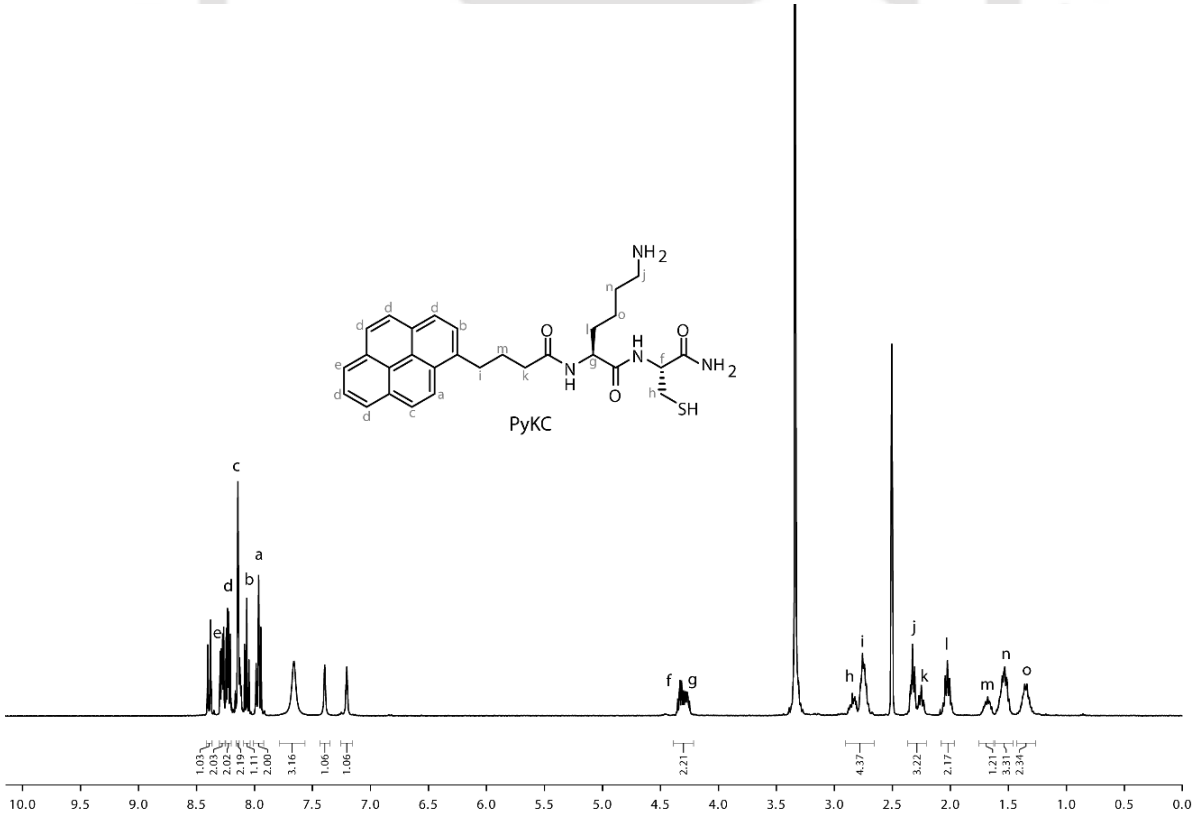

Figure 7.52^{1}H NMR Spectrum of **PyKC** in DMSO-D_6.

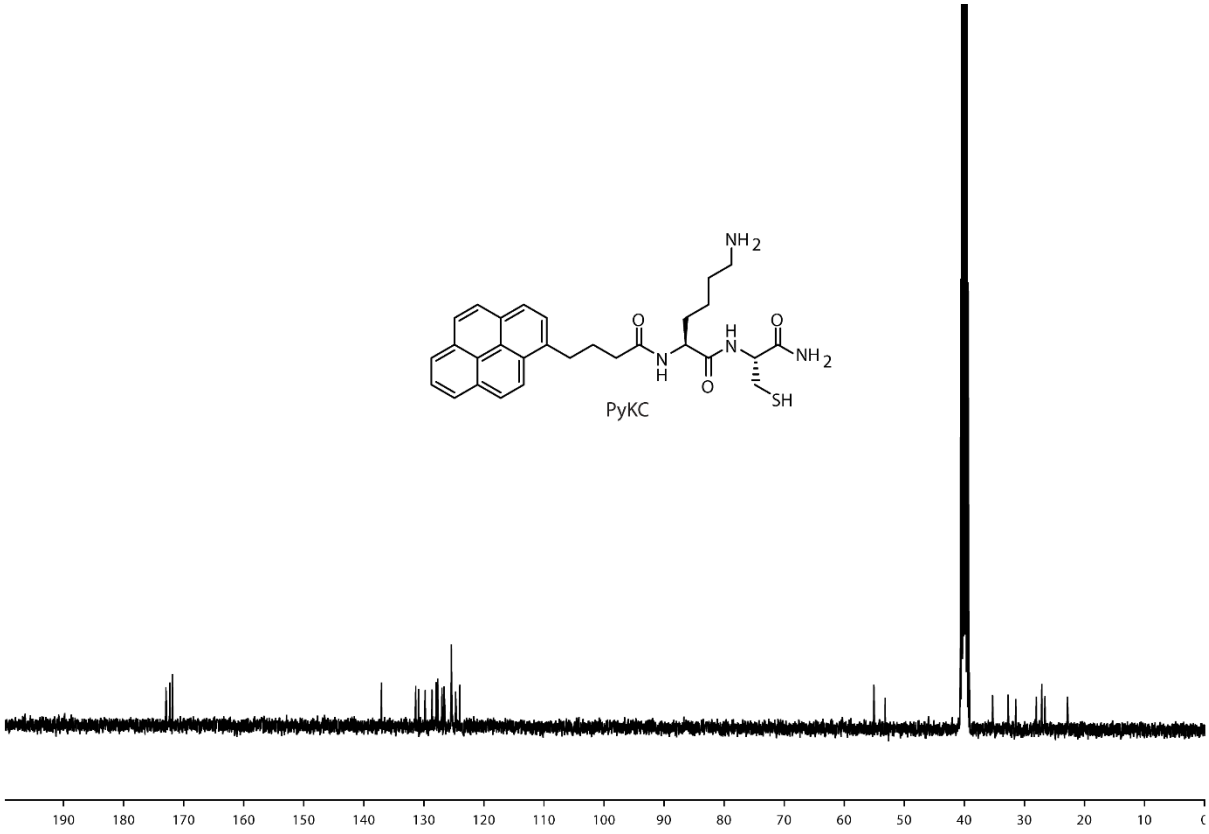

Figure 7.53 ^{13}C NMR Spectrum of **PyKC** in DMSO-d_6.

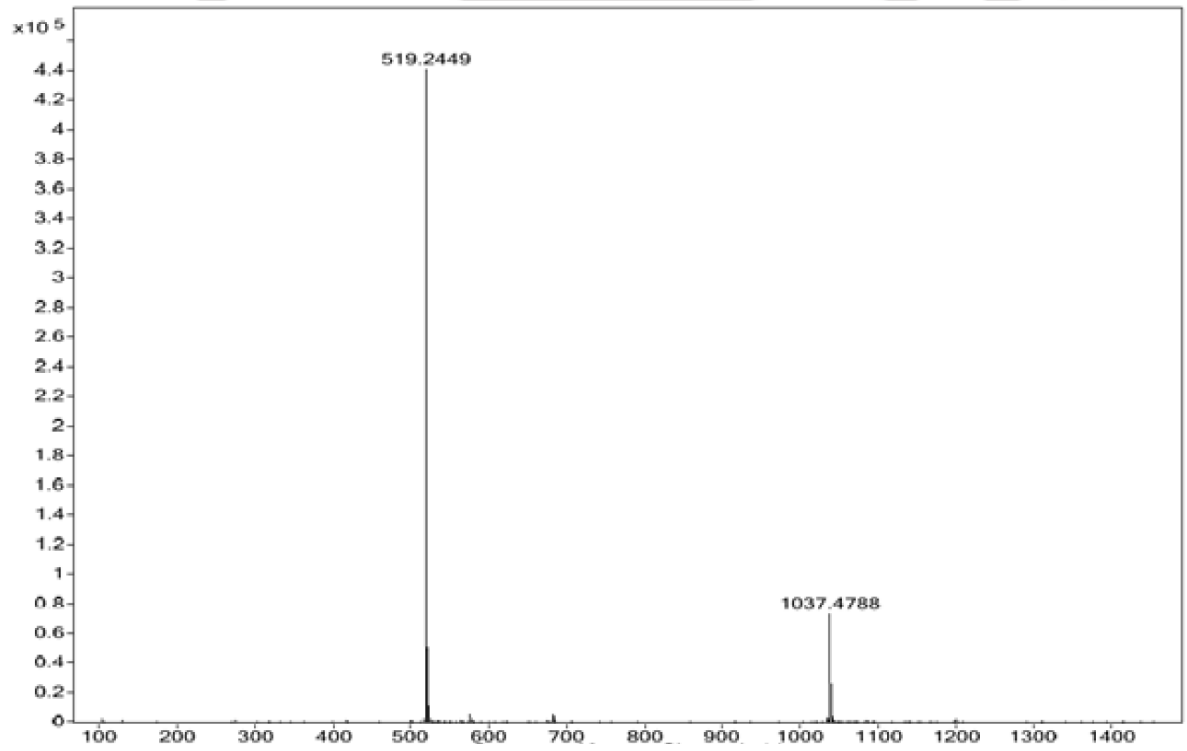

Figure 7.54 ESI-MS Spectrum of **PyKC**.

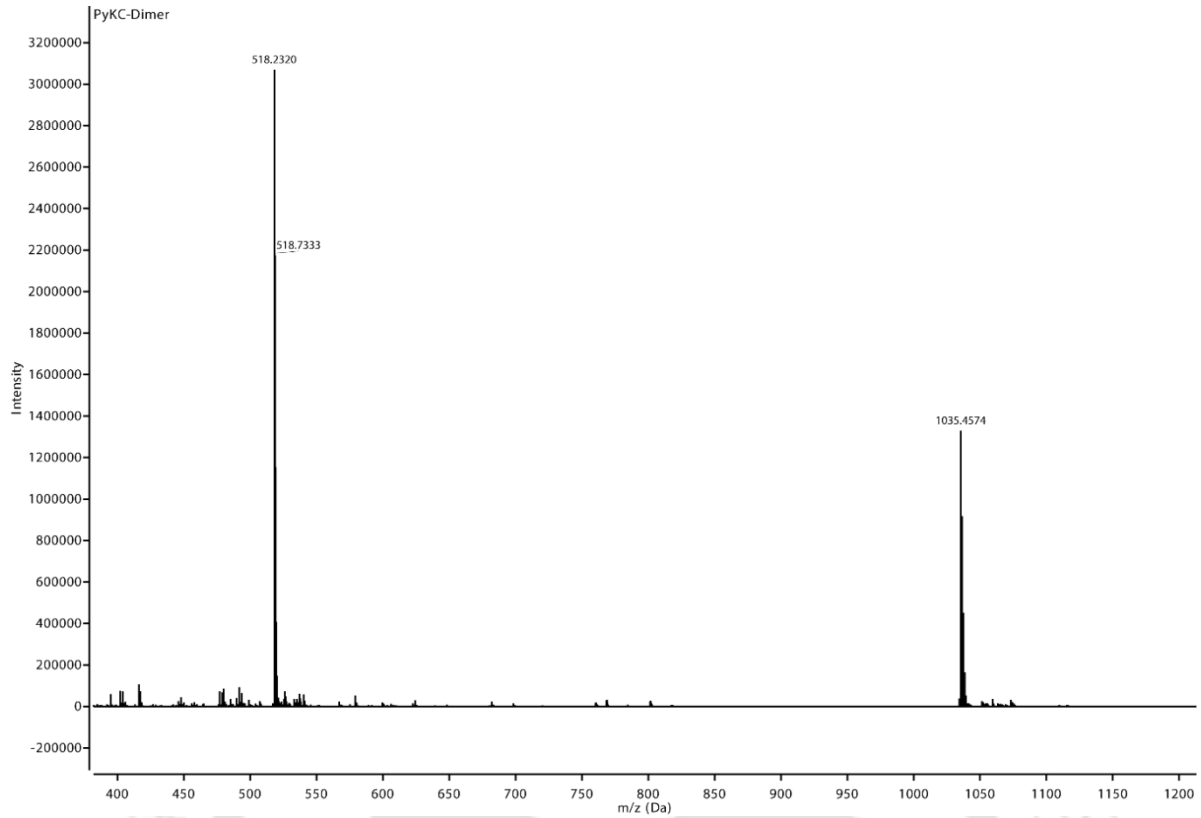

Figure 7.55 ESI-MS Spectrum of PyKC Dimer.

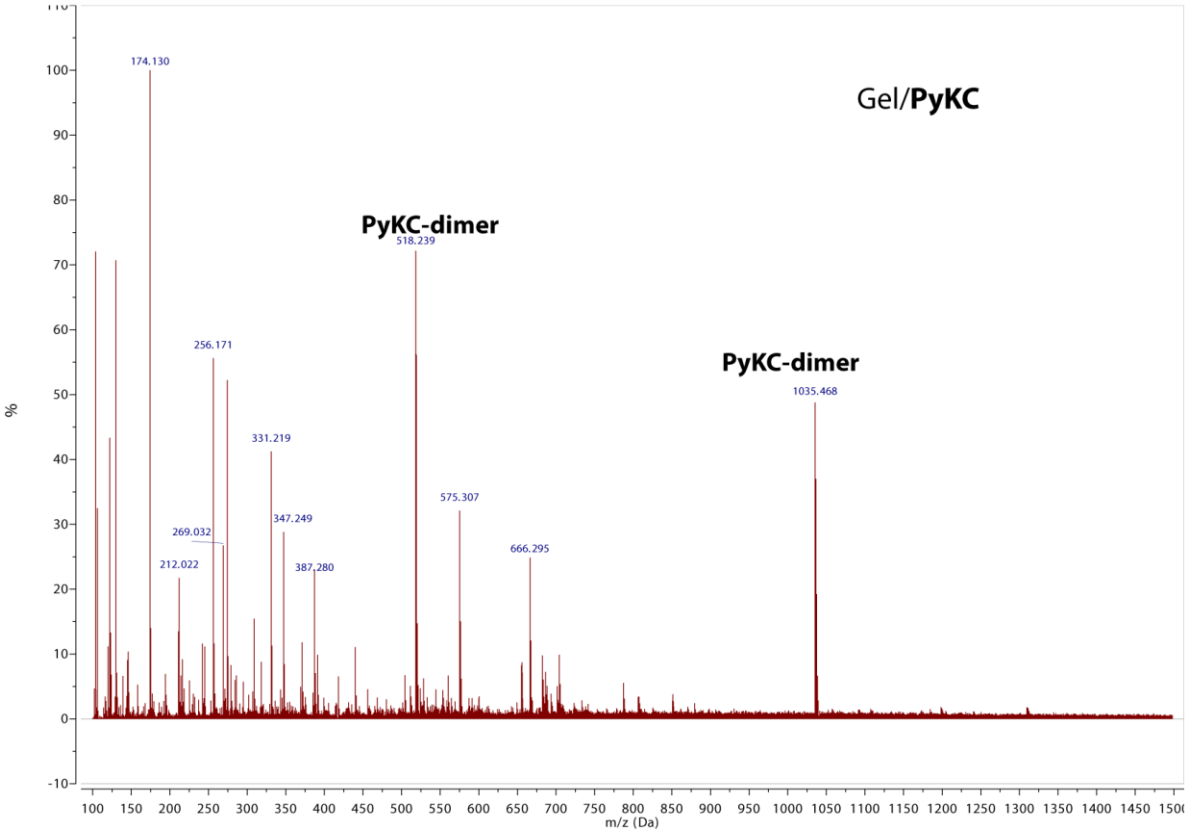

Figure 7.56ESI-MS Spectrum of 24 h matured composite hydrogel of Gel/PyKC.

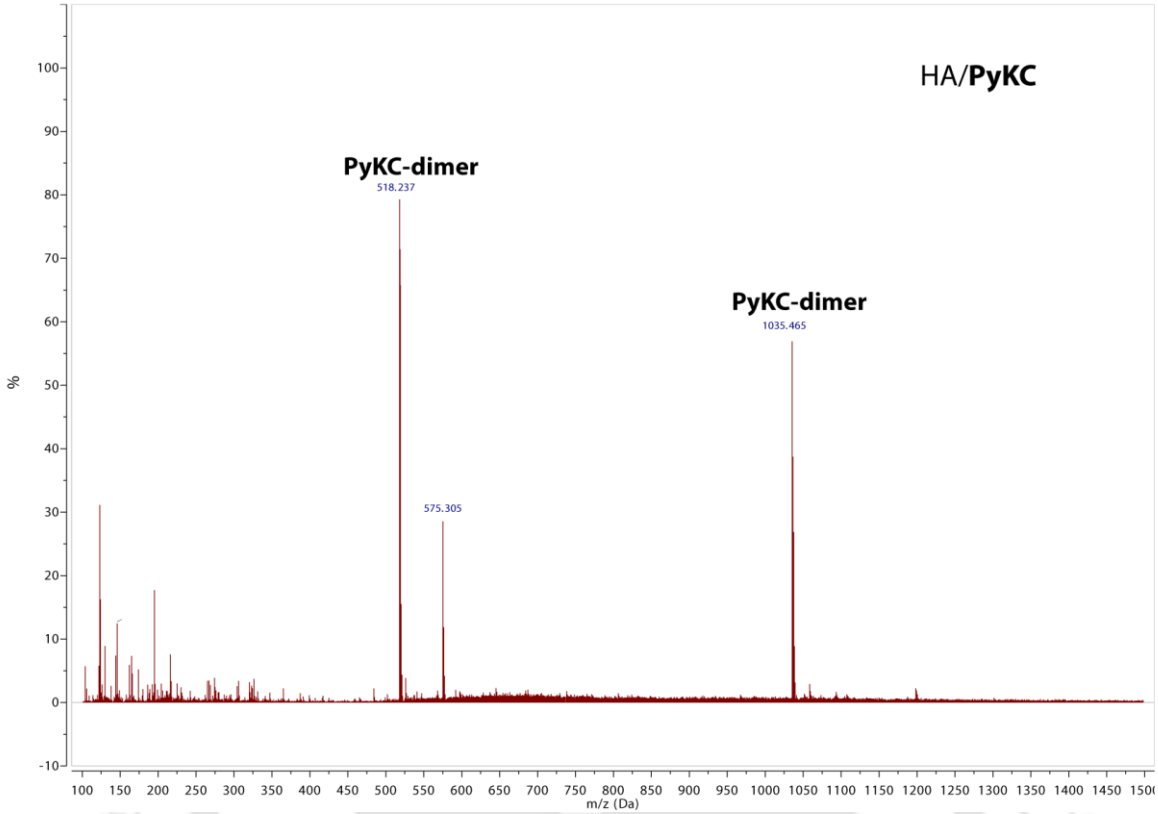

Figure 7.57 ESI-MS Spectrum of 24 h matured composite hydrogel of HA/PyKC.

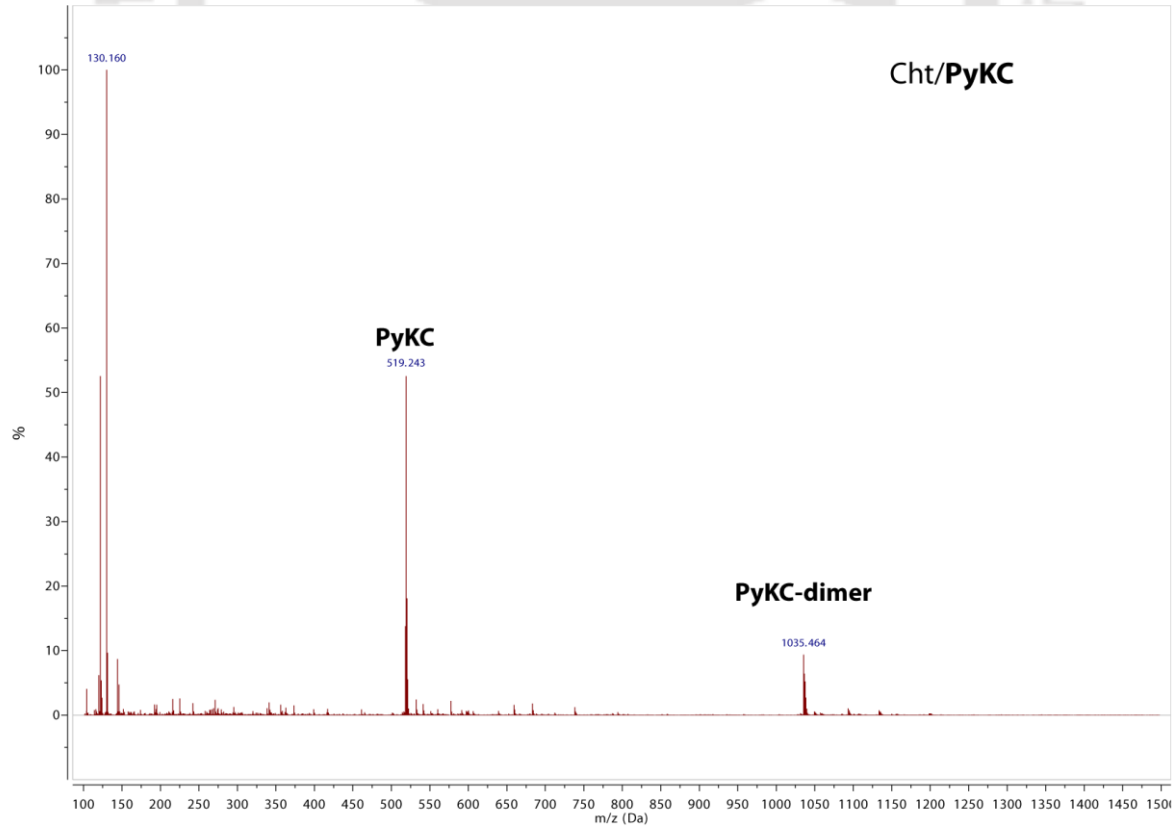

Figure 7.58 ESI-MS Spectrum of 24 h matured composite hydrogel of Cht/PyKC.

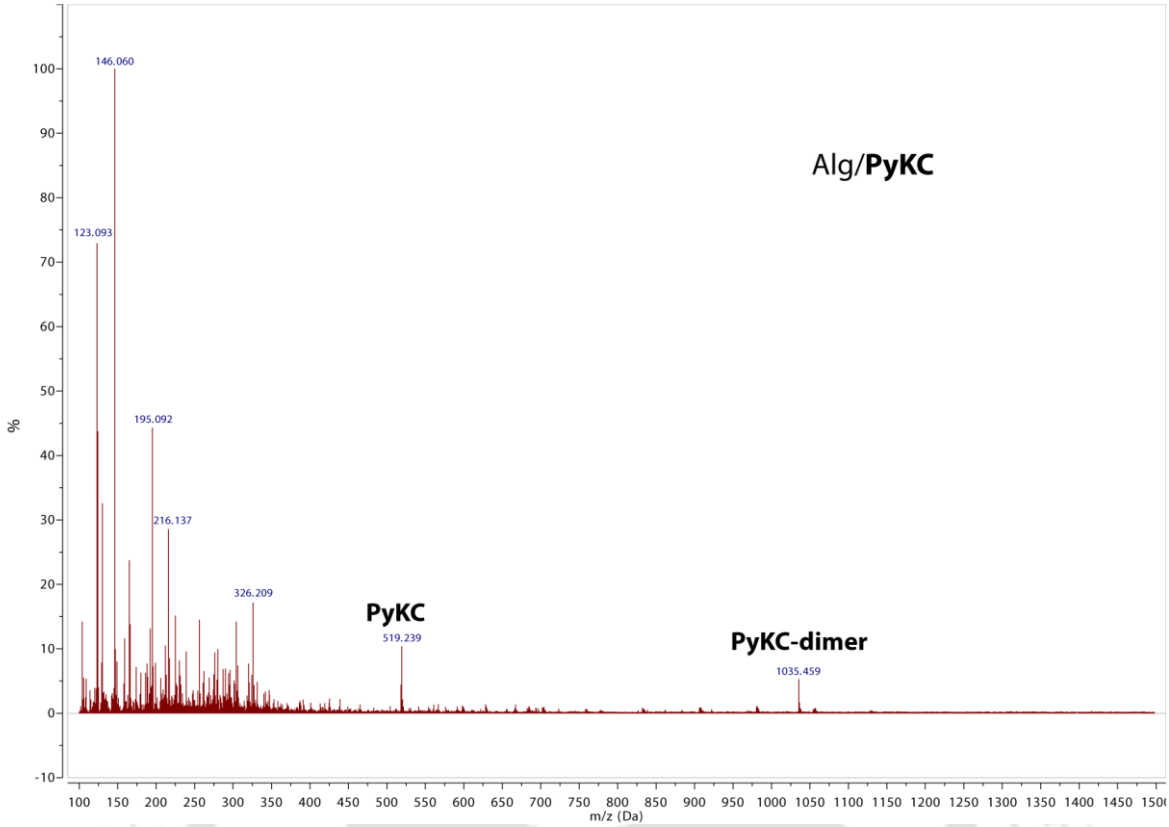

Figure 7.59ESI-MS Spectrum of 24 h matured composite hydrogel of Alg/PyKC.

Chapter 4

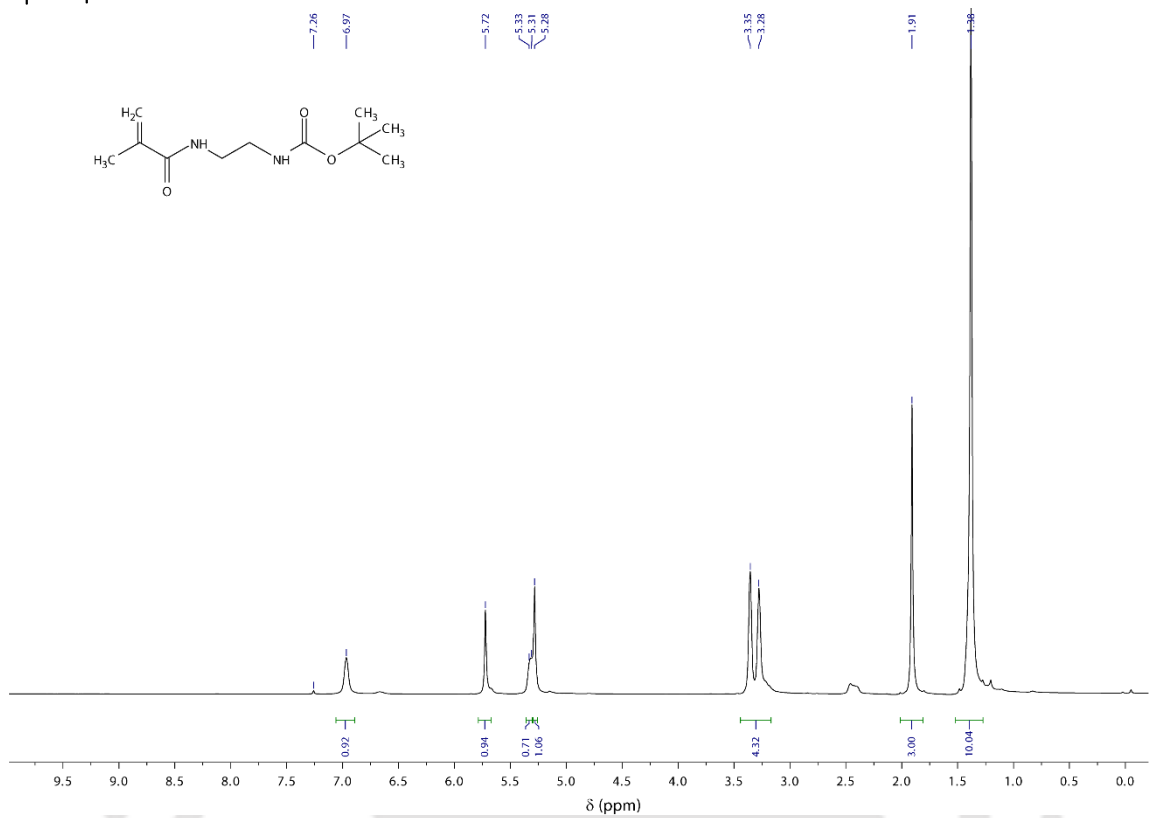

Figure 7.6 ^{1}H Spectrum of Compound **19** in $CDCl_3$.

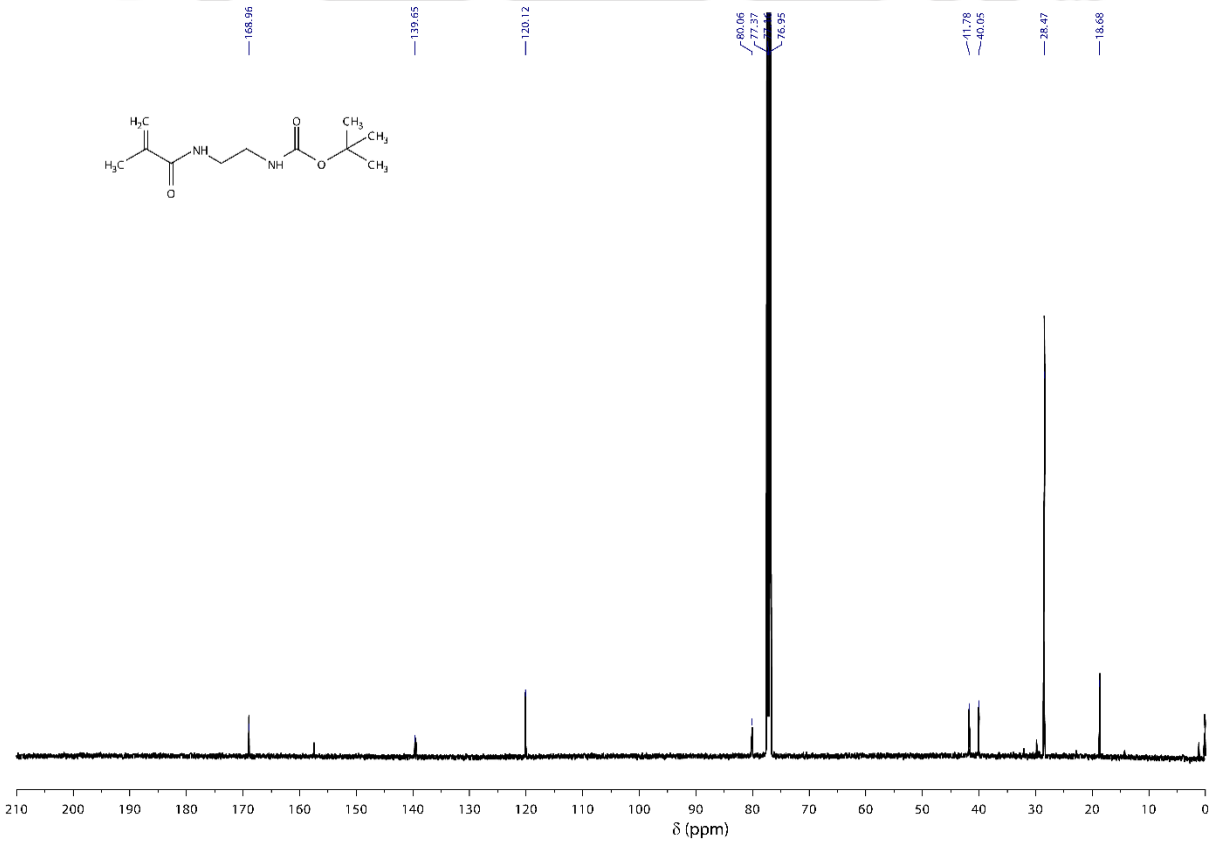

Figure 7.61 ^{13}C Spectrum of Compound **19** in $CDCl_3$.

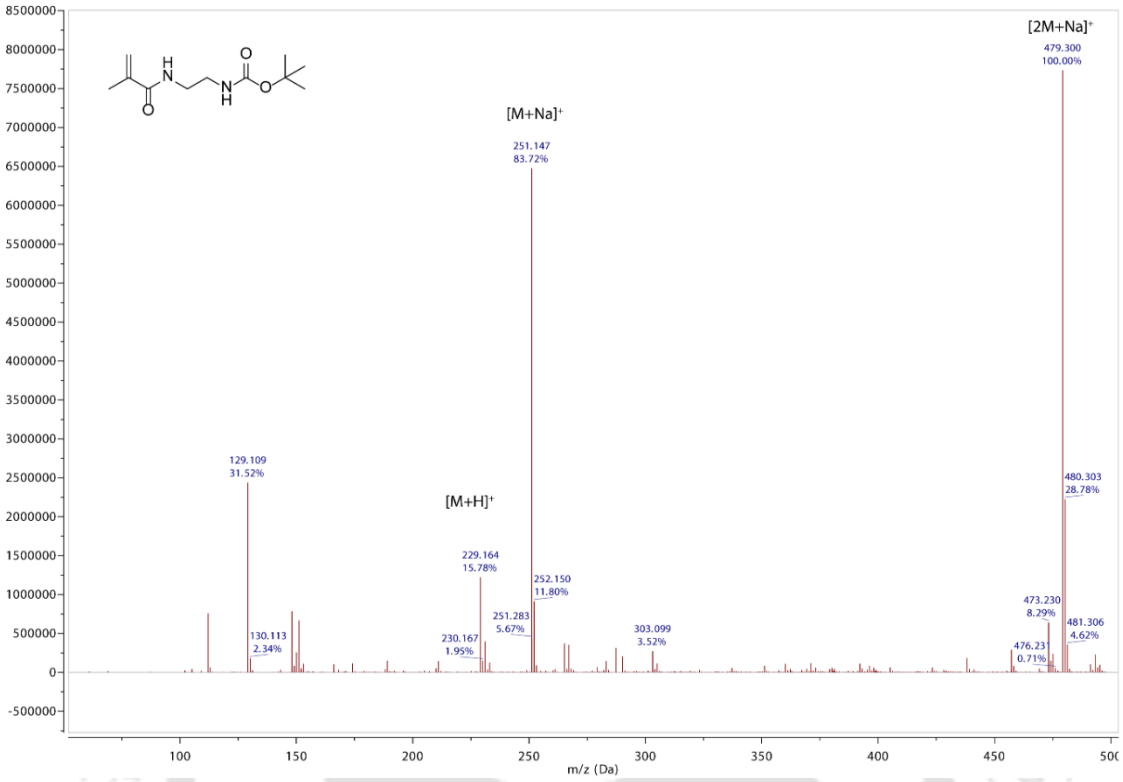

Figure 7.62 ESI-MS **Spectrum** of Compound **19**.

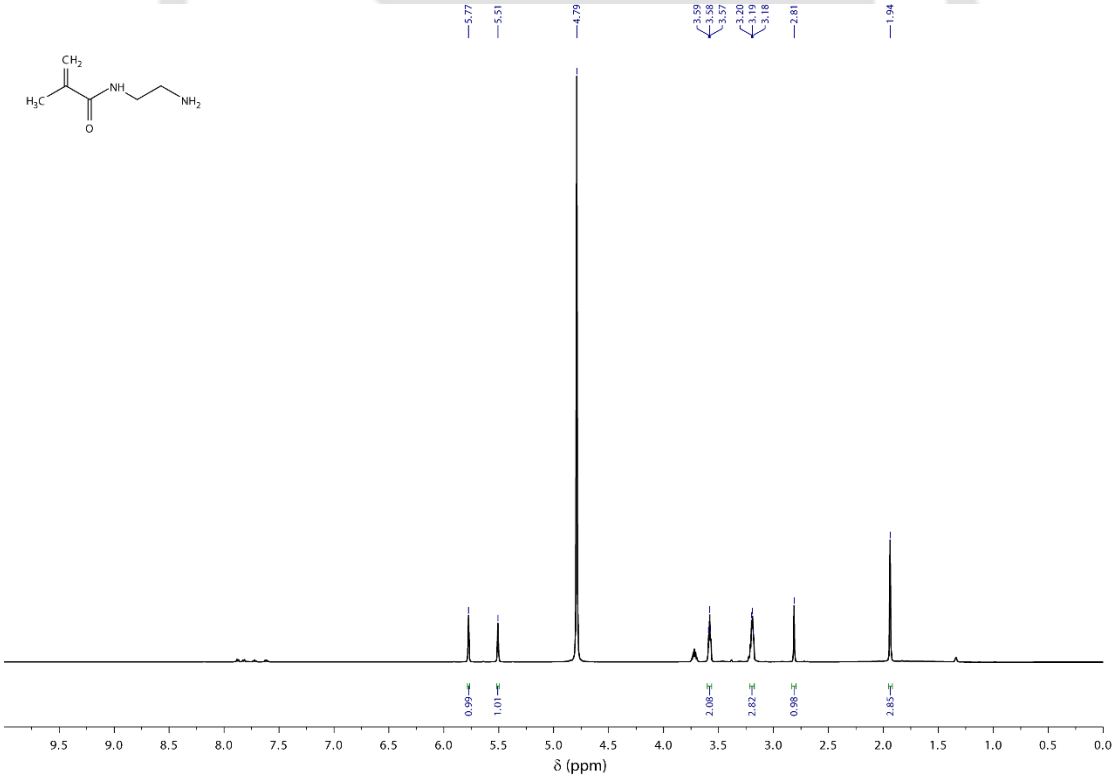

Figure7.63 ^{1}H Spectrum of Compound **20** in D_2O.

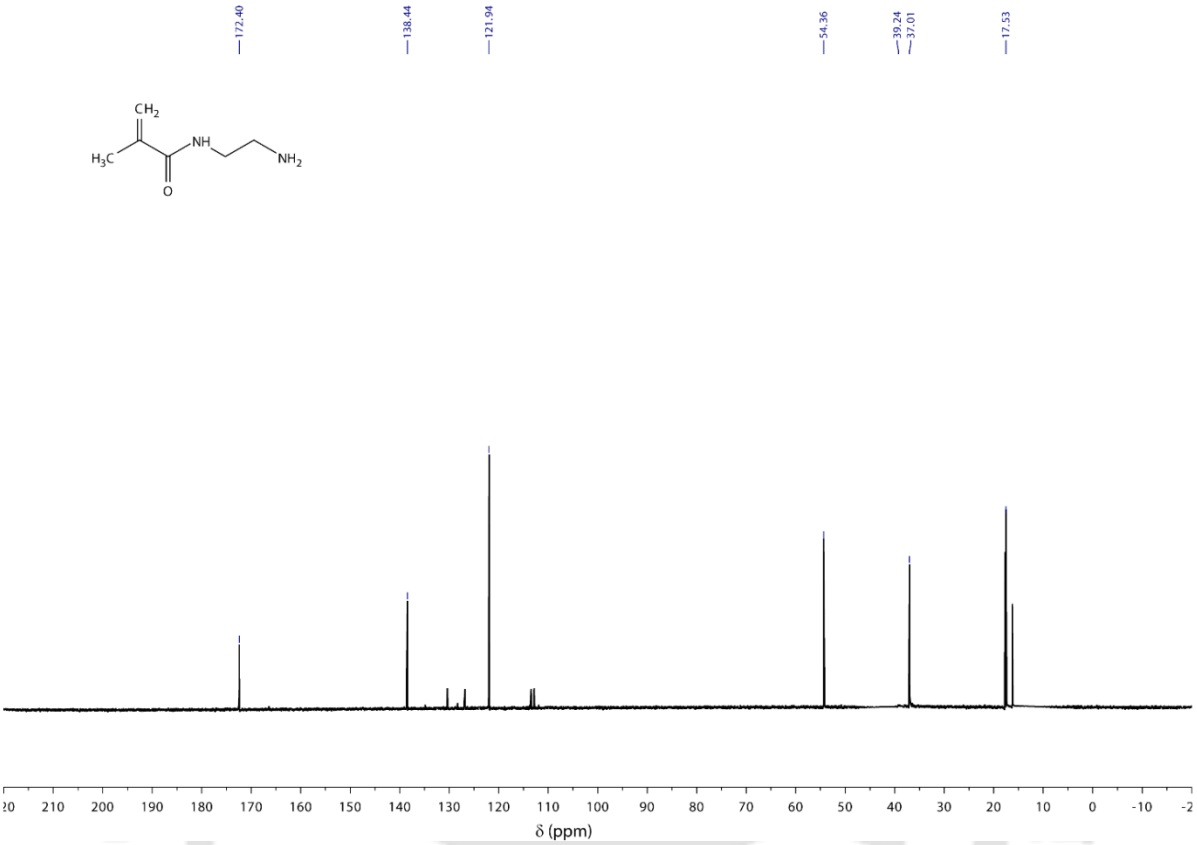

Figure 7.64 ^{13}C Spectrum of Compound **20** in D_2O.

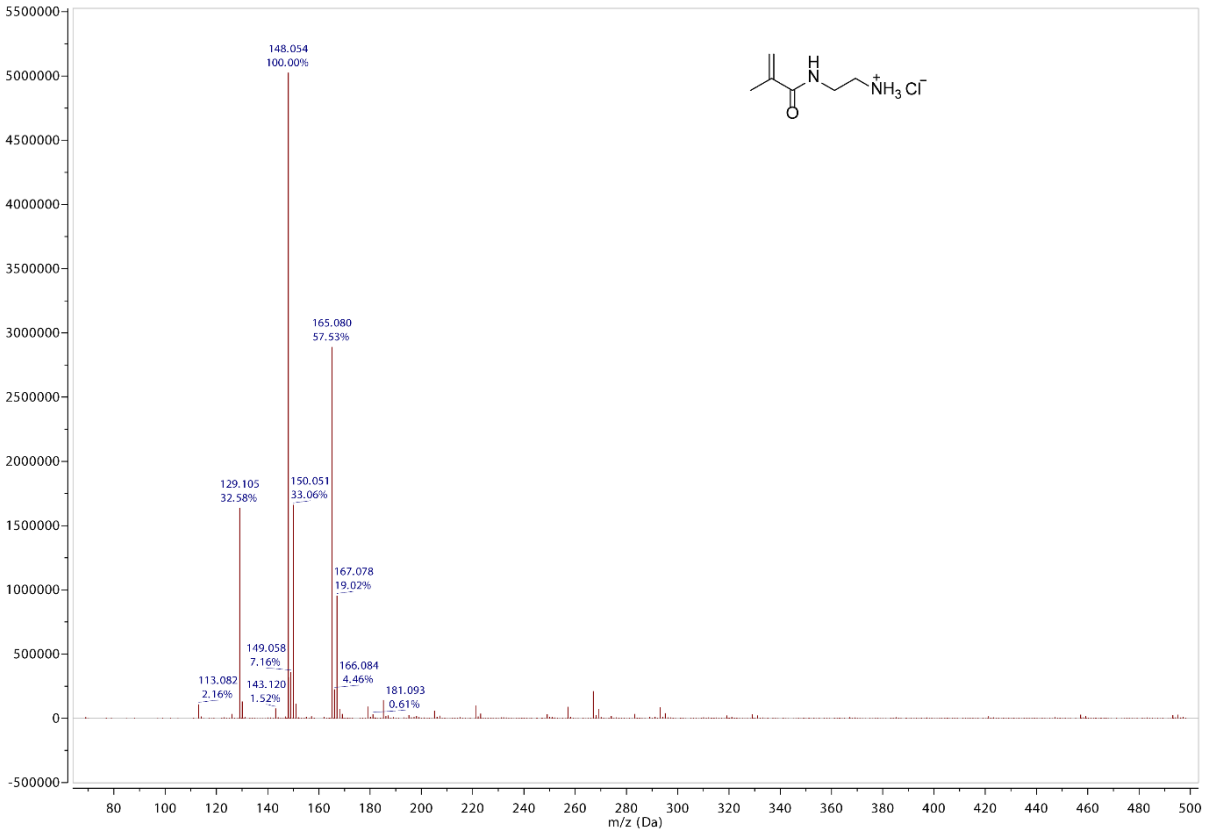

Figure 7.65 ESI-MS Spectrum of Compound **20**.

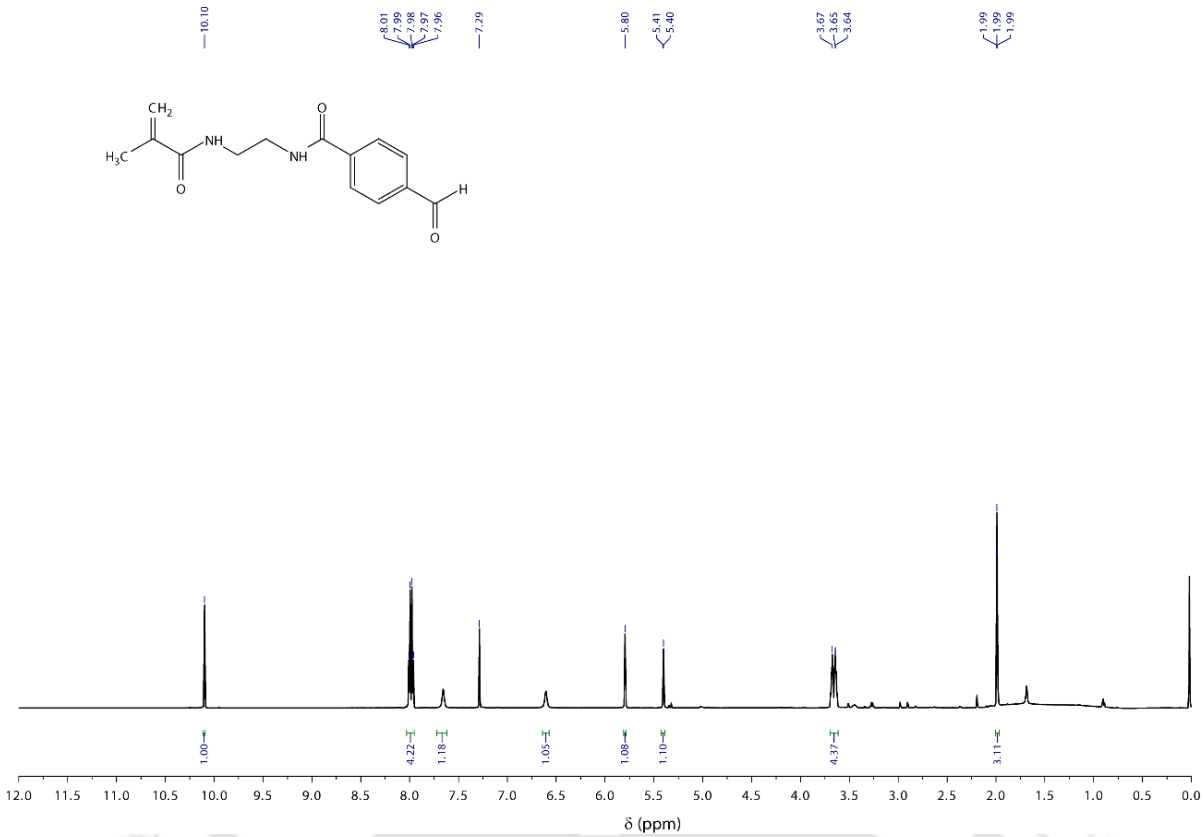

Figure 7.66 ^{1}H NMR Spectrum of Compound **21** in $CDCl_3$.

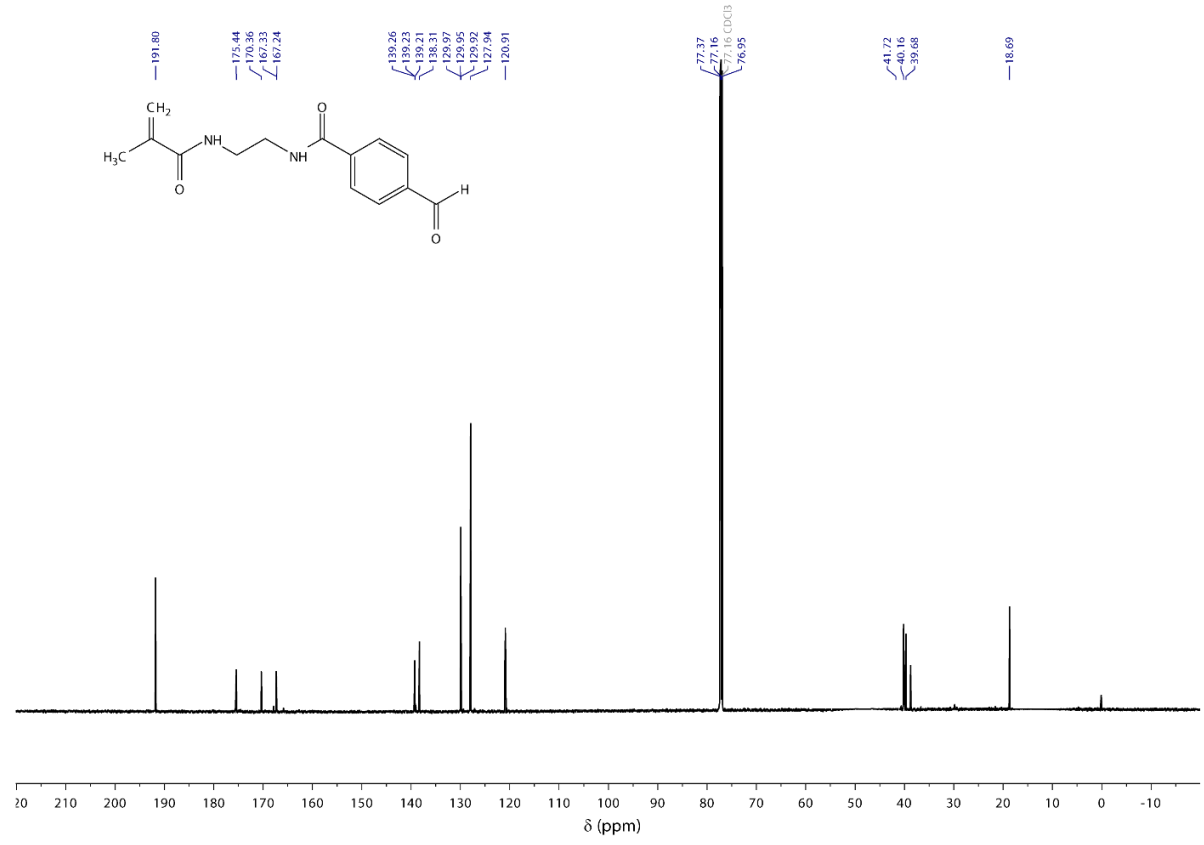

Figure 7.67 ^{13}C NMR Spectrum of Compound **21** in $CDCl_3$.

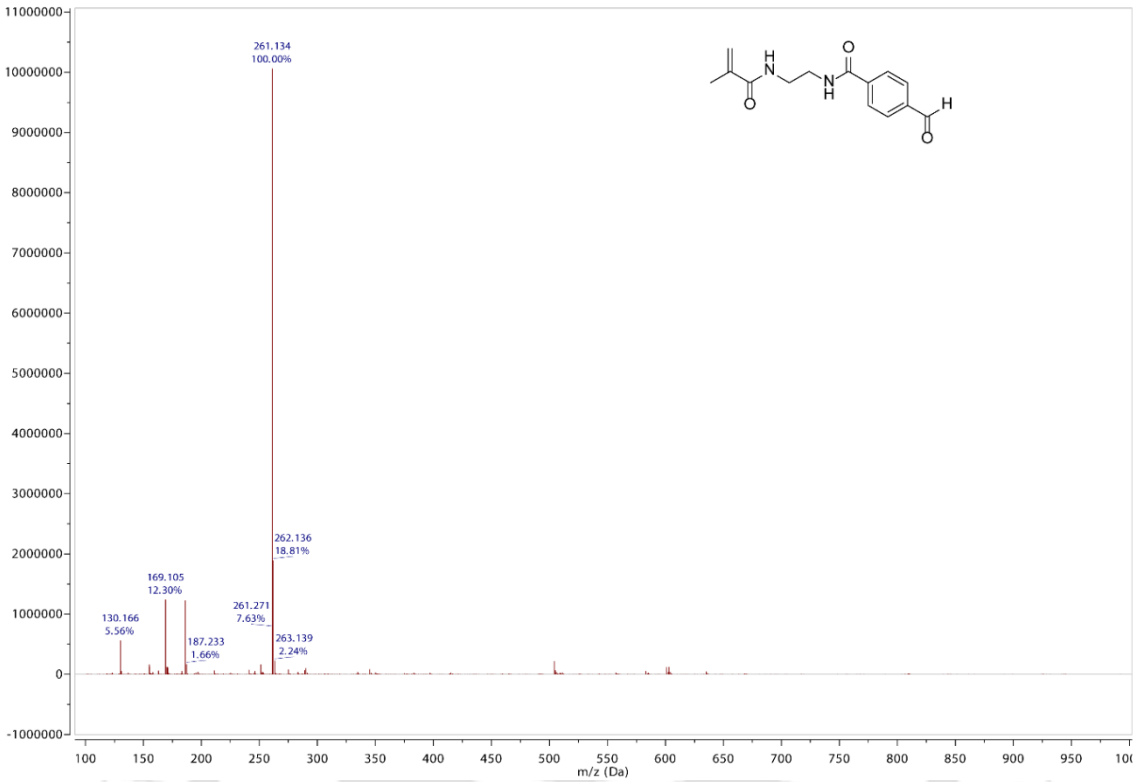

Figure 7.68ESI-MS Spectrum of Compound **21**.

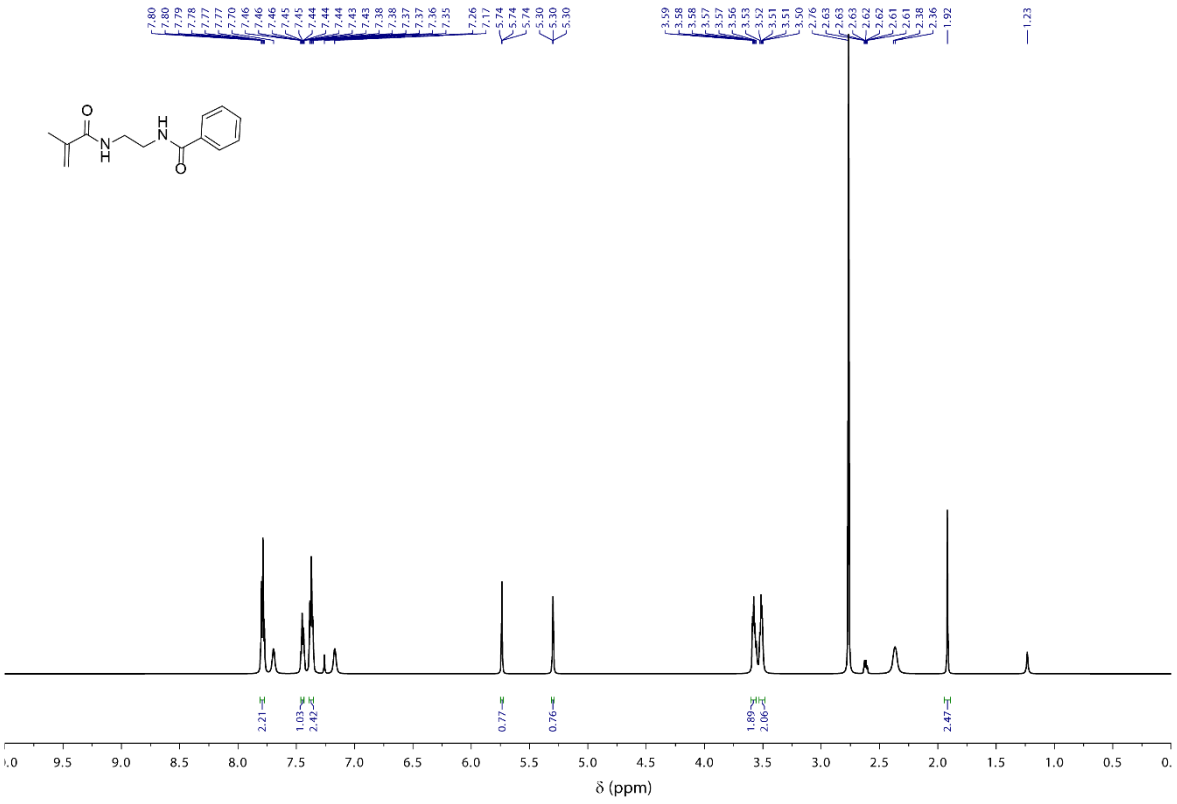

Figure 7.69^{1}H NMR Spectrum of Compound **22**in $CDCl_3$

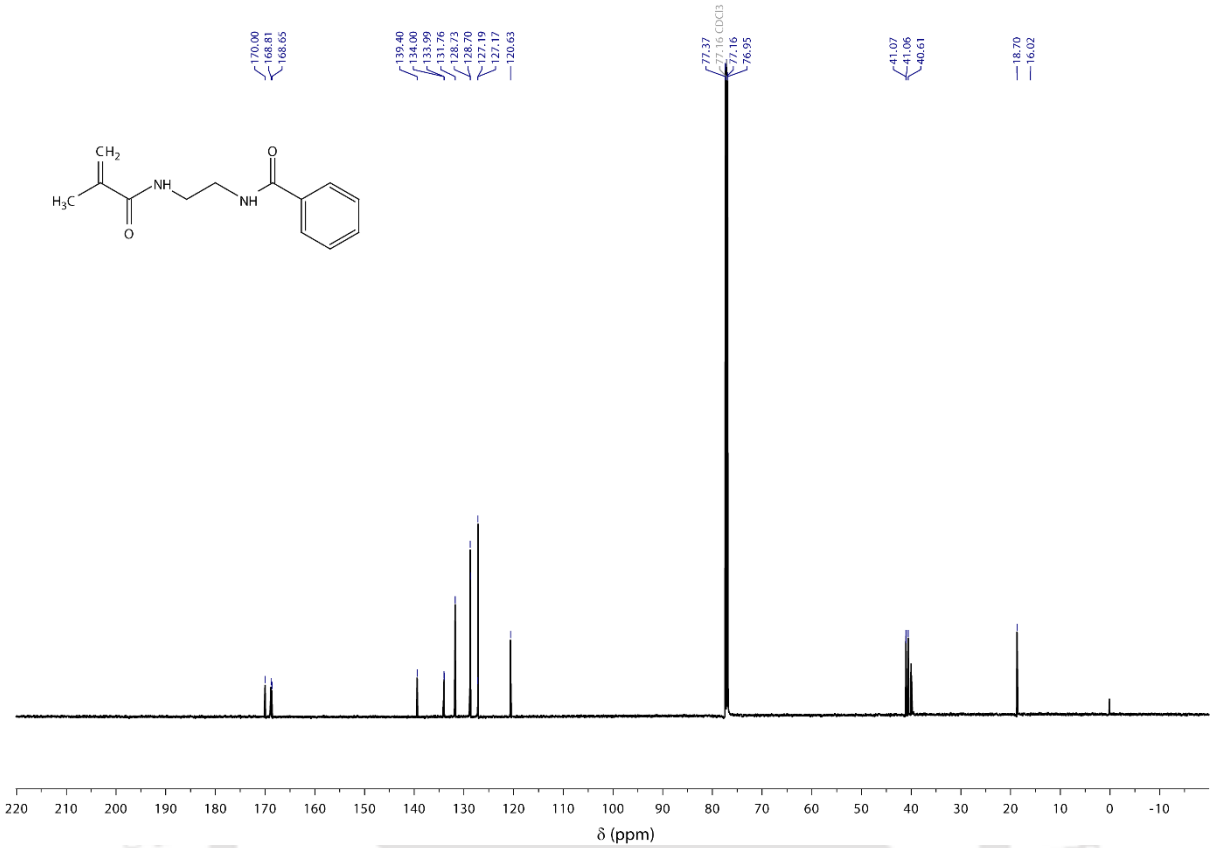

Figure 7.70 ^{13}C NMR Spectrum of Compound **22** in $CDCl_3$.

Figure 7.71 ESI-MS Spectrum ofCompound **22** in $CDCl_3$

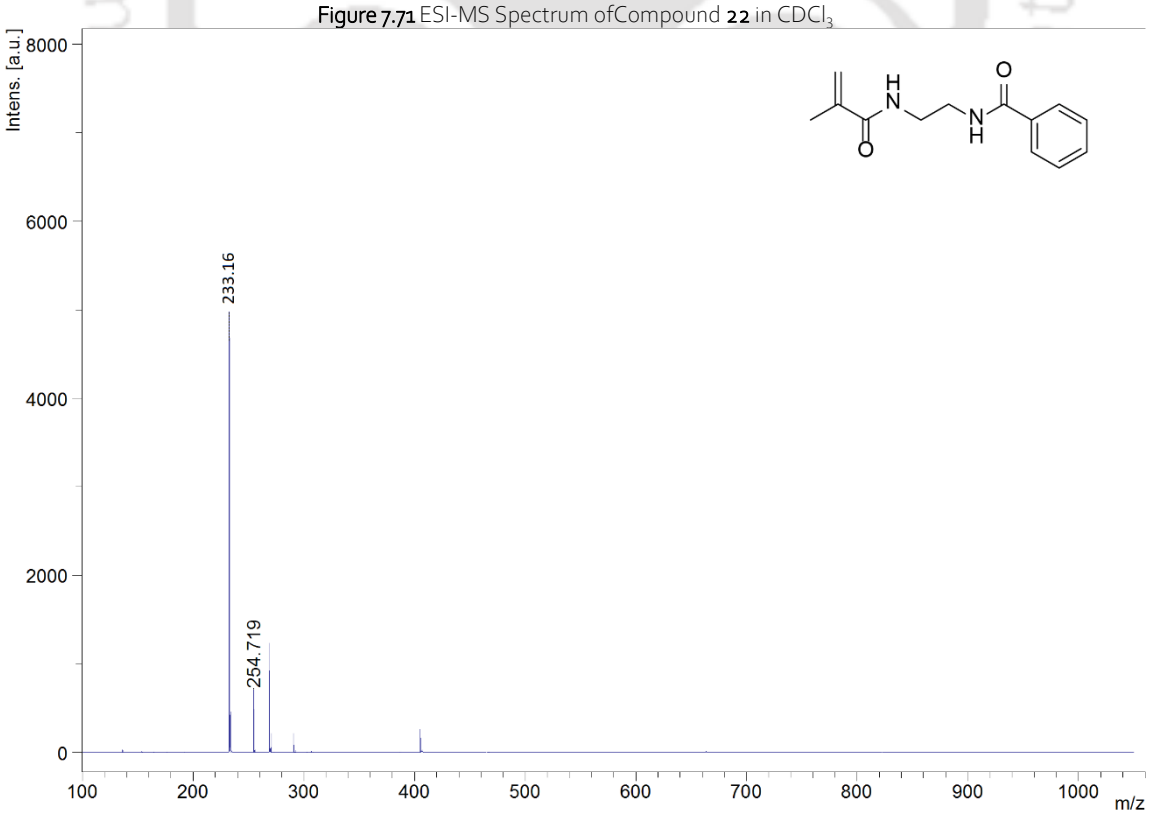

Figure 7.61 ESI-MS SPECTRUMSpectrum of Compound 22 in $CDCl_3$.

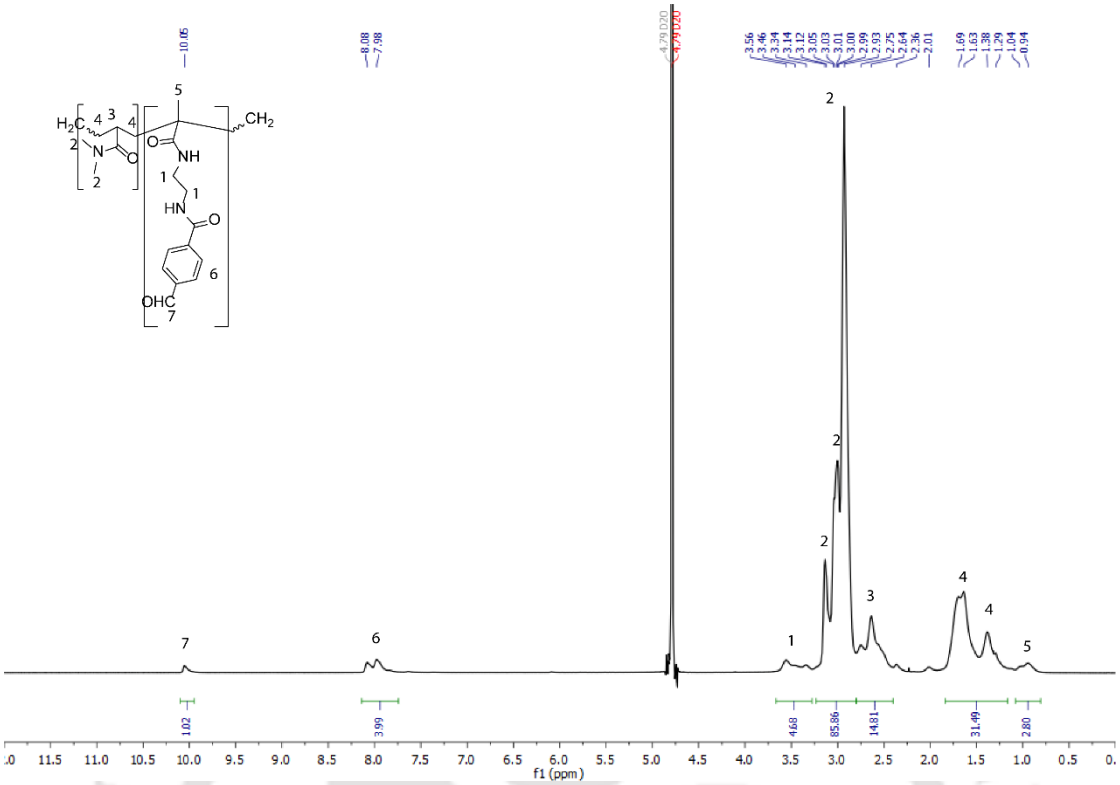

Figure 7.72 ^{1}H NMR Spectrum of Compound **23** in D_2O.

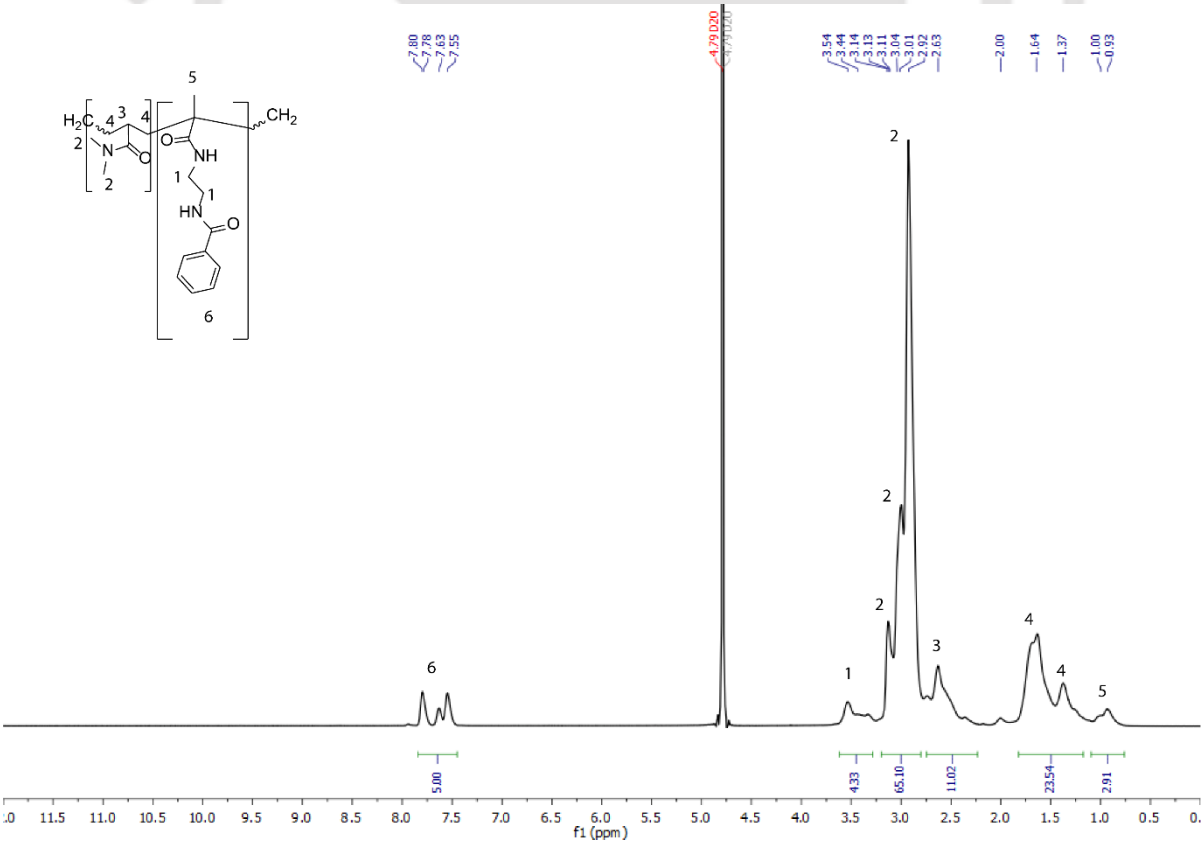

Figure 7.73 ^{1}H NMR Spectrum of Compound **24** in D_2O.

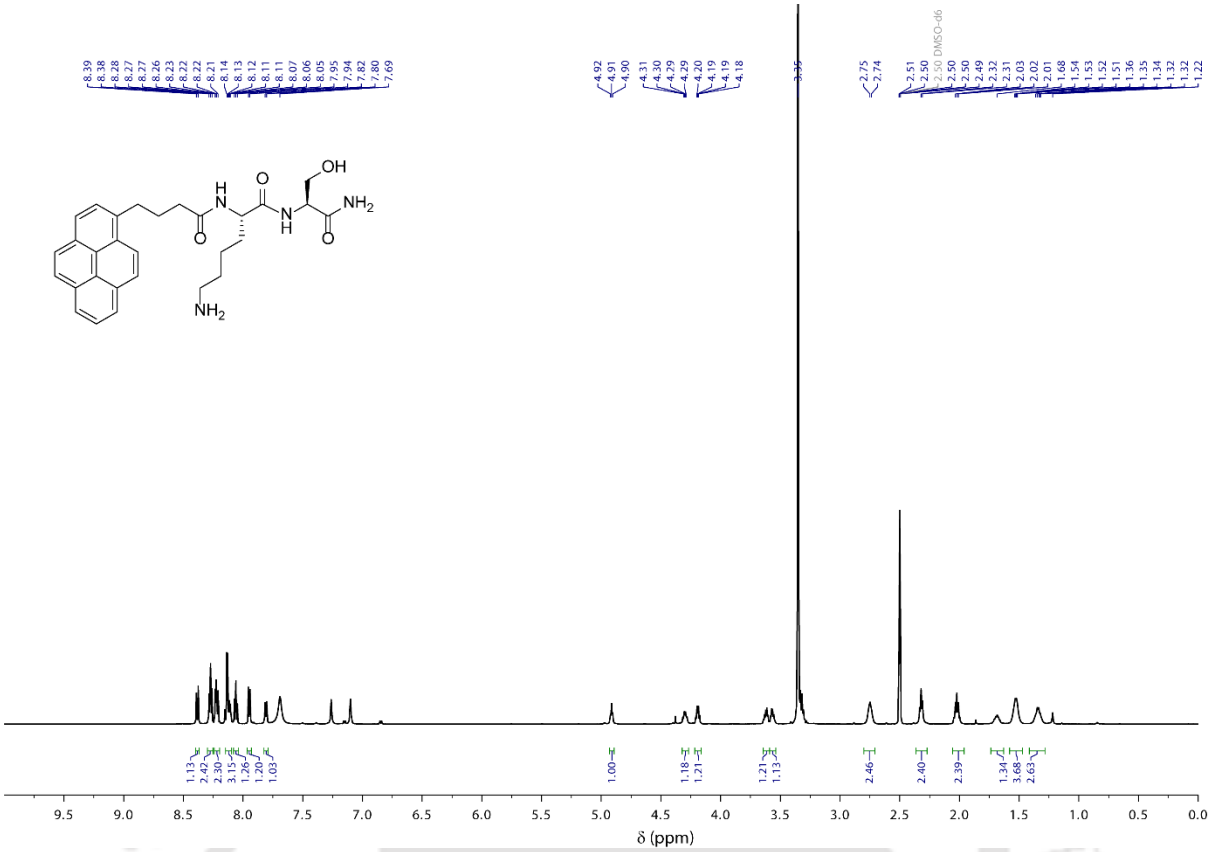

Figure 7.74 ^{1}H NMR Spectrum of **PyKS** in DMSO-D_6.

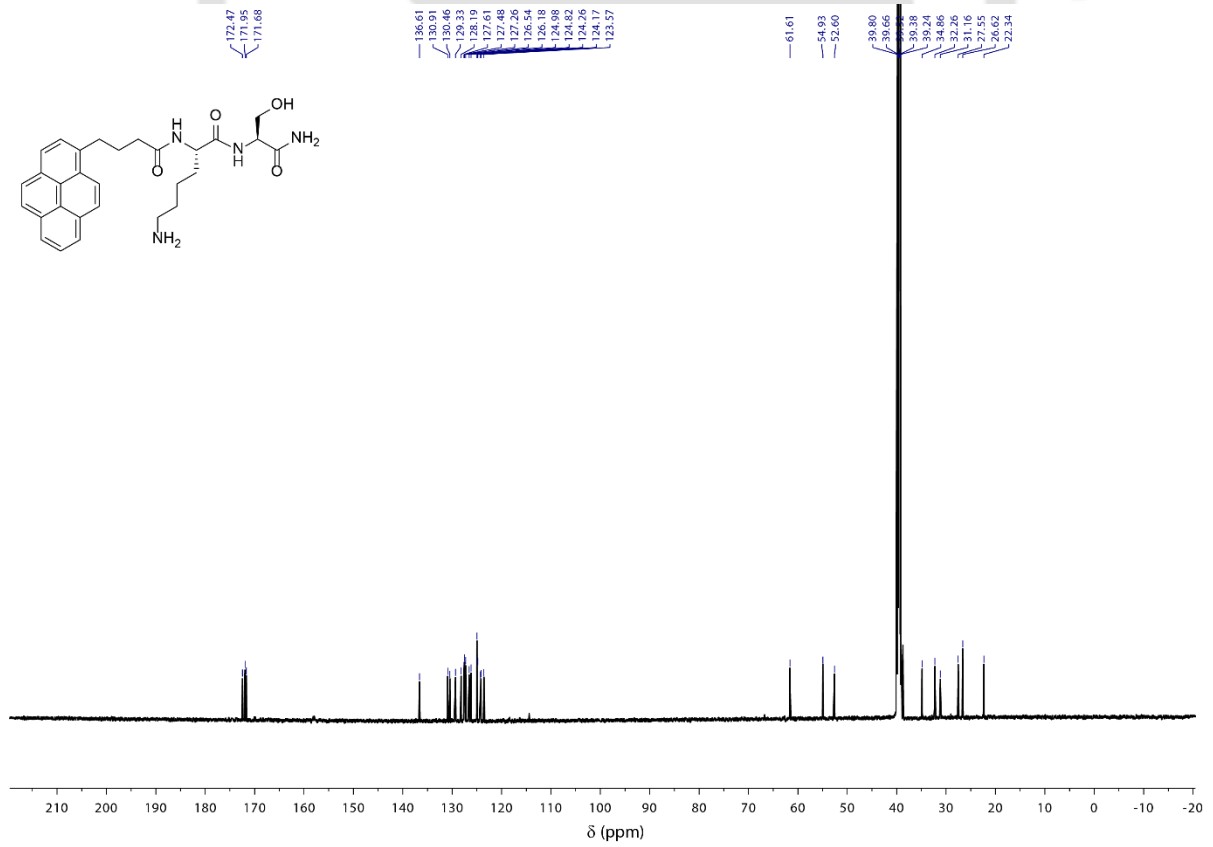

Figure 7.75 ^{1}H NMR Spectrum of **PyKS** in DMSO-D_6.

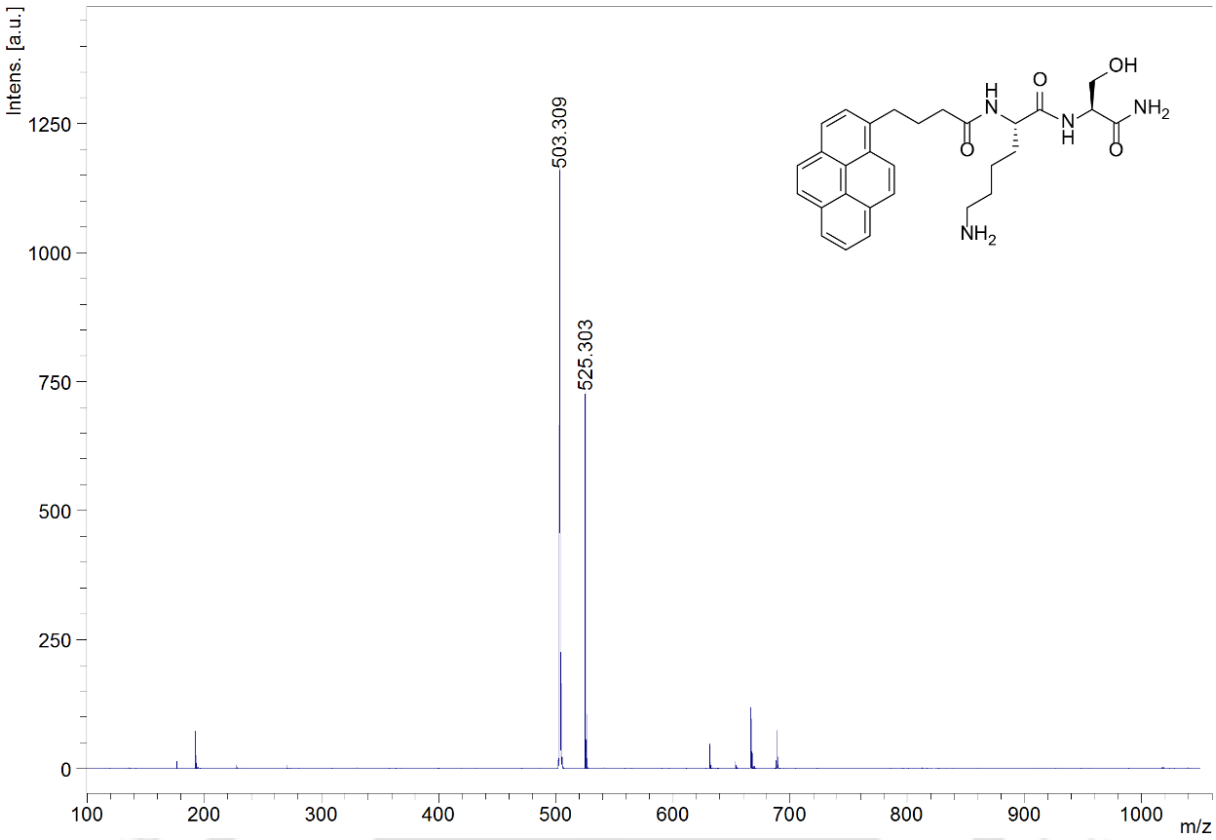

Figure 7.76ESI-MS Spectrum of PyKS

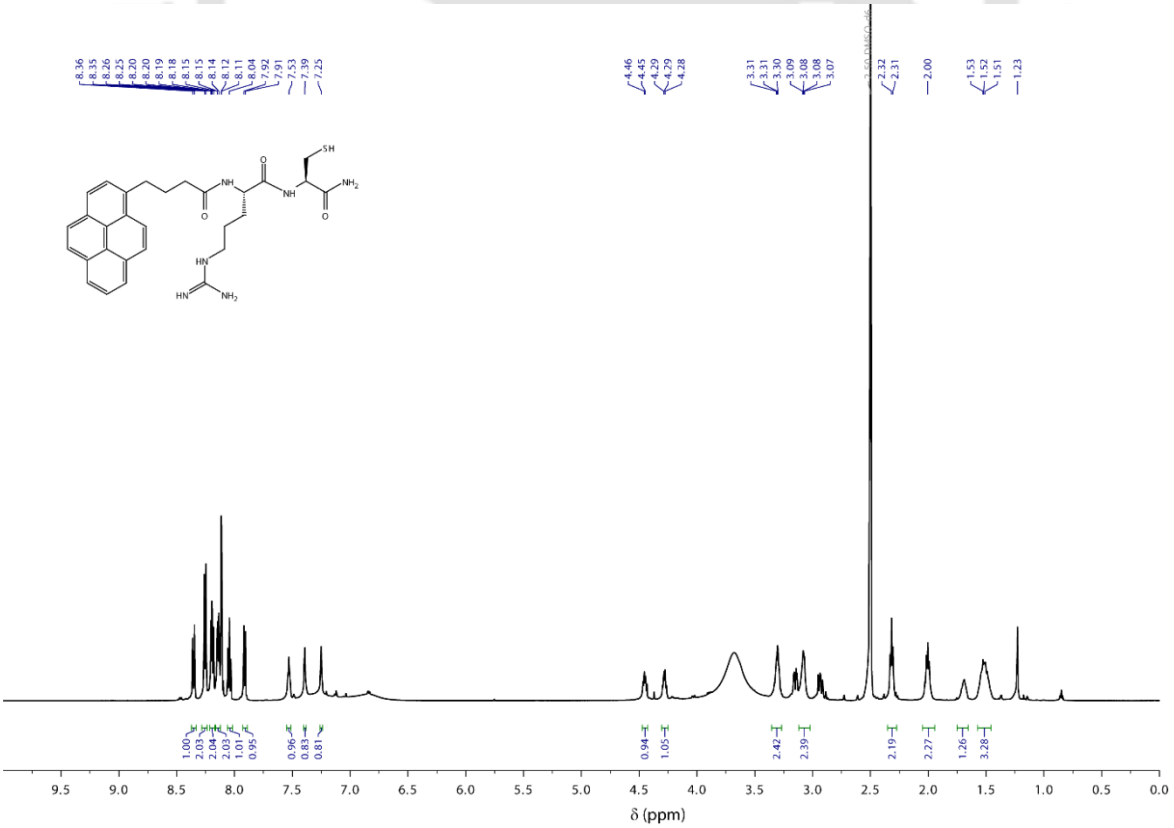

Figure 7.77^{1}H NMR Spectrum of PyRC in DMSO-D_6.

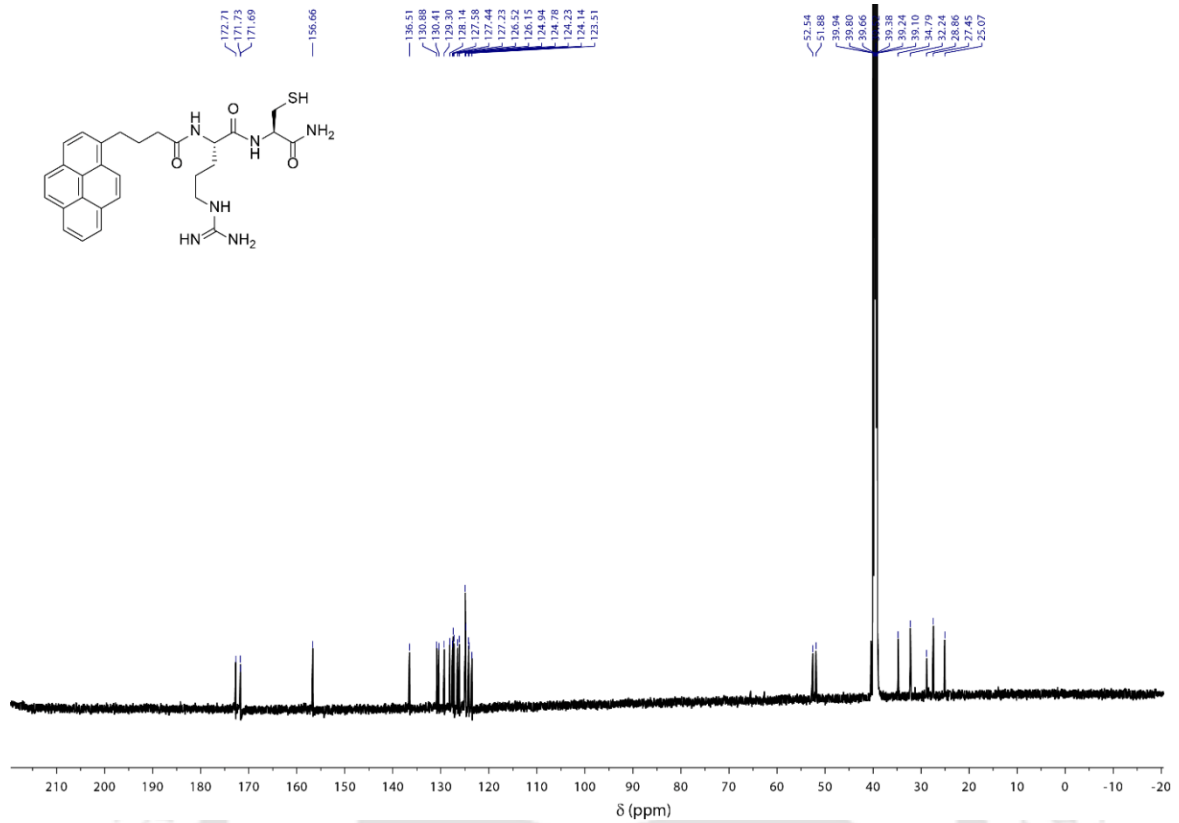

Figure 7.78 ^{13}C NMR Spectrum of **PyRC** in DMSO-D_6.

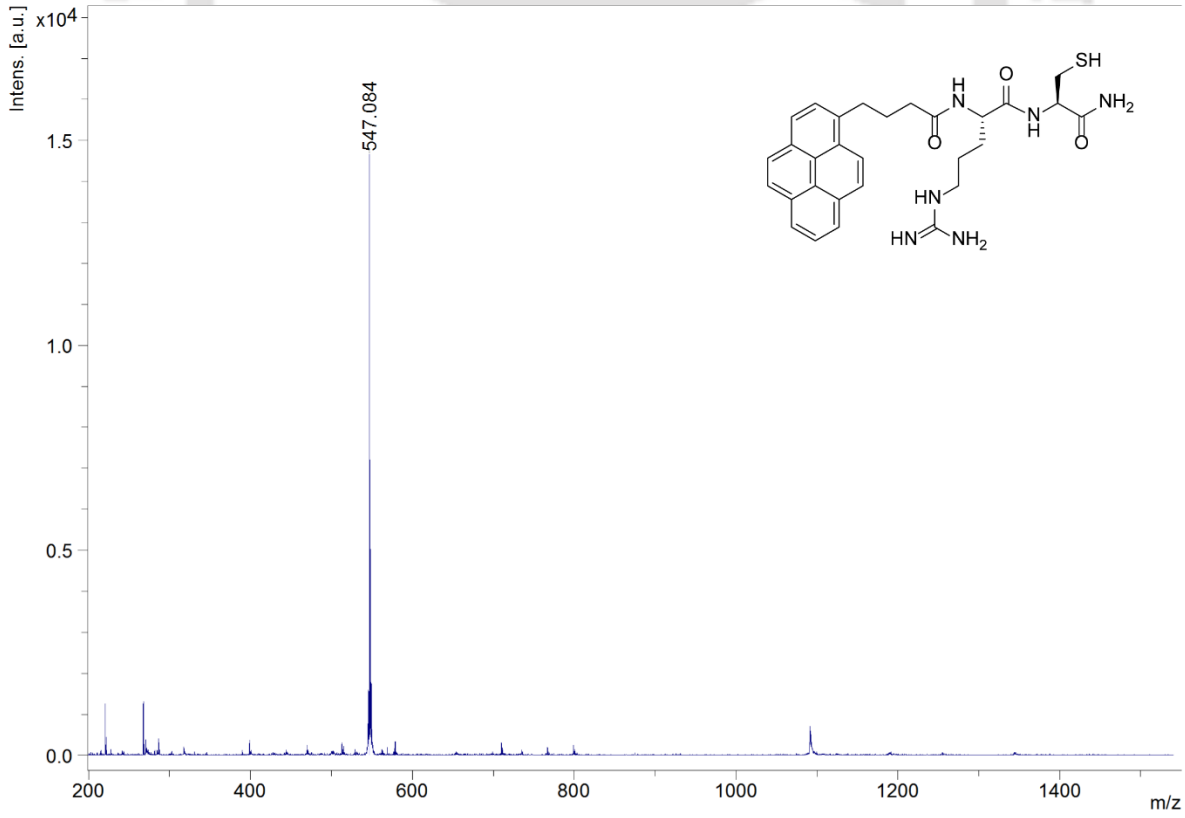

Figure 7.79 ESI-MS Spectrum of **PyRC**.

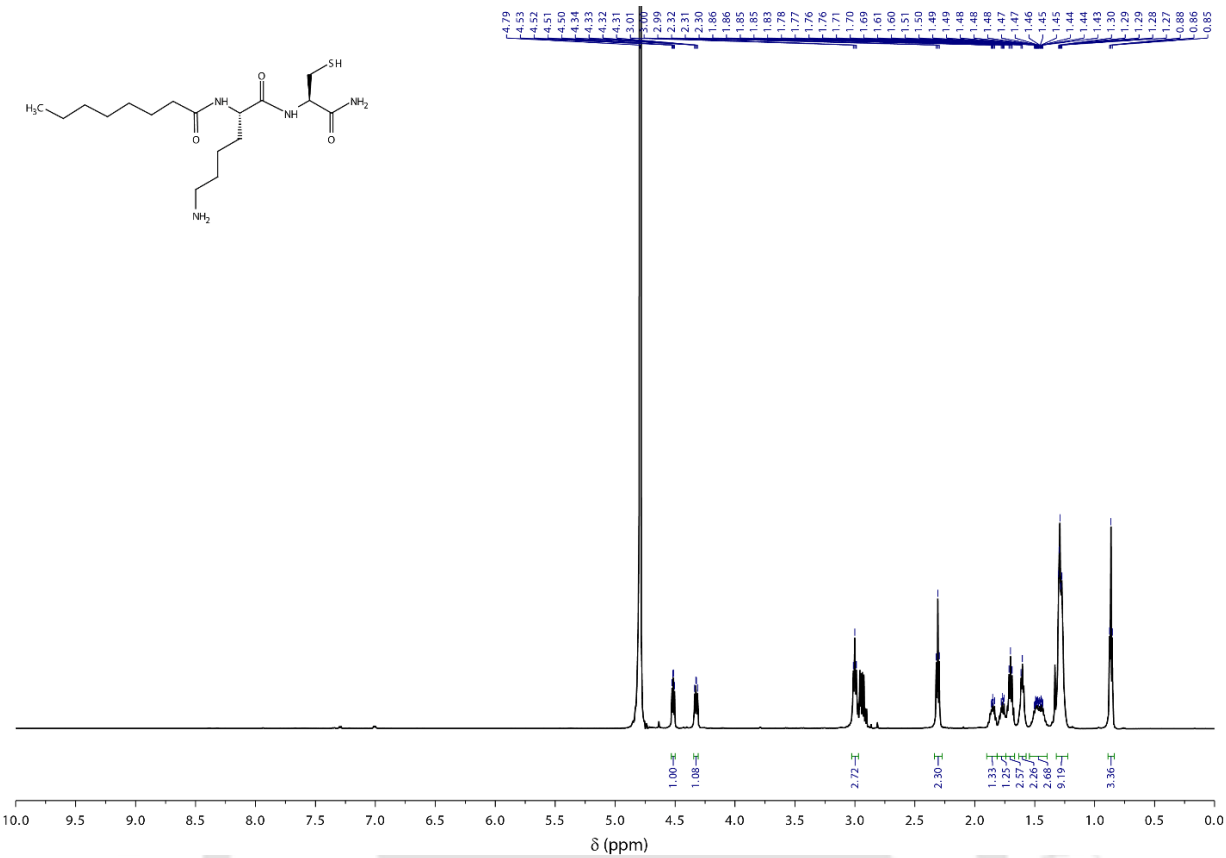

Figure 7.80 ^{1}H NMR Spectrum of C_6KC in D_2O.

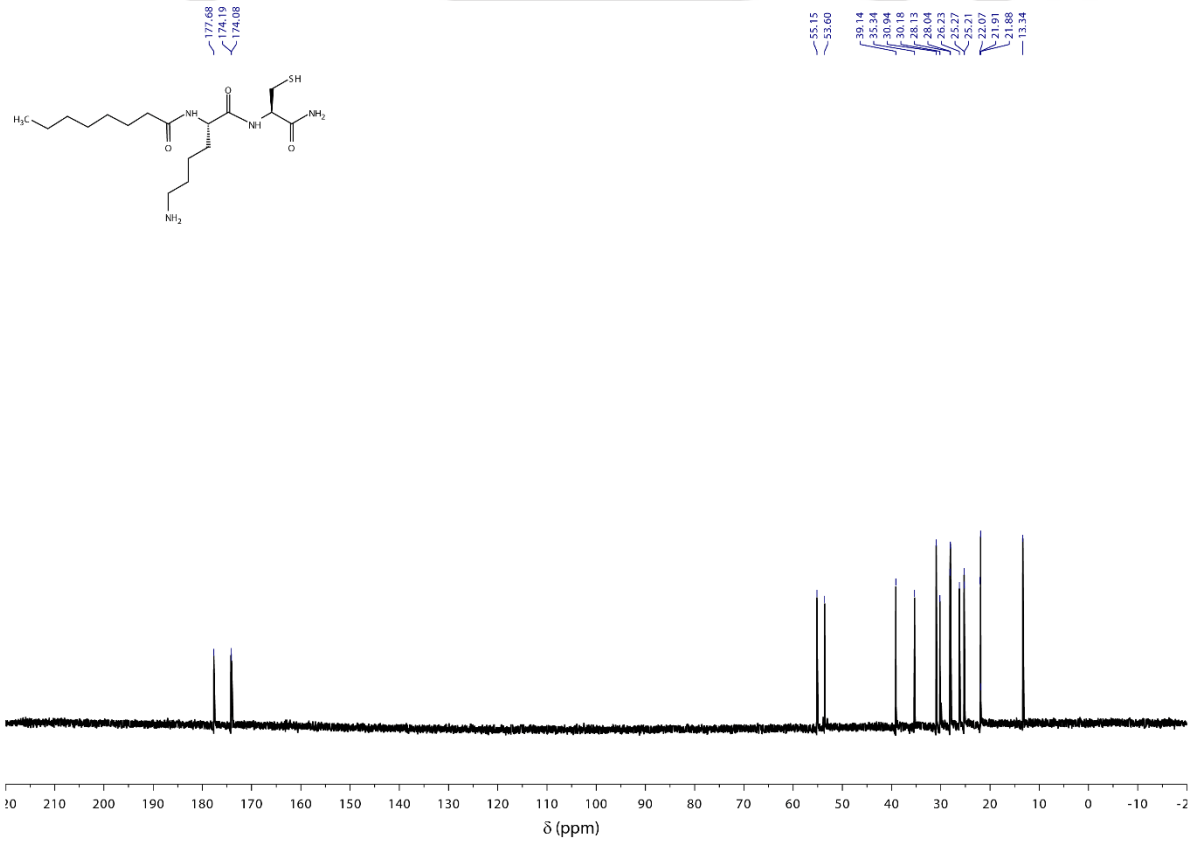

Figure 7.81 ^{13}C NMR Spectrum of C_6KC in D_2O.

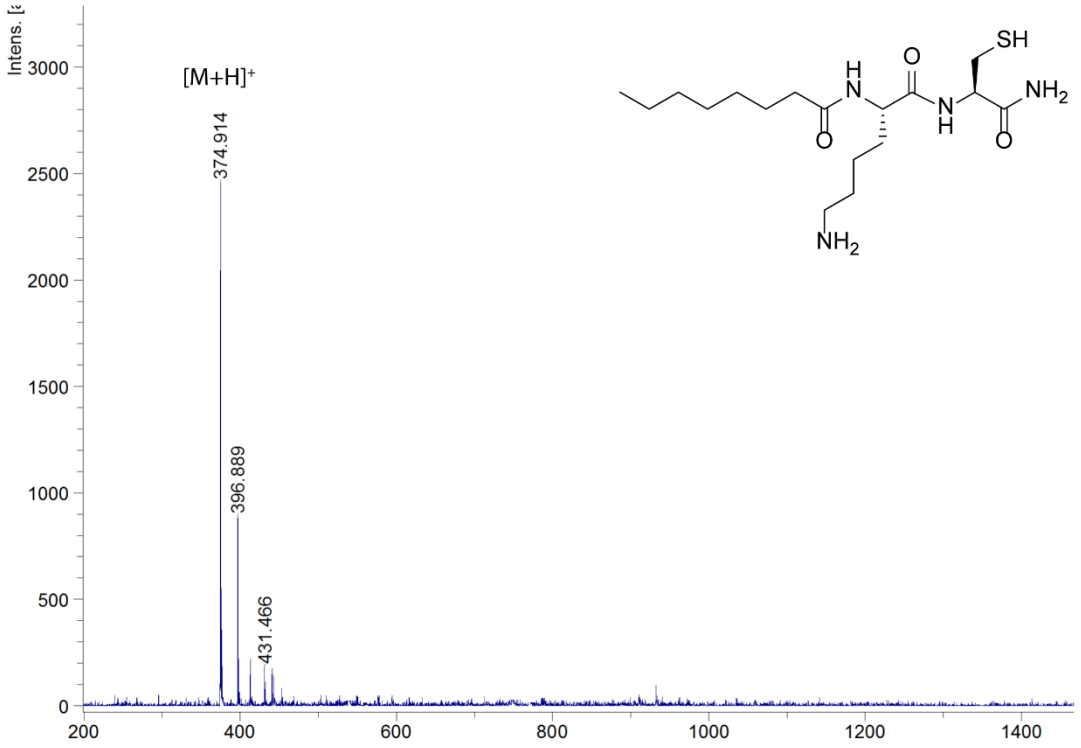

Figure 7.82 ESI-MS Spectrum of C_6KC.